

Electronic Thesis and Dissertation Repository

---

August 2010

# Virtual and Augmented Reality Techniques for Minimally Invasive Cardiac Interventions: Concept, Design, Evaluation and Pre-clinical Implementation

Cristian A. Linte, *University of Western Ontario*

Supervisor: Dr. Terence M. Peters, *The University of Western Ontario*

A thesis submitted in partial fulfillment of the requirements for the Doctor of Philosophy degree in Biomedical Engineering

© Cristian A. Linte 2010

Follow this and additional works at: <https://ir.lib.uwo.ca/etd>



Part of the [Bioimaging and Biomedical Optics Commons](#)

---

## Recommended Citation

Linte, Cristian A., "Virtual and Augmented Reality Techniques for Minimally Invasive Cardiac Interventions: Concept, Design, Evaluation and Pre-clinical Implementation" (2010). *Electronic Thesis and Dissertation Repository*. 4.

<https://ir.lib.uwo.ca/etd/4>

This Dissertation/Thesis is brought to you for free and open access by Scholarship@Western. It has been accepted for inclusion in Electronic Thesis and Dissertation Repository by an authorized administrator of Scholarship@Western. For more information, please contact [wlsadmin@uwo.ca](mailto:wlsadmin@uwo.ca).

**Virtual and Augmented Reality Techniques for Minimally  
Invasive Cardiac Interventions: Concept, Design,  
Evaluation and Pre-clinical Implementation**

(Spine title: Mixed Reality Environment for  
Cardiac Intervention Guidance)

(Thesis Format: Integrated Article)

by

Cristian A. Linte

Biomedical Engineering Graduate Program

Submitted in partial fulfillment  
of the requirements for the degree of  
Doctor of Philosophy

The School of Graduate and Postdoctoral Studies  
The University of Western Ontario  
London, Ontario, Canada

August 2010

© Cristian A. Linte, 2010

THE UNIVERSITY OF WESTERN ONTARIO  
School of Graduate and Postdoctoral Studies

CERTIFICATE OF EXAMINATION

**Supervisor**

**Examiners**

\_\_\_\_\_  
Dr. Terry M. Peters

\_\_\_\_\_  
Dr. James Johnson

**Supervisory Committee**

\_\_\_\_\_  
Dr. Maria Drangova

\_\_\_\_\_  
Dr. Shuo Li

\_\_\_\_\_  
Dr. Gerard M. Guiraudon

\_\_\_\_\_  
Dr. Tim Wilson

\_\_\_\_\_  
Dr. Rajni Patel

\_\_\_\_\_  
Dr. Purang Abolmaesumi

The thesis by

Cristian A. Linte

entitled

Virtual and Augmented Reality Techniques for Minimally  
Invasive Cardiac Interventions: Concept, Design,  
Evaluation and Pre-clinical Implementation

is accepted in partial fulfillment of the  
requirements for the degree of  
Doctor of Philosophy

Date \_\_\_\_\_

\_\_\_\_\_  
Chair of the Thesis Examination Board

*Dedicated to all those who suffer and who one day may hopefully benefit  
from the research conducted worldwide on minimally invasive cardiac interventions.*

## Abstract

While less invasive techniques have been employed for some procedures, most intracardiac interventions are still performed under cardiopulmonary bypass, on the drained, arrested heart. The progress toward off-pump intracardiac interventions has been hampered by the lack of adequate visualization inside the beating heart.

This thesis describes the development, assessment, and pre-clinical implementation of a mixed reality environment that integrates pre-operative imaging and modeling with surgical tracking technologies and real-time ultrasound imaging. The intra-operative echo images are augmented with pre-operative representations of the cardiac anatomy and virtual models of the delivery instruments tracked in real time using magnetic tracking technologies. The virtual models assist the user with the tool-to-target navigation, while real-time ultrasound ensures accurate positioning of the tool on target, providing the surgeon with sufficient information to “see” and manipulate instruments in absence of direct vision.

The targeting accuracy under model-enhanced ultrasound-assisted guidance was studied for procedures simulating direct-access and catheter guided interventions, and compared to the outcomes under model-assisted guidance and US image guidance alone. The proposed guidance environment led to an overall targeting error of under 3 mm, which represented a significant improvement from the accuracy recorded under 2D US image guidance alone. In addition, the real-time US imaging component provided sufficient information to correctly identify the intra-operative surgical target location and to compensate for any positioning errors due to misregistrations present between the heart model and its physical counterpart, ensuring a consistent targeting accuracy within 1-1.5 mm.

The pre-operative anatomical models integrated within the proposed surgical environment are critical for ensuring appropriate tool-to-target navigation. Using techniques previously developed in our laboratory, a method to generate subject-specific cardiac models for use in mitral valve interventional guidance is proposed and val-

idated using MR datasets of healthy subjects. The developed models can predict the location of the mitral valve annulus with a 3.1 mm accuracy throughout the cardiac cycle. Furthermore, these models can be integrated within the intra-operative guidance environment with less than a 5 mm alignment error of the pre- and intra-operative anatomy in the region of interest.

Several pre-clinical acute evaluation studies have been conducted *in vivo* on swine models to assess the feasibility of the proposed environment in a clinical context. Following direct access inside the beating heart using the UCI, the proposed mixed reality environment was used to provide the necessary visualization and navigation to position a prosthetic mitral valve on the the native annulus, or to place a repair patch on a created septal defect *in vivo* in porcine models.

Starting from the fundamental assumption in image-guided interventions that pre-operative images can adequately depict the intra-operative anatomy, the effects of heart displacement during minimally invasive procedure workflow have also been explored. Tracked ultrasound was used to acquire “instances” of the heart at each stage during the peri-operative workflow of model-enhanced ultrasound-guided interventions in porcine subjects and robot-assisted coronary artery bypass graft surgery in patients. In the effort to provide better pre-operative planning for the robot-assisted coronary artery bypass grafting interventions, a method was proposed to predict the intra-operative location of the target vessel based on its pre-operative, CT-derived location and the peri-operative heart migration information.

Following further development and seamless integration into the clinical workflow, we hope that the proposed mixed reality guidance environment may become a significant milestone toward enabling minimally invasive therapy on the beating heart.

**Keywords:** image-guided cardiac surgery; mixed reality environments; pre-operative planning; intra-operative guidance; surgical tracking; *in vivo* clinical translation

## Co-Authorship

The work in Chapter 1 is adapted from **Linte CA**, White J, Eagleson R, Guiraudon GM and Peters TM. Virtual and augmented medical imaging environments: Enabling technology for minimally invasive cardiac interventional guidance. *IEEE Reviews on Biomedical Engineering*. Submitted: July 2010. ©2010 IEEE. Reprinted, with permission, from IEEE. CA Linte performed the literature review and wrote the manuscript. J White contributed to the writing of selected parts of the manuscript. GM Guiraudon and R Eagleson shared their clinical and human-computer interface expertise, respectively, through helpful discussions. All authors provided editorial assistance and approved the final version of the manuscript. The research was performed under the supervision of TM Peters.

The work in Chapter 2 is adapted from **Linte CA**, Moore J, Wiles, AD, Wedlake C and Peters TM. Virtual Reality-Enhanced Ultrasound Guidance: A Novel Technique for Intracardiac Interventions. *Journal of Computer-Aided Surgery*. 13(2):82-94. 2008. CA Linte designed and conducted the experiments, analyzed the data, and wrote the manuscript. AD Wiles performed two of the experiments and wrote selected parts of the manuscript. J Moore provided support with tool design and hardware development. C Wedlake assisted with data acquisition and provided assistance with software support. All authors provided editorial assistance and approved the final version of the manuscript. The research was performed under the supervision of TM Peters.

The work in Chapter 3 is adapted from **Linte CA**, Moore J, Wedlake C and Peters TM. Evaluation of Model-Enhanced Ultrasound-Assisted Interventional Guidance in a Cardiac Phantom. *IEEE Transactions on Biomedical Engineering*. In Press: 2010. DOI: 10.1109/TBME.2010.2050886. ©2010 IEEE. Reprinted, with permission, from IEEE. CA Linte designed and conducted the experiments, analyzed the data, and wrote the manuscript. J Moore provided support with tool design and hardware development. C Wedlake assisted with data acquisition and provided software support. All authors provided editorial assistance and approved the final version of the manuscript. The research was performed under the supervision of TM Peters.

The work in Chapter 4 is adapted from **Linte CA**, Wierzbicki M, Moore J, Guiraudon GM, Little SH and Peters TM. Subject-Specific Models of the Dynamic Heart for Image-Guided Mitral Valve Surgery. *Proc. Med Image Comput Comput Assist Interv. (MICCAI) - Lect Notes Comput Sci.* 4792:94-101, 2007 and Linte CA, Wierzbicki M, Moore J, Guiraudon GM, Jones DL and Peters TM. On Enhancing Planning and Navigation of Beating-Heart Mitral Valve Surgery Using Pre-operative Cardiac Models. *Proc. IEEE Eng Med Biol.* 475-8. 2007. ©2010 IEEE. Reprinted, with permission, from IEEE. CA Linte designed and conducted the experiments, analyzed the data, and wrote both manuscripts. M Wierzbicki provided software support, conducted parts of the experiments, and contributed to the writing of selected parts of the manuscripts. J Moore provided support with tool design and hardware development. C Wedlake assisted with data acquisition and provided software support. SH Little acquired the ultrasound images and provided assistance with feature identification. GM Guiraudon and DL Jones shared their clinical expertise. All authors provided editorial assistance and approved the final versions of the manuscripts. The research was performed under the supervision of TM Peters.

The work in Chapter 5 is adapted from **Linte CA**, Moore J, Wedlake C and Bainbridge D, Guiraudon GM, Jones DL and Peters TM. Inside the Beating Heart: An *In Vivo* Feasibility Study on Fusing Pre- and Intra-operative Imaging for Minimally Invasive Therapy. *International Journal of Computer Assisted Radiology and Surgery* 4(2):113-123. 2009. CA Linte designed and conducted the experiments, analyzed the data, and wrote the manuscript. J Moore provided support with tool design and hardware development. C Wedlake assisted with data acquisition and provided software support. GM Guiraudon, DL Jones and D Bainbridge conducted the surgeries on animal models and moreover, D Bainbridge also acquired the ultrasound images and provided assistance with feature identification. All authors provided editorial assistance and approved the final versions of the manuscripts. The research was performed under the supervision of TM Peters.

The work in Chapter 6 is adapted from **Linte CA**, Carias M, Cho SD, Moore J, Wedlake C, Bainbridge D, Kiaii B and Peters TM. Estimating heart shift and morphological changes during minimally invasive cardiac interventions. *Proc. SPIE*



*Medical Imaging 2010: Visualization, Image-guided Procedures and Modeling*. Vol. 7625. Pp. 762509-1-11. 2010. CA Linte analyzed the data, and wrote the manuscript. M Carias provided assistance with data analysis. DS Cho acquired the data and helped with parts of the data analysis. J Moore and C Wedlake provided assistance with tool design and software support, respectively. B Kiaii performed the surgeries, helped with data acquisition, and provided clinical expertise. D Bainbridge acquired the ultrasound images and identified the features of interest. All authors provided editorial assistance and approved the final versions of the manuscripts. The research was performed under the supervision of TM Peters.

Portions of the work in Chapter 7 appear in **Linte CA**, Moore J and Peters TM. How accurate is accurate enough? An overview on accuracy considerations in image-guided cardiac interventions. *Proc. IEEE Eng Med Biol*. In Press. 2010. ©2010 IEEE. Reprinted, with permission, from IEEE. CA Linte designed and conducted the experiments, analyzed the data, and wrote the manuscript. J Moore provided support with tool design and hardware development. All authors provided editorial assistance and approved the final versions of the manuscripts. The research was performed under the supervision of TM Peters.

The work in Appendix A is adapted from Cho SD, **Linte CA**, Chen E, Wedlake C, Moore J and Peters TM. Predicting Target Vessel Location for Improved Planning of Robot-Assisted CABG Procedures. *Proc. Med Image Comput Comput Assist Interv. - Lect Notes Comput Sci*. In Press: 2010. DS Cho and CA Linte contributed to the experimental design, data acquisition and analysis, and wrote the manuscript. J Moore, C Wedlake and E Chen provided assistance with tool design and also provided suggestions with experimental design and data acquisition. All authors provided editorial assistance and approved the final versions of the manuscripts. The research was performed under the supervision of TM Peters.

## Acknowledgments

The work accomplished over the past four years would not have been the same without the help and support of many whom I do not have enough words to thank.

First and foremost, I would like to take a moment and thank Dr. Terry Peters for giving me the opportunity to be part of his research group and join this great project, for inspiring and challenging me, and for sharing his research insight and passion with me over the past four years. Terry has not been just a great supervisor, but rather a mentor any PhD student strives to find during his/her early research career. I owe Terry many thanks for his constructive criticism, for his support and encouragement with all my extracurricular activities, and for providing me with excellent networking opportunities while attending numerous national and international conferences and scientific meetings around the world.

Valuable guidance has been provided by the members of my advisory committee, Dr. Maria Drangova, Dr. Gérard Guiraudon and Dr. Rajni Patel, whose insightful suggestions, criticisms and encouragements determined me to focus and gave me the motivation to learn and overcome some of the challenges. Thank you for your continuous support and collaboration!

Next, I would like to thank John Moore, Chris Wedlake, Dr. Elvis Chen, Jaques Milner and Dr. Usaf Aladl for their day-to-day help around the lab, valuable advice and suggestions, and for being great friends. On the same note, I would like to thank Dr. Marcin Wierzbicki for his advice and research support in my early days and for helping me pave my research path under his experienced guidance. In addition, I would like to thank Jackie Williams for her editorial assistance with many of my scientific manuscripts and funding applications. Thanks Jackie for trying to make me a better writer ... hopefully one day it will really happen!

Without any doubt, over the past four years I have spent more time at Robarts than anywhere else, while not traveling, of course! I owe my great times and experience in the lab to several people, some still in the lab — Pencilla Lang, Diego Cantor, Feng Li, Daniel Cho, Kamyar Abhari, Feng Li and Mehdi Esteghamatian, some on the verge of moving on — Jessie Guo, Carling Cheung, and Kevin Wang, others who

have already moved on — Andrew Wiles, Danielle Pace, Qi Zhang, Jennifer Lo, and Edward Huang, and one who is no longer with us — Louise, I have always admired you for your strength and compassion! In addition, special thanks go to Petar Seslija and Dr. Veronica Ulici for their friendship and support, as well as Jessica, Gina and Robert Riley, and Flori and Ionut Turlescu for making me feel at home in Windsor even after my parents moved to the West Coast. Thank you all for being there for me!

The clinical aspects of this work would not have been possible without the help and support of a very dedicated clinical team — Dr. Daniel Bainbridge, Dr. Mike Chu, Dr. Gérard Guiraudon, Dr. Douglas Jones, Dr. Bob Kiaii, Dr. Ian Ross and Dr. Stephen Little, and Dr. James White, whom I would like to thank for sharing their expertise and enabling the initiation of the translation of this work from the laboratory and into the operating room. In addition, I would like to thank the animal care staff at CSTAR — Amber Parsons, Karen Siroen, and Sheri van Lingen for their help and support with all the animal studies.

I would like to thank Diana Timmermans, Kimberly Perry, Jackie Battaglia, Ana Pimentel and Anne Leaist for their administrative support and for their last minute assistance with all my funding applications. I would also like to thank Anne for sharing her chocolate supply with me during some of the late late nights at Robarts. Furthermore, I would like to thank Lynn Bowlby and Jodi Janiszewski from the IEEE EMBS Executive Office for all their help and assistance during my mandate as EMBS Student Representative, and Dr. Christopher James from the University of Warwick for his friendship, support and mentorship.

I would like to also acknowledge financial support over the past four years. Amongst other sources, significant support was provided by a Canada Graduate Scholarship from the Natural Sciences and Engineering Research Council and a Doctoral Research Award from the Heart & Stroke Foundation of Canada.

Lastly, I would like to thank my family for their unconditional love and support over the past almost thirty years! I can't believe it has already been thirty years ... don't they go by in a blink?! You have always been there for me! Thank you for everything and for encouraging me to follow my dreams!

# Contents

<b>Certificate of Examination</b>	<b>ii</b>
<b>Abstract</b>	<b>iv</b>
<b>Co-Authorship</b>	<b>vi</b>
<b>Acknowledgements</b>	<b>ix</b>
<b>List of Tables</b>	<b>xvii</b>
<b>List of Figures</b>	<b>xviii</b>
<b>List of Abbreviations</b>	<b>xxi</b>
<b>1 Introduction</b>	<b>1</b>
1.1 Introducing Virtual, Augmented and Mixed Reality Environments . . .	2
1.2 Minimally Invasive Procedures . . . . .	4
1.2.1 Cardiac interventions: A world of their own . . . . .	5
1.2.2 Imaging for Interventional Guidance . . . . .	5
1.2.3 Towards Surgical Guidance Platforms . . . . .	6
1.3 Interventional Platform Architecture . . . . .	7
1.3.1 Imaging . . . . .	7
1.3.1.1 Pre-operative Images . . . . .	7
1.3.1.2 Intra-operative Images . . . . .	9
1.3.2 Segmentation and Anatomical Modeling . . . . .	12
1.3.3 Surgical Instrument Localization and Tracking . . . . .	14
1.3.4 Data Integration . . . . .	16
1.3.4.1 Landmark-based Registration . . . . .	16
1.3.4.2 Geometry and Intensity-based Registration . . . . .	17
1.3.4.3 Deformable Registration . . . . .	18
1.3.5 Visualization and Display . . . . .	18
1.3.5.1 Visualization Platforms . . . . .	18

1.3.5.2	Display Technology . . . . .	21
1.4	Accuracy Considerations . . . . .	22
1.4.1	Clinical Accuracy Constraints . . . . .	23
1.4.2	Engineering Accuracy Considerations . . . . .	23
1.5	From the Laboratory into the Operating Room . . . . .	24
1.5.1	Logistics . . . . .	24
1.5.1.1	<i>In vitro</i> Evaluation . . . . .	25
1.5.1.2	Initiating Clinical Translation . . . . .	25
1.5.2	Psycho-physical Effects: Visualization and Perception . . . . .	26
1.5.2.1	Image Fusion . . . . .	27
1.5.2.2	3D Data Visualization and Interaction . . . . .	27
1.5.2.3	Navigation and Hand-eye Coordination . . . . .	28
1.5.3	Pre-clinical and Clinical Applications . . . . .	28
1.5.3.1	Transapical Aortic Valve Implantation . . . . .	28
1.5.3.2	Ultrasound-guided Robotic Intracardiac Surgery . . . . .	30
1.5.3.3	Model-enhanced Ultrasound-Assisted Guidance . . . . .	31
1.5.3.4	Electro-physiology and Ablation Therapy Guidance . . . . .	31
1.5.3.5	Assessing and Restoring Cardiac Function . . . . .	32
1.6	Caveats in Cardiac Surgical Guidance Environments . . . . .	34
1.6.1	Equipment Constraints . . . . .	34
1.6.2	Calibration and Visualization Constraints . . . . .	36
1.6.2.1	Spatial and Temporal Calibration . . . . .	36
1.6.2.2	3D Data Representation . . . . .	36
1.6.3	User-dependent Constraints . . . . .	37
1.7	Thesis Objectives . . . . .	39
1.8	Thesis Outline . . . . .	40
1.8.1	Chapter 2: Model-enhanced US-assisted Guidance Environ- ment Overview . . . . .	40
1.8.2	Chapter 3: Quantitative Surgical Guidance Evaluation . . . . .	41
1.8.3	Chapter 4: Pre-operative Models for Mitral Valve Interventions . . . . .	41
1.8.4	Chapter 5: <i>In vivo</i> Pre-clinical Feasibility Studies . . . . .	41
1.8.5	Chapter 6: Heart Migration during Minimally Invasive Proce- dures . . . . .	42
1.8.6	Appendix A: Predicting Intra-operative Target Vessel Location . . . . .	42
	<b>References</b> . . . . .	<b>43</b>
<b>2</b>	<b>Model-enhanced Ultrasound Guidance: Concept, Initial Implemen- tation, and Qualitative <i>in vitro</i> Assessment</b> . . . . .	<b>66</b>
2.1	Introduction . . . . .	67
2.2	Surgical Guidance Platform Architecture . . . . .	70
2.2.1	The <i>AtamaiViewer</i> . . . . .	70

2.2.1.1	Components . . . . .	70
2.2.1.2	Applications . . . . .	70
2.2.2	Mixed Reality Environment . . . . .	71
2.2.2.1	Intra-operative Guidance: Echocardiography . . . . .	71
2.2.2.2	Pre-operative Planning and Guidance . . . . .	73
2.2.2.3	Surgical Tool Tracking . . . . .	75
2.3	System Evaluation and Assessment . . . . .	77
2.3.1	Accuracy Assessment . . . . .	77
2.3.1.1	US Calibration Accuracy . . . . .	77
2.3.1.2	Surgical Navigation Accuracy . . . . .	78
2.3.2	Pre-clinical Qualitative Evaluation: <i>In vitro</i> and <i>Ex vivo</i> Mitral Valve Implantation . . . . .	79
2.3.2.1	Cardiac Intervention Phantom Studies . . . . .	80
2.3.2.2	Excised Porcine Hearts Study . . . . .	80
2.3.2.3	Guidance Modalities . . . . .	82
2.4	Discussion . . . . .	85
2.5	Conclusions . . . . .	87
	<b>References</b>	<b>89</b>
<b>3</b>	<b>Quantitative Evaluation of the Model-Enhanced Ultrasound-Assisted Guidance Environment</b>	<b>93</b>
3.1	Introduction . . . . .	94
3.2	Materials and Methods . . . . .	96
3.2.1	Experimental Design . . . . .	96
3.2.2	Visualization and Navigation Environment . . . . .	97
3.2.2.1	Pre-operative Imaging and Modeling . . . . .	98
3.2.2.2	Intra-operative Imaging . . . . .	99
3.2.2.3	Surgical Tracking . . . . .	99
3.2.3	Simulating <i>in vitro</i> Therapy Delivery . . . . .	100
3.2.3.1	Direct Access Closed-Chest Navigation . . . . .	100
3.2.3.2	Endocardial Catheter Navigation . . . . .	101
3.2.3.3	Intra-operative Guidance Modalities . . . . .	102
3.2.3.4	Mimicking Model-to-Subject Misregistrations . . . . .	104
3.2.4	Data Acquisition Module . . . . .	108
3.3	Evaluation and Results . . . . .	109
3.3.1	Direct Access Epicardial Interventions . . . . .	110
3.3.2	Catheter-Driven Endocardial Interventions . . . . .	112
3.3.3	Model-to-Subject Misalignments . . . . .	114
3.3.4	Qualitative Surgical Guidance Environment Evaluation . . . . .	118
3.4	Discussion . . . . .	119
3.5	Conclusions . . . . .	123

<b>References</b>	<b>125</b>
-------------------	------------

<b>4 Subject-Specific Models for Mitral Valve Interventions: Predicting Surgical Target and Enhancing Intra-operative Navigation</b>	<b>128</b>
4.1 Introduction . . . . .	129
4.2 Methodology . . . . .	130
4.2.1 Building Subject-Specific Cardiac Models for Mitral Valve Interventions . . . . .	131
4.2.1.1 Prior High-Resolution Heart Model . . . . .	132
4.2.1.2 Image Acquisition . . . . .	133
4.2.1.3 Anatomical Feature Extraction . . . . .	134
4.2.2 Pre- to Intra-operative Registration . . . . .	136
4.3 Results . . . . .	137
4.3.1 Accuracy Assessment of Model-Predicted Mitral Valve Annulus	137
4.3.2 Pre- to Intra-operative Registration Evaluation . . . . .	139
4.4 Discussion . . . . .	142
4.5 Conclusions . . . . .	145

<b>References</b>	<b>147</b>
-------------------	------------

<b>5 Mitral Valve Implantation and Atrial Septal Defect Repair under Model-enhanced Ultrasound Guidance: <i>In vivo</i> Pre-clinical Feasibility Studies</b>	<b>149</b>
5.1 Introduction . . . . .	150
5.2 Methodology . . . . .	150
5.2.1 Pre-operative Imaging and Modeling . . . . .	151
5.2.1.1 Pre-operative Image Acquisition. . . . .	151
5.2.1.2 Static Cardiac Model . . . . .	152
5.2.1.3 Dynamic Model . . . . .	153
5.2.2 Intra-operative Guidance . . . . .	154
5.2.2.1 Trans-esophageal Echocardiography . . . . .	154
5.2.2.2 Peri-operative Image Acquisition . . . . .	155
5.2.2.3 Peri-operative Image Processing . . . . .	155
5.3 Virtual Environment and Surgical Guidance . . . . .	158
5.3.1 Pre- to Intra-operative Registration . . . . .	158
5.3.2 Image-Guided Therapy Applications . . . . .	160
5.3.2.1 Mitral Valve Implantation . . . . .	161
5.3.2.2 Atrial Septal Defect Repair . . . . .	163
5.4 Discussion . . . . .	164
5.5 Conclusions . . . . .	169

<b>References</b>	<b>171</b>
-------------------	------------

<b>6</b>	<b>Investigating Heart Migration during Minimally Invasive Cardiac Interventions</b>	<b>173</b>
6.1	Introduction . . . . .	174
6.2	Methodology . . . . .	176
6.2.1	Minimally Invasive Procedure Workflow . . . . .	177
6.2.1.1	Direct-access Off-pump Intracardiac Interventions via UCI . . . . .	177
6.2.1.2	Robot-Assisted Coronary Artery Bypass Graft Interventions . . . . .	178
6.2.2	Data Acquisition . . . . .	179
6.2.2.1	Pre-operative Image Acquisition . . . . .	179
6.2.2.2	Peri-operative Image Acquisition . . . . .	179
6.2.2.3	Cardiac Feature Identification . . . . .	181
6.2.3	Data Analysis . . . . .	182
6.2.3.1	Global Heart Movement . . . . .	182
6.2.3.2	Morphological Feature Characterization . . . . .	183
6.3	Results . . . . .	184
6.3.1	Global Heart Displacement . . . . .	184
6.3.1.1	UCI-based Intracardiac Interventions . . . . .	184
6.3.1.2	Robot-assisted CABG Interventions . . . . .	185
6.3.2	Morphological Feature Characterization . . . . .	186
6.4	Discussion . . . . .	187
6.5	Conclusions . . . . .	192
	<b>References</b>	<b>193</b>
<b>7</b>	<b>Summary, Contributions and Future Directions</b>	<b>194</b>
7.1	Summary of Contributions . . . . .	195
7.2	Accuracy Considerations: Revisited . . . . .	198
7.2.1	Examples of Accuracy Expectations in the Clinic . . . . .	199
7.2.2	Identifying Engineering Accuracy Constraints . . . . .	200
7.2.2.1	Modeling Accuracy . . . . .	200
7.2.2.2	Registration Accuracy . . . . .	201
7.2.2.3	Surgical Tracking Accuracy . . . . .	202
7.2.2.4	Overall Targeting Accuracy . . . . .	204
7.2.3	Monitoring, Improving and Providing Accuracy Feedback to the Surgeon . . . . .	204
7.3	Summary of Lessons Learned during Clinical Translation . . . . .	206
7.3.1	Zoom in where Needed: Region of Interest Accuracy . . . . .	206
7.3.2	Cutting-edge Hardware: Surgical Tool Design . . . . .	207
7.3.3	Minimizing “Footprint” in the Operating Room . . . . .	207
7.3.4	Making “the New” Look like “the Old” . . . . .	208



7.3.5	Maximizing Returns: Optimal Information Display . . . . .	209
7.4	Future Directions . . . . .	209
7.4.1	Integration with 3D TEE . . . . .	209
7.4.2	Catheter-guided Atrial Ablation Therapy . . . . .	211
7.5	Concluding Remarks . . . . .	213
<b>References</b>		<b>214</b>
<b>A Predicting Target Vessel Location for Improved Planning of Robot-Assisted CABG Procedures</b>		<b>217</b>
A.1	Background and Motivation . . . . .	218
A.2	<i>In vitro</i> Experimental Validation . . . . .	221
A.2.1	Experimental Apparatus . . . . .	221
A.2.2	Intra-operative Image Acquisition . . . . .	222
A.2.3	Feature-based Registration Technique . . . . .	223
A.3	Assessing Intra-operative LAD Localization . . . . .	224
A.4	Discussion . . . . .	226
A.5	Conclusions . . . . .	227
<b>References</b>		<b>228</b>
<b>B Copyright Releases and Permissions</b>		<b>229</b>
<b>C Research Ethics Approvals</b>		<b>238</b>
<b>Vita</b>		<b>244</b>

# List of Tables

2.1	Accuracy assessment of US calibration using three different transducers	77
2.2	Single point localization accuracy assessment under three distinct guidance modalities . . . . .	79
3.1	Direct Access Procedures: Summary Table . . . . .	110
3.2	Endocardial Catheter Navigation: Summary Table . . . . .	113
3.3	Guidance Accuracy under Model-to-Subject Misregistration: Part 1 .	116
3.4	Guidance Accuracy under Model-to-Subject Misregistration: Part II .	116
3.5	Qualitative Assessment of Surgical Guidance: Expert Evaluation . . .	118
3.6	Qualitative Assessment of Surgical Guidance: Novice Evaluation . . .	119
4.1	Predicted surgical target accuracy . . . . .	138
4.2	Pre- to intra-operative registration error summary across each model structure . . . . .	140
4.3	Pre- to intra-operative registration error (RMS distance error - mm) estimated at four cardiac phases . . . . .	141
5.1	Anatomical alignment achieved using the pre- to intraoperative registration . . . . .	159
6.1	Mitral and aortic valve displacement in swine subjects during UCI-based interventions . . . . .	185
6.2	Mitral and aortic valve displacement in patients during robot-assisted CABG procedures . . . . .	188
6.3	Characterization of valvular morphology during UCI-based interventions	188
6.4	Characterization of valvular morphology during robot-assisted CABG workflow . . . . .	189
A.1	Left Anterior Descending Coronary Vessel Registration Error . . . . .	224
A.2	Anatomical Feature Localization Error . . . . .	225

# List of Figures

1.1	Schematic representation of the reality-virtuality continuum . . . . .	3
1.2	Typical IGI system/procedure workflow . . . . .	6
1.3	Common tracking systems employed in IGI . . . . .	15
1.4	<i>Analyze<sup>TM</sup></i> visualization environment . . . . .	19
1.5	<i>IGSTK</i> surgical navigation environment . . . . .	20
1.6	Intra-operative real-time MR image guidance . . . . .	29
1.7	Myocardial scar imaging for CAR . . . . .	33
1.8	Hybrid vascular-scar models for cellular-based CRT . . . . .	35
1.9	Volume rendering of multi-modality images . . . . .	38
2.1	Model-enhanced US guidance operating room workflow . . . . .	69
2.2	it AtamaiViewer surgical platform environment . . . . .	72
2.3	Examples of interventional US images . . . . .	73
2.4	Subject-specific cardiac model of healthy human volunteer . . . . .	74
2.5	TEE augmented with pre-operative heart model . . . . .	75
2.6	Surgical instrument tracking . . . . .	76
2.7	Cardiac intervention phantom mimicking real anatomy . . . . .	81
2.8	Experimental setup for excised porcine hearts . . . . .	82
2.9	Valve implantation using US image guidance alone . . . . .	83
2.10	Illustration of the navigation-positioning paradigm . . . . .	84
2.11	Valve implantation under model-enhanced US guidance . . . . .	85
3.1	Beating heart phantom used for <i>in vitro</i> evaluation . . . . .	97
3.2	Dynamic CT dataset and virtual models of cardiac phantom . . . . .	98
3.3	Experimental setup mimicking direct-access procedures. . . . .	101
3.4	Experimental apparatus: catheter-driven endocardial procedures . . . . .	102
3.5	Image-guidance modalities employed in the experiments. . . . .	104
3.6	Model-enhanced US anatomy and associated error map . . . . .	105
3.7	Simulated model-to-phantom misregistrations. . . . .	106
3.8	Illustration of the navigation/positioning paradigm. . . . .	109
3.9	Direct-access interventional guidance evaluation. . . . .	112

3.10	Direct-access intervention target distribution maps. . . . .	112
3.11	Catheter-guided endocardial intervention assessment. . . . .	113
3.12	Target distribution maps under catheter guidance. . . . .	115
3.13	Targeting accuracy plot following accurate world registration. . . . .	117
3.14	Targeting accuracy improvements in presence of US imaging. . . . .	117
3.15	Qualitative target distribution maps. . . . .	122
4.1	Constructing subject-specific cardiac models . . . . .	134
4.2	Cardiac motion extraction using non-rigid registration . . . . .	135
4.3	Pre- to intra-operative registration process . . . . .	137
4.4	Predicted vs. ground-truth surgical target location . . . . .	139
4.5	Error distribution across left ventricle model . . . . .	141
4.6	Error distribution across left atrium and aorta . . . . .	142
4.7	Error distribution across right atrium and ventricle . . . . .	143
4.8	Diagram2 . . . . .	144
4.9	Multi-modality imaging visualization and navigation . . . . .	145
5.1	Pre-operative MR image and corresponding model of a porcine heart . . . . .	152
5.2	Porcine heart chamber models extracted from pre-operative MRI . . . . .	153
5.3	Schematic representation of cardiac motion extraction . . . . .	154
5.4	Instances of a dynamic porcine heart model throughout the cardiac cycle . . . . .	154
5.5	Intra-operative US image acquisition for feature reconstruction . . . . .	156
5.6	Schematic representation of the generation of “pseudo” 3D US volumes . . . . .	157
5.7	“Pseudo” 3D ultrasound reconstructions from 2D tracked TEE images . . . . .	157
5.8	Pre- to intra-operative registration diagram . . . . .	158
5.9	Typical multi-modality images employed during <i>in vivo</i> model-enhanced US-assisted guidance . . . . .	160
5.10	Universal Cardiac Introducer — device used to provide access inside the beating heart . . . . .	161
5.11	Model-enhanced US guided mitral valve implantation . . . . .	163
5.12	Model-enhanced US guided ASD repair . . . . .	164
6.1	Pre-operative planning of a robot-assisted CABG procedure . . . . .	174
6.2	Peri-operative workflow during UCI-based intracardiac interventions . . . . .	178
6.3	Peri-operative setup in the operating room . . . . .	180
6.4	Peri-operative US image acquisition and post-processing . . . . .	181
6.5	Peri-operative instances of human heart imaged using tracked TEE . . . . .	182
6.6	Schematic representation of valvular geometry . . . . .	184
6.7	Porcine valvular structures at different workflow stage . . . . .	186
6.8	Porcine heart migration during UCI-based interventional workflow . . . . .	187
6.9	Human valve migration during robot-assisted CABG workflow . . . . .	189
6.10	Human heart migration during robot-assisted CABG workflow . . . . .	190

7.1	Model-enhanced US environment in the context of the reality-virtuality continuum . . . . .	195
7.2	Exploring modeling accuracy - combined . . . . .	201
7.3	Exploring registration accuracy - combined . . . . .	202
7.4	NDI Aurora MTS specifications. . . . .	203
7.5	Model-enhanced US-assisted targeting accuracy - revisited . . . . .	204
7.6	3D TEE images of the mitral apparatus . . . . .	210
7.7	Electro-anatomical modeling for atrial fibrillation therapy . . . . .	211
7.8	Preliminary <i>in vivo</i> model-enhanced US-guided catheter navigation .	212
A.1	Pre-operative planning of a robot-assisted CABG procedure . . . . .	218
A.2	Peri-operative instances of human heart imaged using tracked TEE .	219
A.3	Human heart migration during robot-assisted CABG workflow . . . . .	220
A.4	<i>In vitro</i> cardiac anatomy and image acquisition . . . . .	222
A.5	Simulating robot-assisted CABG heart migration <i>n vitro</i> . . . . .	223
A.6	Multi-feature-based registration evaluation and validation . . . . .	225

# List of Abbreviations

2D	Two-Dimensional
3D	Three-Dimensional
4D	Four-Dimensional
ANOVA	Analysis of Variance
AP	Anterior-posterior
AR	Augmented Reality
ASD	Atrial Septal Defect
AV	Augmented Virtuality
AVA	Aortic Valve Annulus
CABG	Coronary Artery Bypass Graft
CAR	Coronary Artery Revascularization
CBCT	Cone-beam CT
CPB	Cardiopulmonary Bypass
CRT	Cardiac Resynchronization Therapy
CT	Computed Tomography
DOF	Degree-of-freedom
ECG	Electrocardiogram
ED	End-diastole
ES	End-systole
FO	Fossa Ovalis
GPU	Graphics Processing Unit
HMD	Head-mounted Display
ICE	Intracardiac Echocardiography

ICP	Iterative Closest Point
IGI	Image-Guided Interventions
IGS	Image-Guided Surgery
IGSTK	Image-Guided Surgery Toolkit
IGT	Image-Guided Therapy
ITK	Insight Toolkit
LA	Left Atrium
LAA	Left Atrium and Aorta
LAD	Left Anterior Descending
LMCO	Left Main Coronary Ostium
LR	Left-right
LV	Left Ventricle
LVAp	Left Ventricular Apex
MD	Mid-diastolic
MI	Mutual Information
MITK	Medical Imaging Interaction Toolkit
MR	Mixed Reality
MR	Magnetic Resonance
MRA	Magnetic Resonance Angiography
MRI	Magnetic Resonance Imaging
MS	Mid-systole
MTS	Magnetic Tracking Systems
MV	Mitral Valve
MVA	Mitral Valve Annulus
NEX	Number of Excitations
OR	Operating Room
OTS	Optical Tracking Systems
PET	Positron Emission Tomography
RA	Right Atrium
RA	Robot-assisted

RAV	Right Atrium and Ventricle
RMS	Root Mean Squared
RV	Reality-virtuality
RV	Right Ventricle
SI	Superior-inferior
SNR	Signal-to-Noise Ratio
SPECT	Single Photon Emission Computed Tomography
TE	Echo Time
TEE	Transesophageal Echocardiography
TR	Repetition Time
TRE	Target Registration Error
TTE	Transthoracic Echocardiography
UCI	Universal Cardiac Introducer
US	Ultrasound
VR	Virtual Reality
VTK	Visualization Toolkit



# Chapter 1

## Introduction

*Virtual and augmented reality environments have been adopted in medicine as a means to enhance the clinician's view of the anatomy and facilitate the performance of minimally invasive procedures. Their true value becomes transparent during interventions where the surgeon cannot directly visualize the targets to be treated, such as during cardiac procedures performed on the beating heart. These environments must accurately represent the real surgical field and require seamless integration of pre- and intra-operative imaging, surgical tracking, and visualization technology in a common framework centered around the patient. This chapter begins with an overview of minimally invasive cardiac interventions, describes the architecture of a typical surgical guidance platform including imaging, tracking, registration and visualization, highlights both clinical and engineering accuracy limitations in cardiac image-guidance, and discusses the typically encountered challenges during the translation of the work from the laboratory into the operating room.*

---

This work is adapted from Linte CA, White J, Eagleson R, Guiraudon GM and Peters TM. Virtual and augmented medical imaging environments: Enabling technology for minimally invasive cardiac interventional guidance. *IEEE Reviews on Biomedical Engineering*. Submitted: July 2010. ©2010 IEEE. Reprinted, with permission, from IEEE.

## 1.1 Introducing Virtual, Augmented and Mixed Reality Environments

In many engineering applications, computer generated models are used to design the components of a system, simulate their interaction within a complex assembly, and analyze the behaviour of the system prior to its implementation. However, these models are rarely carried forward to the physical implementation stage, where they could assist with task performance. One approach to alleviate these limitations is to complement the user's visual field with necessary information that facilitates the performance of a particular task. This technique is known as augmented reality (AR) and it was first defined broadly by Milgram *et al.* [1], as a technique of “augmenting natural feedback to the operator with simulated cues”. In simple terms, this approach allows the integration of supplemental information with the real-world environment.

AR environments represent the “more real” subset of mixed reality environments. The latter span the entire spectrum of the reality-virtuality continuum (**Fig. 1.1**) and integrate information ranging from purely real (i.e. directly observed objects) to purely virtual (i.e. computer graphic simulations). The spatial and temporal relation between the real and virtual components distinguish AR environments from virtual reality (VR) environments. A commonly interpreted view of a VR environment is one in which the operator is immersed into a synthetic world consisting of virtual representations of the real world that may or may not be representing the properties of the real-world environment [1]. Moreover, mixed realities may include primarily real information complemented with computer-generated data, or mainly synthetic data augmented with real elements [2, 3]. While the former case constitutes a typical AR environment, the latter extends further from AR into augmented virtuality (AV) [4, 5, 6].

These visualization techniques originated in response to the industrial requirements to facilitate task performance. Initially, engineering models were displayed on computer screens and used as “guides” to perform various industrial tasks. A more revolutionary approach was undertaken by an engineering team at Boeing Industries,

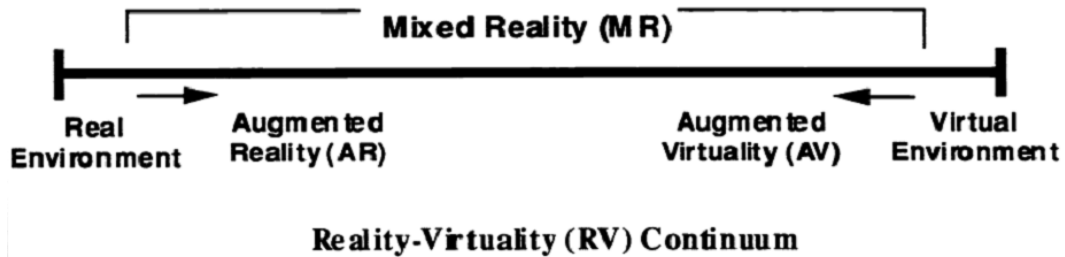


Fig. 1.1: Reality-virtuality continuum spanned by mixed reality (MR) environments ranging from purely real, to fully virtual environments. Image adapted from Milgram *et al.* 1994.

where workers were provided with a natural interface to manufacturing, construction, testing and maintenance information [7]. A see-through display, delivered via a headset worn by the worker, enabled the superposition of computer-generated information (i.e. a computer-aided design model of a device) onto the real field of view (i.e. the physical device). This approach was found to facilitate the task of, for example, identifying the location where a bolt hole was to be drilled inside an aircraft fuselage [7].

The advent of VR and AR environments in the medical world was also driven by the need to enhance or enable therapy delivery under limited visualization and restricted access conditions. Computers have become an integral part of medicine: patient records are stored electronically, computer software enables the acquisition, visualization and analysis of medical images, and computer-generated environments empower clinicians to perform procedures that were rarely successful decades ago [8]. Technological developments and advances in medical therapies have led to the increased use of less invasive treatment approaches for conditions that require a surgical procedure, but involve patient trauma and complications. Today, VR and AR medical environments are employed for diagnosis and treatment planning [9], surgical training [10, 11, 12, 13, 14], pre- and intra-operative data visualization [15, 16, 17, 18], and intra-operative surgical navigation [8, 19, 20, 21, 22].

This chapter provides an overview of the development of virtual and augmented medical imaging environments for visualization and navigation support in image-guided cardiac interventions. Following a brief introduction on mixed reality envi-

ronments, section 1.2 outlines the challenges associated with performing minimally invasive procedures on the heart. Typical pre- and intra-operative imaging modalities, image analysis, segmentation and modeling techniques, as well as data integration, visualization, and display technologies are highlighted in section 1.3. Section 1.4 focuses on surgical guidance evaluation, including both clinical and engineering accuracy assessments, as well as their incorporation in the design of image-guidance platforms. This topic is revisited in Chapter 7, with concrete examples based on the work included in this thesis. Section 1.5 lists common obstacles encountered during the translation of the work from the laboratory and into the operating room (OR) and provides several examples of pre-clinical and clinical minimally invasive cardiac applications. Lastly, several caveats associated with the equipment, logistics, and user interaction are identified in section 1.6. Lastly, section 1.7 outlines the objectives of this thesis in terms of the research questions to be addressed in the upcoming chapters, followed by a brief thesis outline included in section 1.8.

## 1.2 Minimally Invasive Procedures

A large number of conditions require physical therapeutic intervention, which often exposes the patient to additional risks arising from the approach taken to access the target tissue, as opposed to the therapy itself. Cardiac therapy may consist of the replacement or repair of a malfunctioning valve, restoration of myocardial perfusion by inserting a stent or performing a bypass graft, or electrical isolation of tissue regions that cause abnormal heart rhythm by creating scar tissue through heating or freezing.

Cardiac interventions are unique in several perspectives: access, restricted visualization and surgical instrument manipulation, as well as the dynamic nature of the heart. Procedure invasiveness extends beyond the typical measurement of the incision size. Supplying circulatory support via cardiopulmonary bypass (CPB) (i.e. heart-lung machine) represents a significant source of invasiveness that may lead to severe inflammatory response and neurological damage [23]. Moreover, despite various approaches employed to stabilize the motion of the heart at the site of interest during

surgery [24], the delivery of therapy on a soft tissue organ enclosing a blood-filled environment in continuous motion is still a significant challenge. Successful therapy requires versatile instrumentation, robust visualization, and superior surgical skills.

### 1.2.1 Cardiac interventions: A world of their own

Due to the challenges associated with visualization and access, cardiac interventions have been among the last surgical applications to embrace the movement toward minimal invasiveness [25]. This movement originated in the mid-1990s following the introduction of laparoscopic techniques and their use in video-assisted thoracic surgery [26]. The adoption of less invasive techniques posed significant problems in terms of their workflow integration and yield of clinically acceptable outcomes. However, the morbidity associated with the *surgery* rather than the *therapy*, together with the successful experience with the less invasive approaches in other surgical specialties, have fueled their emergence into cardiac therapy.

Multiple access routes, including partial sternotomies, limited access thoracotomies or catheter-based techniques have been used as an alternative to the traditional full median sternotomy [25]. Initial attempts were aimed at performing coronary artery bypass graft (CABG) surgery via minimally invasive access to the arrested heart [27, 28] without CPB [24, 29]. A number of centres reported their experience with robot-assisted atrial septal defect (ASD) and patent foramen ovale closure [30], mitral valve repair and replacement [31], transluminal [32, 33, 34] or transapical [35, 36, 37, 38, 39, 40] aortic valve implantation, or percutaneous pulmonary vein isolation for treatment of atrial fibrillation [41, 42, 43]. The increasing use of endovascular techniques constitutes one of the most rapid changes noted in cardiac interventions. As a result, vascular-guided therapy delivery has become the ultimate, least invasive cardiac therapy approach [44].

### 1.2.2 Imaging for Interventional Guidance

Medical imaging has provided a means for visualization and guidance during interventions where direct visual feedback could not be achieved without significant

trauma; such procedures are commonly referred to as image-guided interventions (IGI). In their recent review [45], Cleary and Peters provided the following statement to serve as a potential definition of IGI: “Image-guided interventions are medical procedures that use computer-based systems to provide virtual image overlays to help the physician precisely visualize and target the surgical site.” Within the IGI community, an image-guided procedure is any minimally invasive intervention that uses imaging for guidance. The typical components/stages of an IGI system/procedure workflow are outlined in **Fig. 1.2**. A detailed presentation of such techniques is available in [46].

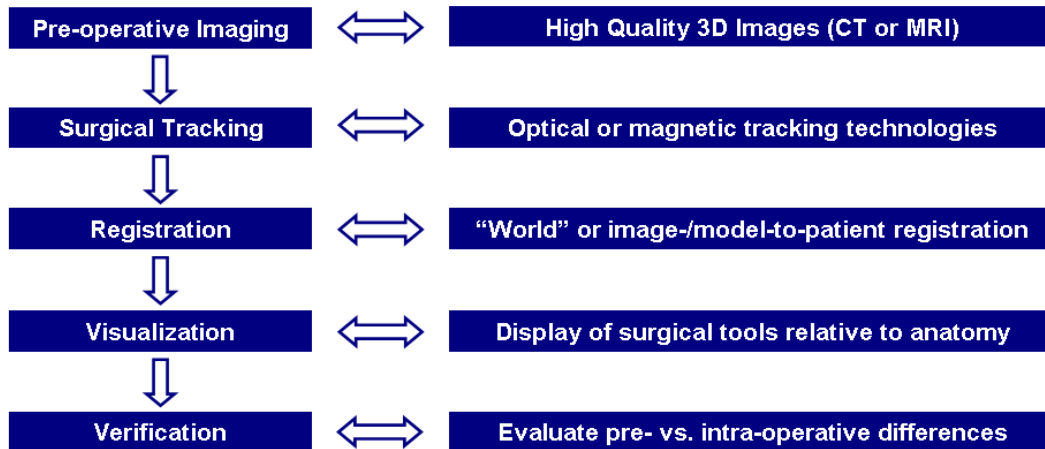


Fig. 1.2: Typical IGI workflow: pre-operative imaging and planning, surgical tracking, patient registration, surgical environment visualization and display, and verification of pre- vs. intra-operative data.

### 1.2.3 Towards Surgical Guidance Platforms

In spite of the wealth of information available to clinicians due to the advances in medical technology, a gap between diagnosis and therapy still exists. If a minimally invasive intervention is the most efficient treatment option, then pre-operative images are employed for diagnosis and treatment planning, while intra-operative imaging is used to guide the procedure. As a result, the interventionalist needs to mentally fuse the surgical plan with the real-time information, while manipulating an instrument

and monitoring therapy delivery. These challenges clearly state the need for interventional guidance platforms that enable the integration of pre- and intra-operative imaging and surgical navigation into a common environment.

## 1.3 Interventional Platform Architecture

### 1.3.1 Imaging

Medical imaging and image guidance may be employed during both on-pump, open-chest procedures, as well as off-pump, beating heart cardiac interventions. While the former may benefit from enhanced visualization available through medical imaging, the latter rely heavily on imaging, enabling clinicians to “see” inside the thoracic cavity and heart chambers in the absence of direct visual access.

#### 1.3.1.1 Pre-operative Images

Pre-operative images are necessary to understand the patient’s heart anatomy, identify a suitable treatment approach, and prepare a surgical plan. These data are often in the form of high-quality images that provide sufficient contrast between normal and abnormal tissue, along with a representation of the patient that is sufficiently accurate for image guidance [47]. Three of the most common imaging modalities employed pre-operatively are described below.

**Computed Tomography** Computed tomography (CT) is an X-ray based imaging method used to generate three-dimensional (3D) image volumes of tissue electron densities [48]. When imaging cardiac anatomy with CT, little image contrast is generally available to allow the differentiation of the structures of interest without additional contrast enhancement. However, following injection of contrast agents, superb images of the cardiac vasculature, blood pool and myocardium can be acquired, allowing high-fidelity reconstructions of the vascular tree, cardiac chambers and myocardial wall.

CT has been employed for both diagnostic imaging [49] and surgical planning [50] for patients with coronary artery disease (CAD). Pre-operative CT images are commonly used to assess patient candidacy for robot-assisted CABG procedures [51] and to identify the optimal port locations such that the surgical target can be reached with the robotic instruments [52].

Classical CT scanners, however, are of limited use intra-operatively. Physicians would need to reach with their hands into the imaging region, if the scanner were to be used for direct guidance [53]. This option is not feasible considering the increased radiation dose during prolonged procedures. In addition, since dynamic CT images are acquired in single axial slices, it is difficult to visualize a catheter that is advanced in the axial direction, as its tip is only visible in the image for a short time. Consequently, CT is more suitable for procedures where the tool is manipulated in the axial plane [54].

**Magnetic Resonance Imaging** Magnetic resonance imaging (MRI) provides excellent soft tissue characterization, allowing a clear definition of the anatomical features of interest. Most cardiac conditions can be diagnosed using MRI, and the diagnostic images are often available to the surgeon in the OR as an aid during procedure guidance.

In addition to its use in morphological imaging, MRI has been extensively employed for cardiac function assessment. Delayed contrast-enhanced MRI provides a quantitative measurement of the transmural effect of the infarct in the myocardium [55, 56, 57]. This technique has evolved into the gold-standard method for assessing myocardial tissue viability [58] for patients suffering from CAD [59, 60]. Another method widely used in characterizing the kinetic properties of the myocardium is MR tagging [61, 62], in which a spatial grid pattern of magnetization is superimposed onto the cardiac image, enabling the estimation of tissue motion during the cardiac cycle.

In interventional radiology, where catheters and probes are navigated through the vasculature and into the heart, MRI presents several advantages over the traditional X-ray fluoroscopy guidance. Not only can it spare both the patient and clinical staff



from prolonged radiation exposure, but also provides superior visualization of the vasculature, catheter, and target organ, often without the need of contrast enhancement. Several designs of intra-operative MR systems have been developed to date, including the General Electric Signa-SP “Double Doughnut” system that allows access to the patient between the two toroidal magnets [63, 64, 65], the Siemens Medical Systems *Magnetom Open* interventional magnet [66], the Philips Panorama<sup>TM</sup> system [67], and lastly the Medtronic Odin PoleStar<sup>TM</sup> N-20 system [68], which has been integrated with the StealthStation<sup>TM</sup> TREON navigation platform. Other MRI guidance systems employ modified versions of clinical MR scanners featuring shorter bores with a larger diameter, enabling the physician to reach inside the magnet and manipulate instruments [69, 70].

**Nuclear Medicine** Nuclear medicine imaging typically refers to Positron Emission Tomography (PET) and Single Photon Emission Computed Tomography (SPECT). In general, these modalities offer little anatomical or morphological information, but rather provide valuable functional information for detection and staging of a disease [71]. PET and SPECT imaging are commonly used to assess myocardial tissue viability in patients suffering from ischemic heart disease. To compensate for the lack of morphological information, nuclear images are paired with morphological images, such as CT [72, 73] or MRI [74], which provide anatomical context for their interpretation.

While the use of such images during interventional guidance is minimal, their pre-operative value is significant, as they can help the surgeon identify the target location and determine the optimal trajectory for therapy. To further exploit its usefulness, the functional information can be mapped onto anatomical models and made available to the clinician intra-operatively.

### 1.3.1.2 Intra-operative Images

Since the surgical field cannot be observed directly, intra-operative imaging is critical for visualization. The technology must operate in real time to provide accurate

guidance, be compatible with the standard OR equipment, but may compromise spatial resolution or image fidelity in favour of the above.

**X-Ray Fluoroscopy** X-ray images were the first medical images employed for guidance. Their first use was reported in Birmingham, UK within months of their discovery in 1895, to remove an industrial sewing needle from a woman’s hand [75]. Despite concerns regarding radiation exposure, X-ray fluoroscopy is the standard imaging modality employed in interventional radiology. The X-ray tube and detector are mounted on a curved arm (C-arm) facing each other, with the patient table lying between them [53] and rapidly collecting two-dimensional (2D) projection images through the body [76] at rates of over 30 Hz. Some C-arm systems are portable, allowing them to be rolled in and out of different operating rooms as needed [77].

Fluoroscopic images possess a high spatial resolution, allowing for sub-millimeter objects to be resolved. They also show clear contrast between different materials, such as a catheter and tissue or bone and liver, and different tissue densities, such as heart and lungs. However, many soft tissues, including cardiac structures, cannot be differentiated without the use of contrast agent. Since fluoroscopic images are 2D projections through 3D anatomy, they appear as a series of “overlapping shadows”. Nevertheless, projection imaging is advantageous, as no post-processing of an image volume is required, thus making it a true real-time imaging modality.

Several extensions of X-ray and fluoroscopy imaging such as CT-fluoroscopy [78, 79, 80] and cone-beam CT (CBCT) systems [81, 82, 83] have been employed for intra-operative guidance. CBCT has evolved from C-arm based angiography and can acquire high-resolution 3D images of organs in a single gantry rotation [84, 85, 86, 87].

To compensate for the lack of anatomical context and soft tissue contrast, fluoroscopic images have been combined with 3D anatomical models, allowing for a better interpretation of the position and orientation of a catheter inside the heart [88]. They also have been integrated into hybrid systems combining X-ray and MR imaging (also referred to as XMR) [89, 90]. In such systems, optical tracking technology [91] is used to determine the transformations that relate the X-ray and MRI coordinate systems [92]. When co-registered, the X-ray and MR images provide both enhanced real-time

navigation information, as well as real-time monitoring of therapy delivery. However, there are several drawbacks associated with the use of XMR suites, including high operation and maintenance costs, as well as incompatibilities with the interventional workflow and OR equipment.

**Ultrasound** Ultrasound (US) has been employed in interventional guidance since the early 1990s [93], initially for neurosurgical procedures. US can acquire real-time images at various user-controlled positions and orientations, with a spatial resolution ranging from 0.2 to 2 mm. Moreover, US systems are inexpensive, mobile, and compatible with the OR equipment.

It is generally agreed that the quality of US images is inferior to that of CT or MR images [66]. The presence of multiple speckle reflections, shadowing, and variable contrast are some of the disadvantages that have contributed to the slow progress of employing US imaging intra-operatively. Several approaches to enhance anatomical visualization have included the acquisition of 2D US image series to generate volumetric datasets [94, 95], optical or magnetic tracking of the 2D US transducer to reconstruct 3D images [96, 97, 98], and fusion of US and pre-operative CT or MRI images [99, 100, 101].

Several US transducers have been employed for cardiac applications. Until recently, when their use for interventional guidance has emerged [102, 103], trans-thoracic echocardiography (TTE) probes were mainly used for diagnosis and intra-operative patient monitoring. However, during an intervention, the surgeon needs to manipulate the instruments at the same time as the US transducer, leading to a cumbersome workflow. As an alternative, trans-esophageal echocardiography (TEE) probes [104] have been widely employed, enabling cardiac image acquisition from the esophagus with remote probe manipulation. Similarly, for intracardiac tissue ablation procedures, intracardiac echocardiography (ICE) probes have also been used [100]. However, given the proximity of the transducer to the imaged tissue, ICE images have a limited field of view and are difficult to interpret without additional anatomical context.

Magnetically tracked 2D TEE has also been employed for intra-procedure guidance

[105]. This technology, as described in the upcoming chapters, is a fundamental feature of the surgical guidance environment proposed in this thesis. The position and orientation of the US transducer is recorded, enabling visualization of the acquired images relative to the tracked surgical instruments. Moreover, recent developments in US technology have led to the launching of 3D TEE transducers. However, the field of view is small, restricting the visualization of both surgical tools and targets in the same volume during guidance. To ameliorate these disadvantage, Gao *et al.* [106] have proposed a rapid registration technique of 3D TEE data to X-ray fluoroscopy images for guidance of cardiac procedures.

### 1.3.2 Segmentation and Anatomical Modeling

Although image-guided surgery (IGS) typically employs medical imaging for guidance, the image datasets can be quite large, making them difficult to manipulate in real time. A common approach is to extract the information of interest and generate models that can be used to plan the procedures and provide visualization during guidance. Anatomical models consisting primarily of a surface of the organ of interest extracted from the volume using image segmentation are commonly employed in IGS. A large and continuously growing body of literature is dedicated to image segmentation, ranging from low-level techniques such as thresholding, region growing, clustering methods, and morphology-based segmentation to more complex, model-based techniques. A review of these methods can be found in [107].

Anatomical models employed for cardiac guidance are usually obtained from pre-operative MRI or contrast-enhanced CT datasets. While manual segmentation has been accepted as the gold-standard approach for segmentation, given the superior soft tissue contrast available in the MR and CT images, various semi- or fully automatic techniques available in open-source packages, such as *ITK-SNAP* (<http://www.itksnap.org/>), can also be employed. Moreover, several model-based techniques, including classical deformable models [108, 109], level sets [110], active shape and appearance models [111, 112], and atlas-based approaches [113, 114] have also been explored. Provided a sufficiently large database is available, a statistical

shape atlas can be generated and fitted to a new subject’s clinical image using non-rigid registration [115]. These modeling techniques were initially developed to enable the quantification of left ventricular ejection fraction for diagnostic purposes, and were shown to yield results more rapidly than manual segmentation, while maintaining anatomical accuracy [115]. Subsequently, similar methods were used [116] to build subject specific heart models to be employed during procedure guidance. In Chapter 4, a method for generating pre-operative, subject-specific heart models capable of predicting the dynamic location of the mitral valve annulus is presented, for use in the guidance of minimally invasive mitral valve interventions.

Surface extraction [117] is a trade-off between the fidelity of the surface and the amount of polygonal data used to represent the organ model: the denser the surface mesh, the better the surface features are preserved, but at the expense of manipulation times. These limitations are addressed via decimation — an algorithm that identifies surface regions with low curvature and replaces several small polygons with a larger one [118]. This post-processing step reduces the amount of polygonal data, while preserving the desired surface features.

Anatomical models are often augmented with functional information. For example, electro-physiological information can be mapped onto a surface model of the heart [119] or a contraction force distribution can be superimposed onto a left ventricular model [120]. The former can be used to identify arrhythmia-related sites, while the latter could depict regions of low myocardial contractility. Other groups have employed similar modeling techniques to assess cardiac function under different conditions. Pop *et al.* [121] conducted a combined theoretical and experimental study to characterize post-infarct scars in porcine heart models, Sermesant *et al.* [122] developed an electromechanical heart model to predict the effects of cardiac resynchronization therapy (CRT), and Fleureau *et al.* [123] constructed a hybrid model of the left ventricle to assess regional cardiac function in patients with heart failure.

The advances in computing technology and the advantage of the power of the graphics processing unit (GPU) have allowed for the construction of four-dimensional (4D) (i.e. 3D + time) heart models using volume rendering of pre-operative MRI and CT datasets [124]. These techniques allow the user to appreciate the full 3D attributes

of the pre-operative images, while maintaining all the original data, rather than discarding most of it during surface extraction using classical segmentation methods.

### 1.3.3 Surgical Instrument Localization and Tracking

Most interventions require precise knowledge of the position and orientation of the surgical instrument with respect to the target at all times during the procedure, making the localization system an essential component of any image-guided intervention platform. Prior to the development of real-time tracking systems, stereotactic frames were employed in neurosurgery to provide a direct spatial relationship between the physical patient, the pre-operative images, and the surgical instruments mounted and guided in the same coordinate system [125, 77]. As computers became more powerful, new instrument localization techniques were developed. In the early stages, mechanical tracking devices consisting of multi-arm systems whose kinematics could be determined and used to infer the position and orientation of the probe [126] were employed. However, their use diminished, as they were bulky and intrusive to the clinical workflow. In the early 1990s, several groups [127, 128] proposed the use of sonic triangulation systems for instrument tracking. These systems suffered from speed of sound fluctuations induced by humidity and temperature variations in the environment, as well as limitations related to the optimal distance between the transmitter and the receiver, which allowed measurable differences in the time-of-flight to enable accurate tracking [129].

The tracking technologies most frequently employed in IGI use either optical [91] or magnetic [130, 131, 132] approaches (**Fig. 1.3**). Common optical tracking systems (OTS) include the Micron Tracker (Claron Technologies, Toronto, Canada), the Optotrak 3020 (Northern Digital Inc, Waterloo, Canada) [133, 134], the Flashpoint 5000 (Boulder Innovation Group Inc., Boulder, Colorado) [135, 136, 137], and the Polaris (Northern Digital Inc.) [138, 139]. In spite of their tracking accuracy on the order of 0.5 mm [91], they require an unobstructed line-of-sight between the transmitting device and the sensors mounted on the instrument, which prevents their use for within-body applications. As such, their application is limited to procedures per-

formed outside the body, or interventions where the rigid delivery instruments extend outside the heart or thoracic cavity.

Magnetic tracking systems (MTS), on the other hand, do not suffer from such limitations and allow the tracking of flexible instruments inside the body, such as a catheter tip [140], endoscope [131, 141] or TEE transducer [105]. However, their performance may be limited by the presence of ferromagnetic materials in the vicinity of the field generator, or inadequate placement of the “surgical field” within the tracking volume of the MTS. Three magnetic tracking systems typically used in IGI include the NDI Aurora<sup>TM</sup> (Northern Digital Inc.), the 3D Guidance system from Ascension (Burlington, VT), and the transponder-based system developed by Calypso Medical Systems (Seattle, WA). As mentioned earlier, magnetic tracking technologies have been employed extensively in the work presented in this thesis, to track both rigid (e.g. pointers, valve-guiding tools or fastening devices), as well as flexible instruments, including catheters or TEE transducers.



Fig. 1.3: Commonly employed optical a) Polaris Spectra<sup>TM</sup> from NDI and b) Micron Tracker<sup>TM</sup> from Claron Technologies (Toronto, Canada), and magnetic tracking systems: c) Aurora<sup>TM</sup> from NDI and d) 3D Guidance<sup>TM</sup> from Ascension. *Images courtesy of Northern Digital Inc., Claron Technologies, and Ascension.*

In addition to optical and magnetic tracking, image-based tracking can also be employed. Novotny *et al.* [142] proposed a detection technique to identify the position of surgical instruments using 3D real-time US imaging. Their algorithm searches the US image volume for long, straight objects to identify the axis of the instruments, and determines their position and orientation based on passive markers attached to the instrument shaft. This technique was implemented on the GPU for rapid execution and enabled nearly real-time instrument tracking at a 3D US image frame rate of 26 Hz. *In vitro* experiments revealed a 1.8 mm and 1.1° accuracy in translation and orientation, respectively. Moreover, subsequent *in vivo* studies demonstrated successful tracking inside a beating swine heart [103].

### 1.3.4 Data Integration

Image registration is the enabling technology for the development of surgical navigation environments. It plays a key role in establishing the relationship between the virtual environment (pre- and intra-operative images and surgical tool representations), and the physical patient [143]. Initially, registration was defined as the process of aligning images such that corresponding features can be easily analyzed [144]. However, over time, the meaning of the term has expanded to include the alignment of images, features or models with other features or models, as well as with corresponding features in the physical space. The latter is known as “world” or subject/patient registration and it determines the relationship between the virtual environment and the subject.

#### 1.3.4.1 Landmark-based Registration

Registration techniques vary from fully manual to completely automatic. A common manual approach is via landmark-based registration, that consists of the selection of homologous landmarks in multiple datasets. This rigid approach is employed to perform the world registration *in vitro*, for studies aimed at evaluating the navigation accuracy of newly-developed guidance environments [145, 146]. Landmarks identified in the pre-procedural CT image of a phantom are matched to their physical coun-



terparts using a tracked pointer. However, considering that such rigid landmarks are very difficult to identify in a pre-operative heart image and also within the patient’s heart during the intervention, other registration methods may be preferred.

#### 1.3.4.2 Geometry and Intensity-based Registration

Automatic registration methods require little or no input from the user and are generally classified into intensity- and geometry-based techniques. Intensity-based methods determine the optimal alignment using different similarity relationships [147, 148] among voxels of the multiple image datasets. Examples are the algorithms developed by Huang *et al.* [101, 149], which use normalized mutual information to register intra-operative 2D or 3D US images to 3D CT or MR images of the heart acquired pre-operatively.

Geometry-based techniques provide a registration using homologous features or surfaces defined in multiple datasets. One of the first algorithms was introduced by Pelizzari *et al.* [150] and is known as the “head-and-hat” technique. In many ways this algorithm is a precursor of what is now commonly known as the iterative closest point (ICP) method introduced independently under its current name by Besl and McKay [151]. Several variations of this technique are often employed in cardiac applications. Ma *et al.* [152] have proposed a method that uses the epicardial surface of the left ventricle and centerline of the ascending aorta to register intra-operative 3D US datasets to the corresponding pre-operative 3D MR datasets.

In Chapter 4 another feature-based registration approach is proposed that employs the mitral and aortic valve annuli, identified both pre- and intra-operatively from MR datasets and magnetically tracked 2D TEE, respectively, to register pre-operative cardiac models to the intra-operative environment for valvular interventional guidance [153]. An extension of this algorithm has been recently employed to study the peri-operative migration of the heart during robot-assisted CABG procedure workflow [154] and to predict the intra-operative location of the target vessel during the same procedures [155], as described in Chapter 6 and Appendix A, respectively.

### 1.3.4.3 Deformable Registration

Due to the soft tissue nature of the heart, deformable registration techniques have been employed extensively for cardiac image registration. Wierzbicki *et al.* [116] used a non-rigid, free-form deformation approach to extract the motion between successive 3D image volumes of the heart acquired throughout the cardiac cycle using electrocardiogram (ECG) gating. Similar techniques were employed to construct statistical-shape atlases of the heart by co-registering multiple patient MR images to a high-resolution cardiac MR dataset [156, 111]. Such atlases can be further used to generate subject-specific models of future subjects' hearts via registration-based segmentation [157, 158].

While these techniques provide robust frameworks for accurate registration of cardiac images, deformable registration algorithms may be computationally expensive and hence inefficient for use during time-critical interventional procedures [47]. Similar issues were raised by Dr. Russell Taylor from Johns Hopkins University at the *Workshop on Image-guided Interventions and Robotics* at the 12th annual *Medical Image Computing and Computer-Assisted Interventions* conference (London, UK, 2009). Similar observations were reiterated by Yaniv *et al.* [147] when establishing the criteria for registration evaluation for interventional guidance, which include performance time, alignment accuracy, robustness, user interaction, and reliability [147]. A thorough description of image registration for interventional guidance is provided in chapters 6 [147] and 7 [159] of the book by Peters and Cleary [160], and additional references are available in Hajnal *et al.* [161].

## 1.3.5 Visualization and Display

### 1.3.5.1 Visualization Platforms

Visualization is an important component of any surgical guidance platform. Whatever the adopted approach may be, it must present the surgical scene in a three-dimensional fashion and provide a high fidelity representation of the surgical field. For most closed-chest cardiac interventions, this information cannot be accessed via

direct vision by the clinician.

Different research groups have employed various custom-developed environments that best suited their applications [162] and were iteratively optimized to address subsequent challenges identified during their use [163]. Among the visualization packages reported in the literature, *Analyze<sup>TM</sup>*, *3D-Slicer*, and *Image-Guided Surgery Toolkit (IGSTK)* are examples of some which have benefited from extensive support over the past decade.

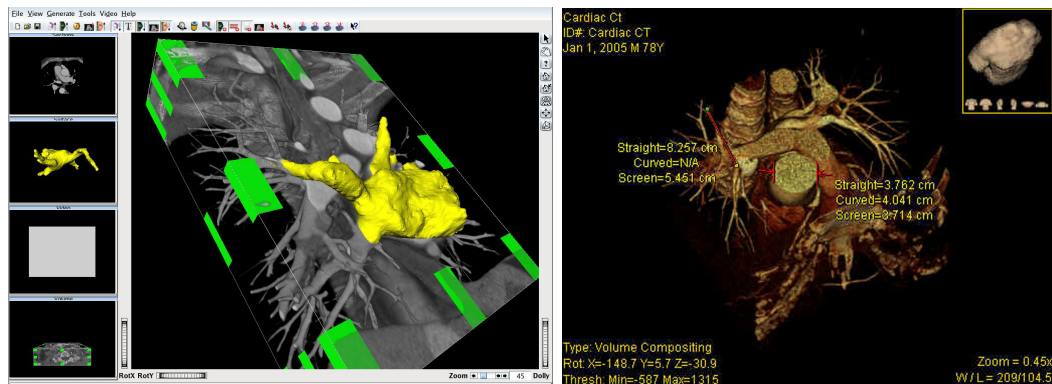


Fig. 1.4: Surface-rendered model of the left atrium and volume-rendered peripheral vasculature obtained from a clinical MRI dataset (left panel), employed here to obtain measurements of the aorta from a volume-rendered image dataset (right panel). *Image courtesy of David R. Holmes III, Mayo Clinic and Graduate School, Rochester, MN.*

*Analyze<sup>TM</sup>* (Biomedical Imaging Resource, Mayo Clinic, Rochester, USA) [164] has grown into one of the longest surviving visualization packages capable of bringing together a wide variety of tools for generalized manipulation, measurement and visualization of multi-dimensional medical images within an interactive and user-friendly environment (**Fig. 1.4**).

The *3D-Slicer* package (Brigham and Women’s Hospital, Harvard University, Boston, USA) [165] makes extensive use of open-source libraries such as the *Visualization Toolkit (VTK)* [166] and the *Insight Toolkit* [167]. By embracing the open-source philosophy and receiving support from the image guidance community, this package has found applications in many laboratories around the world.

The *IGSTK* platform (Georgetown University, Washington, DC) [168] was developed for image-guided interventions and contains basic components to build specific

applications [169] (**Fig. 1.5**). It also supports several tracking systems, including models from NDI, Ascension, Claron, and Atracsys (Renens, Switzerland).

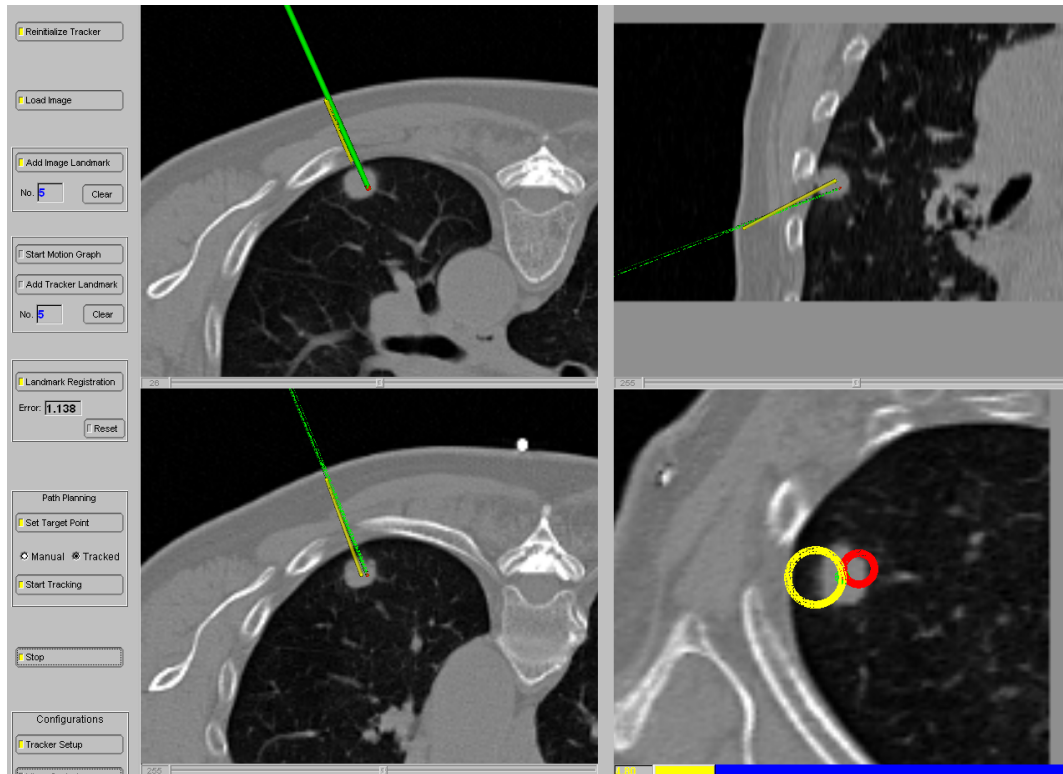


Fig. 1.5: IGSTK-based navigation graphical user interface employed during a clinical lung biopsy procedure. *Image courtesy of Ziv Yaniv, PhD, Georgetown University, Washington DC.*

Other examples include the *Medical Imaging Interaction Toolkit (MITK)* (German Cancer Research Center, Heidelberg), and the *AtamaiViewer* (Robarts Research Institute, London, Canada). The *MITK* is another open-source platform free for development of interactive medical image-processing software. Its newly released image-guided therapy module (*MITK-IGT*) supports various tracking systems and enables the development of image-guided applications [170]. The *AtamaiViewer* comprises a user interface based on Python and VTK and integrates a wide variety of components for image-guided applications, including multi-modality image visualization, anatomical modeling, and surgical tracking [171]. A more detailed description of the various functionalities of the *AtamaiViewer* is provided in Chapter 2, together

with the primary application implemented within the platform — the model-enhanced US-assisted surgical guidance environment.

### 1.3.5.2 Display Technology

In addition to robust visualization, choosing the most appropriate information display technology is another key aspect of an image guidance platform. Although we live in a technology-driven era, it could become overwhelming for surgeons to visualize, analyze, interpret, and fuse all the information available during procedures to allow optimal therapy delivery. VR and AR environments have provided solutions for enhanced visualization, ranging from fully immersive environments that do not provide the user with any real display of the surgical field, to environments that combine computer graphics with a direct or video view of the real surgical scene. The first head-mounted display (HMD)-based AR system was introduced by Sutherland *et al.* in 1968 and combined real and virtual images by means of a semi-transparent mirror. Operating binoculars and microscopes were also augmented using a similar approach, as described by Kelly *et al.* [172] and Edwards *et al.* [173] for applications in neurosurgery, and further improved and exploited by Birkfellner and colleagues [174, 175] for maxillofacial surgery.

Distinct from the user-worn devices, AR window-based displays allow augmentation without using a tracking system. This technology emerged in 1995 with the device introduced by Masutani *et al.* [176]. The proposed system consisted of a transparent mirror placed between the user and the object to be augmented. Another example was the tomographic overlay described in [177, 178], which made use of a semi-transparent mirror to provide a direct view of the patient together with a CT slice correctly positioned within the patient’s anatomy. A comprehensive review of medical AR displays is provided by Sauer *et al.* [179] and Sielhorst *et al.* [180].

Despite these advances, cardiac interventional guidance is still hampered from a visualization perspective, as it uses traditional OR displays to make imaging information available to the physician. Besides the minimally invasive, robot-assisted procedures performed using the da Vinci<sup>TM</sup> surgical system, which provides the sur-

geon with a real-time stereoscopic view of the surgical field, most ORs still employ standard overhead monitors for information display. These devices are 2D displays and cannot efficiently represent 3D data.

Lo *et al.* [181] explored several avenues toward optimizing the display delivery of a VR-enhanced US navigation environment *in vitro*, using phantom experiments, and *in vivo*, during pre-clinical swine studies. These options included a simple computer monitor display, standard OR overhead monitors accessible to each member of the clinical team, HMDs worn by the surgeons, which provided a fully immersed representation of the navigation environment, and a dual-projector stereoscopic display. Three different display paradigms were also tested: a simple user-operated display that integrated two fixed orthogonal views of the surgical scene; an interactive stereoscopic display offering views of the surgical environment updated in real-time by optically tracking the HMDs; and a dynamic, user-controlled display that allowed the operator to adjust the camera angle as needed during navigation [181]. Most users, including collaborating surgeons, were comfortable using overhead monitors, but found the HMDs more intuitive, despite their progressive discomfort experienced with prolonged use.

A similar stereoscopic visualization paradigm was explored by del Nido’s group [182] at Harvard working on US-guided intracardiac interventions on the beating heart. Their study investigated the feasibility of two display systems for intracardiac navigation of a catheter-based ASD patch delivery in swine models: a stereoscopic 3D echocardiography display and a standard 3D US view. The former technology led to shorter procedure times and increased navigation precision, suggesting that stereoscopic displays have the potential to improve safety of intracardiac, beating-heart interventions.

## 1.4 Accuracy Considerations

From a clinical perspective, the success of an intervention is assessed according to the therapeutic outcome. From an engineering view point, navigation accuracy is constrained by the limitations of the IGI system. The overall targeting error within

an IGI framework is dependent on the uncertainties associated with each of the components [183]. Jannin *et al.* [184] emphasized that a proper IGI system validation should estimate the errors at each stage in the image-guided therapy process, and study their propagation through the entire workflow. Following these suggestions, the accuracy challenge can be posed as a series of questions: What is the tolerable clinical error associated with the procedure? How accurate is the pre-operative modeling and planning? How accurate is the image-/model-to-patient registration? How accurate is the surgical tracking system? What is the overall targeting accuracy of the IGI system?

### 1.4.1 Clinical Accuracy Constraints

While a proper formulation is currently lacking, clinical accuracy may be defined as the maximum error that can be tolerated during an intervention without compromising therapy outcome or leading to increased risk to the patient. Such tolerances are difficult to define, as they are procedure and patient specific. Moreover, *in vivo* experiments with properly controlled variables are required to arrive at a robust measure of the clinically-imposed accuracy. This is, however, a very challenging task for most *in vivo* interventions. Instead, researchers often follow the “ad-hoc” approach and state that “according to the expertise of our collaborating clinicians, an overall accuracy on the order of 5 mm or less is considered acceptable for the application [152, 153].” While this may be an adequate “rule of thumb” for some applications, it may lead to significant over- or under-constraints for others.

Once the clinical accuracy constraints are identified, the next step is to evaluate the engineering constraints imposed by the limitations of the system, hoping that the technology meets the clinical requirements.

### 1.4.2 Engineering Accuracy Considerations

The translation of clinical accuracy expectations into engineering accuracy constraints is intuitive in some cases. In other situations, however, it may be difficult to identify exactly when the limitations of the image-guidance platform start to affect

clinical performance. For percutaneous aortic valve implantation, for example, it is difficult to estimate exactly how accurately the coronary ostia need to be localized to allow optimal stent placement. Nevertheless, the accuracy requirement will dictate the engineering approach used — magnetic TEE tracking may be sufficient for ostia localization within 5 mm, but not within 1 mm. In these cases, simulation experiments can be employed to estimate accuracy needs.

According to Jannin’s recommendations [184], the overall system accuracy depends on the limitations of its integrated components. Therefore, it is helpful to consider a typical image guidance environment as consisting of several stages — modeling, registration, surgical tracking, and overall targeting — and assess their individual accuracy constraints. An overview of the accuracy considerations associated with the model-enhanced US-assisted surgical guidance environment, together with several observations related to monitoring, improving and providing accuracy feedback to the surgeon, will be provided in Chapter 7.

## 1.5 From the Laboratory into the Operating Room

### 1.5.1 Logistics

Before being introduced into the OR, new image-guidance platforms must be exhaustively assessed in terms of both their visualization and navigation capabilities. Image processing algorithms employed for segmentation, registration or modeling can be evaluated using non-invasively acquired clinical images of either healthy volunteers or patients [115, 158, 185]. However, the assessment of invasive components, such as tool-to-target navigation, must be evaluated using *in vitro* clinically-relevant settings. For a true accuracy assessment, the experimental design must ensure proper control of all variables, repeatability of the experimental protocol, as well as precise knowledge of both the surgical tool and target locations. While an *in vivo*, beating heart assessment is preferred, this would entail invasive implantation of tracked targets inside the *in vivo* porcine myocardium, closing of the thoracic cavity, pre-operative image acquisition, and ultimately intra-operative navigation. As an alternative, sev-



eral groups have resorted to the use of representative phantoms for *in vitro* simulation and evaluation.

#### 1.5.1.1 *In vitro* Evaluation

Nadkarni *et al.* [186] used 3D dynamic phantoms of the deforming patient myocardia to quantify temporal jitter artifacts in ECG-gated dynamic echocardiography, as well as phantoms mimicking the pulsatile flow for assessment of novel 2D and 3D intravascular ultrasound imaging techniques [187].

Holmes *et al.* [188] developed an approach to build realistic patient-specific anatomic models, so that the guidance procedure could be validated *in vitro* without introducing unnecessary risks to patient or animal models. Starting with a pre-procedural cardiac CT scan, they segmented the blood pool of the left and right atria, converted them into polygonalized models, and used them to build thin-walled patient-specific blood-pool models in a stereo-lithography system. These models were then embedded in a platinum silicone material with similar echogenicity as human tissue, resulting in phantoms mimicking patient-specific cardiac anatomy with sufficient fidelity.

As a next step toward clinical application, Suematsu *et al.* [189] used *ex vivo* porcine hearts to evaluate the feasibility of real-time 3D echocardiography-guided ASD repair procedures. Similarly, we have documented several qualitative assessments of our model-enhanced US-assisted guidance environment *in vitro* using both a cardiac intervention phantom [190, 104], as well as *ex vivo* porcine hearts, as described in Chapter 2. In addition, a thorough quantitative assessment of the targeting accuracy under model-enhanced US guidance was performed *in vitro* using a beating heart phantom [146] as presented in Chapter 3.

#### 1.5.1.2 Initiating Clinical Translation

The initial clinical translation usually consists of *in vivo* evaluation using animal models. This stage helps identify challenges specific to the operating room that had not posed major concerns in the laboratory environment. While all system compo-

nents need to be seamlessly integrated within the IGI platform, it is easy to overlook the fact that they all need to physically fit inside the OR together with the rest of the equipment and without obstructing the workflow. The invasion of technology into the clinical environment is often referred to as the “technology foot-print” and the key objective is to reduce its impact and ensure a smooth transition.

This concept also applies to the various algorithms employed. Although non-rigid registration techniques are thought to be more reliable for *in vivo* soft tissue applications, they are computationally prohibitive for use during surgical procedures [47]. The choice of the appropriate image- or model-to-patient registration technique for intra-operative use is often the best compromise of accuracy for OR feasibility. Achieving adequate anatomical alignment in the region of interest is sufficient to provide context for tool-to-target navigation, and further rely on real-time intra-operative imaging for on-target positioning [140].

Surgical instrument localization is indispensable in image-guided environments. However, while optical tracking systems pose problems due to the interruptions of the line-of-sight between the emitters and the tracked tools, magnetic tracking systems are often affected by large equipment present in the OR. Although a “magnetically clean” environment can be ensured in the laboratory, the presence of ferromagnetic objects in the OR can compromise the accuracy of MTS in clinical practice. Other considerations involve the placement of the field generator such that it does not interfere with the access to the surgical field, but yet is properly positioned to ensure the subject’s heart is located within the optimal tracking volume. For a suitable setup, the field generator can be either inserted within the mattress of the OR table [191] or placed underneath the table [154], as later reiterated in Chapter 7.

### 1.5.2 Psycho-physical Effects: Visualization and Perception

The fundamental objective of surgical platforms is to provide the surgeon with a more intuitive relationship between the medical imaging data, the surgical field, and the patient. Given the integration of several data sources, these environments may result in comprehensive displays that have the tendency to overload the cognitive

channels of the user and consequently hinder the interpretation of the images. Here we identify several factors to be considered when developing new surgical visualization and navigation paradigms: image fusion, 3D data visualization and interaction, and navigation and hand-eye coordination.

### 1.5.2.1 Image Fusion

Image fusion is the integration of multi-modality images registered to one another within a common coordinate space for simultaneous visualization. Intra-operative imaging modalities such as fluoroscopy or US provide real-time information, but to be meaningful, they often need to be registered to high quality pre-operative images to be interpreted in the appropriate context. These displays may also superimpose diagnostic information into the guidance environment, such as the electro-anatomical models generated within CartoMerge<sup>TM</sup> [100]. Instead of looking at several displays, each corresponding to individual imaging devices, a unified display integrating all the required data may streamline the surgical workflow.

### 1.5.2.2 3D Data Visualization and Interaction

Real surgical fields are 3D scenes, and the visualization environments employed in lieu of direct vision must portray these scenes accordingly to ensure proper perception of the correct spatial relationship between different structures [192]. It is a common challenge to provide the user with the correct depth perception, especially when structures are located within other structures. Such examples include the visualization of an arrhythmia-inducing site requiring ablation located on the endocardial surface of the left atrium, or a coronary vessel requiring grafting embedded within the epicardial surface of the heart. When augmenting stereoscopic video images with 3D computer graphics representations of *underlying structures*, the latter often appear *above the surface represented by the video*, misleading the user. To address this issues, Lerotic *et al.* [193] proposed a novel *pq*-space based non-photorealistic rendering technique to provide see-through vision of the embedded virtual object, while preserving the details of the exposed anatomical surface. As an alternative, the video can be “clipped”

to generate a keyhole that enables visualization of the underlying structure, similar to the work proposed by Kutter *et al.* [194] for volume-rendered displays.

### 1.5.2.3 Navigation and Hand-eye Coordination

The desired consequence of 3D data visualization is improved hand-eye coordination. In conventional cardiac procedures, where a direct view of the surgical field is available, the surgeon manipulates the instruments in a coordinate system fixed with respect to the patient. However, during minimally invasive procedures the surgeon uses the virtual surgical display for navigation, where the image is displayed in a coordinate system not intuitively related to the patient, or is oriented differently relative to the direct patient view. When studying the effect of display location on task performance, Hanna *et al.* [195] concluded that the optimal position and orientation of the display was in front of the operator, above the surgical field and at hand level, ensuring direct correspondence between the real body axes of the patient and those of the virtual surgical field. Some hardware displays that suit these requirements and have the potential to provide improved hand-eye coordination during minimally invasive procedures include semi-transparent screens positioned above the patient [177, 196] or HMDs [197, 198] worn by surgeons.

## 1.5.3 Pre-clinical and Clinical Applications

Although the concepts of virtual and augmented medical imaging environments have been around for quite some time, their application in interventional cardiac guidance has expanded over the past years, leading to several pre-clinical and clinical successes in terms of surgical guidance platforms.

### 1.5.3.1 Transapical Aortic Valve Implantation

Transapical aortic valve implantations have received significant attention over the past few years, and such procedures have been proved successful under real-time MR imaging, as well as real-time cone-beam CT and US imaging.

**Real-time MRI Guidance:** McVeigh *et al.* [199] have described an effective interventional navigation platform for planning and guiding transapical aortic valve implantations. Their system employs real-time MRI guidance using a closed-bore system with shorter depth and a wider opening (**Fig. 1.6**). This interventional platform provides continuously updated images of the heart with superior soft tissue contrast and enables real-time monitoring of therapy delivery using high-quality images [200]. To date, the system has also been employed in a number of other pre-clinical studies in swine models, including intra-myocardial injection of stem cells [201], endovascular repair of abdominal aortic aneurysms [202], atrial-septal puncture and balloon septostomy [203], as well as catheterization procedures in humans [204].



Fig. 1.6: Interventional cardiac MRI suite employing a modified clinical scanner with a shorter bore and a wider opening. *Image courtesy of Elliott McVeigh, PhD, Johns Hopkins University, Baltimore, MD.*

**Real-time Fluoroscopy-TEE Guidance:** Walther *et al.* [205] have reported the use of real-time fluoroscopy guidance combined with echocardiography to guide the implantation of aortic valves via the left ventricular apex during rapid ventricular pacing. The guidance environment integrates both a planning and a guidance module. The pre-operative planning is conducted based on DynaCT<sup>TM</sup> Axiom Artis (Siemens Inc., Erlangen, Germany) images and interactive anatomical landmark selection to determine the size and optimal position of the prosthesis. The intra-operative fluoroscopy guidance allows tracking of the prosthesis and coronary ostia, while TEE enables real-time assessment of valve positioning [206]. The main benefit of these contemporary cone-beam CT imaging systems is their ability to provide 3D organ reconstructions during the procedure. Because the fluoroscopy and CT images are intrinsically registered, no further registration is required to overlay the model of the aortic root reconstructed intra-operatively with the real-time fluoroscopy images [207]. Moreover, since this therapy approach makes use of imaging modalities already employed in the OR, it has the potential to be adopted as a clinical standard of care for such interventions.

### 1.5.3.2 Ultrasound-guided Robotic Intracardiac Surgery

Real-time 3D US imaging has not only enabled the performance of new surgical procedures [102], but also made possible real-time therapy evaluation on the beating heart. However, the rapid cardiac motion introduces serious challenges to the surgeons, especially for procedures which require the manipulation of moving intracardiac structures. Howe *et al.* [208] have proposed the use of a 3D US-based robotic motion compensation system to synchronize instrument with the motion of the heart. The system consists of a real-time 3D US tissue tracker that is integrated with a 1 DOF actuated surgical instrument and a real-time 3D US instrument tracker. The device first identifies the position of the instrument and target tissue, then drives the robot such that the instrument matches the target motion.

For mitral valve repair procedures, the motion compensation system was simplified according to the clinical observation that the mitral annulus follows mainly a one-

dimensional translation along the left atrium - left ventricle axis. Two instruments were introduced through the wall of the left atrium: the first deployed an annuloplasty ring with a shape-memory-alloy frame, while the second applied anchors to attach the ring to the valve annulus. This approach allows the surgeon to operate on a “virtually motionless” heart when placing the annuloplasty ring and anchors. Initial studies have demonstrated the potential of such motion-compensation techniques to increase the success rate of surgical anchor implantation. Moreover, in a recent study [209], the group has also reported sub-millimeter accuracy in tracking the mitral valve using a similar motion-compensation approach for catheter servoing.

### 1.5.3.3 Model-enhanced Ultrasound-Assisted Guidance

The development of model-enhanced US assisted guidance draws its origins from the principle that therapeutic interventions consist of two processes: navigation, during which the surgical instrument is brought close to the target, and positioning, when the actual therapy is delivered, by accurately placing the tool on target. The integration of pre- and intra-operative imaging and surgical tracking enables the implementation of the navigation-positioning paradigm formulated in this work and further explored in the chapters to follow. As presented in Chapter 2, the pre-operative anatomical models act as guides to facilitate tool-to-target navigation, while the US images provide real-time guidance for on-target tool positioning. This platform has been employed pre-clinically to guide several *in vivo* interventions in swine models [191], including mitral valve implantation and ASD repair, on the beating heart under direct intracardiac access achieved using the Universal Cardiac Introducer [210]. The implementation of the model-enhanced US guidance technology into the pre-clinical setting is described in Chapter 5.

### 1.5.3.4 Electro-physiology and Ablation Therapy Guidance

One of the systems available on the market designed to provide guidance support for minimally invasive cardiac ablation therapy is the Carto<sup>TM</sup> package (Biosense Webster, Haifa). Traditionally, guidance for these procedures has been provided using

bi-plane fluoroscopy images, but these cannot show the soft tissue in a meaningful way. The physician is required to mentally fuse the navigation data with the electrical signals collected by the reference electrodes and deduce the location of the catheter in the heart during navigation.

To overcome some of these limitations, the Carto<sup>TM</sup> system tracks the catheter using a magnetic sensor, enabling the acquisition of electrical signals from the endocardial surface of the heart together with their 3D spatial location. These data allow the construction of patient-specific electro-anatomical models. Although the reconstructed anatomy was initially rather coarse, it still provided the clinician with intuitive navigation information and real-time feedback on therapy progress [211].

Subsequently, the system was modified to enable the use of more realistic models. Patient-specific left atrial anatomy was extracted from high-quality pre-operative MR or CT images. These models were then integrated into the patient coordinate system by registering them to the endocardial surface points recorded using the tracked catheter. This technology was developed by Siemens Corporate Research [100] in collaboration with Biosense-Webster and later commercialized as the CartoMerge<sup>TM</sup> platform.

### 1.5.3.5 Assessing and Restoring Cardiac Function

**Myocardial Scar Imaging:** Coronary artery revascularization (CAR) and CRT may improve systolic performance, survival, and quality of life in patients with left ventricular dysfunction. However, it has been shown that the presence and extent of myocardial scar [121] within the relevant vascular targets may negate clinical response to these interventions [212, 213, 214, 215]. 3D vascular imaging techniques, such as coronary CT or MR angiography, have been used to characterize vascular targets [216, 217] and to plan both CAR and CRT interventions [218, 219, 220]. More recently, these vascular images have been fused with spatially matched 3D myocardial scar imaging to provide 3D maps of both relevant vascular structures and related myocardial scar (**Fig. 1.7**) [221]. While visual registration of these structures appears to influence therapeutic decisions, the role of these hybrid images for guidance of CAR



or CRT needs further investigation.

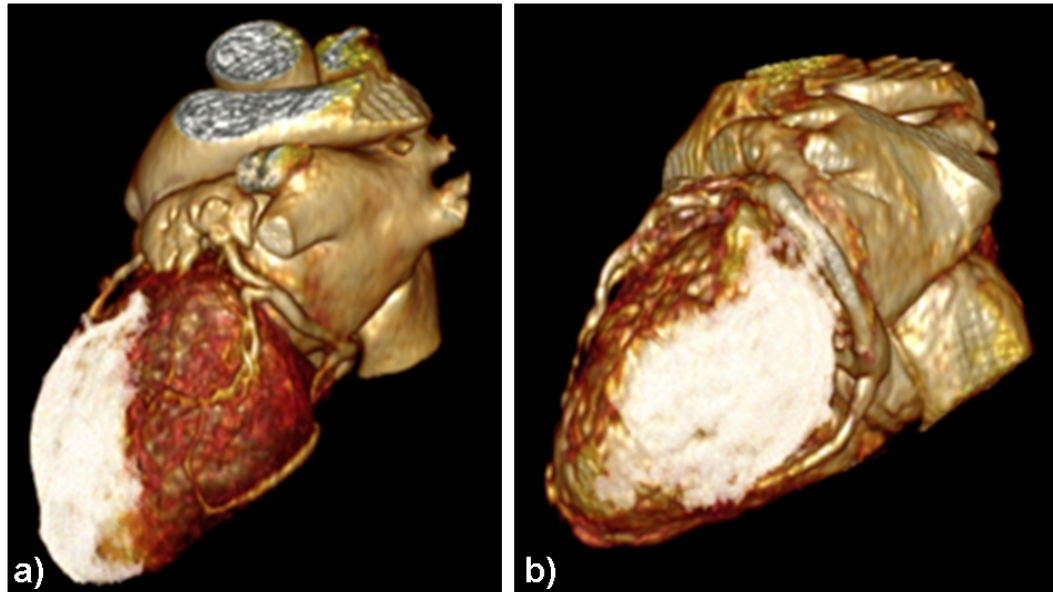


Fig. 1.7: Volume rendering of fused 3D myocardial scar imaging and coronary MRA datasets in two patients with prior myocardial infarction referred for CRT. Patient in (a) has a lateral wall vein without underlying scar despite extensive infarction of the anterior wall. Patient in (b) shows extensive infarction of the lateral wall, but a viable anterior wall beneath the anterior interventricular vein. *Images courtesy of James White, MD, Roberts Research Institute, London, ON.*

**Revascularization and Resynchronization Therapy:** Revascularization procedures are performed using either percutaneous, fluoroscopically-guided delivery of coronary stents, or surgically, through CABG. The pre-procedural vascular-scar models have the potential to guide the selection of vascular targets based on the viability of the tissue in the respective territories [222]. Therefore, a simultaneous, synchronized display of such models during fluoroscopic procedures may be clinically valuable.

This information is also relevant to the delivery of the coronary sinus pacemaker leads for resynchronization therapy. These leads are fluoroscopically guided into branches of the coronary venous system to advance the mechanical activation of delayed myocardial segments. Ideally, the coronary sinus lead is delivered to the most mechanically delayed myocardial segment that demonstrates an absence of scar.

The accomplishment of this goal can be facilitated by the co-registration of multi-component cardiac models to intra-operative fluoroscopy. However, future efforts in the development of lead guidance approaches that integrate vascular models, scar distribution, and activation maps must be invested.

**Cellular-based Cardiac Regenerative Therapy:** Although still under investigation, cellular-based regenerative therapy continues to present an interesting potential for patients with ischemic myocardial injury. While the optimal delivery of this therapy is uncertain, endocardial injection of the stem cells under image guidance is commonly employed [223]. Knowledge of the injection target site relative to myocardial scar morphology may therefore be crucial to the clinical success of this evolving therapy (**Fig. 1.8**). This task could be facilitated by integrating MRI-derived 3D scar models with real-time fluoroscopy during guidance.

Injection under direct MRI visualization has also been investigated [224]. This technique not only provided enhanced soft-tissue characterization during catheter tip placement, but also enabled the visualization of the super paramagnetic iron oxide (SPIO)-labeled stem cell populations following delivery [225]. However, this approach is resource intensive and its incremental clinical value beyond X-ray fluoroscopy guidance remains to be determined.

## 1.6 Caveats in Cardiac Surgical Guidance Environments

### 1.6.1 Equipment Constraints

The approach taken by McVeigh *et al.* [226] described earlier has demonstrated the use of intra-operative MR imaging for interventional cardiac guidance. Moreover, Rhode *et al.* [92] have reported their experience with combined real-time MR and X-ray imaging for catheter navigation. Despite their real-time benefits and high-quality images, these surgical suites are not only expensive and require special infrastructure

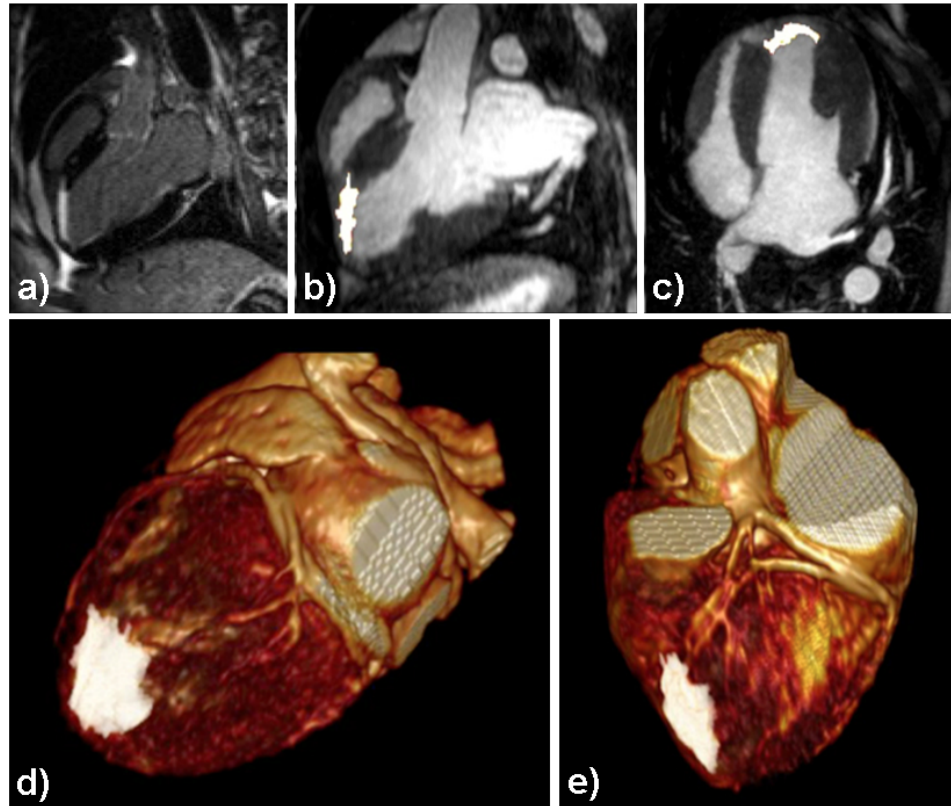


Fig. 1.8: Cardiac MRI of a canine model used for planning an endocardial stem cell injection. a) Delayed-enhanced image showing transmural antero-apical infarction caused by mid-LAD ligation; b) and c) 3D segmentation of myocardial scar displayed together with delayed-enhanced MR image; d) and e) Volume rendering of hybrid dataset including 3D MRA and scar imaging. *Images courtesy of James White, MD, Robarts Research Institute, London, ON.*

for implementation, but also hamper the clinical workflow due to their incompatibility with traditional OR instrumentation.

The restrictive environment inside the beating heart also imposes constraints on surgical tool design. If surgical tracking is employed, the delivery instruments must be built or adapted from existing clinical tools, such that they incorporate the tracking sensors [227]. In addition, most off-the-shelf surgical instruments do not comply with the magnetically clean environment requirement imposed by the presence of magnetic tracking technologies in the OR. Therefore, medical device manufacturers must be involved into the project from the very start to design instruments that are both

appropriate for the application and compatible with the guidance environment.

## 1.6.2 Calibration and Visualization Constraints

### 1.6.2.1 Spatial and Temporal Calibration

Assuming successful integration of the necessary hardware equipment into the surgical suite, adequate calibration and synchronization of all data sources is yet another challenge. All displayed images, models and surgical tool representations must be integrated into a common environment, which, in turn, must be registered to the patient. Moreover, several guidance platforms employ tracked US imaging, in which case an additional calibration steps are required to ensure that the location and geometry of the imaged features are accurately depicted [228, 105].

Besides spatial calibration, temporal synchronization between the information displayed in the visualization environment and the actual anatomy needs to be maintained during real-time visualization. While 3D heart models may be sufficient during the procedure planning stage, minimally invasive, beating heart procedures may require the use of dynamic models “beating” in synchrony with the subject’s heart and optimally registered to the real-time intra-operative images. Ideally, a high-fidelity image guidance environment would enable image acquisition, registration, surgical tracking, and information display at  $\sim 30$  frames per second. However, these processes take time and in spite of the real-time intra-operative imaging, the virtual information is necessarily delayed due to the latency of tracking and rendering [179]. The patient registration also needs to be updated in a nearly real-time fashion, leading to a trade off between accuracy, simplicity, and invasiveness [180]. Thanks to the increasing computational power of modern GPUs, deformable image registration algorithms have been optimized to yield accuracies on the order of 1-2 mm in a few seconds [229, 230].

### 1.6.2.2 3D Data Representation

To appreciate the full 3D attributes of medical data, three major approaches have been undertaken for surgical planning and guidance: slice rendering, surface

rendering, and volume rendering. The slice rendering approach is the most commonly employed in radiology. Clinicians often use this technique to view CT or MR image volumes one slice at a time using the traditional ortho-plane display. This method has been established as the clinical standard approach for visualizing and analyzing medical images. However, this approach may not be optimal for navigation, as it only provides information in the viewing plane and requires further manipulation of the viewing planes to interactively scan through the acquired volume.

Surface rendering provides information beyond that offered via slice rendering and shows three-dimensional representations of the structures of interest. The surfaces are generated via segmentation, which is itself an obstacle, since the complex cardiac structures cannot be easily segmented automatically. In addition, the segmentation process involves a binary decision process to decide where the surface lies, which may in turn affect the fidelity of the models.

Volume rendering techniques, on the other hand, utilize all of the original 3D imaging data, rather than discarding most of it when surfaces are extracted using segmentation. “Viewing rays” are cast through the intact volumes and individual voxels in the dataset are mapped onto the viewing plane, maintaining their 3D relationship while making the display appearance meaningful to the observer (**Fig. 1.9**). Recently, using GPUs, artifact-free, interactive volume rendering of medical datasets were achieved [194] without compromising image fidelity.

### 1.6.3 User-dependent Constraints

Additional constraints associated with the development and implementation of new visualization and navigation paradigms revolve around the interventionalist. In minimally invasive interventions the guidance environment *is* the surgeon’s only visual access to the surgical site, raising the following questions: what information is appropriate, how much is sufficient, when and how should it be displayed, and how can the interventionalist interact with the data?

These environments are far from those clinicians have been accustomed to using. After looking at chest radiographs or conventional views of the heart provided via

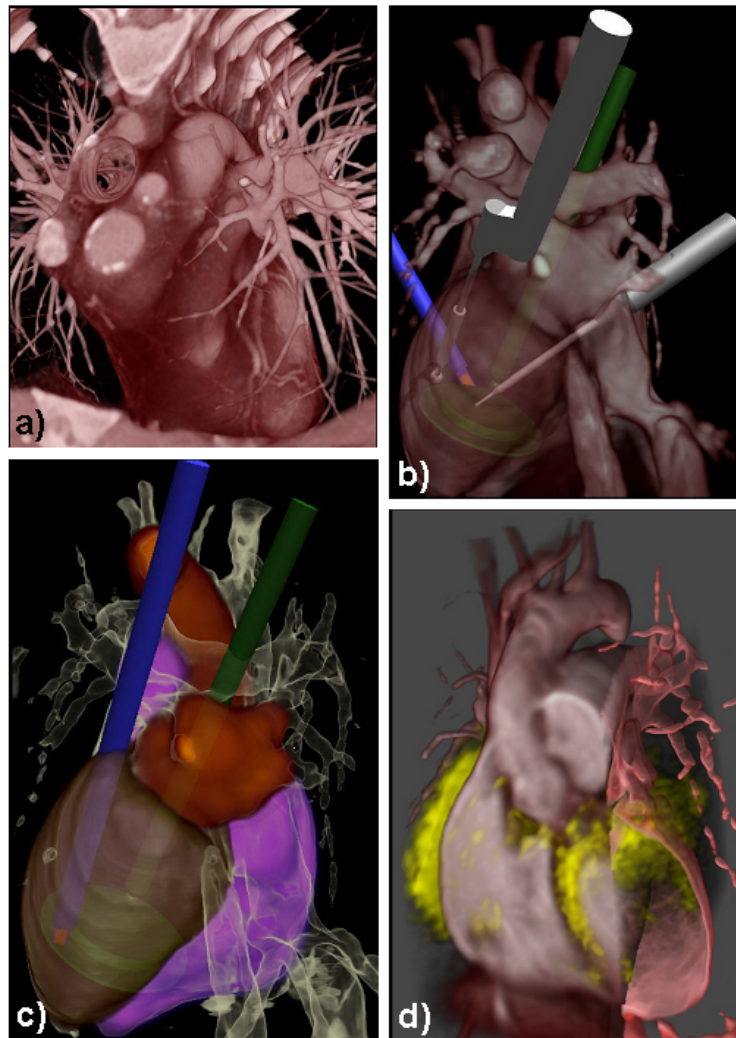


Fig. 1.9: a) Volume rendered contrast-enhanced cardiac CT images, showing peripheral vasculature; b, c) Procedure simulation showing volume rendered cardiac MR dataset augmented with surgical instruments, displayed using different translucency levels for feature enhancement; d) Fused cardiac MR and 3D US datasets, showing enhancement of the pre-operative MR data. *Images courtesy of Qi Zhang, PhD, Robarts Research Institute, London, ON.*

digital medical imaging, and after performing open chest surgery for decades, some clinicians may be intimidated by the novelty of the VR and AR environments and find the complex displays overwhelming rather than intuitive. The appropriate approach is to make “the new” look as much like “the old”, gradually introducing new information to avoid overload, employing standard anatomical views first and progressively

establishing an intuitive transition toward 3D displays. This approach is expected to provide training and sufficient time to explore and understand the guidance platform. Moreover, the clinicians must be actively involved in the development of such environments, as they can raise concerns that may unfortunately be overlooked by the engineers.

Common paradigms for information manipulation and user interaction with classical 2D medical displays include windows, mouse pointers, menus and dials. Despite their extensive use, these approaches do not translate well for 3D displays. In their work, Bowman *et al.* [231] provide a comprehensive overview of 3D user interfaces along with detailed arguments as to why 3D information manipulation is difficult. Furthermore, Reitinger *et al.* [232] have proposed a 3D VR user interface for procedure planning of liver interventions. Both groups concluded that each procedure requires a limited number of meaningful visualization poses suitable for the user. Therefore, environments must be modified to control the degree of user interaction, by identifying the necessary navigation information at each stage in the workflow and ensure its optimal delivery without information overload [233].

## 1.7 Thesis Objectives

The global objective of this work is to demonstrate that a mixed reality environment that integrates both pre- and intra-operative information can be developed to provide the surgeon with the necessary visualization and navigation information for minimally invasive therapy delivery inside the beating heart. Moreover, this surgical guidance environment is based on a fundamental paradigm — *the navigation-positioning paradigm* formulated in this thesis and described in Chapter 2.

The specific objectives are listed below in terms of the following research questions:

- Can a mixed reality environment be developed to replace the surgeons eyes and provide sufficient guidance information to deliver therapy to targets located inside the beating heart in absence of direct vision?
- What is the accuracy with which users can target specific locations using the

model-enhanced US-assisted guidance environment in the context of both direct-access, as well as catheter-guided interventions?

- Can pre-operatively acquired 3D and 4D medical images be used to generate subject-specific anatomical models of the heart that can be integrated within the virtual surgical environment to augment real-time intra-operative US imaging?
- How accurate should these models be to provide sufficient anatomical context to enhance intra-operative navigation during off-pump cardiac interventions?
- What does the clinical workflow entail to accommodate the translation of model-enhanced US guidance into the clinic and is this surgical environment clinically feasible for guiding typical intracardiac procedures?
- What is the effect of the peri-operative workflow associated with these minimally invasive procedures on the global position of the heart, not only in the context of model-enhanced US-guided intracardiac interventions, but also in terms of other minimally invasive applications?
- How can the information related to the global heart displacement be used to improve pre-operative planning of other interventions, such as robot-assisted CABG procedure, for example?

## 1.8 Thesis Outline

### 1.8.1 Chapter 2: Model-enhanced US-assisted Guidance Environment Overview

This chapter describes the concept, design and initial implementation of the model-enhanced US-assisted guidance platform. The overall platform architecture, together with a series of experiments designed to demonstrate the feasibility of the intended environment are presented, including US calibration assessment, preliminary navigation experiments, as well as qualitative assessment of the navigation-positioning



paradigm via *in vitro* and *ex vivo* investigations using a cardiac intervention phantom and excised swine hearts, respectively.

### **1.8.2 Chapter 3: Quantitative Surgical Guidance Evaluation**

A thorough quantitative assessment of the surgical navigation capabilities of the proposed environment is described in this chapter. Using a beating heart phantom, the targeting accuracy under model-enhanced US guidance is studied for procedures simulating direct-access and catheter guided interventions, and compared to the outcomes under model-assisted guidance, US image guidance alone, as well as endoscopic guidance (used as a control modality, due to its resemblance to direct vision).

### **1.8.3 Chapter 4: Pre-operative Models for Mitral Valve Interventions**

According to the navigation-positioning paradigm, virtual representations of the subject's anatomy provide context for the tool-to-target navigation. A method to generate subject-specific heart models that predict the location of the mitral valve with sufficient accuracy is presented, together with a technique to integrate these models within the intra-operative environment to augment real-time US imaging.

### **1.8.4 Chapter 5: *In vivo* Pre-clinical Feasibility Studies**

Following *in vitro* navigation evaluation and assessment of the model-enhanced US environment using images of healthy subjects, this chapter describes the clinical implementation of the environment in a pre-clinical setting, where it was employed to guide *in vivo* mitral valve implantation and ASD repair procedures in swine models.

### **1.8.5 Chapter 6: Heart Migration during Minimally Invasive Procedures**

A common assumption in IGS is that pre-operative information can represent intra-operative morphology with sufficient fidelity. However, for cardiac interventions, this assumption may be invalid, since the overall position of the heart itself may change due to the stages involved in the peri-operative workflow. Here we study the heart migration associated with two procedure workflows: model-enhanced US-guided intracardiac interventions in swine models, and robot-assisted CABG interventions in patients with coronary artery disease.

### **1.8.6 Appendix A: Predicting Intra-operative Target Vessel Location**

The research in this appendix, performed in collaboration with a fellow student in the laboratory (Daniel S. Cho, Biomedical Engineering M.E.Sc. candidate). As a follow-up on the clinical observations arising from the studies on heart migration during robot-assisted CABG procedures, this work describes a method to predict the intra-operative target vessel location based on the pre-operative CT information and the peri-operative heart displacement data. The proposed technique is validated using simulations of the clinically-observed heart migration patterns *in vitro* using a heart phantom.

# References

- [1] P. Milgram, H. Takemura, A. Utsumi, and F. Kishino. Augmented reality: A class of displays on the reality-virtuality continuum. In *Proc. SPIE 1994: Telemanipulator and Telepresence Technology*, volume 2351, pages 282–92, 1994.
- [2] P. Milgram and F. Kishino. A taxonomy of mixed reality visual displays. In *IEICE Trans Inform Syst.*, 1994.
- [3] P. J. Metzger. Adding reality to the virtual. In *Proc. IEEE Virtual Reality International Symposium*, pages 7–13, 1993.
- [4] H. Takemura and F. Kishino. Cooperative work environment using virtual workspace. In *Proc. Computer Supported Cooperative Work*, pages 226–32, 1992.
- [5] M. Kaneko, F. Kishino, K. Shimamura, and H. Harashima. Toward the new era of visual communication. *IEICE Trans Communications*, E76-B(6):577–91, 1993.
- [6] A. Utsumi, P. Milgram, H. Takemura, and F. Kishino. Investigation of errors in perception of stereoscopically presented virtual object locations in real display space. In *Proc. Human Factors and Ergonomics Society*, 1994.
- [7] T. P. Caudell. Introduction to augmented and virtual reality. In *Proc. SPIE 1994: Telemanipulator and Telepresence Technology*, volume 2351, pages 272–81, 1994.
- [8] J. H. Shuhaiber. Augmented reality in surgery. *Arch Surg.*, 139:170–4, 2004.
- [9] G. L. Ettinger, M. E. Leventon, W. E. L. Grimson, R. Kikinis, L. Gugino, W. Cote, L. Sprung, L. Aglio, M. E. Shenton, G. Potts, V. L. Hernandez, and E. Alexander. Experimentation with a transcranial magnetic stimulation system for functional brain mapping. *Med Image Anal.*, 2:477–86, 1998.
- [10] A. Feifer, J. Delisle, and M. Anidjar. Hybrid augmented reality simulator: preliminary construct validation of laparoscopic smoothness in a urology residency program. *J Urol.*, 180:1455–9, 2008.

- [11] D. Magee, Y. Zhu, R. Ratnalingam, P. Gardner, and D. Kessel. An augmented reality simulator for ultrasound guided needle placement training. *Med Biol Eng Comput.*, 45:957–67, 2007.
- [12] K. F. Kerner, C. Imielinska, J. Rolland, and H. Tang. Augmented reality for teaching endotracheal intubation: MR imaging to create anatomically correct models. In *Proc. Annu AMIA Symp*, page 888, 2003.
- [13] J. P. Rolland, D. L. Wright, and A. R. Kancherla. Towards a novel augmented-reality tool to visualize dynamic 3-D anatomy. *Stud Health Technol Inform.*, 39:337–48, 1997.
- [14] S. M. Botden and J. J. Jakimowicz. What is going on in augmented reality simulation in laparoscopic surgery? *Surg Endosc.*, 23:1693–700, 2009.
- [15] A. Koehring, J. L. Foo, G. Miyano, T. Lobe, and E. Winer. A framework for interactive visualization of digital medical images. *J Laparoendosc Adv Surg Tech.*, 18:697–706, 2008.
- [16] E. E. Lovo, J. C. Quintana, M. C. Puebla, G. Torrealba, J. L. Santos, I. H. Lira, and P. Tagle. A novel, inexpensive method of image coregistration for applications in image-guided surgery using augmented reality. *Neurosurgery*, 60:366–71, 2007.
- [17] E. M. Friets, J. W. Strohbehm, and D. W. Roberts. Curvature-based nonfiducial registration for the stereotactic operating microscope. *IEEE Trans Biomed Engin.*, 42:477–86, 1995.
- [18] S. Kaufman, I. Poupyrev, E. Miller, M. Billingham, P. Oppenheimer, and S. Weghorst. New interface metaphors for complex information space visualization: an ECG monitor object prototype. *Stud Health Technol Inform.*, 39:131–40, 1997.
- [19] K. G. Vosburgh and R. San José Estépar. Natural orifice transluminal endoscopic surgery (notes): An opportunity for augmented reality guidance. In *Proc. MMVR*, volume 125 of *Stud Health Technol Inform.*, pages 485–90, 2007.
- [20] S. Vogt, A. Khamene, H. Niemann, and F. Sauer. An AR system with intuitive user interface for manipulation and visualization of 3D medical data. In *Proc. MMVR*, volume 98 of *Stud Health Technol Inform.*, pages 397–403, 2004.
- [21] D. Teber, S. Guven, T. Simpfend'orfer, M. Baumhauer, E. O. Gven, F. Yencilek, A. S. G'ozen, and J. Rassweiler. Augmented reality: A new tool to improve surgical accuracy during laparoscopic partial nephrectomy? preliminary in vitro and in vivo results. *Eur Urol.*, 56:332–8, 2009.

- [22] M. Nakamoto, K. Nakada, Y. Sato, K. Konishi, M. Hashizume, and S. Tamura. Intraoperative magnetic tracker calibration using a magneto-optic hybrid tracker for 3-D ultrasound-based navigation in laparoscopic surgery. *IEEE Trans Med Imaging*, 27:255–70, 2008.
- [23] L. H. Edmunds. Why cardiopulmonary bypass makes patients sick: strategies to control the blood-synthetic surface interface. *Adv Card Surg.*, 6:131–67, 1995.
- [24] V. A. Subramanian, J. C. McCabe, and C. M. Geller. Minimally invasive direct coronary artery bypass grafting: Two-year clinical experience. *Ann Thorac Surg.*, 64:1648–53, 1997.
- [25] M. J. Mack. Minimally invasive cardiac surgery. *Surg Endosc.*, 20:S488–92, 2006.
- [26] M. J. Mack, R. J. Aronoff, T. E. Acuff, M. B. Douthit, Bowman R. T., and W. H. Ryan. Present role of thoracoscopy in the diagnosis and treatment of diseases of the chest. *Ann Thorac Surg.*, 54, 1992.
- [27] H. Reichenspurner, V. Guliemos, J. Wunderlich, M. Dangel, F. M. Wagner, M. F. Pompili, J. H. Stevens, J. Ludwig, W. G. Daniel, and S. Schler. Port-access coronary artery bypass grafting with the use of cardiopulmonary bypass and cardioplegic arrest. *Ann Thorac Surg.*, 65:413–9, 1998.
- [28] K. E. Matschke, J. F. Gummert, S. Demertzis, U. Kappert, M. B. Anssar, F. Siclari, V. Falk, E. L. Alderman, C. Detter, H. Reichenspurner, and W. Harringer. The Cardica C-Port system: Clinical and angiographic evaluation of a new device for automated, compliant distal anastomoses in coronary artery bypass grafting surgery - a multicenter prospective clinical trial. *J Thorac Cardiovasc Surg.*, 130:1645–52, 2005.
- [29] K. D. Stahl, W. D. Boyd, T. A. Vassiliades, and H. L. Karamanoukian. Hybrid robotic coronary artery surgery and angioplasty in multivessel coronary artery disease. *Ann Thorac Surg.*, 74:S1358–62, 2002.
- [30] J. A. Morgan, J. C. Peacock, T. Kohmoto, M. J. Garrido, B. M. Schanzer, A. R. Kherani, D. W. Vigilance, F. H. Cheema, S. Kaplan, C. R. Smith, M. C. Oz, and M. Argenziano. Robotic techniques improve quality of life in patients undergoing atrial septal defect repair. *Ann Thorac Surg.*, 77:1328–33, 2004.
- [31] L. W. Nifong, W. R. Chitwood, P. S. Pappas, C. R. Smith, M. Argenziano, V. A. Starnes, and P. M. Shah. Robotic mitral valve surgery: A United States multicenter trial. *J Thorac Cardiovasc Surg.*, 129:1395–404, 2005.

- [32] D. Dvir, A. Assali, K. Spargias, and R. Kornowski. Percutaneous aortic valve implantation in patients with coronary artery disease: Review of therapeutic strategies. *J Invasive Cardiol.*, 21:E237–41, 2009.
- [33] M. C. Wong, D. J. Clark, M. C. Horrigan, E. Grube, G. Matalanis, and H. M. Farouque. Advances in percutaneous treatment for adult valvular heart disease. *Intern Med J.*, 39:465–74, 2009.
- [34] H. R. Andersen. History of percutaneous aortic valve prosthesis. *Herz*, 34:343–6, 2009.
- [35] T. M. Dewey, T. Walther, M. Doss, D. Brown, W. H. Ryan, Svensson. L., T. Mihaljevic, R. Hambrecht, G. Schuler, G. Wimmer-Greinecker, F. W. Mohr, and M. J. Mack. Transapical aortic valve implantation: An animal feasibility study. *Ann Thorac Surg.*, 82:110–6, 2006.
- [36] M. Bollati, E. Tizzani, C. Moretti, F. Sciuto, P. Omede, G. B. Zoccai, G. P. Trevi, A. Abbate, and I. Sheiban. The future of new aortic valve replacement approaches. *Future Cardiol.*, 6:351–6, 2010.
- [37] J. Ye, A. Cheung, S. V. Lichtenstein, F. Nietlispach, S. Albugami, J. B. Masson, C. R. Thompson, B. Munt, R. Moss, R. G. Carere, W. R. Jamieson, and J. G. Webb. Transapical transcatheter aortic valve implantation: follow-up to 3 years. *J Thorac Cardiovasc Surg.*, 139:1107–13, 2010.
- [38] E. Ferrari, C. Sulzer, C. Marcucci, E. Rizzo, P. Tozzi, and L. K. vonSegesser. Transapical aortic valve implantation without angiography: Proof of concept. *Ann Thorac Surg.*, 89:1925–32, 2010.
- [39] E. Ferrari, C. Marcucci, S. Di Bernardo, and L. Karl von Segesser. Feasibility of transapical aortic valve implantation guided by intracardiac ultrasound without angiography. *J Thorac Cardiovasc Surg., In Press*, 2010.
- [40] T. Walther, G. Schuler, M. A. Borger, J. Kempfert, V. Falk, F. W. Mohr, J. Seeburger, Y. Ruckert, J. Ender, A. Linke, and M. Sholz. Transapical aortic valve implantation in 100 consecutive patients: Comparison to propensity-matched conventional aortic valve replacement. *Eur Heart J.*, 31:1398–403, 2010.
- [41] R. K. Wolf, E. W. Schneeberger, R. Osterday, D. Miller, W. Merrill, J. B. Flege, and A. M. Gillinov. Video-assisted bilateral pulmonary vein isolation and left atrial appendage exclusion for atrial fibrillation. *J Thorac Cardiovasc Surg.*, 130:797–802, 2005.
- [42] S. Janin, M. Wojcik, M. Kuniss, A. Berkowitsch, D. Erkapic, S. Zaltsberg, F. Ecarnot, C. W. Hamm, H. F. Pitschner, and T. Neumann. Pulmonary vein

- antrum isolation and terminal part of the P-wave. *Pacing Clin Electrophysiol., In Press*, 2010.
- [43] M. Castell, D. Pereda, C. A. Mestres, F. Gmez, E. Quintana, and J. Mulet. Thoracoscopic pulmonary vein isolation in patients with atrial fibrillation and failed percutaneous ablation. *J Thorac Cardiovasc Surg., In Press*, 2010.
- [44] C. S. Joels, E. M. Langan III, D. L. Cull, C. A. Kalbaugh, and S. M. Taylor. Effects of increased vascular surgical specialization on general surgery trainees, practicing surgeons, and the provision of vascular surgical care. *J Am Coll Surg.*, 208, 2009.
- [45] K. Cleary and T. M. Peters. Image-guided interventions: Technology review and applications. *Annu Rev Biomed Eng.*, 12:119–42, 2010.
- [46] R. Galloway and T. M. Peters. Overview and history of image-guided interventions. In T. M. Peters and K. Cleary, editors, *Image-guided Interventions: Technology and Applications*, pages 1–21. Springer, Heidelberg, Germany, 2008.
- [47] D. R. Holmes III, M. Rettmann, and R. A. Robb. Visualization in image-guided interventions. In T. M. Peters and K. Cleary, editors, *Image-guided Interventions: Technology and Applications*, pages 45–80. Springer, Heidelberg, Germany, 2008.
- [48] G. N. Hounsfield. Computerized transverse axial scanning (tomography): Part 1: Description of system. *Br J Radiol.*, 46:1016–22, 1973.
- [49] C. A. van Mieghem, M. van der Ent, and P. J. de Feyter. Percutaneous coronary intervention for chronic total occlusions: Value of preprocedural multislice CT guidance. *Heart.*, 93:1492, 2007.
- [50] H. Hoffmann, H. P. Dbel, H. Laube, B. Hamm, and M. Dewey. Triage of patients with suspected coronary artery disease using multislice computed tomography. *Acad Radiol.*, 14:901–9, 2007.
- [51] Jr Damiano, Ralph J. Robotics in cardiac surgery: The emperor’s new clothes. *J Thorac Cardiovasc Surg.*, 134:559–61, 2007.
- [52] A. L. Trejos, R. V. Patel, I. Ross, and B. Kiaii. Optimizing port placement for robot-assisted minimally invasive cardiac surgery. *Int J Med Robot.*, 3:355–64, 2007.
- [53] K. Wong. Imaging modalities. In T. M. Peters and K. Cleary, editors, *Image-guided Interventions: Technology and Applications*, pages 241–73. Springer, Heidelberg, Germany, 2008.

- [54] M. Otsuka, S. Sugahara, K. Umeda, M. Nakamura, A. Nakamura, Y. Bonkohara, and Y. Tsurumi. Utility of multislice computed tomography as a strategic tool for complex percutaneous coronary intervention. *Int J Cardiovasc Imaging.*, 24:201–10, 2008.
- [55] O. Bondarenko, A. M. Beek, M. B. Hofman, H. P. Khl, J. W. Twisk, W. G. van Dockum, C. A. Visser, and A. C. van Rossum. Standardizing the definition of hyperenhancement in the quantitative assessment of infarct size and myocardial viability using delayed contrast-enhanced CMR. *J Cardiovasc Magn Reson.*, 7:481–5, 2005.
- [56] S. Mankad, R. Khalil, and C. M. Kramer. MRI for the diagnosis of myocardial ischemia and viability. *Curr Opin Cardiol.*, 18:351–6, 2003.
- [57] E. Heiberg, H. Engblom, J. Engvall, E. Hedstrm, H. Arheden, and M. Ugander. Semi-automatic quantification of myocardial infarction from delayed contrast enhanced magnetic resonance imaging. *Scand Cardiovasc J.*, 39:267–75, 2005.
- [58] J. Bogaert and S. Dymarkowski. Delayed contrast-enhanced mri: use in myocardial viability assessment and other cardiac pathology. *Eur Radiol.*, 15(Suppl. 2):B52–8, 2005.
- [59] I. Klem, J. F. Heitner, D. J. Shah, M. H. Sketch, R. J. Kim, V. Behar, J. Weunsaft, P. Cawley, M. Parker, M. Elliot, and R. M. Judd. Improved detection of coronary artery disease by stress perfusion cardiovascular magnetic resonance with the use of delayed enhancement infarction imaging. *J Am Coll Cardiol.*, 47:1630–8, 2006.
- [60] M. Maruskova, P. Gregor, J. Bartunek, J. Tintera, and M. Penicka. Myocardial viability and cardiac dyssynchrony as strong predictors of perioperative mortality in high-risk patients with ischemic cardiomyopathy having coronary artery bypass surgery. *J Thorac Cardiovasc Surg.*, 138:62–8, 2009.
- [61] L. Axel and L. Dougherty. MR imaging of motion with spatial modulation of magnetization. *Radiology*, 171:841–5, 1989.
- [62] E. R. McVeigh. Measuring mechanical function in the failing heart. *J Electrocardiol.*, 39:S24–7, 2006.
- [63] P. M. Black, T. Moriarty, E. Alexander 3rd, P. Stieg, R. Kikinis, E. J. Woodard, P. L. Gleason, C. H. Martin, R. B. Schwartz, and F. A. Jolesz. Development and implementation of intraoperative magnetic resonance imaging and its neurosurgical applications. *Neurosurgery*, 41:831–42, 1997.



- [64] J. F. Schenck, F. A. Jolesz, P. B. Roemer, H. E. Cline, R. Kikinis, W. E. Lorensen, S. G. Silverman, C. J. Hardy, W. D. Barber, and Laskaris E. T. Superconducting open-configuration MR imaging system for image-guided therapy. *Radiology*, 195:805–14, 1995.
- [65] T. M. Moriarty, R. Kikinis, F. A. Jolesz, P. M. Black, and E. Alexander 3rd. Magnetic resonance imaging therapy. intraoperative MR imaging. *Neurosurg Clin N Am.*, 7:323–31, 1996.
- [66] R. Steinmeier, R. Fahlbusch, O. Ganslandt, C. Nimsky, W. Huk, M. Buchfelder, M. Kaus, T. Heigl, G. Lens, and R. Kuth. Intraoperative magnetic resonance imaging with the Magnetom Open scanner: Concepts, neurosurgical indications, and procedures: a preliminary report. *Neurosurgery*, 43:739–47, 1998.
- [67] C. J. Seebauer, H. J. Bail, J. C. Rump, T. Walter, and U. K. Teichgraeber. Advancements in orthopedic intervention: Retrograde drilling and bone grafting of osteochondral lesions of the knee using MRI guidance. *Cardiovasc Intervent Radiol.*, 2010. *In press*.
- [68] F. Baumann, C. Schmid, and R. L. Bernays. Intraoperative magnetic resonance imaging-guided transsphenoidal surgery for giant pituitary adenomas. *Neurosurg Rev.*, 33:83–90, 2010.
- [69] R. van der Weide, K. J. Zuiderveld, C. J. Bakker, T. Hoogenboom, J. J. van Vaals, and M. A. Viergever. Image guidance of endovascular interventions on a clinical MR scanner. *IEEE Trans Med Imaging.*, 17:779–85, 1998.
- [70] D. I. Hoult, J. K. Saunders, G. R. Sutherland, J. Sharp, and B. Tomanek. The engineering of an interventional MRI with a movable 1.5 T magnet. *J Magn Reson Imaging.*, 13:78–86, 2001.
- [71] E. Klodas, T. F. Miller, T. D. Christian, D. O. Hodge, and R. J. Gibbons. Prognostic significance of ischemic electrocardiographic changes during vasodilator stress testing in patients with normal SPECT images. *J Nucl Cardiol.*, 10:4–8, 2003.
- [72] B. F. Hutton, M. Braun, L. Thurffjell, and D. Y. Lau. Image registration: An essential tool for nuclear medicine. *Eur J Nucl Med Mol Imaging.*, 29:559–77, 2002.
- [73] G. de Couto, M. Ouzounian, and P. P. Liu. Early detection of myocardial dysfunction and heart failure. *Nat Rev Cardiol.*, 7:334–44, 2010.

- [74] S. G. Nekolla, A. Martinez-Moeller, and A. Saraste. Pet and mri in cardiac imaging: from validation studies to integrated applications. *Eur J Nucl Med Mol Imaging*, 36(Suppl.1):S121–30, 2009.
- [75] E. Burrows. *Pioneers and early years: A history of British radiology*. Colophon Press, Alderney, UK, 1986.
- [76] W. R. Hendee. The information perspective of radiology. *Am J Roentgenol.*, 158:1387–9, 1992.
- [77] T. M. Peters. Image-guided surgery: from X-rays to virtual reality. *Comput Methods Biomech Biomed Engin.*, 4:27–57, 2000.
- [78] K. Masamune, G. Fichtinger, A. Patriciu, R. C. Susil, R. H. Taylor, L. R. Kavoussi, J. H. Anderson, I. Sakuma, T. Dohi, and D. Stoianovici. System for robotically assisted percutaneous procedures with computed tomography guidance. *Comput Aided Surg.*, 6:370–83, 2001.
- [79] S. B. Solomon, A. Patriciu, M. E. Bohlman, L. R. Kavoussi, and D. Stoianovici. Robotically driven interventions: A method of using CT fluoroscopy without radiation exposure to the physician. *Radiology*, 225:277–82, 2002.
- [80] H. Sakurai, N. Mitsuhashi, K. Harashima, H. Muramatsu, and T. Nakano. CT-fluoroscopy guided interstitial brachytherapy with image-based treatment planning for unresectable locally recurrent rectal carcinoma. *Brachytherapy*, 3:222–30, 2004.
- [81] R. Fahrig and D. W. Holdsworth. Three-dimensional computed tomographic reconstruction using a C-arm mounted XRRI: Image-based correction of gantry motion nonidealities. *Med Phys.*, 27:30–8, 2000.
- [82] D. A. Jaffray, J. H. Siewerdsen, J. W. Wong, and A. A. Martinez. Flat-panel cone-beam computed tomography for image-guided radiation therapy. *Int J Radiat Oncol Biol Phys.*, 53:1337–49, 2002.
- [83] J. H. Siewerdsen, D. J. Moseley, S. Burch, S. K. Bisland, D. A. Jaffray, A. Bogaards, and B. C. Wilson. Volume CT with a flat-panel detector on a mobile, isocentric C-arm: Pre-clinical investigation in guidance of minimally invasive surgery. *Med Phys.*, 32:241–54, 2005.
- [84] W. Lauriola, M. Nardella, V. Strizzi, A. Cal, V. D’Angelo, and F. Florio. 3D angiography in the evaluation of intracranial aneurysms before and after treatment: Initial experience. *Radiol Med.*, 109:98–107, 2005.

- [85] R. Manzke, V. Y. Reddy, S. Dalal, A. Hanekamp, V. Rasche, and R. C. Chan. Intra-operative volume imaging of the left atrium and pulmonary veins with rotational X-ray angiography. In *Proc Med Image Comput Comput Assist Interv.*, volume 9 of *Lect Notes Comput Sci.*, pages 604–11, 2006.
- [86] C. Meyer, R. Manzke, J. Peters, O. Ecabert, J. Weese, R. Kneser, V. W. Reddy, and R. C. Chan. Automatic intra-operative generation of geometric left atrium/pulmonary vein models from rotational X-ray angiography. In *Proc Med Image Comput Comput Assist Interv.*, volume 11 of *Lect Notes Comput Sci.*, pages 61–9, 2008.
- [87] R. Manzke, C. Meyer, O. Ecabert, J. Peters, N. J. Noordhoek, A. Thiagalingam, V. Y. Reddy, R. C. Chan, and J. Weese. Automatic segmentation of rotational X-ray images for anatomic intra-procedural surface generation in atrial fibrillation ablation procedures. *IEEE Trans Med Imaging*, 29:260–72, 2009.
- [88] S. A. Baert, E. B. van de Kraats, T. van Walsum, M. A. Viergever, and W. J. Niessen. Three-dimensional guide-wire reconstruction from biplane image sequences for integrated display in 3-D vasculature. *IEEE Trans Med Imaging*, 22:1252–8, 2003.
- [89] A. J. Dick, V. K. Raman, A. N. Raval, M. A. Guttman, R. B. Thompson, C. Ozturk, A. M. Peters, D. C. amd Stine, V. J. Wright, W. H. Schenke, and R. J. Lederman. Invasive human magnetic resonance imaging: feasibility during revascularization in a combined XMR suite. *Catheter Cardiovasc Interv.*, 64:265–74, 2005.
- [90] M. Sermesant, K. Rhode, G. I. Sanchez-Ortiz, O. Camara, R. Adriantsimiabona, S. Hegde, D. Rueckert, P. Lambiase, C. Bucknall, E. Rosenthal, H. Delingette, D. L. Hill, N. Ayache, and R. Razavi. Simulation of cardiac pathologies using an electromechanical biventricular model and XMR interventional imaging. *Med Image Anal.*, 9:467–80, 2005.
- [91] A. D. Wiles, D. G. Thompson, and D. D. Frantz. Accuracy assessment and interpretation for optical tracking systems. In *Proc. SPIE Medical Imaging 2004: Visualization, Image-Guided Procedures and Display*, volume 5367, pages 421–32, 2004.
- [92] K. S. Rhode, M. Sermesant, D. Brogan, S. Hegde, J. Hipwell, P. Lambiase, E. Rosenthal, C. Bucknall, S. A. Qureshi, J. S. Gill, R. Razavi, and D. L. Hill. A system for real-time XMR guided cardiovascular intervention. *IEEE Trans Med Imaging*, 24:1428–40, 2005.
- [93] V. van Velthoven and L. M. Auer. Practical application of intraoperative ultrasound imaging. *Acta Neurochir. (Wien)*, 105:5–13, 1990.

- [94] R. N. Rohling, A. H. Gee, and L. Berman. Automatic registration of 3-D ultrasound images. *Ultrasound Med Biol.*, 24:841–54, 1998.
- [95] A. Fenster, D. Lee, S. Sherebrin, R. Rankin, and D. Downey. Three-dimensional ultrasound imaging of the vasculature. *Ultrasonics*, 36:629–33, 1998.
- [96] A. Khamene and F. Sauer. A novel phantom-less spatial and temporal ultrasound calibration method. In *Proc. Med Image Comput Comput Assist Interv.*, volume 3750 of *Lect Notes Comput Sci.*, pages 671–78, 2004.
- [97] D. F. Pace, A. D. Wiles, J. Moore, C. Wedlake, D. G. Gobbi, and T. M. Peters. Validation of four-dimensional ultrasound for targeting in minimally-invasive beating-heart surgery. In *Proc. SPIE Medical Imaging 2009: Visualization, Image-Guided Procedures and Modeling*, volume 7261, pages 726115–1–12, 2009.
- [98] M. Feuerstein, T. Reichl, J. Vogel, J. Traub, and N. Navab. Magneto-optical tracking of flexible laparoscopic ultrasound: Model-based online detection and correction of magnetic tracking errors. *IEEE Trans Med Imaging*, 28:951–67, 2009.
- [99] R. Comeau, A. F. Sadikot, A. Fenster, and T. M. Peters. Intraoperative ultrasound for guidance and tissue shift correction in image-guided neurosurgery. *Med Phys.*, 27:787–800, 2000.
- [100] Y. Sun, S. Kadoury, Y. Li, M. John, F. Sauer, J. Resnick, G. Plambeck, R. Liao, and C. Xu. Image guidance of intracardiac ultrasound with fusion of pre-operative images. In *Proc. Med Image Comput Comput Assist Interv.*, volume 10 of *Lect Notes Comput Sci.*, pages 60–7, 2007.
- [101] X. Huang, J. Moore, G. M. Guiraudon, D. L. Jones, D. Bainbridge, J. Ren, and T. M. Peters. Dynamic 2D ultrasound and 3D CT image registration of the beating heart. *IEEE Trans Med Imaging*, 28:1179–89, 2009.
- [102] Y. Suematsu, G. R. Marx, J. A. Stoll, P. E. DuPont, R. D. Howe, R. O. Cleveland, J. K. Triedman, T. Migaljevic, B. N. Mora, B. J. Savord, I. S. Salgo, and P. J. del Nido. Three-dimensional echocardiography-guided beating-heart surgery without cardiopulmonary bypass: A feasibility study. *J Thorac Cardiovasc Surg.*, 128:579–87, 2004.
- [103] P. M. Novotny, J. A. Stoll, N. V. Vasilyev, P. J. del Nido, P. E. Dupont, T. E. Zickler, and R. D. Howe. GPU based real-time instrument tracking with three-dimensional ultrasound. *Med Image Anal.*, 11:458–64, 2007.
- [104] C. A. Linte, A. D. Wiles, N. Hill, J. Moore, C. Wedlake, G. M. Guiraudon, D. L. Jones, D. Bainbridge, and T. M. Peters. An augmented reality environment for

- image-guidance of off-pump mitral valve implantation. In *Proc. SPIE Medical Imaging 2007: Visualization and Image-Guided Procedures*, volume 6509, pages 65090N–12, 2007.
- [105] A. D. Wiles, C. A. Linte, J. Moore, C. Wedlake, and T. M. Peters. Object identification accuracy under ultrasound enhanced virtual reality for minimally invasive cardiac surgery. In *Proc. SPIE Medical Imaging 2008: Visualization, Image-Guided Procedures and Modeling*, volume 6918, pages 69180E1–12, 2008.
- [106] G. Gao, G. P. Penney, N. Gogin, P. Cathier, A. Arujuna, M. Wright, D. Caulfield, A. Rinaldi, R. Razavi, and K. S. Rhode. Rapid image registration of 3D transesophageal echocardiography and X-ray fluoroscopy for the guidance of cardiac interventions. In *Proc. IPCAI*, volume 6135 of *Lect Notes Comput Sci.*, pages 124–34, 2010.
- [107] W. Niesses. Model-based image segmentation for image-guided interventions. In T. M. Peters and K. Cleary, editors, *Image-guided Interventions: Technology and Applications*, pages 219–40. Springer, Heidelberg, Germany, 2008.
- [108] O. Ecabert, J. Peters, H. Schramm, C. Lorenz, J. von Berg, M. J. Walker, M. Vember, M. E. Olszewski, K. Subramanyan, G. Labi, and J. Weese. Automatic model-based segmentation of the heart in CT images. *IEEE Trans Med Imaging*, 27:1189–201, 2008.
- [109] J. Huang, X. Huang, D. Metaxas, and L. Axel. Adaptive metamorphs model for 3D medical image segmentation. In *Proc Med Image Comput Comput Assist Interv.*, volume 4792 of *Lect Notes Comput Sci.*, pages 302–10, 2007.
- [110] I. Ben Ayed, S. Li, and I. Ross. Level set image segmentation with a statistical overlap constraint. *Inf Process Med Imaging.*, 21:589–601, 2009.
- [111] A. F. Frangi, D. Rueckert, J. A. Schnabel, and W. J. Niessen. Automatic construction of multiple-object three-dimensional statistical shape models: Application to cardiac modeling. *IEEE Trans Med Imaging*, 21:1151–66, 2002.
- [112] M. S. Renno, Y. Shang, J. Sweeney, and O. Dossel. Segmentation of 4D cardiac images: Investigation on statistical shape models. In *Proc IEEE Eng Med Biol.*, pages 3086–89, 2006.
- [113] E. M. van Rikxoort, I. Isgum, Y. Arzhaeva, M. Staring, S. Klein, M. A. Viergever, J. P. Pluim, and B. van Ginneken. Adaptive local multi-atlas segmentation: application to the heart and the caudate nucleus. *Med Image Anal.*, 14:39–49, 2010.

- [114] X. Zhuang, K. Rhode, S. Arridge, R. Razavi, D. Hill, D. Hawkes, and S. Ourselin. An atlas-based segmentation propagation framework locally affine registration–application to automatic whole heart segmentation. In *Proc Med Image Comput Comput Assist Interv.*, volume 5241 of *Lect Notes Comput Sci.*, pages 425–33, 2008.
- [115] M. Lorenzo-Valdés, G. I. Sanchez-Ortiz, A. G. Elkington, R. H. Mohiaddin, and D. Rueckert. Segmentation of 4D cardiac MR images using a probabilistic atlas and the EM algorithm. *Med Image Anal.*, 8:255–65, 2004.
- [116] M. Wierzbicki, M. Drangova, G. M. Guiraudon, and T. M. Peters. Validation of dynamic heart models obtained using non-linear registration for virtual reality training, planning, and guidance of minimally invasive cardiac surgeries. *Med Image Anal.*, 8:387–401, 2004.
- [117] W. Lorensen and H. Cline. Marching cubes: a high-resolution 3D surface reconstruction algorithm. *Computer Graphics*, 21:163–9, 1987.
- [118] D. Crouch and R. A. Robb. A new algorithm for efficient polygon decimation for virtual reality applications in medicine. In *Proc. SPIE Medical Imaging 1997*, volume 3031, pages 514–7, 1997.
- [119] K. Wilson, G. M. Guiraudon, D. L. Jones, and T. M. Peters. Mapping of cardiac electrophysiology onto a dynamic patient-specific heart model. *IEEE Trans Med Imaging*, 28:1870–80, 2009.
- [120] C. A. Linte, M. Wierzbicki, T. M. Peters, and A. Samani. Towards a biomechanics-based technique for assessing myocardial contractility: an inverse problem approach. *Comput Methods Biomech Biomed Engin.*, 11:243–55, 2008.
- [121] M. Pop, M. Sermesant, T. Mansi, E. Crystal, J. Detsky, Y. Yang, P. Fefer, E. R. McVeigh, A. Dick, N. Ayache, and G. A. Wright. Characterization of post-infarct scars in a porcine model: A combined experimental and theoretical study. In *Proc. FIMH*, volume 5528 of *Lect Notes Comput Sci.*, pages 1–10, 2009.
- [122] M. M. Sermesant, F. Billet, R. Chabiniok, T. Mansi, P., P. Moireau, R. Peyrat, K. S. Rhode, R. Razavi, and N. Ayache. Personalised electromechanical model of the heart for the prediction of the acute effects of cardiac resynchronisation therapy. In *Proc. FIMH*, volume 5528 of *Lect Notes Comput Sci.*, pages 239–48, 2009.
- [123] J. Fleureau, M. Garreau, E. Donal, C. Leclercq, and A. I. Hernández. A hybrid tissue-level model of the left ventricle: Application to the analysis of the regional

- cardiac function in heart failure. In *Proc. FIMH*, volume 5528 of *Lect Notes Comput Sci.*, pages 258–67, 2009.
- [124] Q. Zhang, R. Eagleson, and T. M. Peters. Dynamic real-time 4D cardiac MDCT image display using GPU-accelerated volume rendering. *Comput Med Imaging Graph.*, 33:461–76, 2009.
- [125] A. Olivier, G. Bertrand, and C. Picard. Discovery of the first human stereotactic instrument. *Appl Neurophysiol.*, 46:84–91, 1983.
- [126] S. J. Zinreich, S. A. Tebo, D. M. Long, H. Brem, D. E. Mattox, M. E. Loury, C. A. vander Kolk, W. M. Koch, D. W. Kennedy, and R. N. Bryan. Frameless stereotaxic integration of CT imaging data: Accuracy and initial applications. *Radiology*, 188:735–42, 1993.
- [127] G. H. Barnett, D. W. Kormos, C. P. Steiner, and J. Weisenberger. Use of a frameless, armless stereotactic wand for brain tumor localization with two-dimensional and three-dimensional neuroimaging. *Neurosurgery*, 33:674–8, 1993.
- [128] R. D. Bucholz, H. W. Ho, and J. P. Rubin. Variables affecting the accuracy of stereotactic localization using computerized tomography. *J Neurosurg.*, 79:667–73, 1993.
- [129] T. M. Peters. Image-guidance for surgical procedures. *Phys Med Biol.*, 51:R505–40, 2006.
- [130] W. Birkfellner, F. Watzinger, F. Wanschitz, G. Enislidis, C. Kollmann, D. Rafolt, R. Nowotny, R. Ewers, and H. Bergmann. Systematic distortions in magnetic position digitizers. *Med Phys.*, 25:2242–8, 1998.
- [131] D. D. Frantz, A. D. Wiles, S. E. Leis, and S. R. Kirsch. Accuracy assessment protocols for electromagnetic tracking systems. *Phys Med Biol.*, 48:2241–51, 2003.
- [132] J. B. Hummel, M. R. Bax, M. L. Figl, Y. Kang, C. Maurer Jr., W. W. Birkfellner, H. Bergmann, and R. Shahidi. Design and application of an assessment protocol for electromagnetic tracking systems. *Med Phys.*, 32:2371–9, 2005.
- [133] L. P. Nolte, L. Zamorano, H. Visarius, U. Berlemann, F. Langlotz, E. Arm, and O. Schwarzenbach. Clinical evaluation of a system for precision enhancement in spine surgery. *Clin Biomech.*, 10:293–303, 1995.
- [134] R. Rohling, P. Munger, J. M. Hollerbach, and T. Peter. Comparison of relative accuracy between a mechanical and an optical position tracker for image-guided neurosurgery. *J Image Guid Surg.*, 1:30–4, 1995.

- [135] M. S. Eljamel. Accuracy, efficacy, and clinical applications of the radionics operating arm system. *Comput Aided Surg.*, 2:292–7, 1997.
- [136] J. B. Anon. Computer-aided endoscopic sinus surgery. *Laryngoscope*, 108:949–61, 1998.
- [137] F. Watzinger, W. Birkfellner, F. Wanschitz, W. Millesi, C. Schopper, K. Sinko, K. Huber, H. Bergmann, and R. Ewers. Positioning of dental implants using computer-aided navigation and an optical tracking system: case report and presentation of a new method. *J Craniomaxillofac Surg.*, 27:77–81, 1999.
- [138] R. Khadem, C. C. Yeh, M. Sadeghi-Tehrani, M. R. Bax, and R. Shahidi. Comparative tracking error analysis of five different optical tracking systems. *Comput Aided Surg.*, 5:98–107, 2000.
- [139] S. Schmerber and F. Chassat. Accuracy evaluation of a CAS system: Laboratory protocol and results with 6D localizers, and clinical experiences in otorhinolaryngology. *Comput Aided Surg.*, 6:1–13, 2001.
- [140] C. A. Linte, J. Moore, A. D. Wiles, C. Wedlake, and T. M. Peters. Targeting accuracy under model-to-subject misalignments in model-guided cardiac surgery. In *Proc. Med Image Comput Comput Assist Interv.*, volume 5761 of *Lect Notes Comput Sci.*, pages 361–8, 2009.
- [141] B. J. Wood, H. Zhang, Durrani. A., N. Glossop, A. Durrani, S. Ranjan, D. Lindsch, E. Levy, F. Banovac, J. Borgert, S. Krueger, J. Kruecker, A. Viswanathan, and K. Cleary. Navigation with electromagnetic tracking for interventional radiology procedures: A feasibility study. *J Vasc Interv Radiol.*, 16:493–505, 2005.
- [142] P. M. Novotny, J. A. Stoll, N. V. Vasilyev, P. J. del Nido, P. E. Dupont, and R. D. Howe. GPU based real-time instrument tracking with three dimensional ultrasound. In *Proc. Med Image Comput Comput Assist Interv.*, volume 4190 of *Lect Notes Comput Sci.*, pages 58–65, 2006.
- [143] F. Sauer. Image registration: Enabling technology for image-guided surgery and therapy. In *Proc. IEEE Eng Med Biol.*, pages 7242–5, 2005.
- [144] J. V. Hajnal, D. L. G. Hill, and D. J. Hawkes. Introduction. In *Medical Image Registration*, pages 1–8. CRC Press, Boca Raton, FL, USA, 2001.
- [145] M. E. Rettmann, D. R. Holmes, Y. Su, B. M. Cameron, J. J. Camp, D. L. Packer, and R. A. Robb. An integrated system for real-time image-guided cardiac catheter ablation. In *Proc. MMVR*, volume 119 of *Stud Health Technol Inform.*, pages 455–60, 2006.



- [146] C. A. Linte, J. Moore, C. Wedlake, and Peters. T. M. Evaluation of model-enhanced ultrasound-assisted interventional guidance in a cardiac phantom. *IEEE Trans Biomed Eng., In Press*, 2010.
- [147] Z. Yaniv. Rigid registration. In T. M. Peters and K. Cleary, editors, *Image-guided Interventions: Technology and Applications*, pages 159–92. Springer, Heidelberg, Germany, 2008.
- [148] W. R. Crum, L. D. Griffin, D. L. Hill, and D. J. Hawkes. Zen and the art of medical image registration: Correspondence, homology, and quality. *Neuroimage*, 20:1425–37, 2003.
- [149] X. Huang, J. Ren, G. M. Guiraudon, D. Boughner, and T. M. Peters. Rapid dynamic image registration of the beating heart for diagnosis and surgical navigation. *IEEE Trans Med Imaging*, 28:1802–14, 2009.
- [150] C. A. Pelizzari, G. T. Chen, D. R. Spelbring, R. R. Weichselbaum, and C. T. Chen. Accurate three-dimensional registration of CT, PET, and/or MR images of the brain. *J Comput Assist Tomogr.*, 13:20–6, 1989.
- [151] P. J. Besl and N. D. McKay. A method for registration of 3D shapes. *IEEE Trans Pattern Anal Machine Intell.*, 14:239–55, 1992.
- [152] Y. L. Ma, G. P. Penney, C. A. Rinaldi, M. Cooklin, R. Razavi, and K. S. Rhode. Echocardiography to magnetic resonance image registration for use in image-guided cardiac catheterization procedures. *Phys Med Biol.*, 54:5039–55, 2009.
- [153] C. A. Linte, M. Wierzbicki, J. Moore, G. M. Guidardon, D. L. Jones, and T. M. Peters. On enhancing planning and navigation of beating-heart mitral valve surgery using pre-operative cardiac models. In *Proc. IEEE Eng Med Biol.*, pages 475–78, 2007.
- [154] C. A. Linte, M. Carias, D. S. Cho, , D. Pace, J. Moore, C. Wedlake, D. Bainbridge, B. Kiaii, and T. M. Peters. Estimating heart shift and morphological changes during minimally invasive cardiac interventions. In *Proc. SPIE Medical Imaging 2010: Visualization, Image-guided Procedures, and Modeling*, volume 7625, pages 7625091–11, 2010.
- [155] S. D. Cho, C. A. Linte, E. Chen, J. Moore, J. Barron, B. Kiaii, R. Patel, and T. M. Peters. Predicting target vessel location for improved planning of robot-assisted CABG procedures. In *Proc. Med Image Comput Comput Assist Interv.*, volume *In Press of Lect Notes Comput Sci.*, 2010.

- [156] R. Chandrashekara, A. Rao, G. I. Sanchez-Ortiz, R. H. Mohiaddin, and D. Rueckert. Construction of a statistical model for cardiac motion analysis using nonrigid image registration. *Inf Process Med Imaging*, 18:599–610, 2003.
- [157] D. Perperidis, R. Mohiaddin, and D. Rueckert. Construction of a 4D statistical atlas of the cardiac anatomy and its use in classification. In *Proc. Med Image Comput Comput Assist Interv.*, Lect Notes Comput Sci., pages 402–10, 2005.
- [158] M. Wierzbicki, J. Moore, M. Drangova, and T. M. Peters. Subject-specific models for image-guided cardiac surgery. *Phys Med Biol.*, 53:5295–312, 2008.
- [159] D. J. Hawkes, D. Barratt, T. Carter, J. McClelland, and B. Crum. Nonrigid registration. In T. M. Peters and K. Cleary, editors, *Image-guided Interventions: Technology and Applications*, pages 193–218. Springer, Heidelberg, Germany, 2008.
- [160] T. M. Peters and K. Cleary. *Image-guided Interventions: Technology and Applications*. Springer, Heidelberg, Germany, 2008.
- [161] J. V. Hajnal, D. L. G. Hill, and D. J. Hawkes. *Medical Image Registration*. CRC Press, Boca Raton, FL, USA, 2001.
- [162] A. E. Holsinger, R. C. Wright, S. J. Riederer, F. Farzaneh, R. C. Grimm, and J. K. Maier. Real-time interactive magnetic resonance imaging. *Magn Reson Med.*, 14:547–53, 1990.
- [163] P. Aksit, J. A. Derbyshire, J. M. Serfaty, and E. Atalar. Multiple field of view MR fluoroscopy. *Magn Reson Med.*, 47:53–60, 2002.
- [164] R. A. Robb. 3-D visualization in biomedical applications. *Annu Rev Biomed Eng.*, 1:377–99, 1999.
- [165] D. T. Gering, A. Nabavi, R. Kikinis, N. Hata, L. J. O’Donnell, W. E. Grimson, F. A. Jolesz, P. M. Black, and V. M. Wells. An integrated visualization system for surgical planning and guidance using image fusion and an open MR. *J Magn Reson Imaging.*, 13:967–75, 2001.
- [166] W. J. Schroeder, L. S. Avila, and W. Hoffman. Visualizing with VTK: A tutorial. *IEEE Comput Graph Appl.*, 20:20–7, 2000.
- [167] T. S. Yoo and D. N. Metaxas. Open science – combining open data and open source software: Medical image analysis with the insight toolkit. *Med Image Anal.*, 9:503–6, 2005.

- [168] A. Enquobahrie, P. Cheng, K. Gary, L. Ibanez, D. Gobbi, F. Lindseth, Z. Yaniv, S. Aylward, J. Jomier, and K. Cleary. The image-guided surgery toolkit IGSTK: An open-source C++ software toolkit. *J Digit Imaging*, 20:21–33, 2001.
- [169] Z. Yaniv, P. Cheng, E. Wilson, T. Popa, D. Lindisch, E. Campos-Nanez, H. Abeledo, V. Watson, K. Cleary, and F. Banovac. Needle-based interventions with the image-guided surgery toolkit (IGSTK): From phantoms to clinical trials. *IEEE Trans Biomed Engin.*, 57:922–33, 2010.
- [170] J. Neuhaus, J. Kast, I. Wegner, M. Baumhauer, A. Seitel, I. Gergel, M. Nolden, D. Maleike, I. Wolf, Meinzer H. P., and L. Maier-Hein. Building image guided therapy applications with the medical imaging interactive toolkit. *Int J Comput Assist Radiol Surg.*, 4:267–71, 2009.
- [171] J. Moore, G. M. Guiraudon, D. L. Jones, N. Hill, A. D. Wiles, D. Brainbridge, C. Wedlake, and T. M. Peters. 2D ultrasound augmented by virtual tools for guidance of interventional procedures. In *Proc. MMVR*, volume 125 of *Stud Health Technol Inform.*, pages 322–27, 2007.
- [172] P. J. Kelly, G. J. Alker Jr, and S. Goerss. Computer-assisted stereotactic microsurgery for the treatment of intracranial neoplasms. *Neurosurgery*, 10:324–31, 1982.
- [173] P.J. Edwards, D. J. Hawkes, D. L. Hill, D. Jewell, and M. Gleeson. Augmentation of reality using an operating microscope for otolaryngology and neurosurgical guidance. *J Image Guid Surg.*, 1:172–8, 1995.
- [174] W. Birkfellner, M. Figl, K. Huber, F. Watzinger, F. Wanschitz, J. Hummel, R. Hanel, W. Greimel, P. Homolka, R. Ewers, and H. Bergmann. A head-mounted operating binocular for augmented reality visualization in medicine - design and initial evaluation. *IEEE Trans Med Imaging.*, 21:991–7, 2002.
- [175] W. Birkfellner, K. Huber, F. Watzinger, M. Figl, F. Wanschitz, R. Hanel, D. Rafolt, R. Ewers, and H. Bergmann. Development of the varioscopear: A see-through HMD for computer-aided surgery. In *Proc. IEEE and ACM Int Symp on Augmented Reality*, pages 54–9, 2000.
- [176] Y. Masutani, M. Iwahara, O. Samuta, Y. Nishi, M. Suzuki, N. Suzuki, T. Dohi, H. Iseki, and K. Takakura. Development of integral photography-based enhanced reality visualization system for surgical support. In *Proc. Int Symposium Comput Aided Surg.*, pages 16–7, 1995.
- [177] K. Masamune, Y. Masutani, S. Nakajima, I. Sakuma, T. Dohi, H. Iseki, and K. Takakura. Three-dimensional slice image overlay system with accurate depth

- perception for surgery. In *Proc. Med Image Comput Comput Assist Interv.*, Lect Notes Comput Sci., pages 395–402, 2000.
- [178] M. Blackwell, C. Nikou, A. M. DiGioia, and T. Kanade. An image overlay system for medical data visualization. *Med Image Anal.*, 4:67–72, 2000.
- [179] F. Sauer, S. Vogt, and A. Khamene. Augmented reality. In T. M. Peters and K. Cleary, editors, *Image-guided Interventions: Technology and Applications*, pages 81–119. Springer, Heidelberg, Germany, 2008.
- [180] T. Sielhorst, M. Feuerstein, and N. Navab. Advanced medical displays: A literature review of augmented reality. *J Display Technol.*, 4:451–67, 2008.
- [181] J. Lo, J. Moore, C. Wedlake, G. M. Guiraudon, R. Eagleson, and T. M. Peters. 2D ultrasound augmented by virtual tools for guidance of interventional procedures. In *Proc. MMVR*, volume 142 of *Stud Health Technol Inform.*, pages 162–7, 2009.
- [182] N. V. Vasilyev, P. M. Novotny, J. F. Martinez, H. Loyola, I. S. Salgo, R. D. Howe, and P. J. del Nido. Stereoscopic vision display technology in real-time three-dimensional echocardiography-guided intracardiac beating-heart surgery. *J Thorac Cardiovasc Surg.*, 135:1334–41, 2008.
- [183] W. J. Viant. The development of an evaluation framework for the quantitative assessment of computer-assisted surgery and augmented reality accuracy performance. *Stud Health Technol Inform.*, 81:534–40, 2001.
- [184] P. Jannin, J. M. Fitzpatrick, D. J. Hawkes, X. Pannec, R. Shahidi, and M. W. Vannier. Validation of medical image processing in image-guided therapy. *IEEE Trans Med Imaging*, 21:1445–49, 2002.
- [185] C. A. Linte, M. Wierzbicki, J. Moore, S. H. Little, G. M. Guiraudon, and T. M. Peters. Towards subject-specific models of the dynamic heart for mitral valve surgery. In *Proc. Med Image Comput Comput Assist Interv.*, volume 4792 of *Lect Notes Comput Sci.*, pages 94–101, 2007.
- [186] S. K. Nadkarni, D. Boughner, M. Drangova, and A. Fenster. In vitro simulation and quantification of temporal jitter artifacts in ECG-gated dynamic three-dimensional echocardiography. *Ultrasound med Biol.*, 27:211–22, 2001.
- [187] S. K. Nadkarni, H. Austin, G. Mills, D. Boughner, and A. Fenster. A pulsating coronary vessel phantom for two- and three-dimensional intravascular ultrasound studies. *Ultrasound med Biol.*, 29:621–8, 2003.

- [188] D. R. Holmes III, M. Rettmann, B. Cameron, J. Camp, and R. Robb. Developing patient-specific anatomic models for validation of cardiac ablation guidance procedures. In *Proc. SPIE Medical Imaging 2008: Visualization, Image-Guided Procedures and Modeling*, volume 6918, pages 69181W–8, 2008.
- [189] Y. Suematsu, B. Kiaii, D. T. Bainbridge, P.J. del Nido, and R.J. Novick. Robotic-assisted closure of atrial septal defect under real-time three-dimensional echo guide: In vitro study. *Eur J Cardiothorac Surg.*, 32:573–576, 2007.
- [190] C. A. Linte, J. Moore, A. Wiles, C. Wedlake, and T. Peters. Virtual reality-enhanced ultrasound guidance: A novel technique for intracardiac interventions. *Comput Aided Surg.*, 13:82–94, 2008.
- [191] C. A. Linte, J. Moore, C. Wedlake, D. Bainbridge, G. M. Guitaudon, D. L. Jones, and T. M. Peters. Inside the beating heart: An *in vivo* feasibility study on fusing pre- and intra-operative imaging for minimally invasive therapy. *Int J CARS*, 4:113–122, 2009.
- [192] T. Sielhorst, C. Bichlmeier, S. M. Heining, and N. Navab. Depth perception - a major issue in medical AR: evaluation study by twenty surgeons. In *Proc. Med Image Comput Comput Assist Interv.*, volume 4191 of *Lect Notes Comput Sci.*, pages 364–72, 2006.
- [193] M. Lerotic, A. J. Chung, G. Mylonas, and G. Z. Yang. pq-space based non-photorealistic rendering for augmented reality. In *Proc Med Image Comput Comput Assist Interv.*, volume 4792 of *Lect Notes Comput Sci.*, pages 102–9, 2007.
- [194] O. Kutter, R. Shams, and N. Navab. Visualization and GPU-accelerated simulation of medical ultrasound from CT images. *Comput Methods Programs Biomed.*, 94:250–66, 2009.
- [195] G. B. Hanna, S. M. Shimi, and A. Cuschieri. Task performance in endoscopic surgery is influenced by location of the image display. *Ann Surg.*, 227:481–4, 1998.
- [196] C. Bichlmeier, S. M. Heining, M. Feuerstein, and N. Navab. The virtual mirror: A new interaction paradigm for augmented reality environments. *IEEE Trans Med Imaging*, 28:1498–510, 2009.
- [197] W. Birkfellner, M. Figl, C. Matula, J. Hummel, R. Hanel, H. Imhof, F. Wanschitz, A. Wagner, F. Watzinger, and H. Bergmann. Computer-enhanced stereoscopic vision in a head-mounted operating binocular. *Phys Med Biol.*, 48:49–57, 2003.

- [198] J. Traub, P. Stefan, S. M. Heining, T. Sielhorst, C. Riquarts, E. Euler, and N. Navab. Hybrid navigation interface for orthopedic and trauma surgery. In *Proc. Med Image Comput Comput Assist Interv.*, volume 4191 of *Lect Notes Comput Sci.*, pages 373–80, 2006.
- [199] M. A. Guttman, R. J. Lederman, J. M. Sorger, and E. R. McVeigh. Real-time volume rendered MRI for interventional guidance. *J Cardiovasc Magn Reson.*, 4:431–42, 2002.
- [200] M. A. Guttman, P. Kellman, A. J. Dick, R. J. Lederman, and E. R. McVeigh. Real-time accelerated interactive mri with adaptive TSENSE and UNFOLD. *Magn Reson Med.*, 50:315–21, 2003.
- [201] A. J. Dick and R. J. Lederman. MRI-guided myocardial cell therapy. *Int J Cardiovasc Intervent.*, 7:165–70, 2005.
- [202] A. J. Dick, M. A. Guttman, V. K. Raman, D. C. Peters, B. S. Pessanha, J. M. Hill, S. Smith, G. Scott, E. R. McVeigh, and R. J. Lederman. Magnetic resonance fluoroscopy allows targeted delivery of mesenchymal stem cells to infarct borders in swine. *Circulation*, 108:2899–904, 2003.
- [203] A. N. Raval, P. V. Karmarkar, M. A. Guttman, C. Ozturk, R. Desilva, R. J. Aviles, V. J. Wright, W. H. Schenke, E. Atalar, E. R. McVeigh, and R. J. Lederman. Real-time MRI guided atrial septal puncture and balloon septostomy in swine. *Catheter Cardiovasc Interv.*, 67:637–43, 2006.
- [204] A. J. Dick, V. K. Raman, A. N. Raval, M. A. Guttman, and R. J. Lederman. Invasive human magnetic resonance imaging: Feasibility during revascularization in a combined XMR suite. *Catheter Cardiovasc Interv.*, 64:265–74, 2005.
- [205] T. Walther, T. Dewey, M. A. Borger, J. Kempfert, A. Linke, R. Becht, V. Falk, G. Schuler, F. W. Moher, and M. Mack. Transapical aortic valve implantation: Step by step. *Ann Thorac Surg.*, 87:276–83, 2009.
- [206] M. E. Karar, M. Gessat, T. Walther, V. Falk, and O. Burgert. Towards a new image guidance system for assisting transapical minimally invasive aortic valve implantation. In *Proc. IEEE Eng Med Biol.*, pages 3645–8, 2009.
- [207] J. Kempfert, V. Falk, G. Schuler, A. Linke, D. Merk, F. W. Mohr, and T. Walther. Dyna-CT during minimally invasive off-pump transapical aortic valve implantation. *Ann Thorac Surg.*, 88:2041–2, 2009.
- [208] R. D. Howe. Fixing the beating heart: Ultrasound guidance for robotic intracardiac surgery. In *Proc. FIMH*, volume 5528 of *Lect Notes Comput Sci.*, pages 97–103, 2009.

- [209] S. B. Kesner, S. G. Yuen, and R. D. Howe. Ultrasound servoing of catheters for beating heart valve repair. In *Proc. IPCAI*, volume 6135 of *Lect Notes Comput Sci.*, pages 168–78, 2010.
- [210] G. M. Guiraudon. Universal cardiac introducer. Patent Application, 2005. US 2005/0137609 A1, Appl. No. 10/736,786.
- [211] Y. Sun, F. S. Azar, C. Xu, G. Hayam, A. Preiss, N. Rahn, and F. Sauer. Registration of high-resolution 3D atrial images with electroanatomical cardiac mapping: evaluation of registration methodology. In *Proc. SPIE Medical Imaging 2005: Visualization, Image-Guided Procedures, and Display*, volume 5744, pages 299–307, 2005.
- [212] G. B. Bleeker, T. A. Kaandorp, H. J. Lamb, E. Boersma, P. Steendijk, A. Roos, E. E. van der Wall, M. J. Schalij, and J. J. Bax. Effect of posterolateral scar tissue on clinical and echocardiographic improvement after cardiac resynchronization therapy. *Circulation*, 113:969–76, 2006.
- [213] C. Ypenburg, M. J. Schalij, G. B. Bleeker, P. Steedijk, E. Boersma, P. Dibbets-Schneider, M. P. Stokkel, E. E. van der Wall, and J. J. Bax. Impact of viability and scar tissue on response to cardiac resynchronization therapy in ischemic heart failure patients. *Eur Heart J.*, 28:33–41, 2007.
- [214] R. J. Kim, E. Wu, A. Rafael, E. L. Chen, M. A. Parker, O. Simonetti, F. J. Klocke, R. O. Bonow, and R. M. Judd. The use of contrast-enhanced magnetic resonance imaging to identify reversible myocardial dysfunction. *N Engl J Med.*, 343:1445–53, 2000.
- [215] A. M. Beek, H. P. Kuhl, O. Bondarenko, J. W. Twisk, M. B. Hofman, W. G. van Dockum, C. A. Visser, and A. C. van Rossum. Delayed contrast-enhanced magnetic resonance imaging for the prediction of regional functional improvement after acute myocardial infarction. *J Am Coll Cardiol.*, 42:895–901, 2003.
- [216] H. Gulbins, H. Reichensperner, C. Becker, D. H. Bohem, A. Knez, C. Schmitz, R. Bruening, R. Haberl, and B. Reichart. Preoperative 3D-reconstructions of ultrafast-CT images for the planning of minimally invasive direct coronary artery bypass operation (MIDCAB). *Heart Surg Forum*, 1:1111–5, 1998.
- [217] H. Gasparovic, F. J. Rybicki, J. Millstine, D. Unic, J. G. Byrne, K. Yucel, and T. Mihaljevic. Three dimensional computed tomographic imaging in planning the surgical approach for redo cardiac surgery after coronary revascularization. *Eur J Cardiothorac Surg.*, 28:244–9, 2005.
- [218] N. R. Van de Veire, J. D. Schuijf, J. De Sutter, D. Devos, G. B. Bleeker, A. de Roos, E. E. van der Wall, M. J. Schalij, and J. J. Bax. Non-invasive

- visualization of the cardiac venous system in coronary artery disease patients using 64-slice computed tomography. *J Am Coll Cardiol.*, 48:1832–8, 2006.
- [219] J. P. Singh, S. Houser, K. E. Heist, and J. N. Ruskin. The coronary venous anatomy: A segmental approach to aid cardiac resynchronization therapy. *J Am Coll Cardiol.*, 46:68–74, 2005.
- [220] K. Rioual, E. Unanua, S. Laguitton, M. Garreau, D. Boulmier, P. Haigron, C. Leclercq, and J. L. Coatrieux. MSCT labeling for pre-operative planning in cardiac resynchronization therapy. *Comput Med Imaging Graph.*, 29:432–9, 2005.
- [221] Q. Zhang, R. Eagleson, T. M. Peters, and J. White. A two-level transfer function based method for heart display with vascular tissue and scar enhancement. In *Proc. IEEE International Symposium Biomedical Imaging*, pages 903–6, 2009.
- [222] J. A. White, R. Yee, X. Yuan, A. Krahn, A. Skanes, M. Parker, G. Klein, and M. Drangova. Delayed enhancement magnetic resonance imaging predicts response to cardiac resynchronization therapy in patients with intraventricular dyssynchrony. *J Am Coll Cardiol.*, 48:1953–60, 2006.
- [223] M. Rodriguez-Porcel. In vivo imaging and monitoring of transplanted stem cells: Clinical applications. *Curr Cardiol Rep.*, 12:51–8, 2010.
- [224] C. Rickers, R. gallegos, R. T. Seethamraju, X. Wang, C. Swingen, and M. Jerosch-Herold. Applications of magnetic resonance imaging for cardiac stem cell therapy. *J Interv Cardiol.*, 17:37–46, 2004.
- [225] R. Zhou, D. Idiyatullin, S. Moeller, C. Corum, H. Zhang, H. Qiao, J. Zhong, and M. Garwood. SWIFT detection of SPIO-labeled stem cells grafted in the myocardium. *Magn Reson Med.*, 63:1154–61, 2010.
- [226] E. R. McVeigh, M. A. Guttman, R. J. Lederman, M. Li, O. Kocaturk, T. Hunt, S. Kozlov, and K. A. Horvath. Real-time interactive MRI-guided cardiac surgery: Aortic valve replacement using a direct apical approach. *Magn Reson Med.*, 56:958–64, 2006.
- [227] J. Moore, A. Wiles, C. Wedlake, B. Kiaii, and T. M. Peters. Integration of transesophageal echocardiography with magnetic tracking technology for cardiac interventions. In *Proc. SPIE Medical Imaging 2010: Visualization, Image-guided Procedures and Modeling*, volume 7625, pages 76252Y–1–10, 2010.
- [228] F. Rousseau, P. Hellier, M. M. Letteboer, W. J. Niessen, and C. Barillot. Quantitative evaluation of three calibration methods for 3-D freehand ultrasound. *IEEE Trans Med Imaging*, 2006:1492–501, 25.



- [229] B. Li, A. A. Young, and B. R. Cowan. GPU accelerated non-rigid registration for the evaluation of cardiac function. In *Proc. Med Image Comput Comput Assist Interv.*, volume 5242 of *Lect Notes Comput Sci.*, pages 880–7, 2008.
- [230] X. Gu, H. Pan, Y. Liang, R. Castillo, S. B. Jiang, D. Yang, D. Choi, E. Castillo, A. Majumdar, and T. Guerrero. Implementation and evaluation of various demons deformable image registration algorithms on a GPU. *Phys Med Biol.*, 55:207–19, 2010.
- [231] D. A. Bowman, E. Kruijff, J. J. laViola, and I. Poupyrev. *3D user interfaces: Theory and practice*. Addison Wesley Longman Publishing, Redwood City, CA, USA, 2004.
- [232] B. Reitinger, A. Bornik, R. Beichel, and D. Schmalsteig. Liver surgery planning using virtual reality. *IEEE Comput Graph Appl.*, 2:36–47, 2006.
- [233] S. A. Ahmadi, T. Sielhorst, M. Stauder, M. Horn, H. Feussner, and N. Navab. Recovery of surgical workflow without explicit models. In *Proc. Med Image Comput Comput Assist Interv.*, volume 4190 of *Lect Notes Comput Sci.*, pages 420–8, 2006.

## Chapter 2

# Model-enhanced Ultrasound Guidance: Concept, Initial Implementation, and Qualitative *in vitro* Assessment

*In an effort to reduce morbidity associated with cardiac interventions, we initiated the development of an interventional guidance environment for off-pump cardiac interventions. Our surgical navigation system employs a mixed reality environment that integrates pre-operative anatomical modeling with real-time intra-operative US imaging and surgical tool tracking, providing the surgeon with a broad range of valuable information. This chapter provides an overview of our guidance system together with the initial experiments designed to assess its pre-clinical performance.*

---

This work is adapted from Linte CA, Moore J, Wiles, AD, Wedlake C and Peters TM. Virtual Reality-Enhanced Ultrasound Guidance: A Novel Technique for Intracardiac Interventions. *Journal of Computer-Aided Surgery*. 13(2):82-94. 2008.

## 2.1 Introduction

Minimizing invasiveness inevitably leads to a more limited visual access to the target tissues. This is especially true for intracardiac treatments where the goal is to minimize the physical invasiveness of a full sternotomy. Since these procedures require reaching targets inside the heart, direct visual access is simply not possible while the heart is beating. However, advances in medical imaging technologies have revived opportunities for off-pump intracardiac therapies.

The imaging modalities employed for intra-procedure guidance typically involve X-ray fluoroscopy, magnetic resonance imaging (MRI), and 2D and 3D US, and in most cases image guidance is limited to a simple display of imaging data via a monitor in the operating room (OR) [1, 2, 3, 4]. The limitations associated with these approaches have been outlined in Chapter 1: the surgeon is required to mentally reconstruct the 3D geometry of both surgical tools and patient anatomy from 2D image data, as well as to interpret motion information (e.g. bringing a tool into contact with the target tissue) from a 2D monitor output and then transpose it to 3D motion patterns of real tools in the OR.

In response to these challenges, several groups have addressed some of these limitations by integrating imaging data with various virtual elements to either add spatial context or functional information to the intra-procedure images [5, 6, 7, 8]. Our approach is to rely on echocardiography for intra-operative guidance, fuse it with pre-operative information, and make use of tracking technologies to provide a robust system for surgical guidance, thus eliminating any radiation associated with fluoroscopy. Since real-time US images are displayed within the anatomical context supplied via pre-operative models and virtual surgical instrument representations, we refer to this navigation platform as the model-enhanced US-assisted guidance environment.

In terms of the nomenclature defined by Milgram *et al.* [9] as shown in Chapter 1, this environment is best classified as a mixed reality environment, consisting

of virtual components — pre-operative anatomical models and surgical tool representations, and “peripherally real” components — real-time US images. While the US images do not provide a real view of the patient, they are considered “more real” compared to the purely virtual models of the anatomy and surgical tools; hence, the model-enhanced US guidance environment could be classified as an AR environment. Nevertheless, given the predominance of virtual elements, it could also be interpreted as a VR environment. All three terms — mixed, augmented and virtual reality environment — are often used interchangeably throughout this thesis when referring to the model-enhanced US guidance environment. However, for the sake of consistency with Milgram’s reality-virtuality taxonomy, this environment should be most appropriately identified as a mixed reality environment.

The global objective of our mixed reality surgical platform is to provide the surgeon with a simple, intuitive system for surgical navigation in the absence of direct vision. Specifically, in the context of cardiac surgery, our goal is to build a sufficiently robust and reliable system to benefit most minimally-invasive intracardiac therapies, although our current experience has primarily focused on direct access mitral valve replacement and ASD repairs.

To better illustrate our research goals, we follow the patient through the proposed mitral valve procedure work-flow. First, a pre-operative cine CT or MR image dataset of the subject are acquired. A static 3D subject-specific cardiac model is constructed via either manual or semi-automatic segmentation or an atlas-based approach by registering a high-resolution average heart model containing the segmented surgical target and the surrounding anatomy, to clinical image of the subject’s heart, as described in Chapter 4. After accessing the heart, the intra-operative MVA is defined interactively using tracked 2D TEE, and displayed within the intra-operative subject space. To facilitate tool navigation and improve spatial orientation, the 2D US images are complemented by 3D anatomical models obtained from pre-operative MR images, and combined with virtual representations of the tracked surgical tools.

The pre-operative cardiac models are incorporated within the intra-operative space using a registration technique also presented in Chapter 4.

This chapter provides a generic overview of our model-enhanced US image guidance system, including details on its engineering components, various clinical applications, and different investigations designed to pre-clinically assess the feasibility of the system. Fig. 2.1 presents a schematic representation of our system and its intended configuration in the operating room.

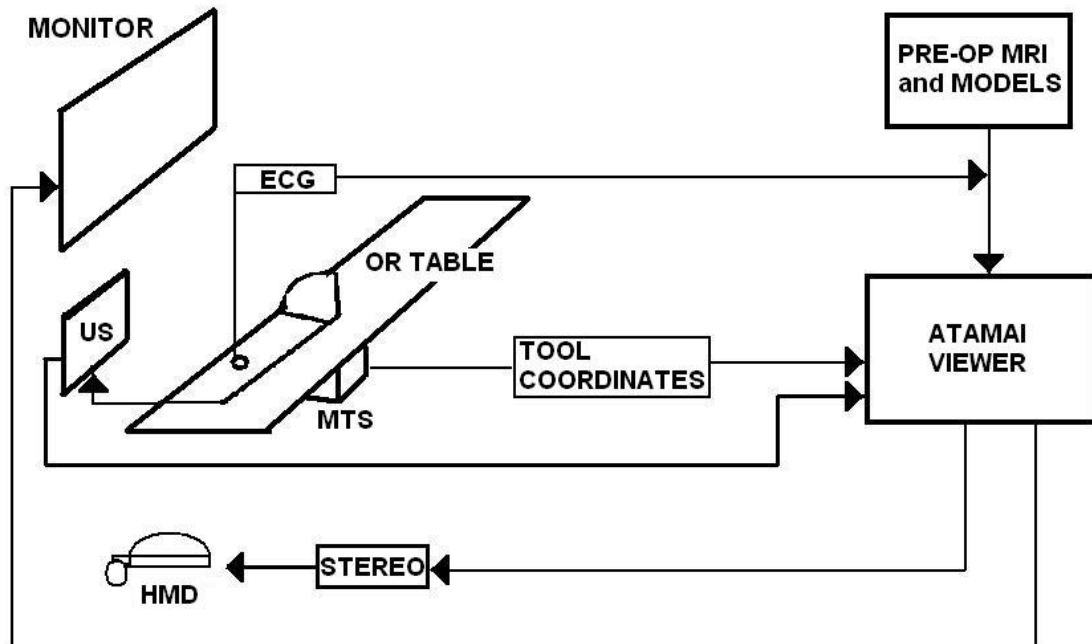


Fig. 2.1: Schematic displaying the layout of our model-enhanced US guidance surgical system, its components and typical configuration within an OR. Integrated ultrasound and virtual reality data can be delivered to the surgeon either via a monitor over the OR table, or via HMDs.

## 2.2 Surgical Guidance Platform Architecture

### 2.2.1 The *AtamaiViewer*

The model-enhanced US-assisted guidance environment is integrated into the *AtamaiViewer* software platform. The *AtamaiViewer* is a robust framework for medical data visualization, interaction and navigation. This software platform is designed to integrate all components necessary for image-guided surgery applications. It is portable across Windows, Linux, and OS-X operating systems, using a Python-based user interface and the Visualization Toolkit (VTK) for rendering and visualization.

#### 2.2.1.1 Components

The *AtamaiViewer* integrates many components necessary for image-guided interventions, including image registration [10], cardiac modeling [11], dynamic MRI-US image registration [12], and procedure planning [13]. Our software platform integrates the visualization of pre-operative multi-modality images with intra-operative US, endoscopic data, tracked surgical tools, haptic devices and virtual models (**Fig. 2.2**). It provides the ability to selectively combine the different imaging components and overlay them using different levels of transparency, display volumetric data on orthogonal or oblique planes, and visualize dynamic data as cine sequences synchronized with the intra-operative ECG [14]. The viewer also permits the incorporation of optical and magnetic tracking systems in a common virtual workspace for a single application, and is designed to support stereoscopic visualization. In addition, the modular design of the platform facilitates the ready addition of new components and features.

#### 2.2.1.2 Applications

A wide variety of applications have been developed within the *AtamaiViewer* environment, several relating to intracardiac image-guided surgery and therapy. These projects include 4D electro-physiology mapping for atrial fibrillation therapy [15], an

AR system for port placement [13], and registration of intracardiac 2D US to pre-operative CT or MR data [16]. The most challenging application implemented within the *AtamaiViewer* is the planning and guidance of mitral valve replacement and ASD repair.

## 2.2.2 Mixed Reality Environment

In this section we show how a series of *AtamaiViewer* components have been integrated to form a mixed reality environment used to guide minimally-invasive interventions. As much of our work has been motivated by the need for less invasive approaches to cardiac surgery, most applications have been designed and implemented in the context of the guidance and navigation of intracardiac procedures on the beating heart.

### 2.2.2.1 Intra-operative Guidance: Echocardiography

To compensate for the lack of direct vision inside the beating heart, our system primarily employs a 4 - 7.5 MHz trans-esophageal echocardiography (TEE) probe for intra-operative imaging. To further assist in visualization, a 3D trans-thoracic echocardiography (TTE) probe is also available to acquire three-dimensional images with a larger field of view. Suematsu *et al.* [2] also raised the necessity of employing 3D echocardiography as a superior technique to 2D US for guiding instruments within the beating heart. They reported their experience using only 3D US as the guidance platform in a laboratory environment, without the benefit of a virtual environment.

Based on our prior experience in intracardiac navigation, we concluded that the use of 2D TEE guidance had significant disadvantages when used as the sole modality for image guidance, even when complemented with 3D TTE. Both anatomical targets and surgical tools were poorly perceived in US images, making it virtually impossible to accurately assess their position and orientation during manipulation, especially

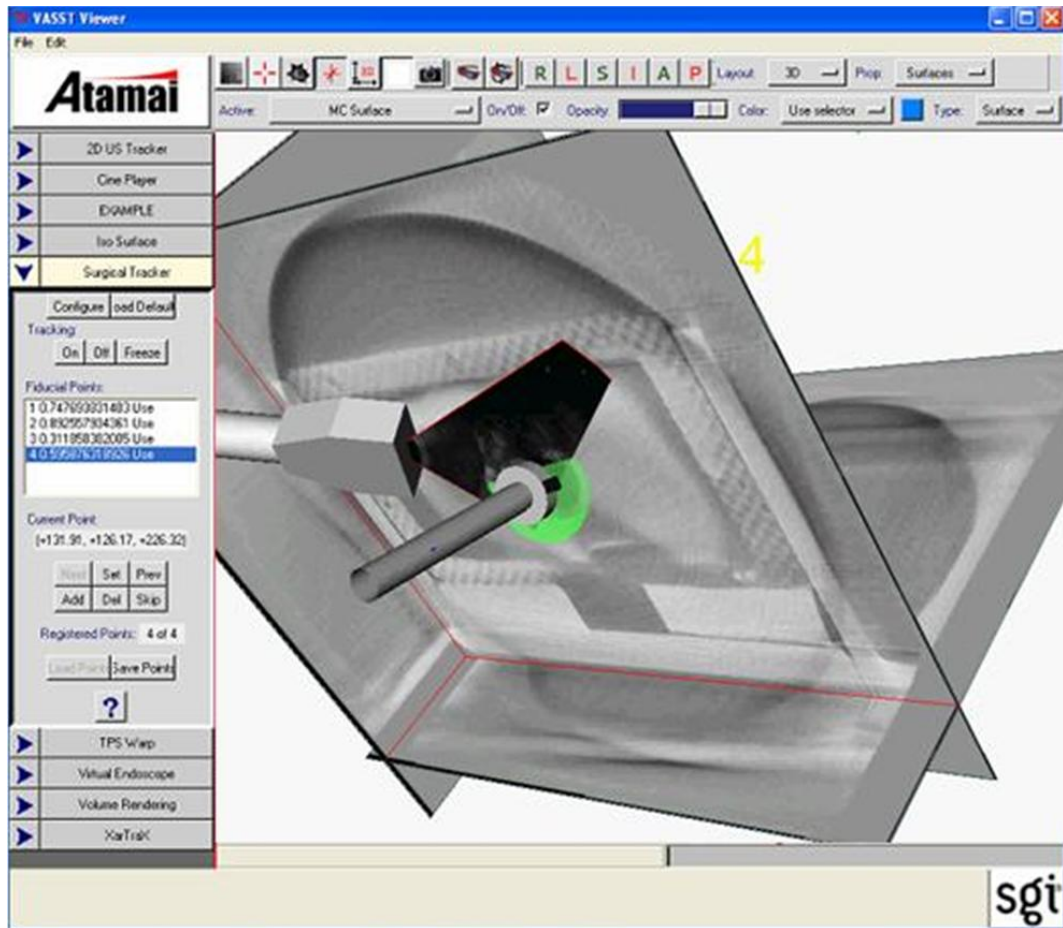


Fig. 2.2: Example image of the *AtamaiViewer* platform, showing the integration of a pre-operative model of a cardiac intervention phantom together with virtual models of a valve-insertion device, and US transducer and imaging fan.

since the 2D cross-sectional images do not provide the necessary context within the 3D cardiac anatomy. Some of the frequent questions arising during the procedure were related to whether the prosthetic valve was within the mitral orifice, or whether the valve skirt was in contact with the valve ring, and answering them was difficult even for an experienced surgical team (**Fig. 2.3**). Although 3D TEE may become a potential future solution, its limited field-of-view and lower resolution compared to 2D US may imposed further challenges in visualizing the surgical tools and target in the same volume. However, in spite of these limitations with respect to image



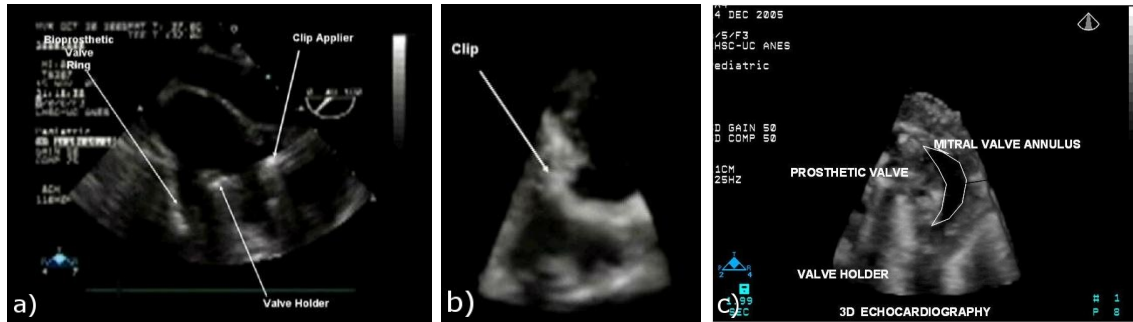


Fig. 2.3: a) 2D TEE image of the valve tool and clip applicator inside a porcine beating heart; b) 3D US image of a similar scene; c) 3D US image showing the mitral valve annulus, prosthetic valve, and valve-insertion tool. Note the difficulty to correctly interpret the anatomical features and surgical tools, especially in the limited field of view of 3D US.

guidance, the Doppler capabilities of US are ideal for assessing the interventions as a function of the blood flow through the valve and abnormalities in flow patterns, such as regurgitant flow through or around the mitral valve, or incomplete ASD repair.

To enhance intra-procedure guidance, we displayed the 2D US data within a more robust anatomical and surgical context. We integrated two main components within the *AtamaiViewer* environment: pre-operative cardiac models, as well as virtual representations of surgical tools and US probe tracked in real time, as described in the upcoming sections.

### 2.2.2.2 Pre-operative Planning and Guidance

**Cardiac Modeling:** Due to their high spatial resolution and tissue characterization, MRI and contrast-enhanced CT images are often used during the procedure planning stage to extract anatomical features of interest. These data can then be used to generate heart models that display the cardiac anatomy as 3D rendered surfaces. 3D subject-specific cardiac models can be constructed either via manual or semi-automatic segmentation or via an atlas-based approach, as described in section 1.3.2.

A similar anatomical modeling technique is described in Chapter 4 to build subject-

specific models from pre-operative 4D MR data to predict the location of dynamic surgical targets (e.g. mitral valve annulus) throughout the cardiac cycle (**Fig. 2.4**). Our models that were specific to the left ventricular myocardium (LV), the left atrium (LA), and the right atrium and ventricle (RA/RV) are accurate within  $5.0 \pm 1.0$  mm,  $4.7 \pm 0.9$  mm, and  $5.3 \pm 1.3$  mm, respectively [17].

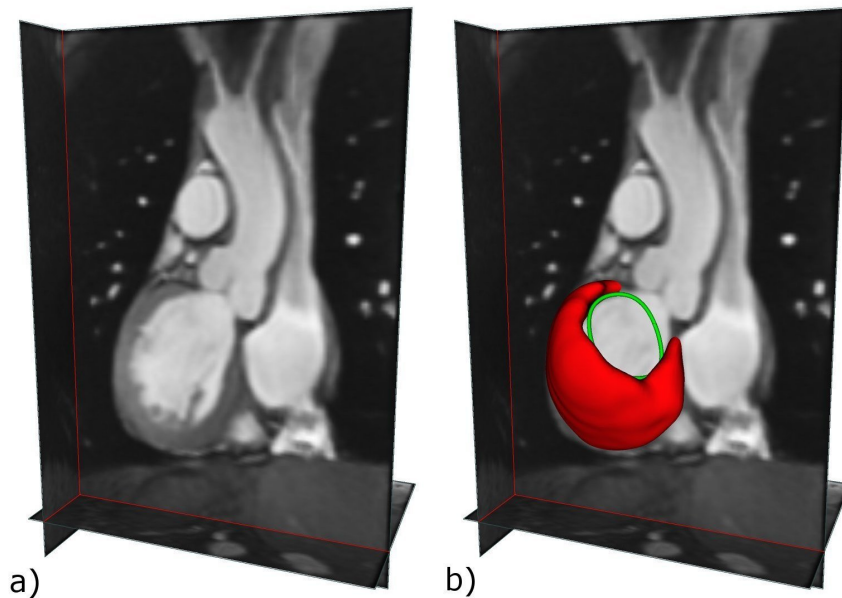


Fig. 2.4: a) Image of the prior high-resolution average heart model at mid-diastole (MD); b) Prior model at mid-diastole showing two segmented features of interest: left ventricle surface and mitral valve annulus.

**Pre- to Intra-operative Registration:** To augment the intra-operative TEE data with the pre-operative cardiac models, we employed a feature-based registration technique. This method is suitable for cardiac interventions, as the selected structures are easily identifiable in both the pre-operative and intra-operative images, and they also ensure a good alignment of the pre-operative and intra-operative surgical targets. As later described in Chapter 4, a RMS distance error of 5.2 mm, 4.1 mm, and 7.3 mm in aligning the pre-operative and intra-operative features located within 10 mm from the valvular region in each of the LV, LA and RA/RV surfaces, respectively [18].

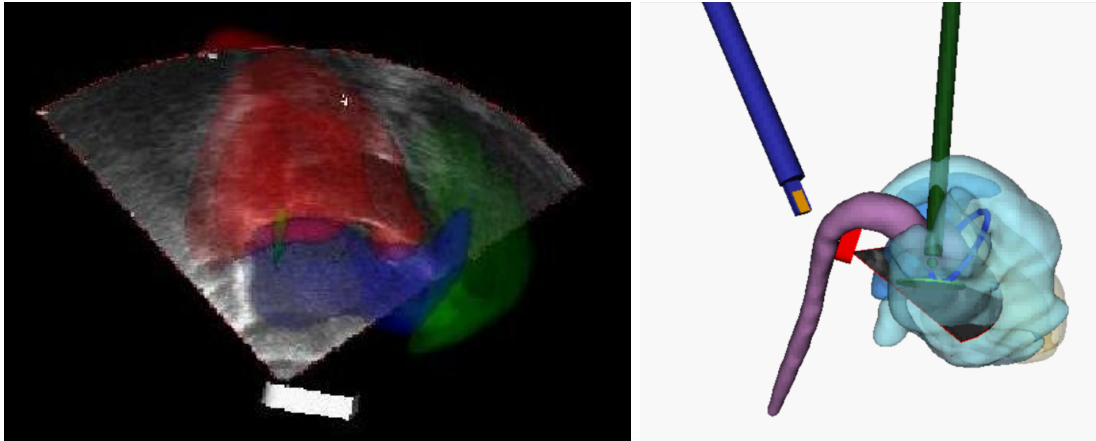


Fig. 2.5: Image showing real-time intra-operative TEE data augmented a pre-operative heart model, using the feature-based registration (left panel); Illustration of the mixed reality environment employed during an *in vivo* porcine study, showing pre-operative heart model, intra-operative TEE image, tracked TEE probe, and surgical tools (right panel).

The pre-operative modeling capabilities employed in our model-enhanced US platform not only offers the feasibility of generating sufficiently accurate models of the subject's heart prior to the procedure, but also facilitates their integration within the intra-procedure environment, leading to an accurate virtual environment for procedure planning and guidance.

### 2.2.2.3 Surgical Tool Tracking

For all off-pump intracardiac procedures, it is crucial for the surgeon to know the position and orientation of the surgical tools with respect to the target at all times during the intervention. As outlined in Chapter 1, the tracking technologies most frequently employed in image-guided therapy use an optical [19] or magnetic [20, 21, 22] approach. However, for procedures where no direct line-of-sight between the sensors mounted on the probe and the transmitting device, magnetic tracking systems are employed exclusively. Our platform employs the the NDI Aurora<sup>TM</sup> MTS. This system consists of three components: a control unit, a magnetic field generator, and miniature 5 or 6 DOF sensors fixed to the ultrasound transducer and

surgical tools.

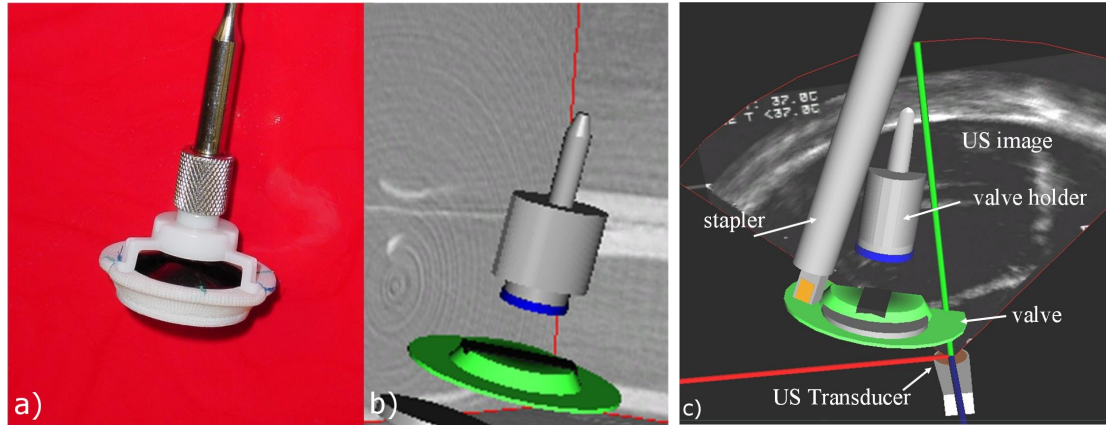


Fig. 2.6: Physical (a) and virtual (b) representation of a mechanical mitral valve attached to the valve-insertion tool; c) Illustration showing the virtual representations of a valve-guiding tool and a fastening device, together with a virtual models of the 2D TEE transducer and the 2D image fan.

As an example, for a typical mitral valve implantation procedure, three virtual objects are required: one for the TEE probe, a second for the valve-guiding tool, and a third for the valve-fastening device. Prior to the procedure, virtual models of both surgical tools and TEE transducer are created using VTK tools. **Fig. 2.6** illustrates a prosthetic valve attached to the valve-insertion tool, accompanied by its virtual representation. Similar virtual models were designed for the US probe and the valve-fastening tool. For the model of the US probe, the image plane automatically adjusts to changes in rotation angle and depth as they are manipulated by the sonographer in the OR (**Fig. 2.5**).

The *AtamaiViewer* platform has many tools for calibration of both tracked surgical tools and US transducers. The tracked US probe is calibrated using either a Z-string device [23] or a phantom-less calibration method, as described in section 2.3.1.1. The valve-guiding tool is calibrated by first defining a transform describing the position and orientation of the tool tip in patient space before the valve is attached. A similar procedure is used to calibrate the valve-fastening tool. In addition, a reference MTS

sensor is attached to a stationary region of the subject to avoid the need to recalibrate the “world” coordinate system in case of accidental motion of the subject or field generator.

## 2.3 System Evaluation and Assessment

Prior to implementing these applications in the clinic, we performed a series of tests to evaluate the surgical guiding system. Two methods for calibrating the tracked TEE transducer were evaluated, then a navigation accuracy assessment was performed, followed by a pre-clinical *in vitro* evaluation of the interventional system in the context of a mitral valve implantation procedure.

### 2.3.1 Accuracy Assessment

#### 2.3.1.1 US Calibration Accuracy

The first set of experiments was designed to evaluate and compare two commonly available calibration methods for the tracked US transducer: the Z-string phantom-based, and the phantom-less calibration approach [24]. In addition, we also described the uncertainty of the system for three US transducers commonly employed in our laboratory (TTE, adult TEE, and pediatric TEE probe), plus each of the calibration methods [25]. To achieve this goal, a point-source was localized (1.6 mm Teflon sphere) in the US image and its position was measured.

Table 2.1: Point-source localization accuracy using three different US probes and two different calibration methods. The root-mean-square (RMS) of the distance errors are provided. \*Please note that the figures presented in this table have subsequently improved following additional experiments. The updated figures are available in Wiles *et al.* [25].

US Probe	RMS Distance (mm)	
	Z-String Calibration	Phantom-Less Calibration
TTE	1.05	1.67
TEE Adult	*4.22	2.83
TEE Pediatric	2.68	2.65

Accuracy was assessed by computing the error between the measured position of the point source and its known position as determined before the experiment. The point-source localization error was estimated as the root-mean-square (RMS) of the distance between the measured and true position of the Teflon sphere. This work was performed in collaboration with another member of the laboratory, and the results are presented in detail by Wiles *et al.* [25]. For the purpose of this thesis, **Table 2.1** includes a summary of the most relevant results.

### 2.3.1.2 Surgical Navigation Accuracy

In the second set of experiments, the accuracy of the virtual reality-enhanced US guidance system was assessed from the surgeon’s point, as described by Wiles *et al.* [26]. Three surgical guidance modalities were tested: (i) 2D US image guidance only (“US only”); (ii) virtual reality guidance with tracked surgical tools (“VR only”); and (iii) 2D US image guidance augmented by virtual reality (“VR + US”). The user was asked to guide a probe tip onto a small target within a cardiac phantom. The *only* information available to the user was the US image, the VR interface, and the VR-augmented US interface for “US only”, “VR only” and “VR + US” guidance modalities, respectively. These results are summarized in **Table 2.2**.

This experiment showed that our VR-enhanced US image guidance system improved the widely used technique of intra-procedure guidance currently only relying on 2D US imaging. While both the “VR only” and “VR + US” modalities showed significantly more accurate targeting than the “US only” approach ( $p < 0.01$ ), the test showed no significant differences between the “VR + US” and “VR only” guidance modalities ( $p > 0.01$ ). The additional errors in the “VR + US” were attributed to the quality of the US images acquired with the trans-esophageal probe. It is anticipated that the “VR + US” will provide a superior solution when used in a dynamic environment such as an actual *in vivo* intracardiac procedure [26].

In addition, the “VR + US” also provides a safety feature in that the surgeon

Table 2.2: Single point localization accuracy assessment. Three users were asked to localize a point three times for each of the three modalities. A two-way analysis of variance (ANOVA) followed by Tukey’s Honestly Significantly Difference post-hoc test showed that only the modality had a significant difference in the achieved targeting accuracy. The “VR only” and “VR + US” modalities showed significantly more accurate targeting than the “US only” guidance modality ( $*p < 0.01$ ).

Modality	RMS (mm)
US Only	*5.42
VR Only	1.02
VR + US	1.47

can use real-time imaging to precisely position devices even if the initial patient-to-image registration has been affected due to organ motion or deformation during the procedure. A significant advantage of the VR-enhanced US guidance approach consists of its navigation versus positioning capabilities. The *virtual reality* components assisted the user mostly with the orientation in space and *navigation towards the surgical target*, while the *US imaging* component provided the user with critical real-time information for *performing detailed on-target manipulations*.

While these results are preliminary in nature, a comprehensive *in vitro* accuracy assessment of the model-enhanced US guidance environment is described in Chapter 3.

### 2.3.2 Pre-clinical Qualitative Evaluation: *In vitro* and *Ex vivo* Mitral Valve Implantation

The following two sets of experiments were designed to assess the success with which an experienced surgeon was able to perform the procedure using our VR-enhanced interventional system, and to compare it to the outcome of the same procedure performed under sole US image guidance. These pre-clinical studies mimicked a mitral valve implantation procedure performed in a cardiac intervention phantom, as well as in *ex vivo* porcine hearts. The surgical task consisted of guiding a prosthetic valve mounted on the valve-insertion tool to the target — the synthetic or native mitral valve annulus, respectively, positioning it correctly, and securing it in place

using a valve-fastening tool.

### 2.3.2.1 Cardiac Intervention Phantom Studies

The first set of experiments were performed on a cardiac intervention phantom (**Fig. 2.7**) built in our laboratory and similar in concept to that described by Rettmann *et al.* [27]. The phantom is made from non-magnetic materials to minimize the interference with the tracking system. A tube descends into the lower part of the phantom simulating the esophagus and facilitating the use of TEE probes. Cardiac tissue was mimicked using poly-vinyl alcohol-cryogel (PVA-C) membranes [28] supported by plexiglass plates. This phantom provides a means of assessing newly-developed intervention procedures under image-guidance in a laboratory that mimic the clinical setting, reducing the reliance on animal studies, with progress being monitored using endoscopic inspection of the target.

### 2.3.2.2 Excised Porcine Hearts Study

To confirm the limitations of US guidance and emphasize the benefits of our virtual environment for navigation while mimicking an *in vivo* setting, *ex vivo* excised porcine hearts were used in the second set of experiments, instead of PVA-C simulated cardiac tissue. The intact porcine hearts were rinsed thoroughly with saline solution and refrigerated for three days prior to the experiment.

The hearts were mounted inside the cardiac phantom and supported using plexiglass plates. To prevent any rigid body translation and rotation, the hearts were anchored in place using a 3 point support (2 lateral and 1 basal), with the apex resting freely on the bottom of the vessel. In order to simulate its *in situ* orientation during the intervention, the hearts were positioned with the left atrium facing upwards, as shown in **Fig. 2.8a**.

Intracardiac cavities were reached using the Universal Cardiac Introducer<sup>®</sup> [29], which is affixed to the left atrial appendage of the excised heart. Note that for an



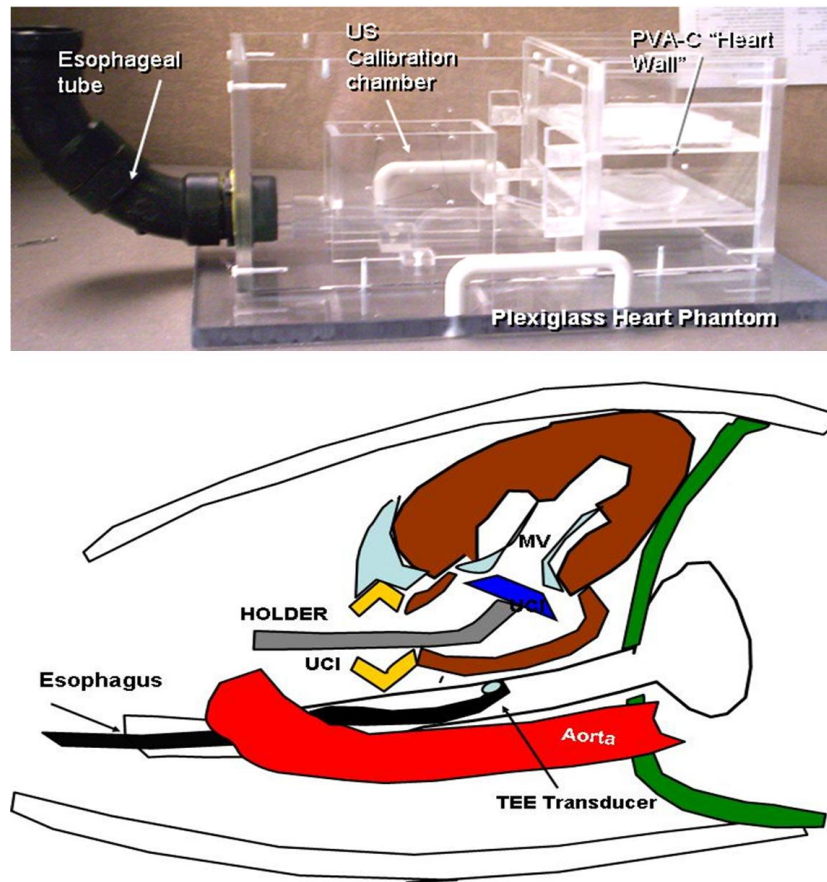


Fig. 2.7: Plexiglass cardiac intervention phantom showing the “esophagus” and PVA-C membranes mimicking the heart wall tissue (upper panel); Equivalent schematic representation of cardiac anatomy for the mitral valve implantation procedure (lower panel).

*in vivo* procedure, the beating heart would be reached via a left-anterior minithoracotomy. The UCI acts as an “air-lock” between the blood-filled cavity and the chest, allowing for the introduction and manipulation of surgical instruments inside the beating-heart with minimal blood loss [29]. The UCI is described in detail in Chapter 5 in the context of our *in vivo* beating therapy studies in animal models.

The valve implantation tasks were first attempted using US guidance alone, followed by guidance using the VR-enhanced system. The surgical target was represented by a 2 cm diameter hole in the PVA-C membrane for the trials performed on

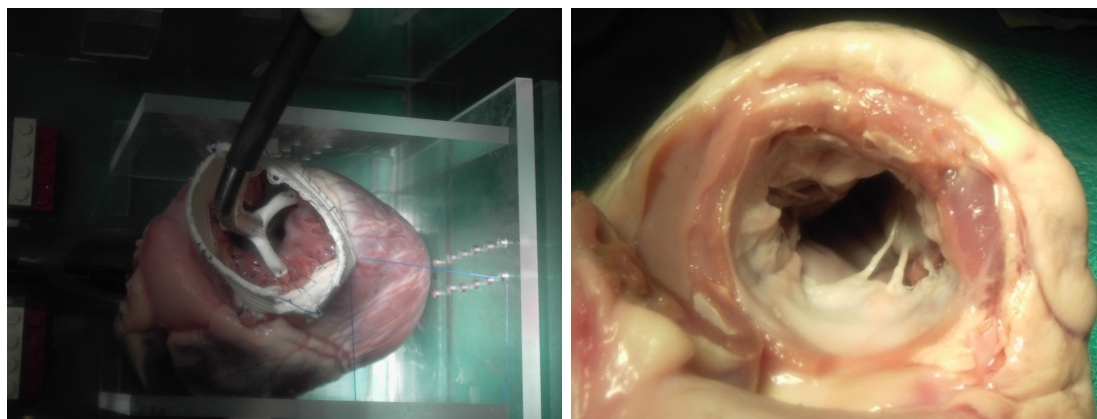


Fig. 2.8: Mounting of the excised heart inside the phantom according to experimental procedure. Note the attachment of the UCI to the heart for intracardiac access (insertion cuff already sutured attached to the left atrial appendage (left panel); Short-axis view of the native mitral valve annulus and parts of the valve leaflets attached to the chordae tendinae in an excised heart (right panel). The mitral annulus represents the target onto which the prosthetic valve must be placed and fastened during implantation.

the cardiac intervention phantom, and by the native mitral annulus for the studies performed on *ex vivo* porcine hearts. The procedure was performed by a surgeon and an echocardiographer, both with extensive experience in mitral valve interventions. All experiments were blinded, with results being recorded for retrospective analysis by an endoscope directed at the target. Intra-operative real-time 2D US images were acquired using the TEE probe descended into the cardiac phantom through the “esophageal tube”.

### 2.3.2.3 Guidance Modalities

**US Image Guidance:** Under US-guidance alone, it was very difficult to identify both the target and the surgical instruments, as well as to determine their exact position and orientation with respect to one another. As a typical observation regarding the valve placement on target in the phantom experiments, positioning that seemed to be correct proved to be several millimeters off-target in both translation and angulation (Fig. 2.9a). The “US-only procedure” was lengthy and consistently

unsuccessful; four clips were fired using the laparoscopic clip-applier, however, none of them efficiently fastened the valve skirt to the underlying membrane.

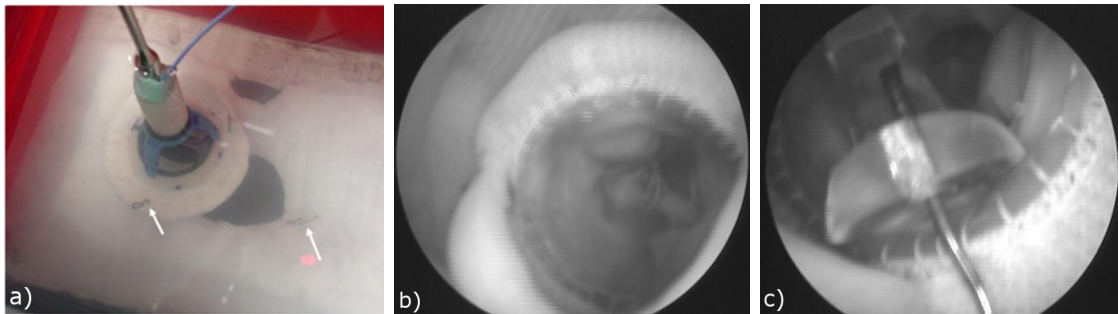


Fig. 2.9: a) Poorly implanted valve under US guidance in the cardiac phantom; b) Endoscopic view showing the valve placement under US guidance in an excised heart; c) Endoscopic view showing an incorrectly inserted fastener under US guidance in an excised heart. Arrows indicate the location of the fasteners.

Similarly, during the trials performed on the *ex vivo* porcine hearts, the 2D US images were misleading even to the experienced surgeons, causing them to rely on previous experience in the clinic. After successive trial-and-error attempts, when it was determined that the valve was in place, the endoscopic camera was employed to assess the position of the valve with respect to the anatomical target (**Fig. 2.9b**). Another endoscopic assessment followed by direct observation revealed that during valve fastening, only one pin was applied in the correct location, but with an incorrect angulation, causing a radial puncture of the ventricle wall (**Fig. 2.9c**).

**VR-Enhanced US Guidance:** In addition to the virtual representations of the tracked TEE transducer and surgical instruments (valve-guiding and valve-fastening devices), our virtual environment also integrated pre-operative “anatomy”, which consisted of an automatically segmented surface model of the cardiac intervention phantom extracted from a CT image acquired prior to the experiments. A virtual target (a 2 cm diameter spline) was interactively reconstructed from the 2D US images by sweeping the tracked US fan across the “mitral annulus” and displayed within the

volume. The “surgical environment” was displayed stereoscopically using HMD units, providing the surgeons with a better spatial perception of the virtual space.

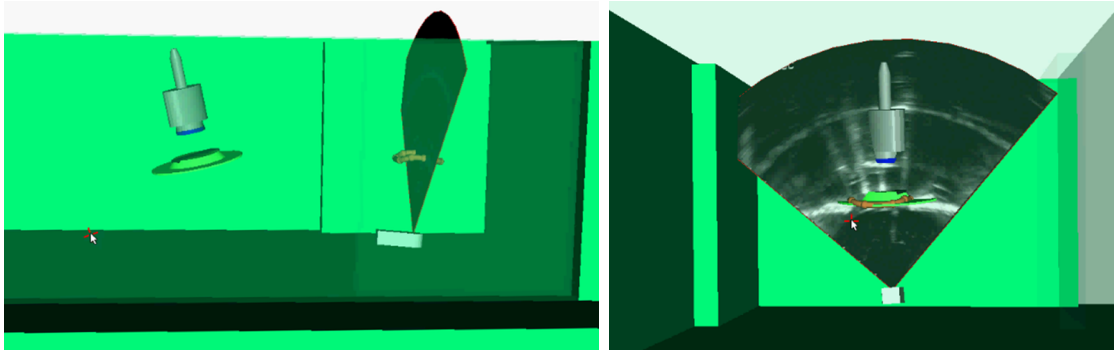


Fig. 2.10: Navigation of the valve-guiding tool toward the defined mitral valve annulus under virtual reality-assisted guidance (left panel), followed by on-target positioning of the valve guiding tool under real-time 2D TEE imaging (right panel).

After displaying the 2D echo images within the context of the 3D “pre-operative anatomy”, navigation of the valve towards the target became almost trivial. The surgeon guided the valve to the target with very little difficulty, relying mainly on the virtual environment. 2D US guidance was employed only to refine the position of the valve and confirm its final correct placement on target. **Fig. 2.10a** illustrates the navigation of the valve-guiding tool toward the defined surgical target by means of the virtual model and magnetically tracked instrument models. Following navigation, the valve-guiding tool was positioned onto the annulus under US image guidance (**Fig. 2.10b**). The real-time imaging capabilities enabled the user to refine the valve positioning on target prior to fastening.

The procedure was finalized by securing the valve in place, using a valve-fastening device. After determining its location in space with respect to the valve, the fastening tool was guided towards the target using the virtual models. Its positioning on target was refined using real-time 2D US and then the clips were applied at multiple locations around the valve skirt (**Fig. 2.11a**).

Guiding the valve to the mitral annulus in the excised hearts using model-enhanced

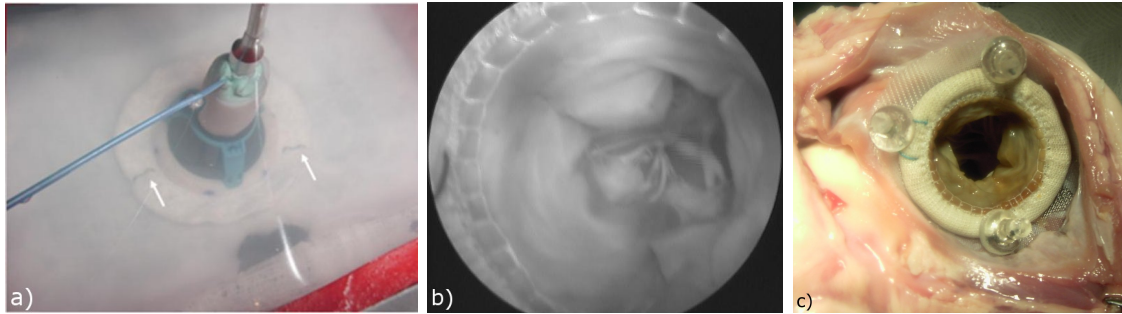


Fig. 2.11: a) Correct valve implantation under model-enhanced US guidance in the cardiac phantom; b) Endoscopic image showing the appropriate positioning (also confirmed by the clear view of the chordae tendinae) of the valve onto the native mitral annulus of an excised heart using US guidance augmented by the VR environment; c) Post-procedure image showing the correct location of the fasteners (push-pins delivered by an instrument consisting of a 6 mm diameter tube custom-developed for initial proof-of-concept) around the valve achieved under US-VR guidance in an excised heart.

US was also a relatively simple task, and again, once on target, the valve positioning was fine-tuned according to the real-time US images. The outcome of the procedure was confirmed by an endoscopic evaluation (**Fig. 2.11b**). Furthermore, the surgeon found it much easier to navigate the tip of the valve-fastening tool to the final target, and then refine its position on target based on the TEE images. Four pins were used to fasten the valve to the underlying tissue, and according to the post-procedure assessment, three of them securely attached the valve (**Fig. 2.11c**), while the fourth pin, although properly located, did not entirely penetrate into the mitral annulus tissue.

## 2.4 Discussion

This paper presents the global architecture of our surgical platform, together with various integrated components, resulting in a complete virtual surgical environment that surgeons can use to plan and guide procedures in the absence of direct vision. These applications emphasize its advantages in assisting with both the navigation

and surgical instrument manipulation inside the beating heart.

Two-dimensional TEE plays a significant role in our interventional system as it provides the operator with real-time intra-procedure information. Nevertheless, these 2D images are ineffective for identifying the position and orientation of surgical tools with respect to the target. Although 3D US may provide images that are easier to interpret, most of these transducers are too large to fit within the esophagus and they also provide a narrow field of view.

To “zoom out” away from the surgical target region and see the “bigger picture”, we augmented 2D intra-procedure imaging with pre-operative models of the heart that provide anatomical context and better spatial orientation. These models can accurately predict the location of the surgical target and can be easily fused with the intra-operative images using a feature-based registration technique. Ultimately, the environment was complemented with virtual representations of the surgical instruments tracked in real-time during the intervention, generating a reliable system for intra-procedure guidance.

To better mimic the environment specific to a real procedure, in addition to the experiments performed in the laboratory, we conducted similar studies on the cardiac intervention phantom in the operating room. These investigations allowed us to identify some of the limitations imposed by the clinical environment which we expected to encounter during *in vivo* interventions.

The implications of using an MTS in the OR are two-fold. First, the “surgical field” must be located within the optimal tracking volume of the field generator to ensure accurate tracking, yet without interfering with the surgical workflow. Secondly, the presence of ferromagnetic objects near the field generator must be avoided [22]. Consequently, this requirement implies also that all surgical instruments must be manufactured from non-ferromagnetic alloys (e.g. high-grade stainless steel or plastic) to minimize tracking error.

Additional constraints are imposed by the size of the surgical instruments used in

the intervention. In our applications, intracardiac cavities are accessed through the left atrial appendage, using the UCI. A potential challenge regarding the instrument size may be reflected in the surgeon's dexterity in maneuvering the valve-insertion and valve-fastening tool not only inside the the UCI, but also within the heart itself. As a concrete example, a slightly larger prosthetic mitral valve may be difficult to insert through the small orifice between the left atrial appendage and the left atrium. Moreover, the valve-fastening device should ideally be situated above the prosthetic valve at all times, as it is used to attach the valve skirt to the mitral annulus.

As our technique constitutes a novel approach to surgery, it is important that the interference with the clinical staff and procedure workflow is minimized. The footprint of our system in the OR is limited to a computer workstation located several meters away from the OR table, and the MTS. Cables are needed to connect the various components: the tracked tools and field generator to the MTS, the ECG and video capture (from the US machine) to the computer, and the computer to either an overhead monitor or to HMD units.

The challenges outlined here represent an initial subset of limitations identified following our preliminary implementation and evaluation of the model-enhanced US guidance environment. Over the course of the upcoming chapters, these challenges, in addition to other emerging caveats associated with the other aspects of the project, will be covered. Ultimately, a full discussion of the lessons learned, presented in the context of the existent literature, will be included in Chapter 7.

## 2.5 Conclusions

To conclude, this initial work has demonstrated the tremendous potential of multi-modality imaging combined with surgical tool tracking for providing the capability to both visualize and assess the surgical intervention in a manner that will ultimately be superior to direct vision, within its inherent limitations. Augmented with US

imaging for real-time guidance for on-target manipulations, and pre-operative cardiac models for anatomical context and spatial orientation for navigation to target, according to our preliminary implementation, our system provides extensive support for target identification, intracardiac route planning, and guidance for direct therapeutic interventions. These key features of the surgical guidance environment will be emphasized in the upcoming chapters, demonstrating the capabilities of this surgical platform toward enabling sufficiently accurate targeting accuracy (Chapter 3), providing enhanced surgical navigation (Chapter 4), and yielding clinically-acceptable surgical outcomes (Chapter 5).



## References

- [1] L. von Segesser, P. Tozzi, M. Augstburger, and A. Corno. Working heart off-pump cardiac repair (OPCARE)—the next step in robotic surgery? *Interact Cardiovasc Thorac Surg.*, 2:120–124, 2003.
- [2] Y. Suematsu, G. R. Marx, J. A. Stoll, P. E. Dupont, R. O. Cleveland, R. D. Howe, J. K. Triedman, T. Mihaljevic, B. N. Mora, B. J. Savord, I. S. Salgo, and P. J. del Nido. Three-dimensional echo-guided beating-heart surgery without cardiopulmonary bypass: a feasibility study. *J Thorac Cardiovasc Surg.*, 128:579–87, 2004.
- [3] E. R. McVeigh, M. A. Guttman, R. J. Lederman, M. Li, O. Kocaturk, T. Hunt, S. Kozlov, and K. A. Horvath. Real-time interactive MRI-guided cardiac surgery: Aortic valve replacement using a direct apical approach. *Magn Reson Med.*, 56:958–64, 2006.
- [4] S. W. Downing and L. H. Edmunds. Release of vasoactive substances during cardiopulmonary bypass. *Ann Thorac Surg.*, 54:1236–43, 1992.
- [5] M. Hastenteufel, S. Yang, C. Christoph, M. Vetter, H. Meinzer, and I. Wolf. Image-based guidance for minimally invasive surgical atrial fibrillation ablation. *Int J Med Robotics Comput Assist Surg*, 2:60–69, 2006.
- [6] J. Dong, T. Dickfeld, D. Dalal, A. Cheema, C. Vasamreddy, C. Henrikson, J. Marine, H. Halperin, R. Berger, J. Lima, D. Bluemke, and H. Calkins. Initial experience in the use of integrated electroanatomic mapping with three-dimensional MR/CT images to guide catheter ablation of atrial fibrillation. *J Cardiovasc Electrophysiol.*, 17:459–466, 2006.
- [7] S. DeBuck, A. Maes, J. Ecto, J. Bogaert, S. Dymarkowski, H. Heidbchel, and P. Suetens. An augmented reality system for patient-specific guidance of cardiac catheter ablation procedures. *IEEE Trans Med Imaging*, 24:1512–1524, 2005.
- [8] K. Rhode, D. Hill, P. Edwards, J. Hipwell, D. Rueckert, G. Sanchez-Ortiz, S. Hegde, V. Rahunathan, and R. Razavi. Registration and tracking to inte-

- grate X-Ray and MR images in an XMR facility. *IEEE Trans Med Imaging*, 22:1369–1378, 2003.
- [9] P Milgram, H. Takemura, A. Utsumi, and F. Kishino. Augmented reality: A class of displays on the reality-virtuality continuum. In *Proc. SPIE 1994: Telemanipulator and Telepresence Technology*, volume 2351, pages 282–92, 1994.
- [10] G. A. Turgeon, G. Lehmann, G. M. Guiraudon, M. Drangova, D. W. Holdsworth, and T. M. Peters. 2D-3D registration of coronary angiograms for cardiac procedure planning and guidance. *Medical Physics*, 32:3737–49, 2005.
- [11] M. Wierzbicki, M. Drangova, G. M. Guiraudon, and T. M. Peters. Validation of dynamic heart models obtained using non-linear registration for virtual reality training, planning, and guidance of minimally invasive cardiac surgeries. *Med Image Anal.*, 8:387–401, 2004.
- [12] X. Huang, N. Hill, J. Ren, G. M Guiraudon, and T. M. Peters. Dynamic 3D ultrasound and MRI image registration of the beating heart. In *Proc. of Med Image Comput Comput Assist Interv.*, volume 3750 of *Lect Notes Comput Sci.*, pages 171–78, 2005.
- [13] J. Marmurek, C. Wedlake, U. Pardasani, R. Eagleson, and T. M. Peters. Image-guided laser projection for port placement in minimally invasive surgery. In *Proc. of Medicine Meets Virtual Reality*, volume 119 of *Stud Health Technol Inform.*, pages 367–72, 2006.
- [14] J Moore, G. M. Guiraudon, D. L. Jones, Hill N., Wiles A. D., D. Bainbridge, C. Wedlake, and Peters T. M. 2D ultrasound augmented by virtual tools for guidance of interventional procedures. In *Proc. of Medicine Meets Virtual Reality*, volume 125 of *Stud Health Technol Inform.*, pages 322–27, 2007.
- [15] K. Wilson, G. Guiraudon, D. Jones, and T. Peters. 4D shape registration for dynamic electrophysiological cardiac mapping. In *Proc. of Med Image Comput Comput Assist Interv.*, volume 4191 of *Lect Notes Comput Sci.*, pages 520–526, 2006.
- [16] X. Huang, N. Hill, J. Ren, G. Guiraudon, and T. Peters. Intra-cardiac 2D US to 3D CT image registration. In *Medical Imaging 2007: Visualization and Image-Guided Procedures*, volume 6509 of *Proc. of SPIE.*, pages 65092E–8, 2007.
- [17] M. Wierzbicki, J. Moore, M. Drangova, and T. M. Peters. Subject-specific models for image-guided cardiac surgery. *Phys Med Biol.*, 53:5295–312, 2008.
- [18] C. A. Linte, M. Wierzbicki, J. Moore, G. M. Guiraudon, D. L. Jones, and T. M. Peters. On enhancing planning and navigation of beating-heart mitral valve

- surgery using pre-operative cardiac models. In *Proc. of IEEE Eng Med Biol Soc.*, pages 475–78, 2007.
- [19] A. D. Wiles, D. G. Thompson, and D. D. Frantz. Accuracy assessment and interpretation for optical tracking systems. In *Proc. SPIE Medical Imaging 2004: Visualization, Image-Guided Procedures and Display*, volume 5367, pages 421–32, 2004.
- [20] W. Birkfellner, F. Watzinger, F. Wanschitz, R. Ewers, and H. Bergmann. Calibration of tracking systems in a surgical environment. *IEEE Trans Med Imaging*, 17:737–42, 1998.
- [21] J. B. Hummel, M. R. Bax, M. L. Figl, Y. Kang, C. Maurer Jr., W. W. Birkfellner, H. Bergmann, and R. Shahidi. Design and application of an assessment protocol for electromagnetic tracking systems. *Med Phys.*, 32:2371–9, 2005.
- [22] C. Nafis, V. Jensen, L. Beauregard, and P. Anderson. Method for estimating dynamic EM tracking accuracy of surgical navigation tools. In *Proc. SPIE Medical Imaging 2006: Visualization and Image-Guided Procedures*, volume 6141, pages 61410K–16, 2006.
- [23] D. G. Gobbi, R. M. Comeau, and T. M. Peters. Ultrasound probe tracking for real-time ultrasound/MRI overlay and visualization of brain shift. In *Lecture Notes in Computer Science*, volume 1679 of *Proc. of Med Image Comput Comput Assist Interv.*, pages 920–927, 1999.
- [24] A. Khamene and F. Sauer. A novel phantom-less spatial and temporal ultrasound calibration method. In *Proc. of Med Image Comput Comput Assist Interv.*, volume 3750 of *Lect Notes Comput Sci.*, pages 671–78, 2004.
- [25] A. D. Wiles, C. A. Linte, J. Moore, C. Wedlake, and T. M. Peters. Object identification accuracy under ultrasound enhanced virtual reality for minimally invasive cardiac surgery. In *Medical Imaging 2008: Visualization, Image-Guided Procedures and Modeling*, volume 6918 of *Proc. of SPIE.*, 2008 - In Press.
- [26] A. D. Wiles, G. M. Guiraudon, J. Moore, C. Wedlake, C. A. Linte, D. L. Jones, D. Bainbridge, and T. M. Peters. Navigation accuracy for an intracardiac procedure using virtual reality-enhanced ultrasound. In *Medical Imaging 2007: Visualization and Image-Guided Procedures*, volume 6509 of *Proc. of SPIE*, pages 61410W–10, 2007.
- [27] M. E. Rettmann, D. R. Holmes, Y. Su, B. M. Cameron, J. J. Camp, D. L. Packer, and R. A. Robb. An integrated system for real-time image-guided cardiac catheter ablation. In *Proc. of Medicine Meets Virtual Reality*, volume 119 of *Stud Health Technol Inform.*, pages 455–60, 2006.

- [28] K. J. M. Surry, H. J. B. Austin, A. Fenster, and T. M. Peters. Poly(vinyl alcohol) cryogel phantoms for use in ultrasound and MR imaging. *Physics in Medicine and Biology*, 49:5529–46, 2004.
- [29] G. Guiraudon, D. Jones, D. Bainbridge, and T. Peters. Mitral valve implantation using off-pump closed beating intracardiac surgery: a feasibility study. *Interact Cardiovasc Thorac Surg.*, 6:603–607, 2007.

## Chapter 3

# Quantitative Evaluation of the Model-Enhanced Ultrasound-Assisted Guidance Environment

*Here we present a comprehensive in vitro evaluation of the our model-enhanced ultrasound guidance environment by simulating clinically relevant interventions on a cardiac phantom. We model therapy delivery simulating blinded, closed-chest, beating heart interventions performed via either direct or percutaneous intracardiac access. Our results demonstrate that the model-enhanced ultrasound guidance environment provides a clinically-desired targeting accuracy of under 3 mm, and maintains this*

---

This chapter is adapted from Linte CA, Moore J, Wedlake C and Peters TM. Evaluation of Model-Enhanced Ultrasound-Assisted Interventional Guidance in a Cardiac Phantom. *IEEE Transactions on Biomedical Engineering*. In Press: 2010. DOI: 10.1109/TBME.2010.2050886. ©2010 IEEE. Reprinted, with permission, from IEEE. Portions of this work also appeared in Linte CA, Moore J, Wiles AD, Wedlake C and Peters TM. Targeting accuracy under model-to-subject misalignments in model-guided cardiac surgery. *Proc. Med Image Comput Comput Assist Interv. (MICCAI). Lect Notes Comput Sci*. 5761:361-8. 2009 and Linte CA, Wiles AD, Moore JT, Wedlake C and Peters TM. Virtual reality-enhanced ultrasound guidance for atrial ablation: In vitro epicardial study. *Proc. Med Image Comput Comput Assist Interv. (MICCAI). Lect Notes Comput Sci*. 5242:644-51. 2008.

*level of accuracy independent of model-to-subject misregistrations typically encountered during the actual procedures. These studies emphasize the direct benefit of integrating real-time imaging with intra-operative model-assisted navigation for therapy guidance, as a means to facilitate tool-to-target navigation challenges in absence of direct vision, especially under misalignments resulting due to limited registration accuracy in the clinic.*

### **3.1 Introduction**

Prior to performing an intervention, diagnostic images of the patient are reviewed off-line, and together with pre-operative images, are used to plan the procedure. It is also commonly assumed that these images represent the intra-operative morphology with sufficient fidelity to enable adequate therapy guidance [1]. Nevertheless, cardiac therapy remains a challenging problem for image guidance due to the complex soft-tissue structure and motion of the heart, and consequently due to the limited accuracy achieved when modeling the intra-operative heart from pre-operative data. Therefore, real-time intra-operative visualization is critical to enable minimally invasive beating heart therapy.

In response to these challenges associated with visualization and guidance during minimally invasive cardiac procedures, we have developed an interventional guidance platform that relies on multi-modality medical imaging for surgical navigation manipulation of intracardiac structures in absence of direct vision [2, 3]. As described in Chapter 2, our platform integrates trans-esophageal echocardiography (TEE) for real-time visualization, augmented with pre-operative models of the cardiac anatomy, and virtual representations of the surgical instruments tracked in real time using magnetic tracking technologies [4]. The end result is a *model-enhanced ultrasound surgical guidance environment* — one of the first attempts toward bridging diagnosis and surgical planning with interventional guidance, allowing the 2D intra-operative

ultrasound US data to be interpreted within the 3D anatomical context provided by the pre-operative models [5].

However, before any novel image guidance platform is translated into the operating room, a robust quantitative assessment of its surgical navigation capabilities is critical. To perform a true surgical accuracy assessment, precise knowledge of both the surgical tool and target locations is required. While an *in vivo*, beating heart assessment is preferred, it would entail a very invasive process of implanting tracked targets inside the *in vivo* myocardium of an animal model, closing up the thoracic cavity, acquiring the necessary pre-operative images, and ultimately performing the procedure. As a trade-off, several groups have resorted to the use of representative phantoms to simulate *in vitro* clinical procedures *in vitro* for image guidance evaluation [6, 7, 8, 9, 10]. We have also used various phantoms to conduct qualitative assessments of the model-enhanced US guidance environment in the context of mitral valve implantation as described in Chapter 2, both *in vitro* in tissue mimicking poly-vinyl alcohol cryogel phantoms [11] and *ex vivo* in excised porcine hearts [2].

The work described here complements our previous studies [2, 4, 12] described in Chapter 2 and presents an *in vitro* quantitative evaluation of the surgical feasibility of our model-enhanced US guidance system. To overcome the difficulties of an *in vivo* intracardiac accuracy study, while maintaining its clinical relevance, we model our experiments in the context of blinded closed-chest beating heart interventions. We use a beating heart phantom to simulate closed-chest epicardial and endocardial procedures, where the “sites to be treated” are reached either via direct access, using rigid laparoscope-like instruments, or via transluminal access, by means of a steerable catheter. During the surgical planning stage, the targets are identified and marked onto the pre-operative cardiac model, which is then integrated into the intra-operative visualization environment to assist with surgical guidance. The “surgical task” consists of guiding a tracked surgical instrument (i.e. a rigid pointer tool or a steerable catheter) to specific targets under guidance provided via model-enhanced US.

We evaluate the performance of our model-enhanced US guidance platform by comparing the resulting targeting accuracy and procedure duration to those achieved under two other guidance modalities: endoscopic and US image guidance. The former modality may be employed for epicardial procedures, but conventional endoscopic imaging cannot provide visualization inside the blood-filled cavities of the beating heart [13]. Nevertheless, for the purpose of our study, endoscopic imaging constitutes a control modality, one that resembles guidance under direct vision. The latter guidance approach, US imaging, represents a clinically-established modality typically employed for cardiac interventional monitoring and guidance. In addition, to better replicate the clinical challenges associated with inaccuracies introduced during the model-to-patient registration [14, 15, 16], we also evaluate the efficacy of model-enhanced US guidance in presence of misregistrations between the physical and virtual phantom model. We hypothesize that model-enhanced US-assisted guidance improves targeting accuracy to a less than 3 mm targeting error and results in shorter procedure duration than real-time 2D US image guidance alone. We also expect the novel environment to enable consistent targeting accuracy under model-to-subject misregistrations, leading to overall lower targeting errors than those achieved under model-guided or US-guided therapy alone.

## 3.2 Materials and Methods

### 3.2.1 Experimental Design

To simulate cardiac anatomy *in vitro*, we used a realistic beating heart phantom (The Chamberlain Group, Great Barrington, MA, USA), which exhibits similar characteristics to both human and porcine hearts, with a highly detailed exterior, and comparable size, anatomy and movement patterns. The phantom is driven by a pneumatic actuator which allows heart rates of 60, 90 and 120 beats per minute. In



addition, the phantom features sufficiently acceptable echogenic properties to mimic US imaging of a typical human/porcine heart, and also enables the extraction of high-fidelity models from CT image datasets (**Fig. 3.1**).

The original phantom underwent a series of modifications to suit the study design. Ten CT-visible fiducial markers (3.2 mm diameter fiducials) were attached on the epicardial surface of the phantom to assist with the model-to-phantom registration. Four 3.2 mm CT and US visible Teflon spheres representing the surgical targets were attached to the epi- and endocardial surfaces of the phantom. The former setup

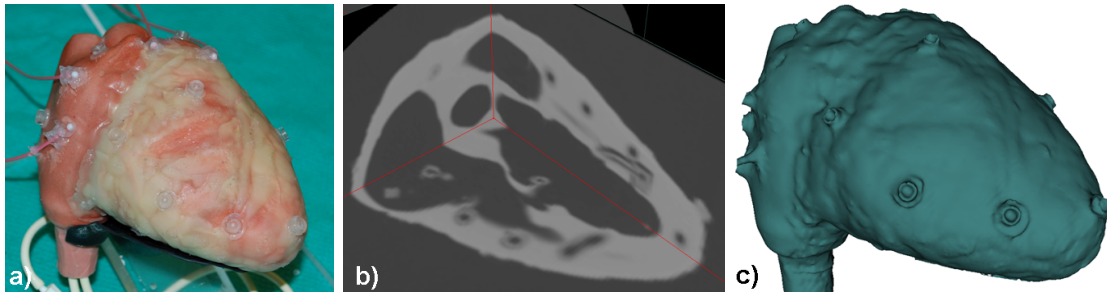


Fig. 3.1: a) Beating heart phantom showing fiducial markers used for world registration and Teflon spheres representing surgical targets; b) Ortho-plane display showing 3D CT volume of cardiac phantom and (c) corresponding surface model.

was designed to simulate a direct-access, laparoscopic targeting of epicardial sites under closed-chest conditions, where the surgical targets were embedded into the epicardial surface of the phantom (section 3.2.3.1). The latter setup was designed to mimic intracardiac therapy, where endocardial targets embedded within the endocardial right atrial wall of the phantom were accessed via a tracked steerable catheter (sections 3.2.3.2 and 3.2.3.4).

### 3.2.2 Visualization and Navigation Environment

During the planning stage of a typical procedure, the clinician employs pre-operative images to identify the surgical targets and associate them with a pre-operative model of the patient's heart. During the intervention, the pre-operative

model featuring the surgical targets is registered to the patient using a feature-based approach [16, 17] and used alongside intra-operative US to guide the intervention. Similarly, here we generate a dynamic model of the phantom from a 4D CT dataset, register the model to its physical counterpart, and complement the environment with virtual representations of the tracked tools and US probe.

### 3.2.2.1 Pre-operative Imaging and Modeling

A pre-operative dynamic image dataset of the cardiac phantom was acquired on a 64 Slice LightSpeed VCT scanner (General Electric, Milwaukee, WI, USA). The image acquisition was gated at a heart rate of 60 beats per minute, and 20 cardiac volumes (0.48 mm x 0.48 mm x 1.25 mm) were acquired depicting the heart at 20 phases over the cardiac cycle.

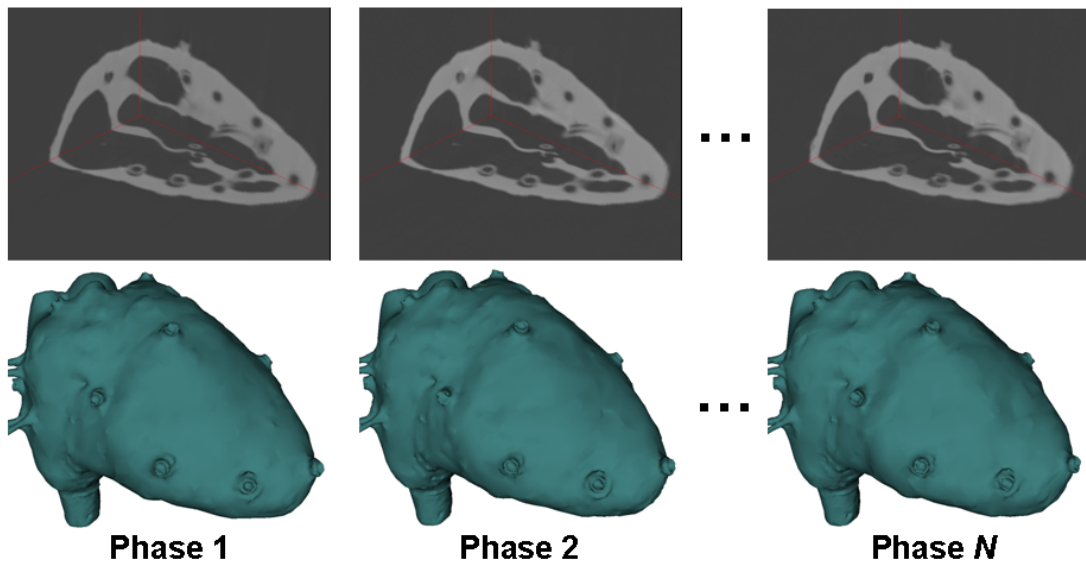


Fig. 3.2: Upper panels show tri-planar views of the CT volume of the phantom at different cardiac phases, while the lower panels show the corresponding surface-rendered view at each cardiac phase.

Using automatic segmentation tools available in the Vascular Modeling Toolkit (<http://www.wmtk.org>), we reconstructed virtual models of the phantom at each

cardiac phase (**Fig. 3.2**). A pre-operative, dynamic model of the beating heart phantom displaying the motion of the surgical targets was obtained by rendering the surface sequence in cine mode for dynamic visualization.

### 3.2.2.2 Intra-operative Imaging

Real-time imaging is critical for intra-operative guidance, and thanks to its excellent real-time capabilities and OR compatibility, US imaging, and specifically TEE, is extensively used in cardiac interventional guidance. In the clinic, the probe is inserted in the esophagus and manipulated by the echocardiographer; similarly, we employed the Philips 2D TEE transducer, imaging the phantom from above, enabling acquisition of different views. As mentioned in Chapter 2, a distinct feature of our surgical platform is the ability to acquire *tracked 2D US* images in real-time. The TEE probe is tracked magnetically, enabling the display of the acquired 2D images relative to the pre-operative anatomy and virtual tool representations.

### 3.2.2.3 Surgical Tracking

Surgical tracking is an essential component of any intra-operative image-guidance system. For procedures performed inside the human body, with non-rigid instruments and no direct line-of-sight between the sensors mounted on the probe and the transmitting device, magnetic tracking systems [18, 19] need to be employed [18, 20, 21].

For all experiments presented here, we employ the NDI Aurora<sup>TM</sup> MTS. The surgical instruments (i.e. the pointer tool and steerable catheter) are tracked using 6 DOF magnetic sensors rigidly attached close to the tips of the tools. Similarly, the US transducer is tracked using a 6 DOF magnetic tracking sensor fixed to the head of the probe. In addition to tracking the surgical instruments and the US transducer, in these experiments we also track the surgical targets, using 5 DOF magnetic sensors rigidly embedded within each Teflon sphere. The coordinates reported by the tracking system were treated as the dynamic ground truth locations of the surgical targets.

Following the attachment of the magnetic sensors, each tracked instrument was calibrated to identify the rigid transform between the instrument and the attached magnetic sensor. While the Teflon spheres only required a tool-tip calibration, the pointer and catheter were calibrated with respect to their tool-tip position as well as orientation. The US transducer was calibrated using a Z-string approach [22, 23], where the probe-to-sensor transform is determined using a least-square fit between the coordinates of a set of points identified in the acquired US images and their known, gold-standard coordinates in tracking space.

### 3.2.3 Simulating *in vitro* Therapy Delivery

#### 3.2.3.1 Direct Access Closed-Chest Navigation

This study simulated a minimally invasive intervention where epicardial targets are accessed using laparoscopic-like instruments. The cardiac phantom equipped with the tracked epicardial Teflon spheres was submerged in a water bath to enable US image acquisition (**Fig. 3.3**). The “surgical setup” was blinded to the user to mimic a closed-chest intervention where surgeons would not have access to direct target visualization. Rather, the users only relied on the use of various visualization modalities to assist them with the performance of the surgical task — placing the tip of the pointer in contact with the sphere.

Both expert clinicians and novice users conducted the *in vitro* procedure on four surgical targets. Each target was randomly approached 3 times by each user under each guidance modality: endoscopic visualization, US image guidance alone, and model-enhanced US guidance. Prior to data acquisition, each user was allotted a short time to become accustomed to the performance of the surgical task under each visualization modality. The procedure outcome was assessed according to the accuracy and duration of each “therapeutic” trial.

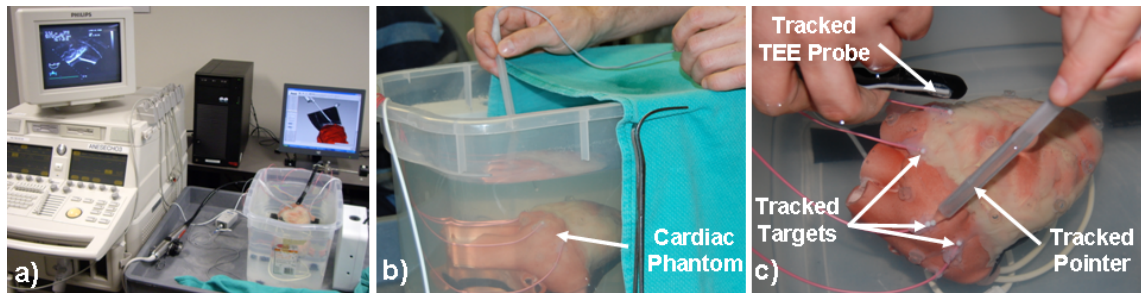


Fig. 3.3: Experimental setup simulating direct-access procedures: a) *in vitro* anatomy (heart phantom), magnetic tracking system, US scanner, and data acquisition system; b) Heart phantom submerged in a water bath showing the user navigate a rigid pointer to selected epicardial targets; c) Endoscopic snapshot of the “surgical field” inside the “closed-chest” showing the tracked pointer probing the phantom surface under TEE visualization.

### 3.2.3.2 Endocardial Catheter Navigation

A wide range of intracardiac interventions employ catheters guided to the surgical sites under real-time imaging. To simulate intracardiac therapy, the surgical targets (i.e. tracked Teflon spheres) were embedded within the right atrial endocardial wall (**Fig. 3.4**). Their locations were carefully chosen in consultation with a cardiac surgeon to represent clinically relevant sites, and be readily reached with the modified steerable catheter. We employed a unidirectional steerable Medtronic CryoCath 7F catheter (Medtronic Inc., Denver, USA), modified by attaching a 6 DOF magnetic sensor near its tip, as described in section 3.2.2.3.

Each user was prompted to approach the targets in an arbitrarily generated order, ensuring that each target was approached four times under three different guidance modalities: endoscopic visualization, US imaging alone, and model-enhanced US guidance. Similar to the previous experiment, prior to acquiring the measurements, each user was allowed a short training period to become accustomed to the surgical visualization and navigation environment.

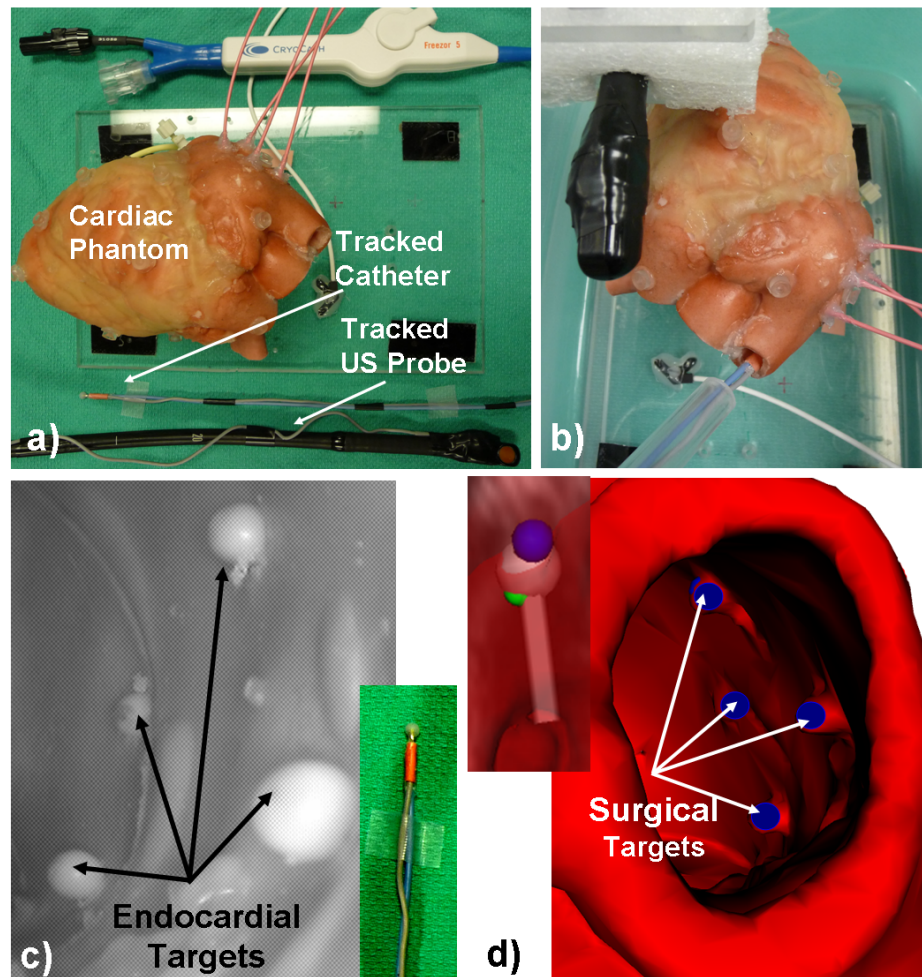


Fig. 3.4: a) Components and experimental setup (b) of the apparatus used to simulate catheter-driven endocardial procedures; c) Endoscopic image inside the right atrium showing embedded surgical targets and magnetically tracked catheter; d) View inside the right atrium showing the surgical targets identified pre-operatively and a virtual representation of the catheter tip.

### 3.2.3.3 Intra-operative Guidance Modalities

Three distinct visualization modalities were used to perform the surgical task in each experiment: endoscopic visualization — employed as a positive control, resembling direct vision; US imaging — an intra-operative imaging modality commonly employed in interventional guidance; and model-enhanced US guidance — the newly

developed guidance environment under evaluation.

**Endoscopic Guidance:** To establish a baseline with respect to the procedure outcome when comparing different visualization modalities, we used a standard surgical endoscope (Intuitive Surgical, Sunnyvale, USA) as a guidance modality mimicking direct vision. The endoscopic video feed provided a realistic appearance of the surgical field, allowing simultaneous visualization of the epi- or endocardial phantom surface, surgical targets, and pointer or catheter tip.

For the first study mimicking direct-access epicardial procedures, the device was mounted above the phantom, providing an entire perspective view of the surgical field (**Fig. 3.5a**), similar to that provided by the da Vinci robot when performing surgery within a body cavity. For the intracardiac catheter navigation studies, the endoscope was introduced into the right atrium of the phantom (**Fig. 3.5b**).

**Ultrasound Image Guidance:** Minimally invasive interventional navigation has been attempted and performed clinically under US image guidance [24, 25, 26] to reduce and potentially eliminate the use of fluoroscopy imaging and its well-known limitations (i.e. dose to both patient and clinical staff, poor soft tissue contrast and lack of anatomical context). In these experiments, users employed 2D real-time US imaging as the only source of intra-operative visualization available to depict the three dimensional surgical scene (**Fig. 3.5 c,d**) and bring the tool tip in contact with the sphere.

**Model-enhanced Ultrasound Guidance:** Enhanced visualization was achieved by augmenting real-time US imaging with the phantom model and virtual representation of the pointer or steerable catheter tip — the model-enhanced US guidance environment (**Fig. 3.5 e,f**). In terms of the navigation-positioning paradigm, this environment provides sufficient information for both tool-to-target navigation via the use of virtual phantom and tool models, as well as precise on-target positioning, pro-

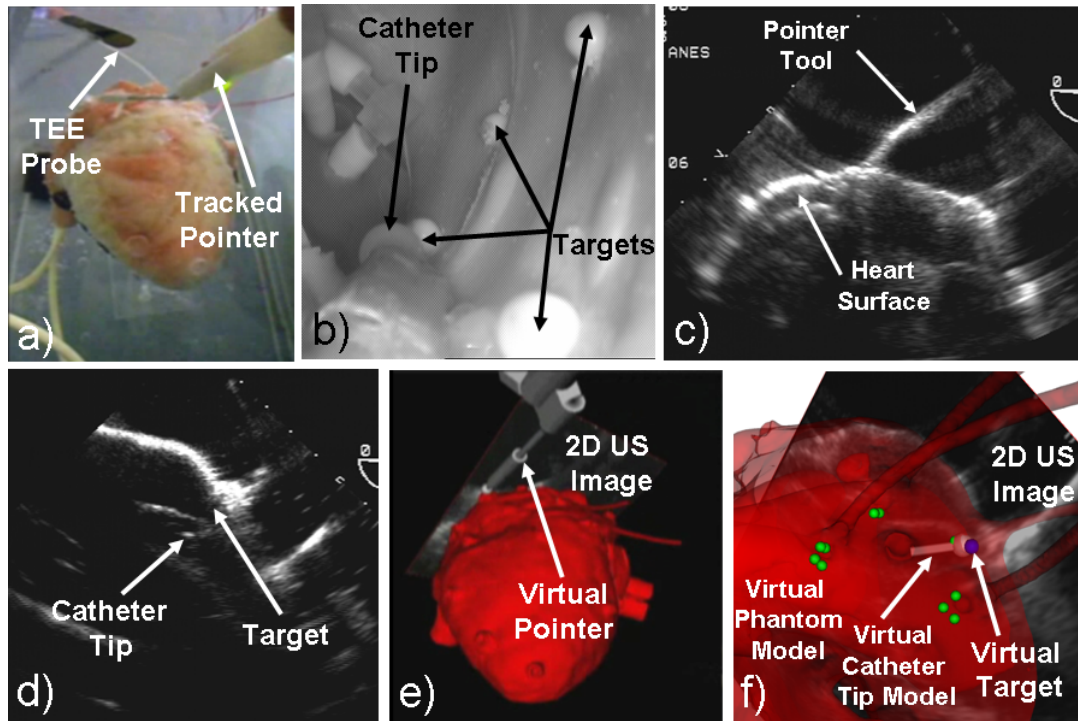


Fig. 3.5: Intra-operative endoscopic image showing (a) direct-access epicardial pointer navigation and (b) intracardiac catheter guidance; (c) Pointer-to-target navigation and (d) catheter tip-to-target navigation under typical 2D US image guidance; Therapy delivery under model-enhanced US guidance for (e) direct epicardial access (e) and endocardial catheter guidance (f).

vided via the tracked 2D real-time US images displayed relative to the virtual tool models. Moreover, the real-time imaging component provides a significant clinical advantage, as it allows for precise targeting in the event of slight misregistrations between the model and the subject's heart as shown in section 3.2.3.4.

### 3.2.3.4 Mimicking Model-to-Subject Misregistrations

Due to their complexity and computational inefficiency, some registration algorithms may not be suitable for use in time-critical interventional applications in the operating room (OR). Instead, fast, simple, and OR-friendly registration techniques are often employed, however at the expense of misregistrations (**Fig. 3.6**) present in the visualization environment [27].



Recently, Ma *et al.* [15] proposed a feature-based registration technique that relies on the alignment of the left ventricular surface and centerline of the descending aorta to fuse pre- and intra-operative data using a weighted iterative closest point (ICP) registration approach; similarly, we have shown clinically-suitable fusion of pre-operative models and intra-operative US data via alignment of reconstructed valve annuli [16, 17], as later described in Chapter 4. While the features driving the registration are different, both techniques provide comparable anatomical alignment (4-5 mm) of the pre- and intra-operative data. However, the achieved alignment may not be suitable for model-guided therapy alone, without refined guidance provided via real-time intra-operative imaging.

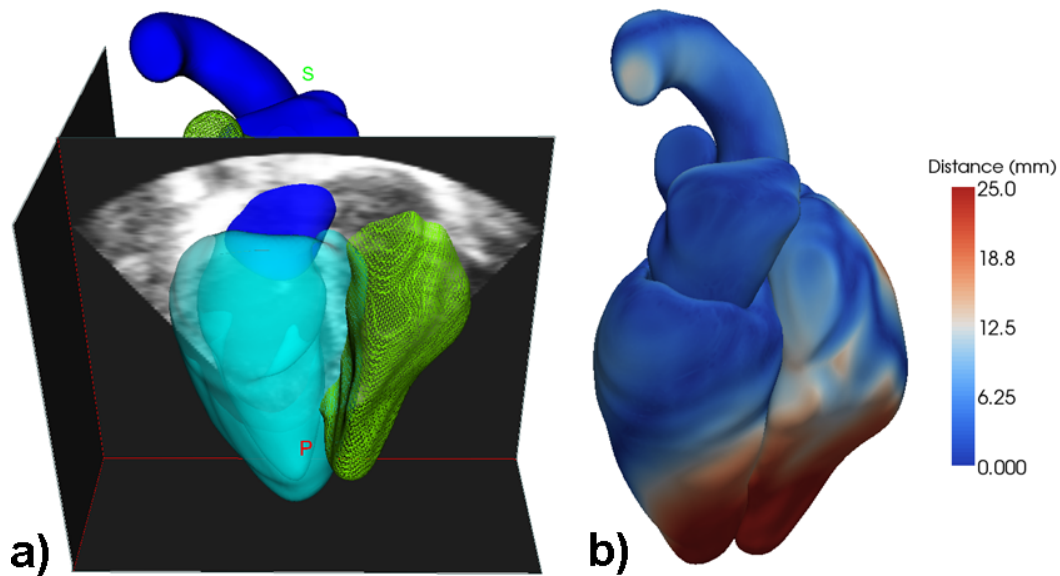


Fig. 3.6: a) Pre-operative anatomical model registered to intra-operative US image using the feature-based model-to-subject registration approach, and b) error map displaying the anatomical misalignments following registration distributed across the surface model.

The first two studies presented here were performed following accurate (0.8 mm RMS target registration error (TRE)) “world registration” — the registration of the virtual components to their real counterparts, as described in section 3.2.3.4. However, considering the common challenges encountered clinically regarding misalignments caused by the model-to-subject registration, surgical target locations, although

accurately labeled pre-operatively, may no longer align with their intra-operative locations; furthermore, they may even appear outside the cardiac chamber (**Fig. 3.7**), where careless navigation may lead to severe outcomes.

To address these challenges, we took the intracardiac catheter navigation study to the next level and evaluate the performance of the model-enhanced US guidance environment in presence of model-to-subject misalignments. We mimicked *in vitro* model-to-subject misregistrations similar to those encountered in the clinic, and showed how our guidance platform provides sufficient navigation information to maintain accurate targeting, in spite of slight misalignments.

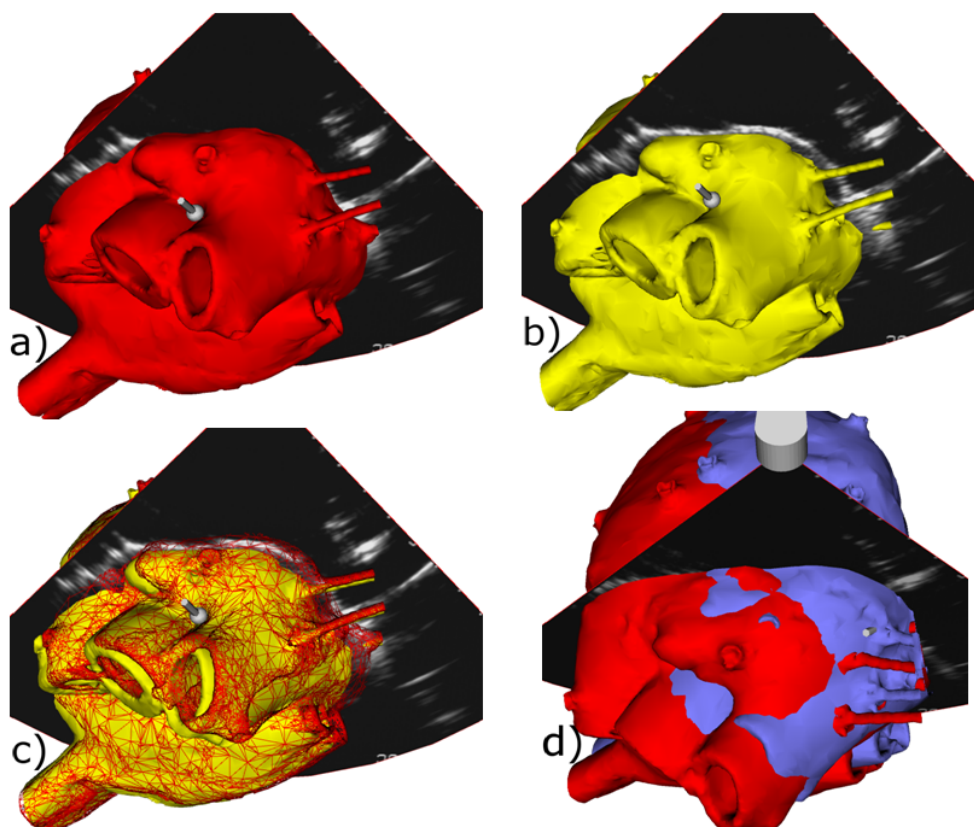


Fig. 3.7: Example of a (a) well-aligned and (b) misaligned phantom model with respect to the physical phantom (note misalignment between the epicardial contour of the phantom model and its US image); c) Superimposed display showing well-aligned (red wireframe) phantom model and the “inward” (yellow surface) and “outward” (blue surface) misaligned model.

**Virtual-to-Real World Registration:** The key to building accurate navigation environments lies within the registration of all components into a common framework. The virtual models of surgical tools, US transducer and image fan are intrinsically registered to the tracking coordinate system and to each other via their respective tool-to-sensor calibration transforms. The challenging step is the registration of the patient to the pre-operative model. For our *in vitro* experiments, we used a point-based registration algorithm involving the 10 epicardial fiducial markers to register the physical phantom to its virtual model using a magnetically tracked pointer. Temporal alignment was achieved by synchronizing the heart rate of the model with the ECG signal driving the actuator, resulting in visualization that is close to real time.

**Inducing Model-to-Subject Misregistrations:** Because of misregistrations often encountered in the OR due to a slightly different orientation of the patient's heart between the pre- and intra-operative stage, the opening of the chest and pericardial sac or other changes induced during the workflow, we simulated two misalignment scenarios: the former misregistration simulates an "inward" misalignment, where the model-depicted endocardial targets are *actually* located within the cardiac chamber; the latter mimics an "outward" misalignment, where targets located on the endocardial wall according to the pre-operative model are *actually* located outside the heart phantom.

The model-to-subject misalignments were achieved by replacing the well-aligned model with new, misregistered models obtained by transforming the well-aligned model, following world registration, to their new, misregistered locations by means of the misalignment transforms. In both cases, rigid-body transforms were chosen to provide a target misregistration on the order of 3-5 mm in the surgical target region; these transforms were manually applied to the well-aligned model of the phantom to obtain the misregistered models. As the phantom model was mapped to its new, misregistered location using the misalignment transforms explained above, the position

and orientation of the tracked tools and US probe remained the same with respect to one another and to the physical phantom.

**Surgical Guidance:** To evaluate the effect of model-to-subject misregistration on targeting accuracy, we conducted several experiments where users relied solely on model-guided visualization or model-enhanced US guidance, under both well-aligned, as well as misaligned conditions. As users were blinded as to whether or not the model was properly registered to the phantom, a specific therapy delivery workflow was adopted. An initial tool to target navigation was performed under model-assisted guidance; once on target, the model display was dimmed, while the tracked 2D US image was emphasized, allowing users to identify the true target location and refine their tool location based on the virtual tool representation and the real-time US image (**Fig. 3.8**).

### 3.2.4 Data Acquisition Module

All data were collected using a custom-designed module integrated within the *AtamaiViewer*. The data acquisition module was designed to record the 4 x 4 transformation matrix indicating the position and orientation of both the tracked surgical targets (i.e. the gold-standard target location) and surgical tool (i.e. targeted site), as well as the elapsed time required for the target to be reached. In addition, the module also allowed easy randomization of both the surgical target and visualization modalities. As such, for each new therapeutic trial the user was prompted to approach a specific target under a specific visualization modality, avoiding any bias caused by the development of a training effect. Several other features available within the *AtamaiViewer* were incorporated into the data acquisition module, providing the user with the flexibility of choosing the optimal information to be displayed for visualization. These techniques enabled variable opacity settings, slicing and cropping of the model, as well as the option of displaying the tracked components of interest.

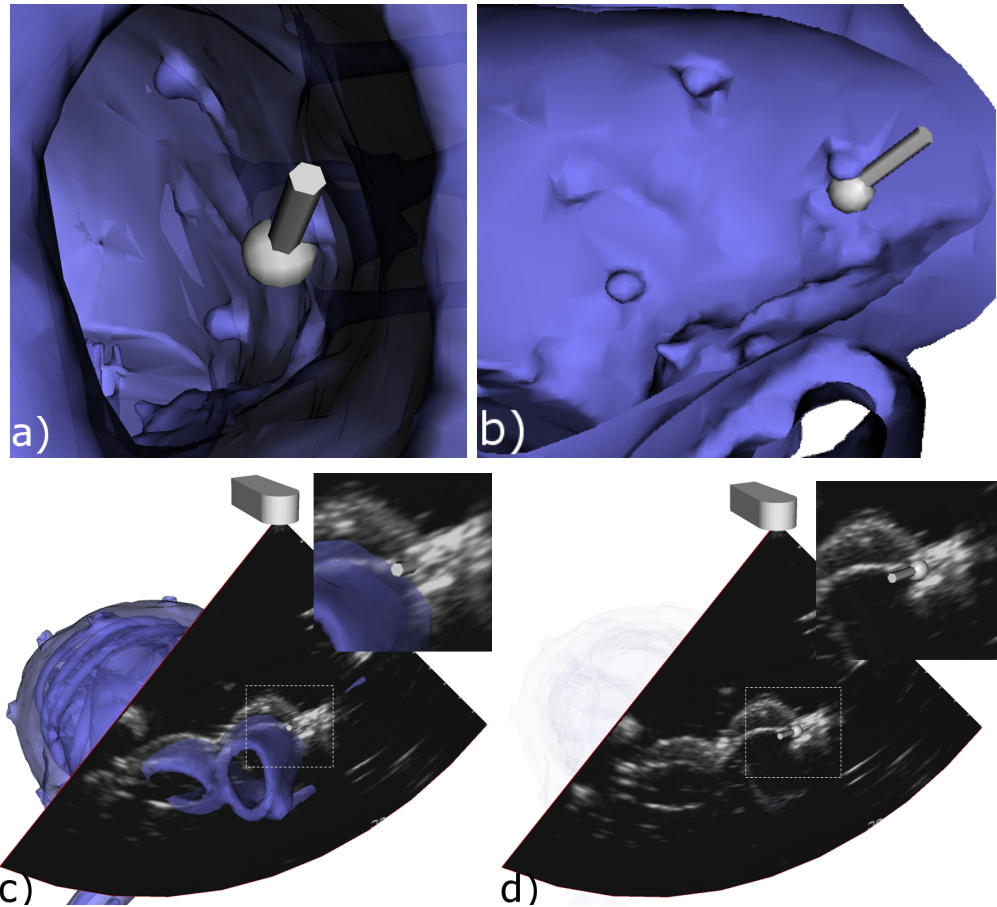


Fig. 3.8: US enhanced model-assisted guidance work flow: initial navigation via virtual anatomy and tool model using two orthogonal views (a) and (b), followed by US model enhancement (c), and final target identification and tool tip positioning performed under real-time US guidance (d).

### 3.3 Evaluation and Results

The objective of these experiments was to quantitatively evaluate therapy delivery, in terms of both targeting accuracy and duration, under model-enhanced US-assisted surgical guidance *in vitro* and to assess the therapeutic outcomes against those achieved under endoscopic and US image guidance. Targeting accuracy was determined as the distance between the tip of the surgical instrument (targeted site) and the surgical target location (ground truth target location) as recorded by the tracking system, following an adjustment equal to the sum of the radii of the spherical

tool tip and spherical targets. Targeting duration was measured directly by the data acquisition module, as the time elapsed until targets were reached by the user. Data analysis was performed using a parametric, two-way Analysis of Variance (ANOVA) technique followed by Tukey’s Honestly Significant Difference post-hoc test. All statistical analyses were performed using the GraphPad Prism 4.0 package to compare the achieved procedure accuracy and duration with respect to the guidance modality employed, the level of expertise of the users, or the location of the physical targets, according to the experimental protocol for each of the conducted studies.

### 3.3.1 Direct Access Epicardial Interventions

Four expert clinicians and four novice users randomly attempted to reach the four targets three times each under each visualization modality; when in contact according to the visualization display, the positions of the target and pointer tip were recorded, along with the duration of the attempt. **Table 3.1** summarizes the distance errors and procedure time, according to the users’ expertise and guidance modality employed.

Table 3.1: Direct Access Epicardial Procedures: Summary of guidance accuracy (Targeting Error - mm) and procedure time (Mean  $\pm$  Std. Error) reported according to user’s expertise and guidance modality.

<b>Guidance</b>	<b>Endoscopic Guidance</b>		<b>US Image Guidance</b>		<b>Model-enhanced US Guidance</b>	
Distance Error (mm)	1.9 $\pm$ 0.1		3.4 $\pm$ 0.3		2.6 $\pm$ 0.1	
RMS Error (mm)	2.5		4.4		2.8	
Elapsed Time (sec)	6.4 $\pm$ 1.1		13.3 $\pm$ 1.6		11.3 $\pm$ 1.8	
<b>Expertise</b>	<b>Experts</b>	<b>Novice</b>	<b>Experts</b>	<b>Novice</b>	<b>Experts</b>	<b>Novice</b>
Distance Error (mm)	2.0 $\pm$ 0.2	1.8 $\pm$ 0.2	3.1 $\pm$ 0.4	3.7 $\pm$ 0.4	2.6 $\pm$ 0.2	2.5 $\pm$ 0.2
RMS Error (mm)	2.3	2.1	4.0	4.7	2.8	2.7
Elapsed Time (sec)	4.4 $\pm$ 0.9	7.5 $\pm$ 1.4	7.7 $\pm$ 0.6	20.1 $\pm$ 1.8	9.9 $\pm$ 1.0	12.6 $\pm$ 1.4

According to the presented results, model-enhanced US-assisted guidance led to more accurate targeting compared to US guidance alone ( $p < 0.05$ ) across both user groups, and also comparable to the accuracy achieved under endoscopic guidance, our baseline positive control modality. In addition, the level of expertise of the users had

no significant effect on procedure accuracy ( $p > 0.05$ ), as both the expert and novice group achieved comparable targeting accuracy under model-enhanced US guidance (**Fig. 3.9**). However, further analysis of the intra-modality targeting data shows that the expert group managed to achieve better accuracy under US image guidance alone compared to the novice group — an intuitive observation considering their extensive exposure to US interventional guidance. On the other hand, the novice group performed slightly more accurately than the expert group under model-enhanced US guidance; they nevertheless experienced a highly significant ( $p < 0.001$ ) improvement in targeting accuracy under model-enhanced US guidance compared to US image guidance alone.

We also analyzed the distribution of the targeted sites with respect to the actual target location. **Fig. 3.10** shows that both the novice and expert groups achieved comparable targeting precision (i.e. a more compact distribution of the targeted sites) under model-enhanced US guidance and endoscopic guidance, our positive control modality. US image guidance, on the other hand, led to greater targeting variability amongst both groups, mainly a result of poor tool-to-target navigation under 2D image guidance alone.

The navigation duration results suggested that model-enhanced US guidance led to slightly longer targeting times than US image guidance alone for the expert group, while the novice group experienced a decrease in procedure time. In addition, both groups showed similar targeting duration between model-enhanced US and endoscopic guidance ( $p > 0.05$ ). Considering that experts are highly accustomed to interventional US, the use of the model-enhanced US display led to longer procedure times, but also more accurate targeting. For the novice group, not only the procedure times were reduced ( $p < 0.05$ ) under model-enhanced US guidance, but the new guidance environment led to significantly higher targeting accuracy ( $p < 0.001$ ). Considering that neither group had previously employed model-assisted guidance, we therefore expect that procedure times will improve with adequate training.

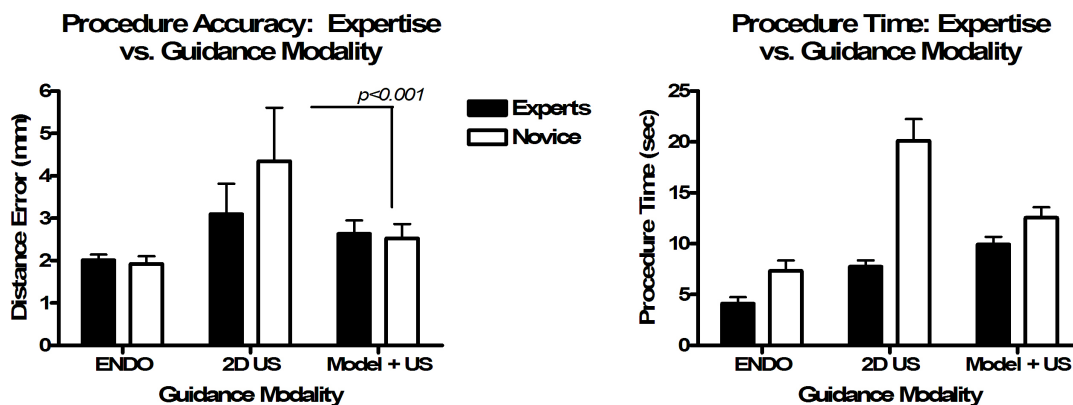


Fig. 3.9: Procedure accuracy and duration achieved by the expert and novice groups under both guidance modalities. Note the significantly more accurate targeting ( $*p < 0.001$ ) achieved by the novice group under model-enhanced US guidance compared to that achieved under US image guidance alone. Moreover, the procedure times recorded for the novice group were also significantly shorter ( $p < 0.05$ ) under model-enhanced US guidance compared to those recorded using US imaging alone.

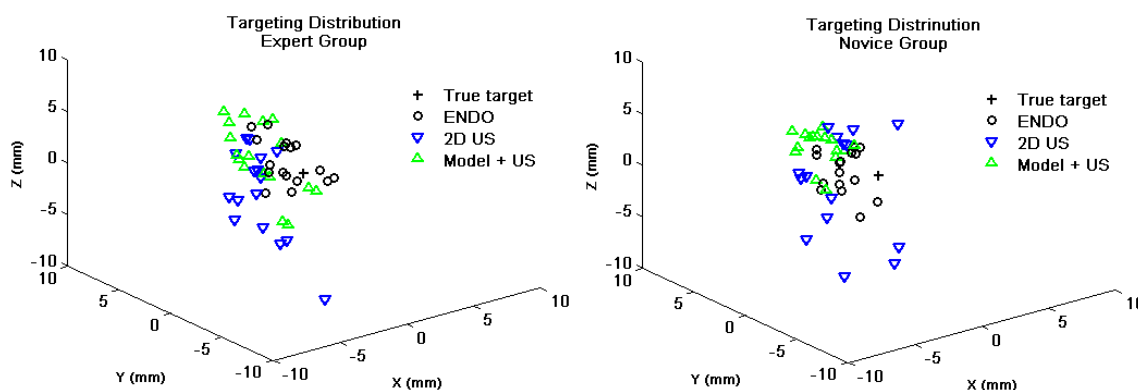


Fig. 3.10: Distribution of targeted locations around the true target achieved using both guidance modalities. Note that model-enhanced US guidance led to more consistent targeting.

### 3.3.2 Catheter-Driven Endocardial Interventions

Four users conducted the *in vitro* catheter navigation on the four surgical targets embedded within the endocardial right atrial wall of the phantom. Procedure outcome was assessed according to the targeting error and duration, reported according to the RMS and 95% confidence interval, and mean and standard error, respectively, and summarized in **Table 3.2**.



Table 3.2: Endocardial Catheter-Guided Procedures: Guidance Accuracy (RMS Targeting Error - mm) and Procedure Duration (Mean  $\pm$  Standard Error)

Guidance Modality	Endoscopic		Model-enhanced US		2D US Imaging	
RMS Error (mm)	0.63		1.10		12.9	
Duration (sec)	$6.4 \pm 0.5$		$31.5 \pm 2.8$		$55.7 \pm 5.1$	
Target Analysis	RMS (mm)	Duration (sec)	RMS (mm)	Duration (sec)	RMS (mm)	Duration (sec)
Target 1	0.5	$8.3 \pm 1.5$	0.9	$25.3 \pm 5.1$	10.3	$52.7 \pm 7.9$
Target 2	0.7	$6.0 \pm 0.8$	1.5	$35.0 \pm 5.2$	11.9	$61.4 \pm 9.1$
Target 3	0.6	$6.4 \pm 0.7$	0.8	$38.9 \pm 6.0$	18.4	$77.8 \pm 13.3$
Target 4	0.7	$5.2 \pm 0.7$	1.0	$25.3 \pm 5.7$	9.1	$29.7 \pm 5.6$

Our results show that model-enhanced US-assisted guidance led to significantly more accurate targeting ( $p < 0.001$ ) and shorter procedure times ( $p < 0.001$ ) than 2D US imaging alone. Moreover, the targeting accuracy achieved under model-enhanced US guidance showed no significant difference ( $p > 0.05$ ) from that achieved under endoscopic guidance, once again employed to establish a positive control with respect to the procedure outcome (Fig. 3.11).

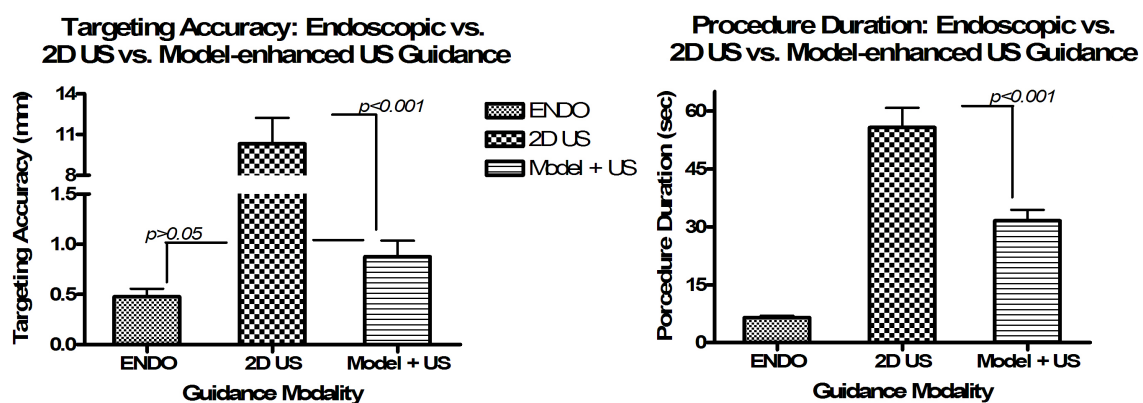


Fig. 3.11: Graphical representation of targeting accuracy and procedure duration achieved under endoscopic, model-enhanced US (model + US), and 2D US image guidance. Note a significant improvement in both targeting accuracy and procedure duration under model-enhanced US guidance with respect to 2D US imaging alone ( $p < 0.001$ ). Moreover, no statistical difference ( $p > 0.05$ ) was shown between the targeting accuracy achieved under model-enhanced US and endoscopic guidance, the control modality.

The difficulties encountered by all users during task completion under US image guidance are not only reflected in procedure accuracy, but also in procedure duration, which was significantly reduced ( $p < 0.05$ ) under model-enhanced US ( $\sim 32$  sec) to almost half the values recorded under US image guidance ( $\sim 58$  sec), but not quite as low as the values recorded achieved under endoscopic guidance ( $\sim 7$  sec). A plausible explanation for these longer trial times may be formulated in terms of the orientation of the model-enhanced US display, the necessity to zoom in or out or to manipulate the views for according to the user’s needs.

In addition, model-enhanced US catheter navigation led to a more consistent distribution of the targeted sites. **Fig. 3.12** shows the distribution of targeted sites (i.e. location of the catheter tip) around the true target location for each of the four targets, under each guidance modality. Endoscopic guidance led to most consistent targeting, model-enhanced US guidance showed comparable performance, while US image guidance alone showed poor precision (**Fig. 3.15**) across all targets. The inaccuracies observed under US image guidance may be easily explained in terms of the navigation-positioning paradigm introduced previously and further discussed in section **3.4**.

### 3.3.3 Model-to-Subject Misalignments

To illustrate the limitations of model-guided therapy in the presence of model-to-subject misregistrations, in addition to the visual blinding and randomization of both the targets and guidance modalities described in the previous experiment, the users had no prior knowledge of the model-to-phantom registration within the model-enhanced US visualization environment. The users were also prompted to perform the surgical task under model-assisted guidance alone, and the outcomes were recorded and compared to those results obtained under model-enhanced US guidance (**Table 3.3** and **Table 3.4**).

Our study following accurate model-to-phantom registration described in section

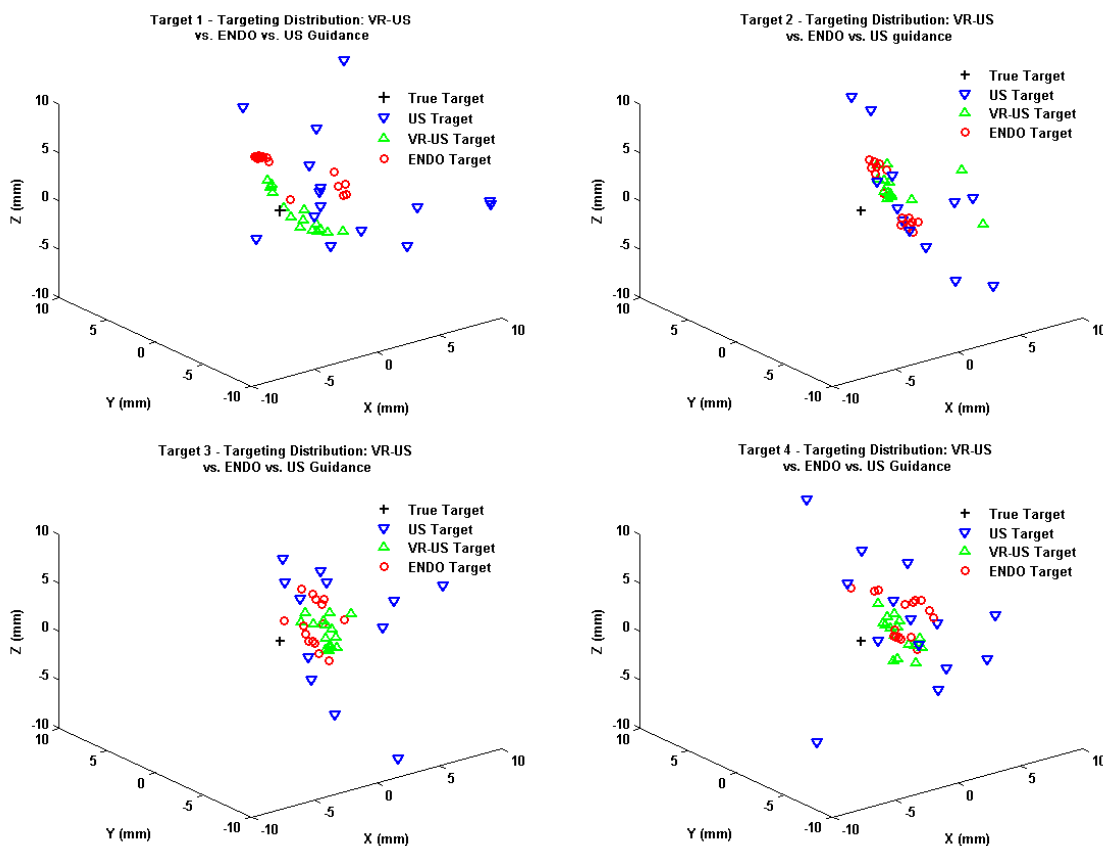


Fig. 3.12: Distribution of targeted sites with respect to the true target location shown for all targets under all three guidance modalities: endoscopic, model-enhanced US and 2D US image guidance. Note that increased targeting accuracy and precision was achieved under model-enhanced US guidance compared to 2D US guidance alone. In addition, the model-enhanced US targeted sites were within 2 mm away from the true target location.

**3.3.2** showed that both the model-assisted and model-enhanced US-assisted guidance led to significantly more accurate targeting ( $p < 0.001$ ) than 2D US imaging alone; moreover, no significant difference was observed between the endoscopic and the two model-assisted guidance modalities ( $p > 0.05$ ) (**Fig. 3.13**).

The chosen misalignment transforms resulted in an overall 3-5 mm misregistration across the four targets. Following model-assisted guidance, we observed a significant decrease in targeting accuracy ( $p < 0.001$ ) compared to that recorded under well-aligned conditions (**Fig. 3.13**). While targeting precision was maintained, users

Table 3.3: Summary of Guidance Accuracy (RMS Distance Error - mm) under Model-to-Subject Misregistrations. Part I: Well-Registered Model

Guidance Modality	Well-Registered Model			
	Endoscopic	US Imaging	Model Assisted	Model + US
Global	0.5	14.8	0.9	0.7
Target 1	0.4	13.4	0.8	0.8
Target 2	0.4	14.8	1.0	0.8
Target 3	0.5	20.3	0.7	0.7
Target 4	0.6	9.4	1.1	0.5

Table 3.4: Summary of Guidance Accuracy (RMS Distance Error - mm) under Model-to-Subject Misregistrations. Part II: Inward- and Outward Misalignments

Guidance Modality	Inward Misalignment (IWD)		Outward Misalignment (OWD)	
	Model Assisted	Model + US	Model Assisted	Model + US
Global	2.9	1.1	3.4	1.4
Target 1	3.2	0.9	3.1	1.1
Target 2	2.4	1.2	3.2	1.7
Target 3	2.9	1.4	3.4	1.6
Target 4	3.1	0.8	3.7	0.9

consistently approached the incorrect targets; hence the trueness of their targeting estimate remained low. After mapping the targeted sites using the inverse of the misalignment transforms, we were able to reconstruct the true locations of the surgical targets, thereby confirming that the navigation errors were in fact induced by the misleading environment.

Once model-assisted guidance was augmented with real-time US, we observed a significant improvement in targeting accuracy. For the “inward” misalignment case, targeting accuracy achieved under model-assisted guidance alone dropped to an overall 3 mm RMS; however, it was restored to an overall 1.1 mm RMS error via US-enhanced guidance ( $p < 0.001$ ). Similarly, for the “outward” misalignment case, model-assisted guidance accuracy was significantly improved with the addition

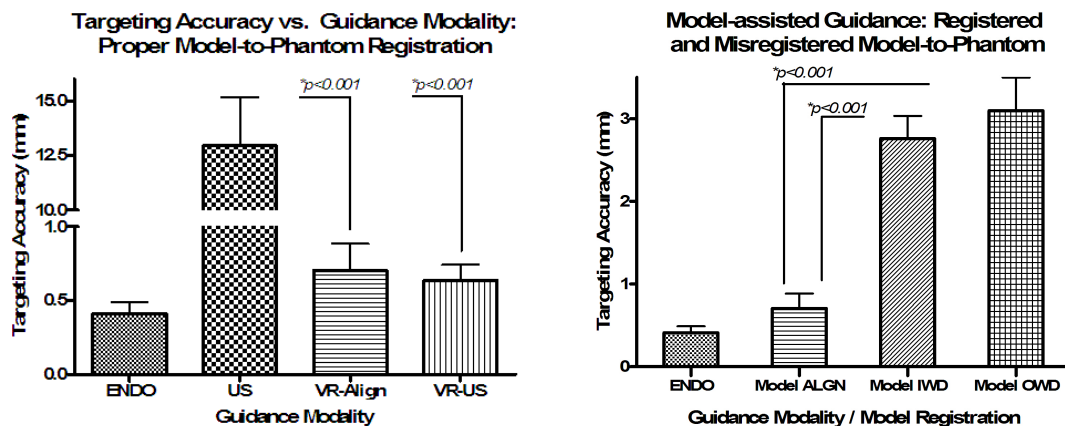


Fig. 3.13: Following accurate model-to-phantom registration (left panel), comparable targeting accuracy was achieved under both model-assisted guidance alone (VR-Align) and model-enhanced US-assisted (model + US) guidance, and superior ( $*p < 0.001$ ) to that achieved under US image guidance alone; However, following induced misregistrations (right panel), the accuracy achieved under model-assisted guidance alone (Model ALGN) was significantly reduced ( $*p < 0.001$ ) under both inward (Model IWD) and outward (Model OWD) misalignments.

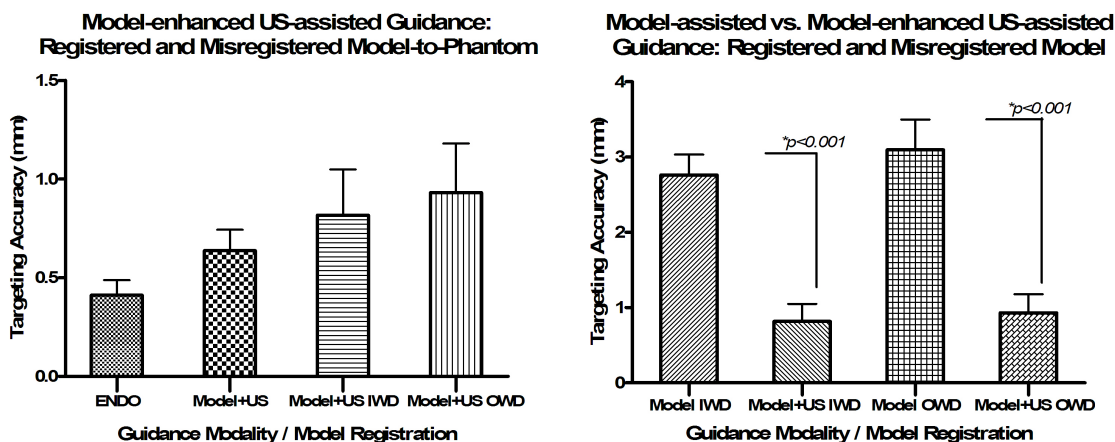


Fig. 3.14: Model-enhanced US-assisted guidance (Model + US) shows consistent targeting accuracy independently of model-to-subject registration, under both inward (Model + US IWD) and outward (Model + US OWD) misalignment conditions (left panel); Note the significantly improved accuracy ( $*p < 0.001$ ) with model-enhanced US-assisted (Model + US) guidance compared to model-assisted guidance alone (Model) under both inward (IWD) and outward (OWD) misregistration conditions.

of US imaging, from 3.1 mm targeting error to 1.4 mm RMS (**Fig. 3.13**). Moreover, model-enhanced US guidance maintained a high level of accuracy regardless of the model-to-subject registration ( $p < 0.001$ ) (**Fig. 3.14**).

### 3.3.4 Qualitative Surgical Guidance Environment Evaluation

Following the *in vitro* therapy experiments, each user completed a survey designed to qualitatively assess the overall performance and clinical value of the surgical visualization and guidance modalities employed in this study on a scale from 1 (highly ineffective) to 5 (highly effective). The evaluation criteria were selected to reflect the guidance environment, the effects of the visualization modality, intuitiveness of the display, user’s confidence during guidance, navigation vs. positioning capabilities, and clinical relevance (**Table 3.5** and **Table 3.6**).

Table 3.5: Expert Qualitative Guidance Assessment: Summary Table

Modality Evaluation Criteria	Expert Users		
	Endoscopic Guidance	US Imaging	Model-enhanced US Guidance
Display Quality	4.75	1.75	4.5
Intuitiveness	4.5	1.75	4.25
Overall Usability	4.75	3.0	4.5
Navigation Capabilities	4.25	1.75	4.75
Positioning Capabilities	4.5	4.5	4.5
User’s Confidence	4.75	2.5	4.75
Clinical Relevance	4.25	4.0	4.75

In summary, both the experts and novice users agreed that endoscopic guidance is a good representation of direct visualization. However, all users identified consistent challenges with respect to the use of real-time US imaging as the sole guidance modality. Specifically, the tool-to-target navigation often involved a backward-and-forward iterative approach, where the target was first identified using US imaging, followed by

Table 3.6: Novice Qualitative Guidance Assessment: Summary Table

Modality Evaluation Criteria	Novice Users		
	Endoscopic Guidance	US Imaging	Model-enhanced US Guidance
Display Quality	4.25	2.25	3.75
Intuitiveness	4.5	1.75	4.5
Overall Usability	4.75	2.0	4.25
Navigation Capabilities	4.5	1.25	4.75
Positioning Capabilities	4.5	3.75	4.5
User’s Confidence	4.5	2.25	4.25
Clinical Relevance	4.75	3.5	4.75

a search for the tool tip while panning the US fan. This process was repeated several times until the perceived tool and target were both viewed in the same 2D US image, leading to prolonged navigation times. Moreover, given the experience of the expert users in interpreting the US information, the novice users experienced additional difficulties with US image guidance compared to the trained group. Nevertheless, both user groups appreciated the superior visualization and guidance capabilities provided by the model-enhanced US guidance environment, which in turn, lead to increased guidance intuitiveness, greater confidence, and a more user-friendly display.

### 3.4 Discussion

The aim of this work was to evaluate the performance of the model-enhanced US guidance environment *in vitro* by simulating minimally invasive closed-chest, beating heart procedures using direct access or catheter-driven approach, as well as mimicking clinically encountered challenges, such as model-to-subject misregistrations. The study began with the hypothesis that model-enhanced US-assisted guidance would lead to improved targeting accuracy (overall targeting accuracy less than 3 mm) and shorter navigation times over 2D US image guidance alone. Furthermore, in the con-

text of model-to-subject misregistrations, we hypothesized that real-time US imaging would contribute to maintaining a consistent targeting accuracy compared to therapy delivery guided using the pre-operative model alone.

We have shown that model-enhanced US guidance led to more accurate targeting than US image guidance alone across all three simulated procedures, resulting in an overall RMS targeting error of under 3 mm, where the baseline accuracy measurements achieved under endoscopic guidance were on the order of 1-2 mm RMS. On the other hand, targeting error achieved under US image guidance ranged from as little as 4-5 mm to over 15 mm, where the large errors were associated with the poor navigation capabilities available to the user through the 2D imaging modality.

Our results also show that while the expert group achieved more accurate targeting ( $\sim 4.0$  mm RMS) than the novice group ( $\sim 4.7$  mm RMS) under 2D US image guidance alone, both groups achieved comparable targeting accuracy ( $\sim 2.7$  mm RMS) under model-enhanced US guidance. Moreover, there was no significant difference between the accuracy achieved by the two groups under the novel guidance modality; nevertheless, the novice group, which demonstrated considerably worse performance than the expert group under US imaging alone, showed a significant improvement in the targeting accuracy under model-enhanced US guidance, which was also accompanied by faster navigation times.

The elapsed time was the period required to navigate the tool to the target and it was mainly dictated by the visualization information available to perform the task. Considering the poor information provided by the 2D US images, (i.e. 2D images cannot easily portray a 3D scene), the elapsed time was longer for the novice group compared to the expert group, due to their reduced exposure to US-assisted navigation. The novices, nevertheless, showed a significant improvement in both navigation time and targeting accuracy under model-enhanced US-assisted guidance. The overall reduction in navigation time was in fact experienced due to the augmentation of the 2D US images with anatomical context via the virtual models. The latter provided



users with an intuitive 3D navigation perspective as opposed to having to iteratively sweep the US fan to visualize the tool and target.

As a consequence of these findings, for the catheter navigation experiments, where catheter manipulation itself is an acquired skill and therefore improves with practice, we resorted to users who had minimal exposure to any sort of catheter navigation and provided them with the same training period (30 mins) under each guidance modality prior to collecting the measurements. This methodological approach ensured that all users were given an equal opportunity to become familiar to the catheter navigation in the same training environment, therefore eliminating any bias from the collected data that may have been related to their expertise in catheter manipulation.

In addition to demonstrating the feasibility of model-enhanced US guidance for beating heart interventions via different access routes, the performance evaluation under model-to-subject misregistration represents a key component of this work. While model-to-patient misalignments are commonly encountered in cardiac interventions, the real-time imaging component of the surgical guidance platform provides sufficient information to identify the correct intra-operative target location following model-assisted navigation, and compensate for the positioning error, ultimately enabling consistent targeting within 1-1.5 mm.

For qualitative evaluation, we recorded targeting maps after each therapy delivery session (**Fig. 3.15**). A compact distribution of targeted sites was observed under endoscopic guidance, and maintained under both model-assisted and US-enhanced model-assisted guidance. In the context of the formulated navigation-positioning paradigm, poor positioning is usually characterized by small errors, where the user-interpreted target location is slightly removed from its true location; on the other hand, inadequate navigation is associated with rather large errors, often due to either mis-registrations between the real and virtual representations, or simply a poor visualization environment, such as that provided by 2D US imaging alone. In fact, the main drawbacks of US image guidance alone arose due to limited information

provided for navigation, including lack of context, poor instrument perception, and the inability of 2D images to adequately portray the 3D surgical scene. The catheter to target navigation was further hampered by the inability to identify the catheter tip in the US image. Nevertheless, model-enhanced US guidance did ameliorate these limitations, and hence targeting accuracy was significantly improved, reaching comparable values to those achieved under endoscopic guidance.

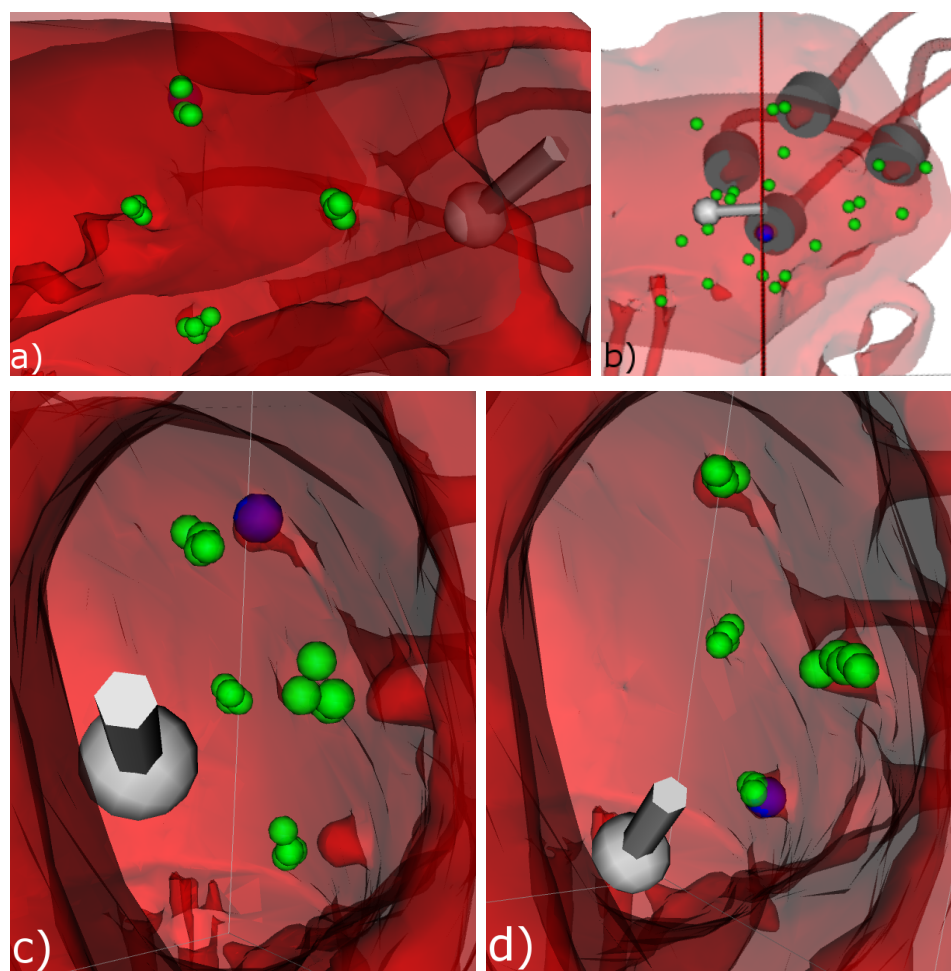


Fig. 3.15: Post-therapy qualitative targeting distribution achieved under a) endoscopic, b) US image guidance alone; c) Model-assisted, and d) Model-enhanced US guidance. Note the prescribed surgical targets displayed in blue and targeted sites displayed in green.

In addition to its demonstrated advantages, the model-enhanced US guidance environment raises several challenges with respect to the employed technology and its

impact on the clinical workflow. The use of magnetic tracking imposes stringent limitations on the workspace and tools used in the procedure. However, the magnetic tracking manufacturers are designing newer and smaller sensors to fit both needles and catheters, as well as magnetic field generators compatible with fluoroscopy imaging and metal tables. We are currently exploring the integration of the tracking technologies within conventional surgical tools, and it is only a matter of time until these sensors will become fully integrated within the instruments. We have recently integrated the 6 DOF NDI Aurora magnetic sensor within the casing of a transesophageal ultrasound transducer [28] and have employed the newly integrated probe for patient image acquisition for a different application.

A natural extension of this work is to initiate its translation into the clinic and illustrate its advantages over traditional real-time US image guidance, as well as a potential solution toward reducing and eventually eliminating the use of X-ray fluoroscopy for intracardiac catheter navigation. To date, we have performed a preliminary *in vivo* study comparing catheter navigation to clinically relevant sites in the right atrium of a porcine model under model-enhanced US-assisted guidance vs. real-time US guidance. Our results have reported targeting errors of less than 5 mm and navigation times of  $\sim 20$  seconds under the hybrid guidance environment — an improvement over US image guidance alone, which led to errors as high as 30 mm after double the hybrid navigation time.

### 3.5 Conclusions

These studies demonstrated that our model-enhanced US-assisted guidance environment can lead to improved targeting accuracy (less than 3 mm) and procedure times compared to the outcomes achieved under traditional real-time US imaging alone. In addition, the environment also supplied sufficient information to allow consistent targeting accuracy (less than 1.5 mm) in presence of commonly encountered

model-to-subject misalignments. Provided further *in vivo* evaluations, we foresee this navigation environment as a less invasive and equally efficient alternative to conventional image-guided cardiac therapy, and a suitable approach to reduce and eventually eliminate the use of X-ray fluoroscopy for catheter navigation.

# References

- [1] T. M. Peters. Image-guidance for surgical procedures. *Phys Med Biol.*, 51:R505–40, 2006.
- [2] C. A. Linte, A. D. Wiles, N. Hill, J. Moore, C. Wedlake, G. M. Guiraudon, D. L. Jones, D. Bainbridge, and T. M. Peters. An augmented reality environment for image-guidance of off-pump mitral valve implantation. In *Proc. SPIE Medical Imaging 2007: Visualization and Image-Guided Procedures*, volume 6509, pages 65090N–12, 2007.
- [3] A. D. Wiles, G. M. Guiraudon, J. Moore, C. Wedlake, C. A. Linte, D. L. Jones, D. Bainbridge, and T. M. Peters. Navigation accuracy for an intracardiac procedure using virtual reality-enhanced ultrasound. In *Proc. SPIE Medical Imaging 2007: Visualization and Image-Guided Procedures*, volume 6509, pages 65090W–10, 2007.
- [4] C. A. Linte, J. Moore, Wiles A. D., C. Wedlake, and T. M. Peters. Virtual reality-enhanced ultrasound guidance: A novel technique for intracardiac interventions. *Comput Aided Surg.*, 13:82–94, 2008.
- [5] F. Sauer. Image registration: Enabling technology for image-guided surgery and therapy. In *Proc. IEEE Eng Med Biol.*, pages 7242–45, 2005.
- [6] D. R. Holmes III, M. Rettmann, B. Cameron, J. Camp, and R. Robb. Developing patient-specific anatomic models for validation of cardiac ablation guidance procedures. In *Medical Imaging 2008: Visualization, Image-Guided Procedures and Modeling*, volume 6918 of *Proc. of SPIE.*, pages 69181W–8, 2008.
- [7] J. Dineley, S. Meagher, T. L. Poepping, W. N. McDicken, and P.R. Hoskins. Design and characterization of a wall motion phantom. *Ultrasound Med Biol.*, 32:1349–57, 2006.
- [8] S. K. Nadkarni, H. Austin, G. Mills, D. Boughner, and A. Fenster. A pulsating coronary vessel phantom for two- and three-dimensional intravascular ultrasound studies. *Ultrasound med Biol.*, 29:621–8, 2003.

- [9] Y. Suematsu, B. Kiaii, D. T. Bainbridge, P.J. del Nido, and R.J. Novick. Robotic-assisted closure of atrial septal defect under real-time three-dimensional echo guide: in vitro study. *Eur J Cardiothorac Surg.*, 32:573–576, 2007.
- [10] S. K. Nadkarni, D. Boughner, M. Drangova, and A. Fenster. In vitro simulation and quantification of temporal jitter artifacts in ecg-gated dynamic three-dimensional echocardiography. *Ultrasound med Biol.*, 27:211–22, 2001.
- [11] T. M. Peters, C. A. Linte, A. D. Wiles, N. Hill, J. Moore, C. Wedlake, D. Jones, D. Bainbridge, and G. M. Guiraudon. Development of an augmented reality approach for closed intracardiac interventions. In *Proc. IEEE International Symposium on Biomedical Imaging*, pages 1004–7, 2007.
- [12] C. A. Linte, A. D. Wiles, J. Moore, C. Wedlake, and T. M. Peters. Virtual reality-enhanced ultrasound guidance for atrial ablation: In vitro epicardial study. In *Proc. of Med Image Comput Comput Assist Interv.*, volume 5242 of *Lect Notes Comput Sci.*, pages 644–51, 2008.
- [13] K. Masamune, T. Horiuchi, M. Mizutani, H. Yamashita, H. Tsukihara, N. Motomura, S. Takamoto, H. Liao, and T. Dohi. Novel endoscope system with plasma flushing for off-pump cardiac surgery. In *Proc. of Med Image Comput Comput Assist Interv.*, volume 5761 of *Lect Notes Comput Sci.*, pages 451–458, 2009.
- [14] Y. L. Ma, G. P. Penney, C. A. Rinaldi, M. Cooklin, R. Razavi, and K. S. Rhode. Echocardiography to magnetic resonance image registration for use in image-guided cardiac catheterization procedures. *Phys Med Biol.*, 54:5039–55, 2009.
- [15] Y. L. Ma, K. Rhode, A. P. King, D. Cauldfield, M. Cooklin, R. Razavi, and G. P. Penney. Echocardiography to magnetic resonance image registration for use in image-guide electrophysiology procedures. In *Medical Imaging 2009: Visualization, Image-Guided Procedures and Modeling*, volume 7261 of *Proc. of SPIE.*, pages 72610Q–8, 2009.
- [16] C. A. Linte, M. Wierzbicki, J. Moore, G. M. Guiraudon, D. L. Jones, and T. M. Peters. On enhancing planning and navigation of beating-heart mitral valve surgery using pre-operative cardiac models. In *Proc. IEEE Eng Med Biol.*, pages 475–78, 2007.
- [17] C. A. Linte, J. Moore, C. Wedlake, G. M. Guiraudon, D. Bainbridge, D. L. Jones, and T. M. Peters. Inside the beating heart: An *in vivo* feasibility study on fusing pre- and intra-operative imaging for minimally invasive therapy. *Int J CARS*, 4:113–122, 2009.
- [18] W. Birkfellner, F. Watzinger, F. Wanschitz, R. Ewers, and H. Bergmann. Calibration of tracking systems in a surgical environment. *IEEE Trans Med Imaging*, 17:737–42, 1998.

- [19] D. D. Frantz, A. D. Wiles, S. E. Leis, and S. R. Kirsch. Accuracy assessment protocols for electromagnetic tracking systems. *Phys Med Biol.*, 48:2241–51, 2003.
- [20] J. B. Hummel, M. R. Bax, M. L. Figl, Y. Kang, C. Maurer Jr., W. W. Birkfellner, H. Bergmann, and R. Shahdi. Design and application of an assessment protocol for electromagnetic tracking systems. *Med Phys.*, 32:2371–9, 2005.
- [21] C. Nafis, V. Jensen, L. Beauregard, and P. Anderson. Method for estimating dynamic EM tracking accuracy of surgical navigation tools. In *Medical Imaging 2006: Visualization and Image-Guided Procedures*, volume 6141 of *Proc. of SPIE.*, pages 61410K–16, 2006.
- [22] D. G. Gobbi, R. M. Comeau, and T. M. Peters. Ultrasound probe tracking for real-time ultrasound/MRI overlay and visualization of brain shift. In *Proc. of Med Image Comput Comput Assist Interv.*, volume 1679 of *Lect Notes Comput Sci.*, pages 920–927, 1999.
- [23] A. D. Wiles, C. A. Linte, J. Moore, C. Wedlake, and T. M. Peters. Object identification accuracy under ultrasound enhanced virtual reality for minimally invasive cardiac surgery. In *Proc. SPIE Medical Imaging 2008: Visualization, Image-Guided Procedures and Modeling*, volume 6918, pages 69180E–12, 2008.
- [24] F. E. Silvestry, R. E. Kerber, M. M. Brook, and M. A. Wood. Echocardiography-guided interventions. *J Am Soc Echocardiogr.*, 22:213–31, 2009.
- [25] S. Saksena, A.M. Simon, P. Mathew, and R. Nagarakanti. Intracardiac echocardiography-guided cardiac resynchronization therapy: technique and clinical application. *Pacing Clin Electrophysiol.*, 32:1030–39, 2009.
- [26] Y. Okumura, B. D. Henz, S. B. Johnson, C. J. O’Brien, A. Altman, A. Govari, and D.L. Packer. Three-dimensional ultrasound for image-guided mapping and intervention: methods, quantitative validation, and clinical feasibility of a novel multimodality image mapping system. *Circ Arrhythm Electrophysiol.*, 1:110–9, 2008.
- [27] T. M. Peters and K. Cleary. *Image-guided Interventions: Technology and Applications*. Springer, Heidelberg, Germany, 2008.
- [28] J. T. Moore, A. D. Wiles, C. Wedlake, and T. M. Peters. Integration of transesophageal echocardiography with magnetic tracking technology for cardiac interventions. In *Proc. of SPIE. - Medical Imaging 2010*, volume 7625, pages 76252Y–1–10, 2010.

## Chapter 4

# Subject-Specific Models for Mitral Valve Interventions: Predicting Surgical Target and Enhancing Intra-operative Navigation

*For the guidance of minimally invasive mitral valve interventions on the beating heart, surgeons need a robust interventional system capable of providing reliable, real-time information related to the surgical targets and delivery instruments to compensate for the lack of direct vision during the procedure. Here we describe a means of gen-*

---

This chapter is adapted from the following work:

- Linte CA, Wierzbicki M, Moore J, Guiraudon GM, Little SH and Peters TM. Subject-Specific Models of the Dynamic Heart for Image-Guided Mitral Valve Surgery. *Proc. Med Image Comput Comput Assist Interv. (MICCAI) - Lect Notes Comput Sci.* 4792:94-101, 2007;
- Linte CA, Wierzbicki M, Moore J, Guiraudon GM, Jones DL and Peters TM. On Enhancing Planning and Navigation of Beating-Heart Mitral Valve Surgery Using Pre-operative Cardiac Models. *Proc. IEEE Eng Med Biol.* 475-8. 2007. ©2010 IEEE. Reprinted, with permission, from IEEE.



*erating dynamic, pre-operative, subject-specific cardiac models that depict the surgical targets and surrounding anatomy. In addition to their procedure planning value, these models also provide cues during surgical navigation, by supplying anatomical context to the real-time US imaging employed for guidance. The accuracy of the model-predicted surgical target is assessed against the accuracy of the equivalent structures extracted from 3D US images. In addition, a method to enhance intracardiac visualization and navigation by registering the pre-operative models to the intra-operative US imaging data is presented.*

## 4.1 Introduction

Intracardiac procedures have challenged surgeons and researchers ever since the pioneers of modern cardiac surgery performed the first interventions on the beating heart [1, 2]. However, their outcomes were compromised by inadequate visualization of intracardiac structures. These concerns led to the use of CPB as part of the traditional approach, to allow these procedures to be performed under direct vision, on the arrested, drained heart.

Minimally-invasive cardiac procedures can potentially reduce complications arising from surgical interventions by minimizing the size of the incision required to access the heart, while employing medical imaging to visualize intracardiac targets without direct vision [3, 4] and robotic and laparoscopic technologies to minimize tissue exposure. However, most of these approaches still require the use of CPB, which may lead to adverse effects, such as severe inflammatory responses [5] and neurological dysfunction [6].

During a mitral valve implantation or repair procedure, the surgeon navigates an instrument (e.g. a guiding tool with an attached prosthetic valve, or a fastening device) to the surgical target — the mitral valve annulus (MVA). Hence, the guidance of such procedures on the beating-heart requires detailed information about the

dynamic behaviour of the mitral valve and the surrounding anatomy. This information is not clearly portrayed by the TEE images, as 2D ultrasound (US) images lack anatomical context. Although 3D TEE might become a potential future solution to this problem, its narrow field of view may impose further challenges towards visualizing the tools and target in the same volume. To address these limitations, we include pre-operative, patient-specific models derived from MRI, which incorporate a dynamic representation of the gross cardiac anatomy (e.g. myocardium) and surgical target — MVA within the intra-operative VR environment. As a result, the intra-operative TEE information can be interpreted within a rich, high-quality 3D context [7] for improved procedure planning and navigation of surgical tools, while on-target positioning and detailed manipulations are performed under real-time US guidance.

Our first objective is to generate subject-specific models of the heart that can display the location of the mitral valve annulus throughout the cardiac cycle, with sufficient fidelity to provide the surgeon with the appropriate information during both procedure planning and guidance. To assess the accuracy of the generated models, the model-predicted mitral valve annuli are compared to their ground-truth representations extracted from 3D TTE images of the same subjects and acquired at the same cardiac phases.

Our next objective is to make these 3D anatomical data available to the surgeon during intra-operative guidance, requiring the development of a suitable approach to register the subject-specific models to the “subject”, such that they can augment the tracked real-time 2D US images, enabling their interpretation within the subject-specific anatomical context.

## 4.2 Methodology

Our proposed surgical procedure consists of several stages, which we have implemented and tested using “artificial data” acquired from healthy volunteers. Pre-

operative 3D MR images of the subjects were acquired throughout the cardiac cycle, and processed to obtain a subject-specific cardiac model that included anatomical features of interest (i.e. left ventricular myocardium - LV, left atrium and aorta - LAA, right atrium and ventricle - RA/RV, AVA and surgical target - the MVA [8].

During an actual procedure, intra-operative visualization is typically achieved with a 2D TEE probe tracked using a magnetic tracking system (MTS), allowing for an easy 3D reconstruction of the MVA within the surgical VR environment. However, to determine the accuracy with which the subject-specific models can depict the mitral valve throughout the cardiac cycle and demonstrate how the pre-operative models may be integrated within the intra-operative environment, (i.e. how well the pre-operative models align with the intra-operative anatomy), we required a gold-standard representation of the MVA. Therefore, for these experiments, we used 3D TTE to acquire subject images that allowed us to further reconstruct the MVA, and display it within the VR intra-operative environment, mimicking those typically identified intra-operatively using 2D TEE.

Finally, the pre-operative subject-specific model is integrated within the intra-operative VR environment using a feature-based registration approach, as presented in section 4.2.2. The success in aligning the pre-operative and intra-operative anatomy was quantified by the target registration error (TRE) between selected pre-operative and intra-operative cardiac chambers (i.e. LV, LAA and RA/RV).

#### **4.2.1 Building Subject-Specific Cardiac Models for Mitral Valve Interventions**

Subject-specific cardiac models can be generated by expert manual segmentation of a pre-operative MRI or contrast-enhanced CT image dataset. The features of interest can be identified within the inherent limitations of the image dataset, allowing the identification of all features of interest, within the inherent limitations associated

with the manual segmentation of the pre-operative dataset.

Here we briefly describe the workflow involved in the development of subject-specific cardiac models from pre-operative MR images of healthy subjects and the protocol used to assess their accuracy in predicting the surgical target. We use a high-resolution heart model previously constructed from multiple-subject 4D MRI datasets [8] to segment the surgical target (MVA) and other relevant cardiac anatomy by registering the prior model to a subject-specific pre-operative MR image dataset. The resulting subject-specific MVA was then compared to its true location, obtained by manual segmentation of 3D full-volume US images acquired throughout the cardiac cycle. The accuracy with which the MVA could be identified, using the prior model, was assessed by quantifying the target registration error (TRE) between the model-predicted annuli, and those extracted manually from US images.

#### 4.2.1.1 Prior High-Resolution Heart Model

Given its superior soft tissue contrast and 4D imaging capabilities, MRI is often considered the gold-standard modality for cardiac imaging. However, clinical MR images may exhibit low spatial resolution, low signal-to-noise ratio (SNR), and motion artifacts. Consequently, surgical targets extracted directly from these clinical images may not be sufficiently accurate for the planning and guidance of the proposed mitral valve surgery. To address this concern, we used a high-quality prior heart model to characterize the surgical targets in the low-quality subject images. This model was built from low-resolution MR images of 10 subjects (6 mm slice thickness). Various anatomical features (i.e. left ventricular myocardium, right ventricle and atrium, etc.) were manually segmented from each image and the resulting data was then co-registered into a common high-resolution reference image (1.5 mm slice thickness) [9]. The model takes into account both image variability (i.e. measure of the appearance of the heart in the MR images), as well as geometric variability (i.e. measure of the size and shape variation of the features of interest) of the heart. The image variability

was obtained by performing a principal component analysis on the co-registered data. The geometric variability consisted of the anatomical features of interest described earlier, which were segmented in the reference image, and corrected to fit the average shape of the population [8].

The prior model is used to segment anatomical features from routinely-acquired low-resolution cardiac MR images, by fitting the image and geometry components simultaneously to a subject-specific dynamic image dataset. A similar approach was undertaken by Lorenzo-Valdès *et al.* [10], who constructed and segmented an average heart model based on population images, and registered it to target images to automate segmentation. The final models specific to the left ventricular myocardium (LV), left atrium (LA) and right atrium and ventricle (RA/RV) were previously shown to be accurate to within  $5.4 \pm 0.8$  mm [8], despite the low resolution of the subject data.

For this study, in addition to the previously identified anatomical features, the MVA was included in the geometry of the prior model (**Fig. 4.1a**), representing the surgical target during mitral valve interventions.

#### 4.2.1.2 Image Acquisition

**MR Imaging:** Coronal images of the healthy subjects were acquired using a 1.5 T CVi scanner (GE Medical Systems, Milwaukee, USA). The imaging protocol employed an ECG-gated gradient echo pulse sequence, a  $256 \times 128$  image matrix, two signal averages (NEX),  $20^\circ$  flip angle, 7.6 ms TR, and 4.2 ms TE. The dataset consisted of 20 3D images throughout the cardiac cycle, with an in-plane resolution of  $1.5 \times 1.5$  mm<sup>2</sup>, 6.0 mm slice thickness, and a total scan duration of approximately 20 min. To minimize breathing artifacts, 20 sec breath holds were employed during the acquisition of each slice.

**US Imaging:** 3D trans-thoracic US images of the same subjects were acquired throughout the cardiac cycle on a Philips SONOS 7500 scanner. Full-volume apical

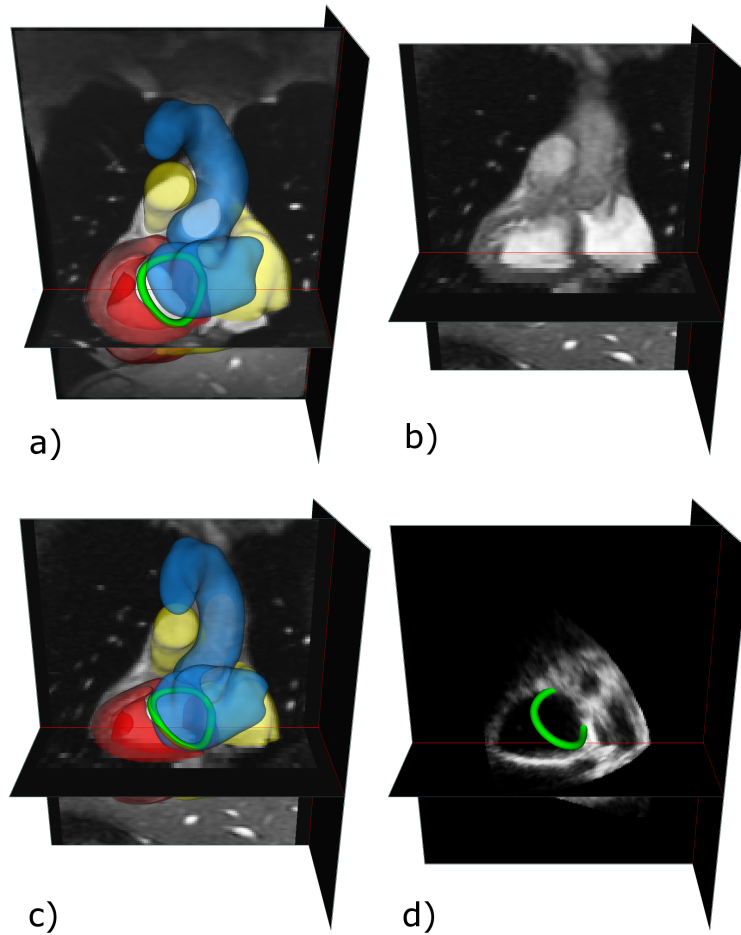


Fig. 4.1: a) Prior high-resolution cardiac model at mid-diastole (MD), containing segmented LV, LA, RA/RV and MVA structures; b) Low-resolution subject MR image at MD; c) Low-resolution MD subject MR image segmented using the prior model; d) 2D US subject image at MD showing the manually segmented MVA.

images of the heart were acquired with a 19 Hz frame-rate and a 14 cm depth-of-focus, with the subject in the left lateral decubitus position. Breath-holds of 5-10 sec were employed to minimize artifacts due to respiratory motion.

#### 4.2.1.3 Anatomical Feature Extraction

**MR Image Segmentation:** In addition to the anatomical features already present, the prior model introduced in section 4.2.1.1 was modified to include the surgical

target — the MVA. The annulus was segmented manually under the assistance of an experienced echocardiographer, by interactively selecting points on the 3D image of the prior model depicting the heart at mid-diastole (MD). We employed a custom-developed spline-based segmentation tool similar to that available for clinical application within the TomTec 4D MV Assessment Software (Unterschleissheim, Germany). The new prior model consisted of a high-quality image component, gross cardiac anatomy, and MVA (**Fig. 4.1a**).

This model was then registered to the low-quality, mid-diastole MR image of the subject (**Fig. 4.1b**). The initial model-to-subject registration was performed using an affine transformation, which was then refined using a non-rigid transformation, to account for the remaining morphological differences between the source and target images. Registration was achieved by maximizing the mutual information between the model and subject image, while ensuring the prior geometry remained consistent with user-selected points in the subject image [8].

The resulting subject-specific model at MD (**Fig. 4.1c**) was then animated over the cardiac cycle to generate a 4D dynamic model. The cardiac motion was extracted using non-rigid registration of the MD subject image to the remaining images in the 4D image dataset (**Fig. 4.2**). These transforms were then used to deform the MD subject-specific model throughout the cardiac cycle [11].

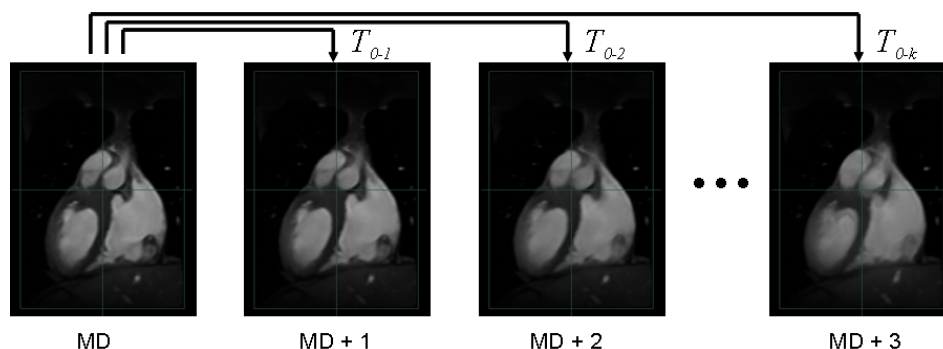


Fig. 4.2: Schematic representation of motion extraction using nonrigid registration of the MD image to the remaining frames in the 4D dataset.

**US Image Segmentation:** The segmentation of the 3D US volumes was performed manually under the guidance of an experienced cardiologist. The same spline-based technique used to segment the MR model was also employed to outline the MVA contour from the subject US images at various time points throughout the cardiac cycle (**Fig. 4.1d**). In addition, the LV geometry was manually segmented from the MD image, and used to register these images to the MR image space. The US to MR registration was performed using an ICP algorithm that aligned the geometric features — the left ventricular myocardia, using an affine transformation.

### 4.2.2 Pre- to Intra-operative Registration

Cardiac therapy guided solely by a pre-operative model is not feasible given the limitations with respect to both building accurate heart models and registering them to the subject with sufficient accuracy. As intra-operative imaging is indispensable for these applications, an OR-friendly approach for building US-enhanced model-guided therapy environments is highly desired. The model-guided component of such environments assists surgeons with the navigation to target, while the US imaging component provides real-time information on the surgical target and tool locations. Hence, a clinically suitable technique should provide intra-operative feasibility from two perspectives: employ readily-identifiable anatomical features and provide adequate anatomical alignment in the regions of interest.

A feature-based registration algorithm was used to augment the intra-operative images with the pre-operative subject-specific cardiac models. This registration consisted of aligning the pre-operatively defined AVA and MVA with those identified intra-operatively, using a two-stage approach. First, we determined unit vectors normal to the pre- and intra-operative AVA and MVA. An initial alignment between the pre-operative and intra-operative annuli was obtained by minimizing the distance between both their centroids, as well as the tips of their corresponding unit vectors. Following initial alignment, the downhill simplex optimizer [12] was used to further



minimize the distance between the two sets of annuli.

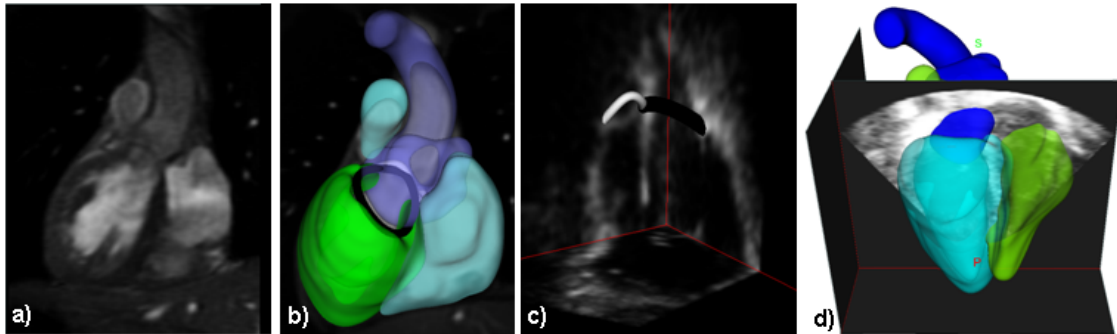


Fig. 4.3: a) Subject MR image at mid-diastole; b) Subject-specific model at MD containing segmented surfaces of the LV, LAA, RA/RV; c) Subject US image at MD acquired “intra-operatively” showing the reconstructed MVA and AVA structures; d) AR environment obtained by integrating the pre-operative subject-specific model within the intra-operative virtual surgical environment by means of feature-based registration.

This technique is straight-forward to implement in the OR, since the structures used to drive the registration can be easily identified. Moreover, it is expected to provide a good alignment of the pre- and intra-operative regions of interest, while adding anatomical context to the otherwise “context-less” intra-operative US images (Fig. 4.3c).

## 4.3 Results

### 4.3.1 Accuracy Assessment of Model-Predicted Mitral Valve Annulus

Our main goal was to determine the accuracy of our model-based segmentation approach in predicting the location of dynamic surgical targets. The accuracy was assessed by computing the root-mean-squared (RMS) TRE between the model-based MVA, and the MVA extracted manually from 3D US images and registered to the MR image space. The TRE was quantified at four different time points in the cardiac

cycle: end-diastole (ED), mid-systole (MS), end-systole (ES), and mid-diastole (MD). In addition, we also estimated the perimeter for both the model-extracted and gold-standard annuli at each of these cardiac frames. A summary of these results is presented in **Table 4.1**.

Table 4.1: Mitral valve annulus perimeter and TRE values of the model-predicted MVA geometry and the gold-standard MVA, quantified at four phases throughout the cardiac cycle, using motion information extracted from both MR and US image datasets.

Cardiac Phase	MR-extracted Motion			US-Extracted Motion		
	Mean Perimeter (mm)		TRE	Mean Perimeter (mm)		TRE
	Model	Gold-Std. (US)	(mm)	Model	Gold-Std. (US)	(mm)
ED	119.9	114.4	2.6	119.9	114.4	2.6
MS	121.3	118.0	7.9	113.0	118.0	3.5
ES	118.5	117.4	10.5	113.5	117.4	3.3
MD	114.3	109.7	2.9	114.3	109.7	2.9

Based on these results, the perimeter of the model-predicted MVAs were within 4.8 % of the perimeter of the annuli extracted from 3D US images, throughout all cardiac frames. As the mitral valve annulus perimeter is not expected to change throughout the cardiac cycle, this measure demonstrated consisted extraction of the annuli from both modalities. Nevertheless, a poor TRE of the two annuli sets was observed during the systolic phases, when the dynamic pre-operative surgical targets were obtained using motion information extracted from the 4D MR image dataset.

According to our analysis, these inconsistencies occurred predominantly on the mitral-aortic valve boundary. The main motion observed in this region of the MVA was caused by the systolic thrust, which is physiologically counteracted by the tension generated within the chordae tendinae by the papillary muscles. However, due to the limited information provided in this region by the low-resolution, thick-slice MR data, these intricate MVA motion patterns could not be correctly reconstructed using the MR images. On the other hand, 3D US images possess a much higher resolution, especially in the valve region, allowing for a clear identification of the valve leaflets.

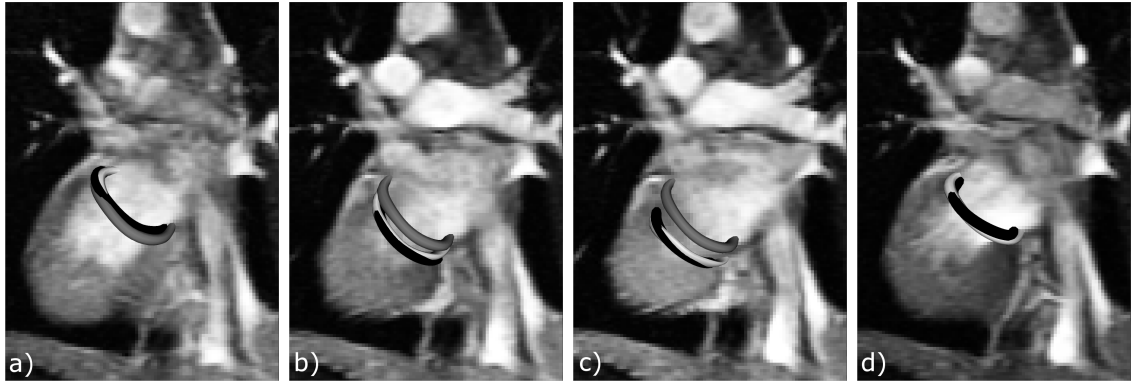


Fig. 4.4: Diagram showing the subject-specific MVA geometry extracted using three different approaches: gold-standard US-based MVA (black), model-based MVA animated using MR motion extraction (grey) and model-based MVA animated using US motion extraction (white). All annuli are registered to the MR space, and displayed at four cardiac phases: a) ED; b) MS; c) ES; d) MD. Note how systolic MVA inaccuracies caused by MR motion extraction (grey vs. black annuli) were significantly improved using US motion extraction (white vs. black annuli).

Therefore, given their high level of detail, the same non-rigid registration algorithm was next employed to extract the cardiac motion from the 4D US image datasets. The resulting TRE during the systolic phases was significantly improved, as reported in **Table 4.1** and **Fig. 4.4**.

### 4.3.2 Pre- to Intra-operative Registration Evaluation

After identifying the pre-operative and intra-operative aortic and mitral annuli, we employed our feature-based registration technique to integrate the pre-operative model within the intra-operative VR space. This enabled us to overlay the 3D subject-specific cardiac model onto the US image, providing additional anatomical context for enhanced intra-procedure visualization and navigation.

Our next goal was to estimate the accuracy of the augmented reality environment, by determining how well the pre-operative models and intra-operative anatomy were aligned using our registration approach. We measured accuracy for each cardiac surface (LV, LAA and RA/RV), by quantifying the RMS distance between the surface

obtained using the feature-based registration versus a previously validated MR to US registration technique (i.e. gold-standard) [8]. This latter transform involved an iterative closest point (ICP) approach to align the LV myocardial surface predefined in both the pre-operative and intra-operative images.

The TRE data were classified into different bins according to the distance from each point on the surface to the mitral/aortic valve annuli. A summary of the TRE values specific to each of the LV, LAA and RA/RV structures was reported in **Table 4.2**. As this work is targeted towards mitral valve image-guided procedures, we tabulated the TRE for the first five bins in each structure, since these regions are located within 50 mm from the surgical target, and are of greatest interest to the surgeons.

In order to interpret these results from a geometric perspective, we reconstructed TRE maps for the LV (**Fig. 4.5**), LAA (**Fig. 4.6**), and RA/RV (**Fig. 4.7**), and displayed them over each surface obtained using the gold-standard registration technique. As expected, low-error regions were located in the vicinity of the mitral and aortic valve annuli, while slightly higher errors were observed with increasing distance from the AVA/MVA.

In addition, we extended this evaluation throughout the cardiac cycle, and assessed robustness of the registration at two diastolic and two systolic phases. A summary of the TRE values specific to each of the LV, LAA and RA/RV structures is reported

Table 4.2: Pre- to intra-operative registration error (RMS distance error - mm) across each model component (LA, LAA and RA/RV).

BIN No. [DISTANCE $d$ (mm)]	Geometry TRE (mm)		
	LV	LAA	RA/RV
<b>BIN 1</b> [ $0 \leq d < 10$ ]	5.2	4.1	7.5
<b>BIN 2</b> [ $10 \leq d < 20$ ]	6.5	4.5	7.4
<b>BIN 3</b> [ $20 \leq d < 30$ ]	7.9	5.1	7.7
<b>BIN 4</b> [ $30 \leq d < 40$ ]	8.8	5.6	11.8
<b>BIN 5</b> [ $40 \leq d < 50$ ]	10.1	5.3	13.2

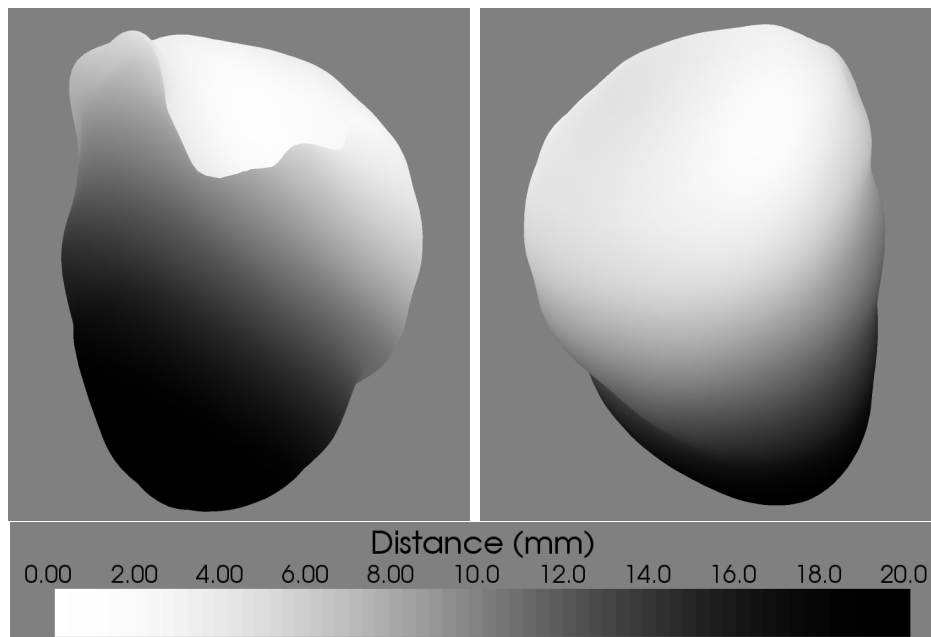


Fig. 4.5: TRE (mm) distribution over the LV surface between the feature-based registration and the ICP-based registration (gold-standard): posterior (left) and anterior (right) view.

in **Table 4.3** for the four cardiac phases: end-diastole (ED), mid-systole (MS), end-systole (ES), and mid-diastole (MD). As this work is targeted towards mitral valve image-guided procedures, we tabulated the TRE for the first four bins in each structure, since these regions are located within 40 mm of the valvular region, and are of greatest interest both for valve procedures, as well as left atrial interventions.

To better interpret these results, we also reconstructed registration error maps for the LV, LAA and RA/RV components (**Fig. 4.8**) at the four cardiac phases.

Table 4.3: RMS TRE across each model component (LV, LAA, RA/RV) at four cardiac phases — end-diastole (ED), mid-systole (MS), end-systole (ES), and mid-diastole (MD) — and binned according to distance from the valves.

Distance Bin $d$ (mm)	ED (mm)			MS (mm)			ES (mm)			MD (mm)		
	LV	LAA	RA/RV	LV	LAA	RA/RV	LV	LAA	RA/RV	LV	LAA	RA/RV
$0 \leq d < 10$	5.4	3.9	7.5	5.5	4.0	7.3	5.3	4.3	7.3	5.3	4.1	7.5
$10 \leq d < 20$	6.6	4.3	7.3	6.4	4.3	7.3	6.4	4.4	7.3	6.6	4.5	7.4
$20 \leq d < 30$	8.0	5.1	7.6	7.9	5.1	8.6	7.8	5.1	8.7	8.0	5.1	7.7
$30 \leq d < 40$	9.0	5.5	11.4	9.1	5.7	12.1	9.0	5.7	12.1	8.9	5.6	11.8

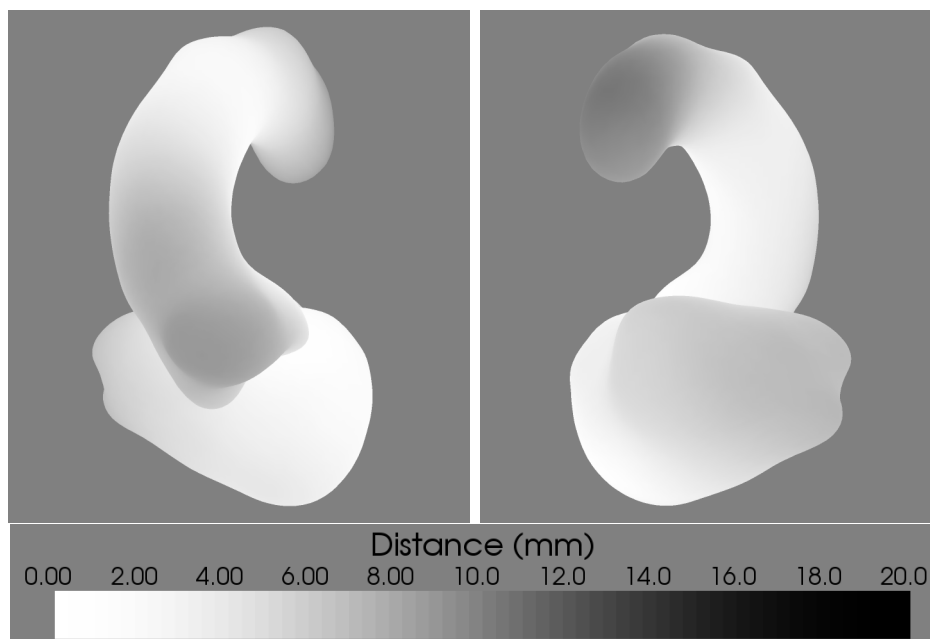


Fig. 4.6: TRE (mm) distribution over the LAA surface, between the feature-based registration and gold-standard: anterior (left); posterior (right) view.

The corresponding registration error is displayed over each surface model component mapped using the gold-standard registration technique as the appropriate cardiac phase. As expected, low-error regions were located in the vicinity of the mitral and aortic valve annuli, while slightly higher errors were observed with increasing distance from the AVA/MVA.

## 4.4 Discussion

This work initiates the investigation of employing pre-operative, subject-specific, dynamic models for enhancement of planning, and navigation of valvular procedures using a VR environment. Specifically, we determined the location of the surgical targets predicted by the pre-operative subject-specific dynamic models to be accurate within 3.1 mm with respect to their true gold-standard location extracted from 3D US images. This study clearly identified weaknesses regarding the extraction of accurate

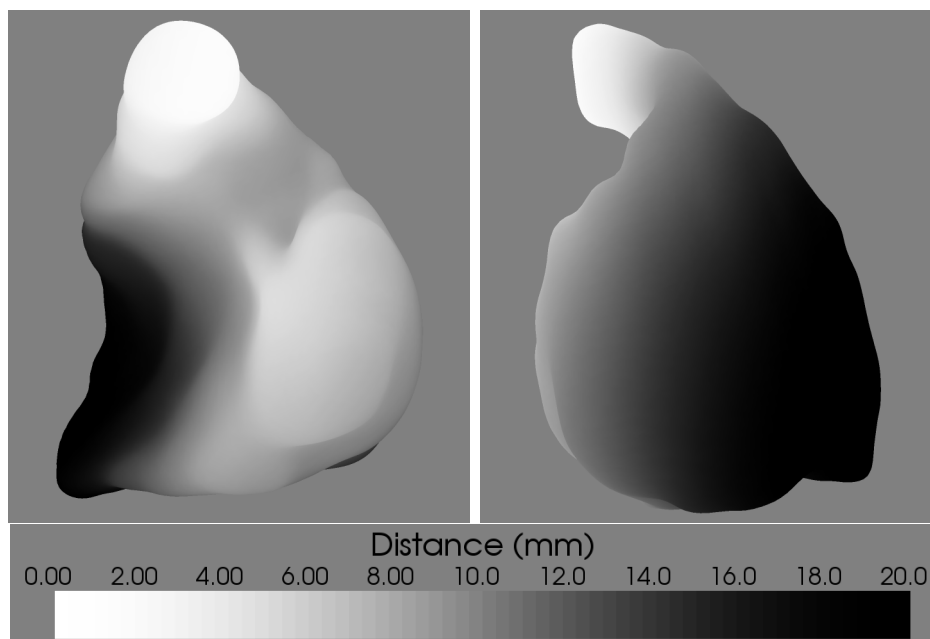


Fig. 4.7: TRE (mm) distribution over the RA/RV surface, between the feature-based registration and gold-standard: posterior (left); anterior (right) view.

valvular motion patterns from clinically feasible MR images, and highlighted the need to acquire a set of full-volume 3D US images of the subject during the proposed clinical protocol, to assist in building accurate pre-operative subject-specific dynamic models.

In term of predicting the dynamic location of the mitral valve, our subject-specific models demonstrated sufficient accuracy, despite the small variations in anatomical structures identified in the MR and US images, as well as any subject-specific physiological variations between the times at which the images were acquired. These cardiac models can be used to augment the surgical virtual environment during image-guided mitral valve interventions. While enhancing procedure visualization by complementing the intra-operative space with 3D anatomical context, these models constitute a significant navigation aid. According to our collaborating cardiac surgeon, a misalignment on the order of approximately 5 mm is tolerable, as these models will be used to facilitate the navigation of instruments towards the surgical targets, whereas

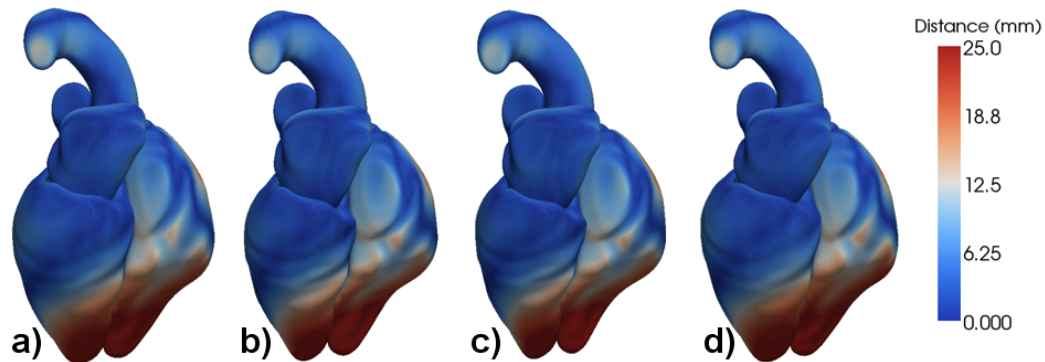


Fig. 4.8: a) Pre- to intra-operative registration error maps achieved via the feature-based registration technique shown for all model components at four cardiac phases: a) ED; b)MS; c) ES; and d) MD.

on-target positioning and fine tuning will be performed under real-time US guidance. In addition, the relative accuracy of the tracked surgical tools is on the order of 1-2 mm [13], leading to an accurate virtual tool-to-US navigation.

Our method of augmenting the intra-operative VR environment with pre-operative anatomy is suitable for interventional applications. It involves the selection of easily identifiable landmarks using intra-operative US imaging, and ensures an accurate registration of the surgical targets. According to our collaborating cardiac surgeon, a misalignment on the order of  $\sim 5$  mm is tolerable, as these models are used to facilitate navigation of surgical instruments inside the heart, whereas on-target positioning and fine-tuning is performed under real-time US guidance. Referring to section 4.3.2, our results were consistent with the objective. We accurately aligned the pre-operative and intra-operative anatomy adjacent to the valvular region in the left ventricle - 5.1 mm (**Fig. 4.5**), as well as the left atrium, and base of the aorta - 4.1 mm (**Fig. 4.6**). This is an important result, given that we use the left atrial appendage as intracardiac port-access for our image-guided off-pump cardiac procedures. Nevertheless, larger errors were recorded for structures further away from the surgical targets, such as posterior and apical regions of the left ventricle (**Fig. 4.5**), as well as the anterior and right-lateral region of the right ventricle, right atrium, and pulmonary artery



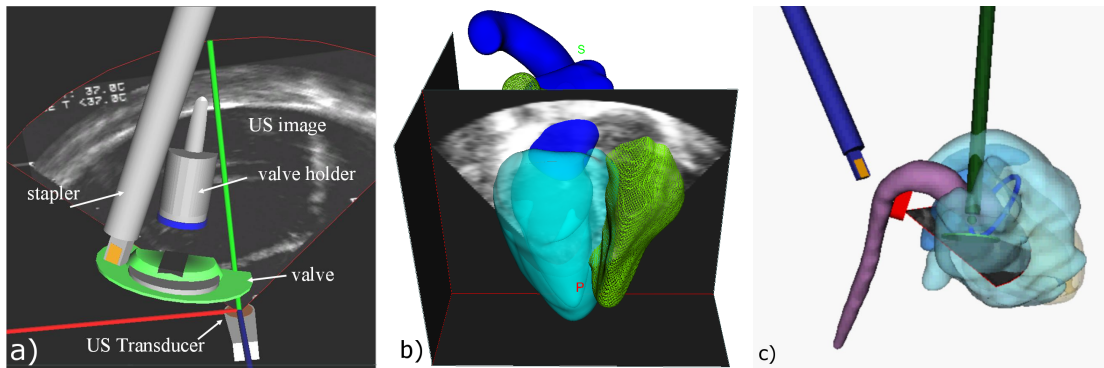


Fig. 4.9: a) Surgical VR environment consisting of 2D US probe and image, valve-guiding tool, and valve-fastening tool; b) Pre-operative subject-specific model displaying LV, LA, and RA/RV surfaces registered to the intra-operative space for visualization and navigation enhancement (note alignment of ventricular septum in model and US); c) Illustration of the mixed reality environment employed during an *in vivo* porcine study, showing pre-operative heart model, intra-operative TEE image, tracked TEE probe, and surgical tools.

(Fig. 4.7).

## 4.5 Conclusions

To conclude, the proposed model-based segmentation approach can be used to generate subject-specific dynamic model of the cardiac anatomy that can predict the location of surgical targets or features of interest (in this case the mitral valve annulus), with a 3.1 mm accuracy throughout the cardiac cycle. Moreover, these dynamic pre-operative models could be integrated within the intra-operative imaging environment using registration, to enhance intra-procedure planning and navigation of image-guided mitral valve surgery.

The accuracy of the augmented environment was assessed by quantifying the target registration error achieved using our feature-based registration relative to a previously validated gold-standard technique in our laboratory. According to our findings, the environment was accurate within less than 5 mm for regions located in the vicinity of the surgical target ( $\sim 0 - 15$  mm away from the MVA), while larger errors occurred

at remote locations.

As part of our future research, we plan to further optimize the feature-based registration approach to improve the overall alignment of pre-operative and intra-operative anatomy. Our ultimate objective is to extend this work towards *in vivo* studies involving animal subjects in the operating room, to validate it using 2D TEE for real-time intra-operative visualization, and to illustrate the direct benefits of employing these anatomical models on enhancing surgical navigation. However, a database of porcine cardiac MR images is not currently available in our laboratory, and manual and semi-automatic segmentation techniques are employed to generate anatomical models from the pre-operative MR images, as described in Chapter 5.

# References

- [1] D.E. Harken, L.B. Ellis, and P.F. Ware. The surgical treatment of mitral stenosis: valvuloplasty. *N Engl J Med.*, 239:801–9, 1948.
- [2] J.R. Gibbon. Application of a mechanical heart and lung apparatus to cardiac surgery. *Minn Med.*, 37:171–85, 1954.
- [3] A. P. Kypson, J. E. Felger, L. W. Nifong, and W. R. W. R. Chitwood. Robotics in valvular surgery: 2003 and beyond. *Curr Opin Cardiol.*, 19:128–33, 2004.
- [4] A. Vahanian and C. Acar. Percutaneous valve procedures: What is the future? *Curr Opin Cardiol.*, 20:100–106, 2005.
- [5] S.w. Downing and L.H. Edmunds. Release of vasoactive substances during CPB. *Ann Thorac Surg.*, 54:1236–43, 1992.
- [6] J. Zeitlhofer, S. Asenbaum, C. Spiss, A. Wimmer, N. Mayr, and E. Wolner. Central nervous system after . *Eur Heart J.*, 14:885–90, 1993.
- [7] F. Sauer. Image registration: Enabling technology for image-guided surgery and therapy. In *Proc. IEEE Eng Med Biol.*, pages 7242–45, 2005.
- [8] M. Wierzbicki. Subject-specific models of the heart from 4D images. PhD Dissertation, 2006. Medical Biophysics, The University of Western Ontario, Canada.
- [9] J. Moore, M. Drangova, M. Wierzbicki, J. Barron, and T.M. Peters. A high-resolution dynamic heart model based on averaged MRI data. In *Proc. Med Image Comput Comput Assist Interv.*, volume 2878 of *Lect Notes Comput Sci.*, pages 549–55, 2003.
- [10] M. Lorenzo-Valdés, G.I. Sanchez-Ortiz, D. Mohiaddin, and D. Rueckert. Atlas-based segmentation and tracking of 3D cardiac mr images using non-rigid registration. In *Proc. Med Image Comput Comput Assist Interv.*, volume 2488 of *Lect Notes Comput Sci.*, pages 642–50, 2002.
- [11] M. Wierzbicki, M. Drangova, G. M. Guiraudon, and T. M. Peters. Validation of dynamic heart models obtained using non-linear registration for virtual reality

training, planning, and guidance of minimally invasive cardiac surgeries. *Med Image Anal.*, 8:387–401, 2004.

- [12] W. H. Press and B. P. *et al.* Flannery. *Numerical recipes in C: The arts of scientific computing*. Cambridge University Press, Cambridge, England, 1992.
- [13] A. D. Wiles, G. M. Guiraudon, J. Moore, C. Wedlake, C. A. Linte, D. L. Jones, D. Bainbridge, and T. M. Peters. Navigation accuracy for an intracardiac procedure using virtual reality-enhanced ultrasound. In *Proc. SPIE Medical Imaging 2007: Visualization and Image-Guided Procedures*, volume 6509, pages 61410W–10, 2007.

## Chapter 5

# Mitral Valve Implantation and Atrial Septal Defect Repair under Model-enhanced Ultrasound Guidance: *In vivo* Pre-clinical Feasibility Studies

*In Chapter 3 we assessed the guidance capabilities of the model-enhanced US-assisted platform and in Chapter 4 we proposed a method to generate pre-operative subject-specific models of the heart and integrate them into the intra-operative environment. Here we present our experience in translating this work to pre-clinical studies, to guide typical intracardiac interventions — mitral valve implantations and ASD repair procedures, in vivo in swine models.*

---

This work is adapted from Linte CA, Moore J, Wedlake C and Bainbridge D, Guiraudon GM, Jones DL and Peters TM. Inside the Beating Heart: An *In Vivo* Feasibility Study on Fusing Pre- and Intra-operative Imaging for Minimally Invasive Therapy. *International Journal of Computer Assisted Radiology and Surgery* 4(2):113-123. 2009.

## 5.1 Introduction

In the previous chapters we described the new model-enhanced US-assisted guidance environment intended to facilitate the delivery of intracardiac therapy with minimal invasiveness, in absence of direct vision [1, 2, 3]. Spatially tracked 2D TEE images are augmented with pre-operative anatomy and virtual representations of the delivery instruments tracked in real time using magnetic tracking technology [2, 3], enabling their interpretation within the appropriate 3D anatomical context for enhanced intra-operative guidance.

This chapter describes the workflow involved in augmenting real-time US imaging with pre-operative cardiac models and virtual representations of the surgical instruments during pre-clinical studies conducted *in vivo* on swine models. Furthermore, our preliminary experience related to the clinical implementation of the model-enhanced US environment to guide mitral valve implantations and ASD repairs in a minimally invasive manner, is reported.

All animal experiments described in this study were approved by the Animal Care and Use Committee of The University of Western Ontario and followed the guidelines of the Canadian Council on Animal Care.

## 5.2 Methodology

The *in vivo* clinical routine associated with this surgical technique involves several stages, which we describe here by following a typical porcine subject through the protocol. Pre-operatively, a dynamic MR cardiac image dataset of the subject is acquired and used to generate a subject specific dynamic heart model. Intra-operatively, TEE is employed for real-time interventional guidance, permitting a fast reconstruction of the intra-operative cardiac anatomy. The feature-based registration technique described in section 4.2.2 is used to map the pre-operative cardiac models onto the intra-operative anatomy imaged via ultrasound. Ultimately, the virtual surgical envi-

ronment is further augmented with representations of the surgical instruments tracked in real-time using a MTS.

## 5.2.1 Pre-operative Imaging and Modeling

The high spatial resolution and excellent capabilities for soft tissue characterization without contrast enhancement promote MRI as a suitable modality for acquiring high-quality dynamic cardiac datasets. These images allow for a clear definition of various anatomical features of interest and can therefore be utilized to construct pre-operative models of the heart.

### 5.2.1.1 Pre-operative Image Acquisition.

The animal was initially anesthetized using Telazol (5 mg/kg) reconstituted with 5 ml of Rompum (100 mg/ml at a dose of 2 ml/50 kg) and Atropine (0.04 mg/kg). At the imaging facility, the subject was intubated with an endotracheal tube and ventilated with oxygen (900 ml/min), nitrous oxide (800 ml/min), and isoflurane (1.5-2%) delivered via a mechanical ventilator.

The pig was imaged using a 1.5 T MRI scanner (General Electric, Milwaukee, WI, USA), using a flexible, phased-array cardiac radio-frequency coil. Cardiac image acquisition was gated to the R-wave of the animal's ECG and 20 images were reconstructed per slice, depicting the heart at different cardiac phases. The fast cine gradient-echo pulse sequence was employed, with a 10.4 msec repetition time (TR), 5.8 msec echo time (TE), 35° flip angle, 8 views per segment, 3 signal averages (NEX), 256 x 128 image matrix, and a 28 mm field of view. To ensure that all slices were acquired at the same point in the respiratory cycle and to minimize the image artifacts due to breathing [4], each slice was acquired while the pig's respiration was consistently suspended at end-expiration using the mechanical ventilator; the animal was re-ventilated for 2 mins after each slice acquisition. The complete image dataset

consisted of 50 sagittal image slices at each cardiac phase, with a 2.0 mm slice thickness and a 1.09 mm x 1.09 mm in-plane resolution. Each slice was acquired over 21 sec, as governed by the average length of the animal’s cardiac cycle ( $\sim 0.9$  sec), resulting in a total scan time of approximately 18 minutes for the entire volume.

### 5.2.1.2 Static Cardiac Model

The dynamic MR image dataset was processed to generate a pre-operative cardiac model of the pig’s heart. Our approach to cardiac modeling consists of first generating individual models for different cardiac components, and then assembling them according to the complexity of the image-guided procedure performed. The main features of interest include the left ventricle myocardium (LV), the left atrium (LA), and the right atrium and ventricle (RA/RV).

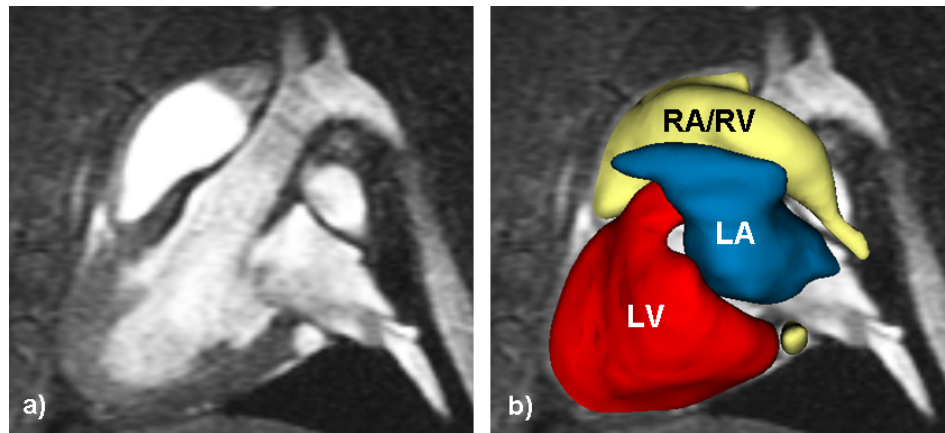


Fig. 5.1: a) Porcine heart image at mid-diastole (MD); b) Porcine heart model at MD showing the left ventricle (LV), left atrium (LA) and right atrium & ventricle (RA/RV).

We extracted all anatomical features using manual segmentation of the mid-diastole (MD) image in the 4D dataset (**Fig. 5.1**). We chose the MD image as the reference because the heart is relatively static during this phase, and hence this image exhibits a low susceptibility to motion artifacts. The image was segmented on a slice-by-slice basis by outlining the region enclosed by the endocardial and epicardial



contours. The outflow tract regions were segmented along the median planes delimiting the LV from the left atrium and aorta, therefore providing a relatively “clean” separation of the cardiac structures. The binary image obtained during segmentation was then processed using the marching cubes algorithm [5] to generate a surface model of each organ component (**Fig. 5.2**). Each surface was smoothed using a Gaussian filter and decimated to increase rendering speed [6].

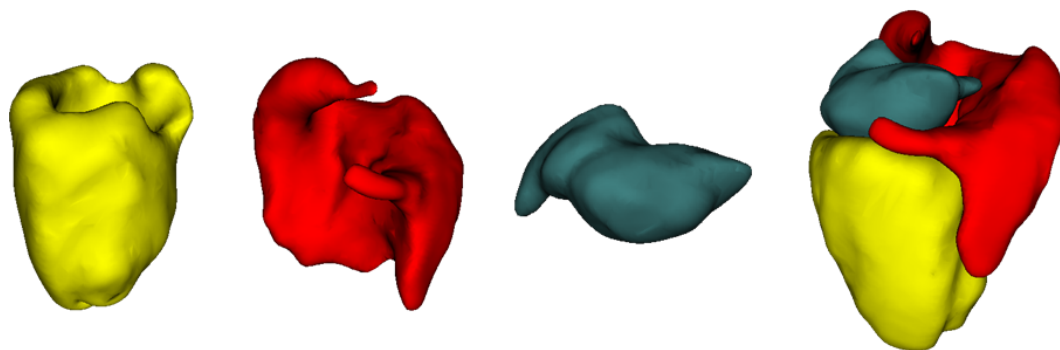


Fig. 5.2: Anatomical models of left ventricle (LV), right atrium and ventricle (RA/RV), left atrium (LA), and complete heart (shown from left to right) extracted from the pre-operative MR dataset of the porcine subject at mid-diastole.

### 5.2.1.3 Dynamic Model

Static anatomical models are of value when performing interventions on organs in the human body that do not undergo significant physiological or intra-procedural deformations. As this characteristic is not applicable to the heart, we employed a technique previously developed in the lab to reconstruct the heart motion throughout the cardiac cycle. A 3D free form deformation field that describes the trajectories of all points in the surface model was extracted using non-rigid image registration, according to the technique described by Wierzbicki *et al* [7].

Using the mid-diastole (MD) heart image as a reference, the frame-to-frame motion vectors ( $T_{0-k}$ , where  $k = 1$  to 19) were computed by non-rigidly registering the 3D MD image (corresponding to  $k = 0$ ) to each of the remaining frames in the 4D

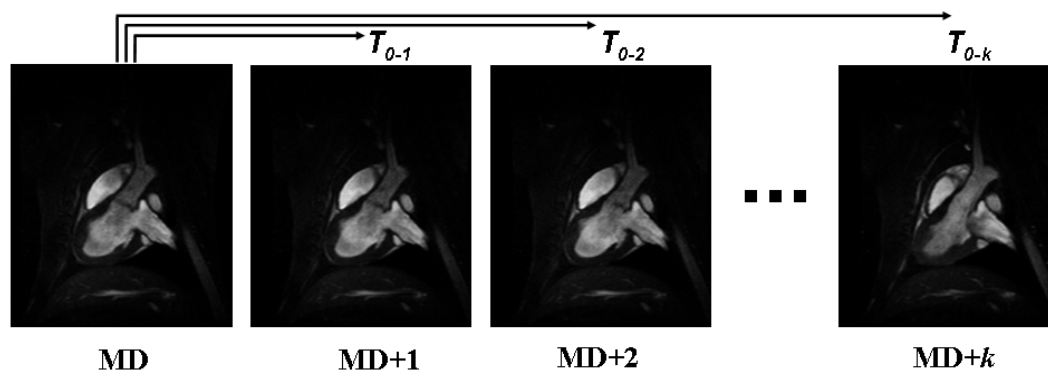


Fig. 5.3: Schematic representation of motion extraction using non-rigid registration of the MD porcine cardiac image to the rest of the frames in the 4D dataset.

dataset (Fig. 5.3).

Ultimately, a dynamic cardiac model was obtained by sequentially propagating the static model throughout the cardiac cycle using the motion vectors previously estimated, and rendered to portray the cardiac dynamics (Fig. 5.4).

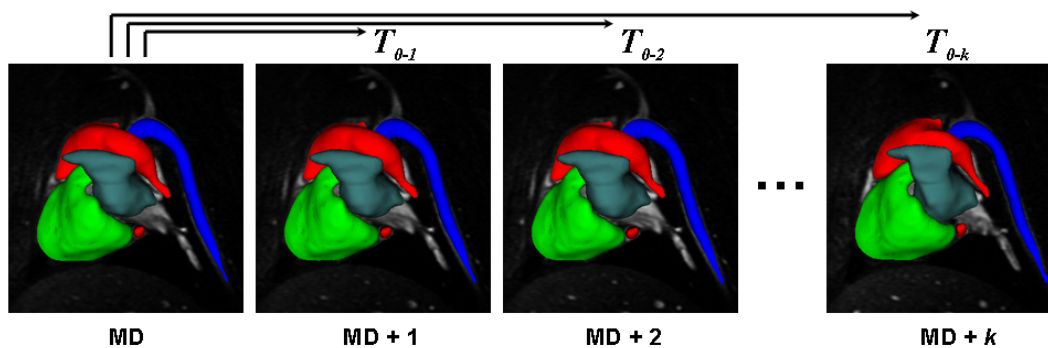


Fig. 5.4: Dynamic cardiac model displayed at different phases in the cardiac cycle, obtained by animating the static model with the transforms obtained using image registration.

## 5.2.2 Intra-operative Guidance

### 5.2.2.1 Trans-esophageal Echocardiography

Two dimensional TEE offers flexibility in acquiring good-quality images, and also eliminates the interference between probe manipulation and surgical work-flow. Nev-

ertheless, the main disadvantage of interventional 2D US is the inadequate representation of the anatomical targets and surgical tools. To address these limitations, the 2D intra-procedure images were augmented with anatomical context supplied by the subject-specific models derived pre-operatively. Peri-operatively, TEE images of the heart were acquired to will serve as the “target image” to which the pre-operative models were registered, using the feature-based registration approach described in Chapter 4.

### 5.2.2.2 Peri-operative Image Acquisition

2D TEE images were acquired using a Philips SONOS 7500 machine (Philips Ultrasound Division, Bothell, WA, USA). The images were encoded spatially using the tracking information provided by the NDI Aurora MTS (Northern Digital Inc., Waterloo, ON, Canada). A 6 DOF magnetic sensor coil was rigidly attached to the US probe and calibrated using a Z-string phantom [8] prior to its insertion in the esophagus. The image acquisition was gated to the R-wave of the animal’s ECG using a standard 3-lead configuration. All images were acquired during breath-holding, by shutting off the mechanical ventilator at end-expiration. A subset of 19 2D images with a 10 cm field of view, and 0.3 mm x 0.3 mm resolution, and a 5 MHz frequency were acquired at each cardiac phase by rotating the TEE transducer about its normal axis at 10° angular increments (**Fig. 5.5**).

### 5.2.2.3 Peri-operative Image Processing

“Pseudo” 3D US images were reconstructed at each cardiac phase, by inserting each of the 2D US image frames into its appropriate location within a 3D image volume, according to its position and orientation information recorded by the magnetic tracking system (**Fig. 5.6**). Ideally, the 2D image frames would only differ from each other by the acquisition angle, as the 2D acquisition fan was rotated at equi-angular increments about the normal axis of the transducer. Moreover, the tracking informa-

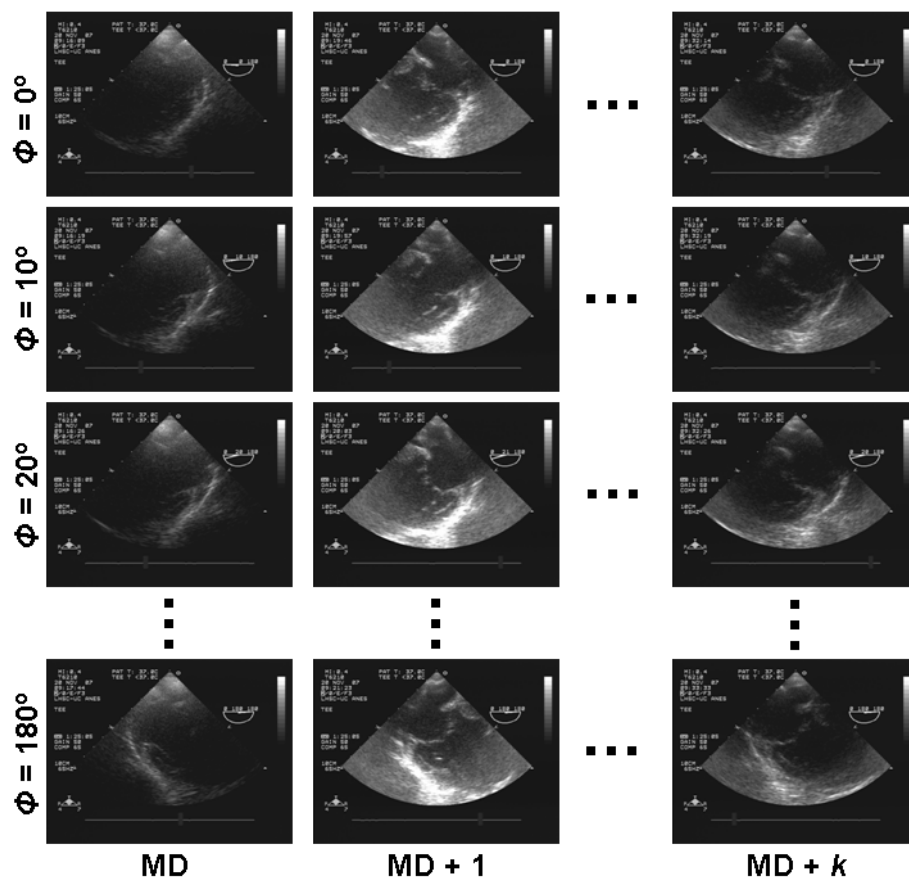


Fig. 5.5: Schematic illustration of the complete US image dataset acquisition. Subsets of 19 2D images of the heart were acquired at equi-angular increments of  $10^\circ$  at each phase in the cardiac cycle, using a magnetically-tracked TEE probe. The acquisition started at mid-diastole and was gated to the animal's ECG, resulting in multiple image datasets, each depicting the heart at a different cardiac phase.

tion could also be used to correct for any undesired motion of the transducer during acquisition prior to the insertion of each 2D image frame into the 3D volume. In addition to their spatial stamp, each image was also inserted into the appropriate cardiac phase volume, as prescribed by the time stamp encoded by the ECG gating. This process ultimately led to a set of volumetric displays of the intra-operative anatomy reconstructed by assembling all angular frames acquired at each cardiac phase (**Fig. 5.7**). The resulting 3D displays are not continuous images, but rather collections of 2D US images arranged according to their position in space and time

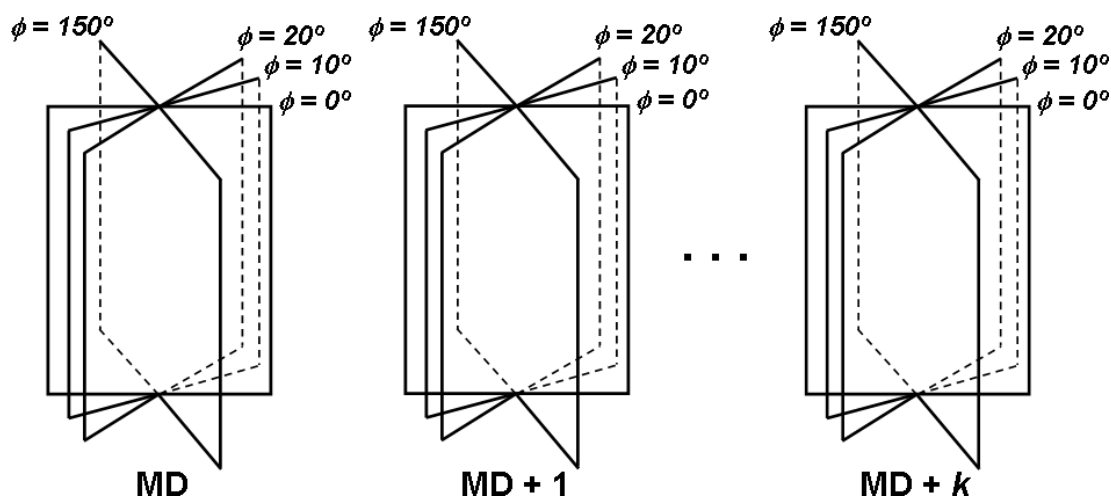


Fig. 5.6: Schematic representation of the generation of “pseudo” 3D US volumes: each 2D US image is inserted into the 3D volume according to its spatial stamp, recorded by the MTS, and temporal stamp, recorded by the ECG gating.

that provide a 3D perspective of the intra-operative cardiac anatomy.

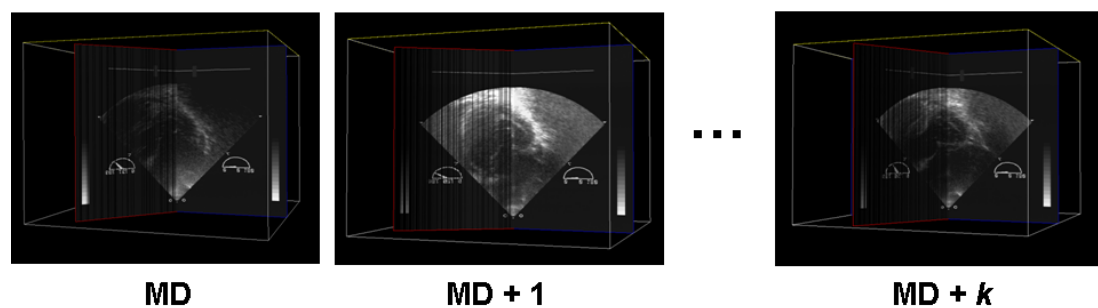


Fig. 5.7: “Pseudo” 3D reconstruction of the intra-operative anatomy images at different cardiac phases. Each image is obtained by inserting the intra-operatively acquired 2D US image frames at their appropriate location within the 3D volume, as prescribed by their spatial and temporal information encoded using magnetic tracking and ECG gating.

These “pseudo” 3D displays allow us to extract features of interest from the intra-operative cardiac anatomy. By aligning the visualization plane with the individual 2D US images, the user can select points of interest in each image of the 3D dataset, ultimately resulting in a 3D reconstruction of the feature of interest over the entire dataset. In our case, we use the “pseudo” 3D US volumes to select anatomical structures — the mitral (MVA) and aortic (AVA) valve annuli — used for registration.

## 5.3 Virtual Environment and Surgical Guidance

### 5.3.1 Pre- to Intra-operative Registration

The feature-based registration technique presented in § 4.2.2 was employed to augment the intra-operative US images with the pre-operative cardiac models. Easily identifiable targets — the mitral (MVA) and aortic (AVA) valve annuli — in both the pre- and intra-procedure datasets, were chosen to drive the model-to-subject registration algorithm (**Fig. 5.8b**).

The pre-operative annuli were segmented manually from the cardiac MR image under the guidance of an experienced cardiologist, using a custom-developed spline-based segmentation technique. The intra-operative annuli were extracted by an experienced echocardiographer from the “pseudo” 3D US volume generated in the peri-operative stage. The visualization plane was interactively aligned with each of the angular 2D US images in the dataset and the end-points of the mitral and aortic valve annuli were selected. Ultimately, 3D splines were used to connect the selected points corresponding to the mitral, and respectively, the aortic annulus.

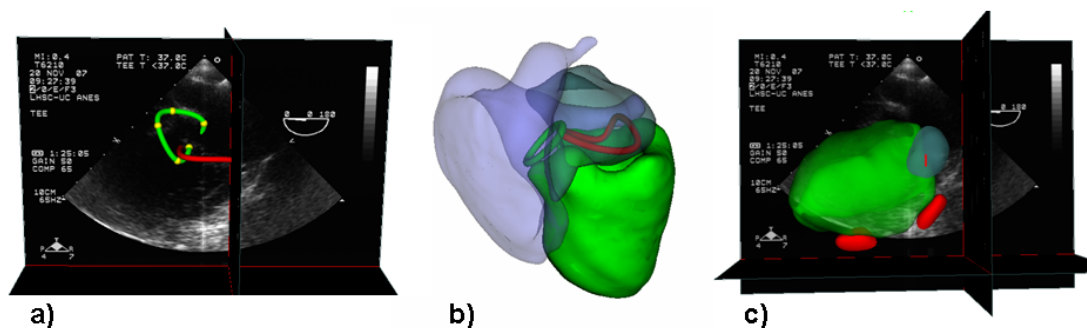


Fig. 5.8: a) Intra-operatively reconstructed 3D US image at mid-diastole containing the intra-operative MVA and AVA; b) Pre-operative heart model at mid-diastole also showing the segmented MVA and AVA; c) Pre-operative heart model fused with the intra-operative US image after performing the model-to-subject registration using the feature-based technique.

The feature-based registration technique presented in Chapter 4 was employed to

overlay the pre-operative 3D model onto the 2D TEE US image (**Fig. 5.8c**). This registration technique is suitable for cardiac interventions, as the selected valvular structures are easily identifiable in both the pre-operative and intra-operative datasets, and they also ensure a good alignment of the pre- and intra-operative surgical targets. Furthermore, given the location of the features used to drive the registration, we expect reasonable anatomical alignment in the surrounding regions, enabling us to employ this technique for a variety of image-guided interventions inside the heart.

Table 5.1: Alignment accuracy achieved via feature-based registration estimated over the anatomical features of interest. Note: Alignment error is reported as RMS (mm) and binned according to the distance of the surface points from the mitral and aortic valves.

Distance $d$ (mm) from AVA & MVA	RMS Alignment Error (mm)		
	LV	LA	RA/RV
$0 \leq d < 10$	5.2	4.1	7.5
$10 \leq d < 20$	6.5	4.5	7.4
$20 \leq d < 30$	7.9	5.1	7.7

As shown in the previous chapter, the accuracy achieved in aligning the pre-operative models with the intra-operative anatomy was on the order of 5.2 mm, 4.1 mm and 7.5 mm for the regions of the left ventricle (LV), left atrium (LA), and right atrium and ventricle (RA/RV), respectively, located within 10 mm from the mitral and aortic valve annuli. Furthermore, an accuracy of approximately 6 mm was maintained for the chambers of interest across regions located 20-30 mm away from the valves. **Table 5.1** summarizes the root-mean-squared (RMS) distance error resulted in aligning the pre- and intra-operative structures, estimated across regions located within 30 mm from the mitral and aortic valves.

Following the model-to-patient registration, the surgeon had access to the complete AR environment during intra-procedure guidance, as opposed to just the 2D intra-operative US images. **Fig. 5.9a** shows an example of a 2D intra-procedure image used for guidance during a different experiment, displayed within the pre-

operative anatomical context. Ultimately, the virtual environment is complemented with the representations of the surgical instruments also built pre-operatively and used to track the position and orientation of the physical instruments within the virtual surgical space (**Fig. 5.9b**).

### 5.3.2 Image-Guided Therapy Applications

We next describe our preliminary experience in the OR employing such AR environments to guide typical intracardiac procedures on the beating heart in porcine subjects, including a mitral valve implantation procedure and an ASD closure intervention. For all studies, direct vision was substituted by our augmented virtual environment integrating real-time US imaging, pre-operative anatomical images, and virtual models of the magnetically tracked surgical tools, all displayed on a single flat screen monitor, and stereoscopically via HMDs worn by the surgeons.

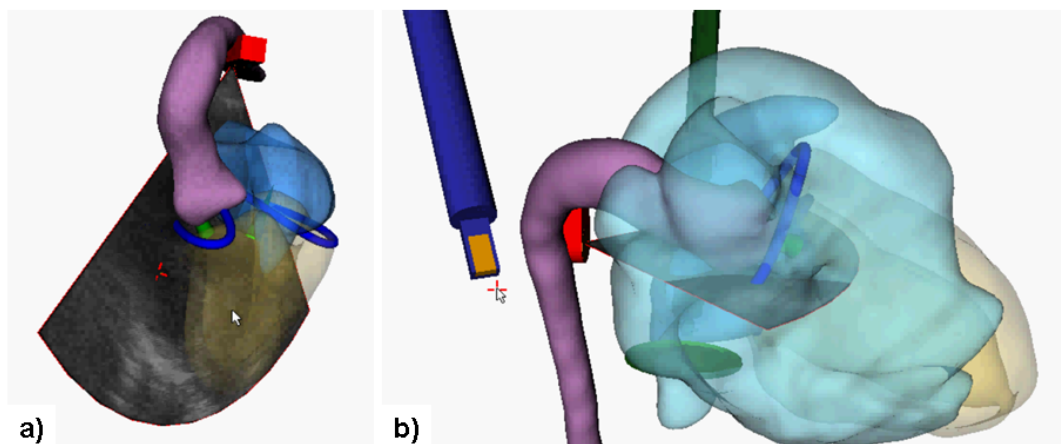


Fig. 5.9: a) Intra-operative 2D US image displayed within anatomical context provided by the pre-operative cardiac model; b) Complete AR environment including pre-operative model, intra-operative US image, TEE transducer, and virtual models of the surgical instruments.

Direct intracardiac access was achieved via the UCI [9], a device used to gain access inside beating heart, briefly mentioned in Chapter 2. The UCI had previously



undergone extensive testing using animal studies to demonstrate its feasibility for endocardial ablation for atrial fibrillation, and mitral valve implantation. This device provides safe port access to intracardiac cavities and targets, and can be removed at the end of the intervention. The UCI is designed as an “air lock” between the blood-filled cardiac cavities and the atmosphere of the chest, and it consists of an insertion cuff, attached at one end to the atrial appendage, and at the other end to the introductory chamber. This chamber has sleeves that allow the introduction of up to four different surgical instruments (e.g. laparoscopic tools, pressure line, endoscope, etc.) inside the beating heart with minimal blood loss, through the specially-designed access ports (Fig. 5.10). The introducer is safe and versatile and does not extensively compromise the manipulation of tools.

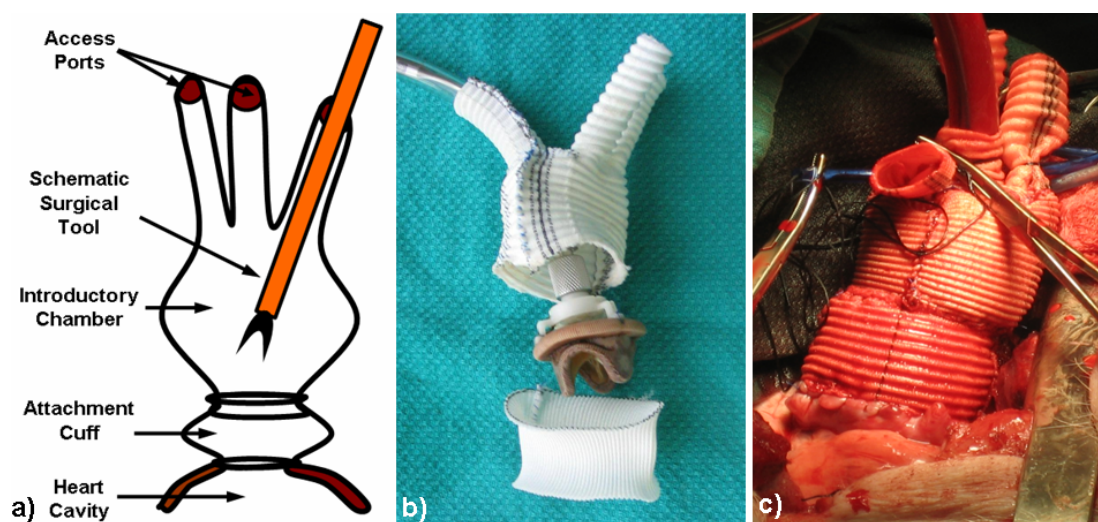


Fig. 5.10: a) Schematic representation of the Universal Cardiac Introducer (UCI); b) UCI displaying the attachment cuff and the introductory chamber with the access ports containing and a valve-guiding tool and prosthetic valve; c) UCI attached to the heart chamber during an *in vivo* porcine study.

### 5.3.2.1 Mitral Valve Implantation

One of the most challenging interventions that we have attempted using our hybrid image-guidance system is the implantation of a mitral valve, procedure that typically

requires a direct access approach to surgery under CPB. Catheter-based navigation techniques are highly preferred for implanting an aortic valve, given the self-centering effect of the collapsible valve within the artery after deployment. However, such methods are not ideal for implanting an artificial mitral valve, mainly due to the challenges encountered while correctly positioning and fastening the prosthetic valve.

Following the success achieved during our *in vitro* studies in the laboratory [2], we initiated the translation of the work into the OR in porcine models. Direct intracardiac access was achieved using the the UCI, attached to the left atrial appendage of the pig's heart via a left side minithoracotomy. A magnetically-tracked 2D trans-esophageal US transducer was used for real-time intra-procedure image-guidance. Pre-operatively generated models of the pig's heart were registered to the intra-procedure imaging space using the feature-based registration approach described earlier. The surgical tools employed in this intervention consisted of a valve-guiding tool, to which the prosthetic valve was attached via a release mechanism, and a fastening tool — a laparoscopic clip applier.

The prosthetic valve was positioned onto the native mitral annulus, and then fastened to the underlying tissue using the clip applier. Both steps entailed two distinct tasks: the former consisted of navigating the valve-guiding tool and valve-fastening tool to the target, under guidance provided by the virtual tool and organ models. The latter involved the actual therapy delivery, represented by the correct positioning of the valve onto the mitral annulus, followed by the correct application of the surgical clips at the desired locations, performed under real-time US image guidance (**Fig. 5.11**). Intra-operative procedure assessment using Doppler US imaging confirmed successful implantation of the valve, as observed in the post-procedure analysis.

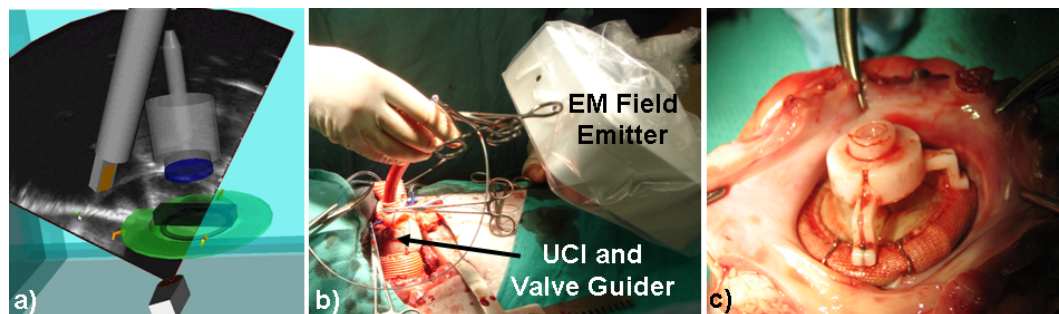


Fig. 5.11: a) AR environment displaying a virtual model of the US transducer, 2D image fan, and two virtual models of the surgical tools: the valve-guiding tool and valve-fastening tool; b) Typical OR setup during a mitral valve implantation procedures; c) Post-procedure assessment image showing the prosthetic valve successfully positioned over the native mitral annulus.

### 5.3.2.2 Atrial Septal Defect Repair

Any optimal minimally invasive ASD closure procedure should combine off-pump techniques with the effectiveness and versatility of the traditional open-heart approach. Here we report our experience in guiding an off-pump ASD repair in porcine models under model-enhanced US-assisted guidance. Our goal was first to create an ASD over the fossa ovale (FO), and then close it by positioning a patch over its surface. The right atrium (RA) of the pig was exposed via a right-lateral thoracotomy, and the UCI was attached to an excluded segment of the free right atrial wall.

The septal defect was created using a custom made punch tool (15 mm diameter) (**Fig. 5.12a**) introduced via the UCI and used to extract a circular region of tissue from the FO under real-time US guidance (**Fig. 5.12b**). After resection of the FO, the blood flow through the ASD was identifiable on Doppler US. A repair patch attached to a guiding tool and the laparoscopic clip applicator, as a fastening device, were then introduced into the RA via the UCI. Using the pre-operative anatomical information and the virtual models of the surgical tools, the patch was guided to the target. One minor challenge resulted due to the slightly large clip applicator tool used to fasten the patch, which collided with the patch guiding tool during navigation, given the confined

intracardiac space. After navigating the tools on target, the surgeon relied on the real-time US images to correctly position the patch onto the created ASD and attach it to the intra-atrial septum. The correct placement of the patch completely occluding the ASD orifice was also confirmed in the post-procedure assessment (**Fig. 5.12c**).

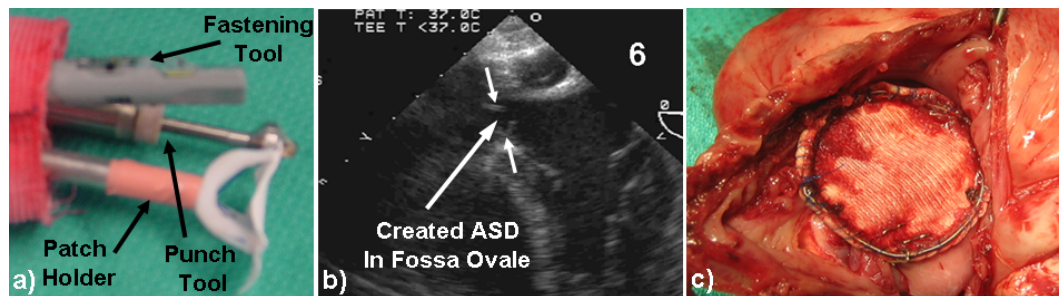


Fig. 5.12: a) Image showing three tools employed during the creation and repair of an ASD procedure; b) 2D intra-operative US image showing a “hole” in the FO after the creation of the ASD; c) Image showing the successful ASD repair: note the repair patch covering the previously created septal defect.

The attachment of both the prosthetic valve and septal repair patch, using the laparoscopic stapler, was adequate given the acute nature of these studies; however, we still need to further investigate and improve the durability and robustness of the fastening. These initial studies have focused on correctly navigating and positioning the valve and repair patch on target using the novel guidance environment, and we chose this fastening technique to anchor the valve and patch in place sufficiently well to enable post-procedure assessment. However, proper fastening tools specific for these applications are currently under design and provided they comply with the requirements, we plan to use them in future *in vivo* clinical evaluation studies.

## 5.4 Discussion

Since the surgeon is not able to directly observe the endocardial surfaces of the heart while it is beating, we employ pre-operative anatomical models and real-time TEE imaging to replace the traditional view of the surgical field with an AR environ-

ment. This environment resembles the real surgical space — the cardiac chambers, structures of interest and surgical tools, and consists of images of the heart gathered both before and during the operation, complemented with models of the instruments used in surgery.

Although two-dimensional TEE plays a significant role in our interventional system, providing the operator with real-time intra-procedure information, the 2D images are of limited use when identifying the position and orientation of the surgical instruments with respect to the target. Pre-operative models, on the other hand, enhance surgical navigation, but surgeons need to be aware that a perfect correspondence between the real and virtual anatomy cannot be achieved. These models are not sub-millimeter replicas of the subject's heart, registration techniques cannot provide a sub-millimeter alignment between the model and the subject's heart, and moreover, because of latencies associated with the image processing, it is virtually impossible to achieve accurate real-time synchronization between the model and the actual beating heart.

During a typical surgical procedure, US images of the heart are acquired peri-operatively, after accessing the thoracic cavity via a minithoracotomy and attaching the UCI. Hence, the intra-operative anatomy imaged via US already reflects the changes in geometry of the heart chambers induced by accessing the intracardiac targets. On the other hand, the cardiac geometry depicted by the pre-operative models is based on closed-chest data, and may therefore differ slightly from the intra-operative geometry. This issue is ameliorated by registering the pre-operative model to the true, intra-operative anatomy imaged via real-time US, after opening the chest and accessing the intracardiac space. However, pre-operative models of the heart that take into account physiological and positional changes arising due to the surgical access are unlikely to be generated; hence, surgeons cannot rely solely on these models for procedure guidance, and therefore must make use of US imaging for real-time visualization. It is important to understand that the virtual anatomical models consist

of an aid to improve anatomical context and facilitate the navigation to target, while TEE consists of the true, real-time visualization modality employed when performing all on-target, detailed manipulations.

Also from a modeling perspective, the use of virtual representations of the surgical instruments, as opposed to just relying on their representation in US images, emphasize the superior surgical guidance capabilities of our platform. While these instruments may not be clearly identified in the US images, they can easily be viewed as 3D objects in the virtual environment. In addition, given our accurate virtual tool-to-US registration, the surgical instruments are aligned with their US representations at all times, ultimately facilitating both their visualization and navigation.

The quality of the pre-operatively acquired images may also impose certain limitations upon how much detail can be achieved when segmenting the anatomy of certain organs. For mitral valve applications, it may be challenging to identify and segment the anatomy of the mitral apparatus from clinical quality, 6 mm slice thickness MR data. Similar challenges may be encountered whenever the surgical targets consist of delicate anatomical structures that are not readily identifiable in low resolution images. In response to these limitations, we have developed a technique that involves a registration-based segmentation of pre-operative images by means of an average anatomical model built from images acquired from a population of subjects [5, 10]. As described in § 4.2.1.1, we have constructed a database of human cardiac models based on a population of 10 individuals, and built a high-resolution average cardiac model of a healthy human heart. Using a registration-based segmentation approach, the high-resolution average heart model has been used to segment cardiac MR images of human subjects that were not part of the database, generating segmented anatomical structures which were validated to be accurate within  $5.0 \pm 1.0$  mm,  $4.7 \pm 0.9$  mm, and  $5.3 \pm 1.3$  mm for the left ventricle, left atrium, and the right atrium and ventricle, respectively. While this technique has been applied and validated on human subject MR data [11], we are currently in the process of building a similar database from

porcine images, and employ this technique to automatically generate the anatomical models as an alternative to manual segmentation. However, for the time being, we have to resort to the manual segmentation approach to generate the anatomical models for our animal studies. Given this disadvantage, the pre-operative imaging must take place a few days prior to the scheduled procedure, to allow sufficient time for image segmentation and model generation.

Our preliminary translational studies in the operating room (OR) have allowed us to identify several constraints specific to “live” interventions in the clinic that had not been previously observed in the laboratory. Given that the tracking accuracy of the MTS decreases away from the magnetic field generator, the latter must be located within 20-30 cm from the surgical field. To further avoid any interference between the setup and the clinical work-flow, we embedded the magnetic field generator within the foam of the OR bed, underneath the pig’s thorax. An evolution of this approach has been NDI’s recent announcement of a flat field generator that can be placed on the OR table, even if it has a steel top.

While these interventional procedures are currently performed manually, a natural extension would be to perform it using robot assistance. Under these conditions, it would be worth while exploring the use of algorithms that track the beating heart motion, and integrate motion compensation into the robot dynamics [12, 13, 14, 15]. However, the need for such an approach, even with robot control, is still open to debate and currently part of our ongoing work, given that the valve or patch application device acts as a natural stabilizer when in contact with the target. An additional advantage of the manual approach is the inherent haptic feedback transmitted to the surgeon through the rigid instrument shaft, a feature that robotic instruments currently lack.

Several approaches have been considered regarding the most appropriate means of delivering the multi-modality imaging data to the physician. The information may be displayed via a traditional computer monitor, a translucent flat panel overlaid onto the

patient and located directly above the surgical field, a stereoscopic display enabling 3D visualization, or via HMDs which allow the operators to “navigate” within the virtual environment, as suggested by Sauer *et al.* [16] or Birkfellner [17]. To date, we have employed the traditional overhead monitor approach, as well as the use of the HMDs, which the surgeons found to be relatively comfortable, in spite of the progressive discomfort experienced with prolonged use. However, investigating the human-computer interaction between the surgeons and the mixed reality environment, and optimizing the information display during image-guided interventions is still an active topic of research in the laboratory.

**Clinical Limitations.** One of the most frequent issues in image-guided interventions is surgical accuracy. Furthermore, we must also keep in mind that, unlike orthopedic or neurological applications, cardiac image-guided procedures will always be prone to higher inaccuracies arising from the difficulty in building perfect anatomical models of the heart, and the limitations of the registration algorithms used to map these models to the intra-operative patient anatomy. These bottlenecks are, of course, further amplified by the rapid movement of cardiac tissue and the limitations of working in a blood-filled environment.

The registration technique used to augment the intra-operative images with the pre-operative models ensures a  $\sim 4.5$  mm alignment accuracy for the cardiac structures located within 10 mm from the valvular region. Moreover, the surgical instruments are also tracked with respect to the ultrasound image, since US imaging does provide the ultimate information for on-target positioning and therapy delivery. Under the inherent limitations of the system (i.e. minimizing the presence of ferro-magnetic materials near the field generator, tracking the instruments within the optimal tracking volume (500 mm x 500 mm x 500 mm from the field generator), and quasi-static conditions - smooth motion of the tracked tools), the typical performance of the NDI Aurora 5 DOF sensors ranges from 0.9 mm to 1.4 mm in translation



and approximately  $0.3^\circ$  in orientation, while the 6 DOF sensors are typically accurate within 0.9 - 1.6 mm in translation and  $0.8^\circ$  -  $1.1^\circ$  in orientation. According to the *in vitro* targeting accuracy results described in section 3.3.1, users achieved an overall RMS targeting accuracy of 4.4 mm under sole US imaging, and a 2.8 mm RMS accuracy under model-enhanced US-assisted guidance [18]. The dramatic accuracy improvement is attributed to the augmentation of the “context-less” 2D US images with the virtual object representations, which significantly facilitate surgical instrument navigation.

While we have been able to quantify the *in vitro* targeting error via cardiac phantom experiments, *in vivo* quantification is much more challenging. Clinically, surgical accuracy is often denoted by a successful procedure, which, although performed via minimally invasive approaches, should still lead to the same clinical outcome and maintain the efficacy of the traditional approach. Based on the acute *in vivo* studies performed to date, we can conclude that these investigations have demonstrated the feasibility of the model-enhanced US platform in guiding mitral valve implantations and ASD repairs. To further strengthen the efficiency and benefits introduced by this novel surgical platform, we will focus on expanding the clinical evaluation toward chronic animal studies. In addition, similar to our *in vitro* work, we plan not only to assess the therapeutic success, but also to consider parameters such as procedure time and the rate of conversion from this minimally invasive off-pump guidance method to the traditional approach.

## 5.5 Conclusions

In conclusion, this initial work has demonstrated the tremendous potential of multi-modality imaging and surgical tool tracking for both visualization and assessment of surgical interventions in a manner that will ultimately be superior to direct vision. Nevertheless, our clinical translation experience is still in its infancy and

further experiments are necessary to better evaluate and report the clinical efficacy of the interventional platform. Hence, our future goals consist of further evaluating the interventional platform *in vivo* on porcine models, while optimizing tool design, and building surgical instruments compatible with the anatomy, standard imaging modalities, and tracking systems.

# References

- [1] C. A. Linte, J. Moore, A. D. Wiles, C. Wedlake, and T. M. Peters. Virtual reality-enhanced ultrasound guidance: A novel technique for intracardiac interventions. *Comput Aided Surg.*, 13:82–94, 2008.
- [2] C. A. Linte, A. D. Wiles, N. Hill, J. Moore, C. Wedlake, G. M. Guiraudon, D. L. Jones, D. Bainbridge, and T. M. Peters. An augmented reality environment for image-guidance of off-pump mitral valve implantation. In *Medical Imaging 2007: Visualization and Image-Guided Procedures*, volume 6509 of *Proc. of SPIE*, pages 65090N–12, 2007.
- [3] A. D. Wiles, G. M. Guiraudon, J. Moore, C. Wedlake, C. A. Linte, D. L. Jones, D. Bainbridge, and T. M. Peters. Navigation accuracy for an intracardiac procedure using virtual reality-enhanced ultrasound. In *Medical Imaging 2007: Visualization and Image-Guided Procedures*, volume 6509 of *Proc. of SPIE*, pages 61410W–10, 2007.
- [4] R. Smolíková-Wqchowiak, M. P. Wachowiak, A. Fenster, and M. Drangova. Registration of tow-dimensional cardiac images to preprocedural three-dimensional images for interventional applications. *J Magn Reson Imaging*, 22:219–28, 2003.
- [5] M. Wierzbicki, M. Drangova, G. M. Guiraudon, and T. M. Peters. Validation of dynamic heart models obtained using non-linear registration for virtual reality training, planning, and guidance of minimally invasive cardiac surgeries. *Med Image Anal.*, 8:387–401, 2004.
- [6] W. J. Schroeder, J. A. Zarge, and W. E. Lorensen. Decimation of triangle meshes. In *Computer Graphics - SIGGRAPH 92*, pages 65–70, 1992.
- [7] M. Wierzbicki and T. M. Peters. Determining epicardial surface motion using elastic registration: Towards virtual reality guidance of minimally-invasive cardiac interventions. In *Proc. of Med Image Comput Assist Interv.*, volume 2878 of *Lect Notes Comput Sci.*, pages 722–29, 2003.
- [8] D. G. Gobbi, R. M. Comeau, and T. M. Peters. Ultrasound probe tracking for real-time ultrasound/MRI overlay and visualization of brain shift. In *Lecture*

- Notes in Computer Science*, volume 1679 of *Proc. of Med Image Comput Comput Assist Interv.*, pages 920–927, 1999.
- [9] G. M. Guiraudon. Universal cardiac introducer. Patent Application, 2005. US 2005/0137609 A1, Appl. No. 10/736,786.
- [10] M. Wierzbicki. *Subject-specific models of the heart from 4D images*. Phd dissertation, University of Western Ontario, Canada, 2006.
- [11] C. A. Linte, M. Wierzbicki, J. Moore, G. M. Guiraudon, S. H. Little, and T. M. Peters. Towards subject-specific models of the dynamic heart for mitral valve surgery. In *Proc. of Med Image Comput Comput Assist Interv.*, volume 4792 of *Lect Notes Comput Sci.*, pages 94–101, 2007.
- [12] O. Bebek and M. C. Cavusoglu. Intelligent control algorithms for robotic-assisted beating heart surgery. *IEEE Trans Rob Autom.*, 23:468–80, 2007.
- [13] O. Bebek and M. C. Cavusoglu. Model based control algorithms for robotic assisted beating heart surgery. In *Proc. of IEEE Eng Med Biol Soc.*, volume 1, pages 823–8, 2006.
- [14] L. Cuvillon, J. Gangloff, M. De Mathelin, and A. Forgione. Towards robotized beating heart tecabg: assessment of the heart dynamics using high-speed vision. *Comput Aided Surg.*, 11:267–77, 2006.
- [15] D. T. Kettler, R. D. Plowes, P. M. Novotny, N. V. Vasilyev, P. J. del Nido, and R. D. Howe. An active motion compensation instrument for beating heart mitral valve surgery. In *Proc. of IEEE/RSJ International Conference on Intelligent Robots and Systems*, volume 1, pages 1290–5, 2007.
- [16] S. Vogt, A. Khamene, H. Niemann, and F. Sauer. An AR system with intuitive user interface for manipulation and visualization of 3D medical data. In *Proc. of Medicine Meets Virtual Reality*, volume 98 of *Stud Health Technol Inform.*, pages 397–403, 2004.
- [17] W. Birkfellner, M. Figl, C. Matula, J. Hummel, R. Hanel, H. Imhof, F. Wanschitz, A. Wagner, F. Watzinger, and H. Bergmann. Computer-enhanced stereoscopic vision in a head-mounted operating binocular. *Phys Med Biol.*, 48:49–57, 2003.
- [18] C. A. Linte, A. Wiles, and J. *et al.* Moore. Virtual reality-enhanced ultrasound guidance for atrial ablation: In vitro epicardial study. In *Lect Notes Comput Sci.*, volume 5242, pages 644–51, 2008.

## Chapter 6

# Investigating Heart Migration during Minimally Invasive Cardiac Interventions

*IGS relies on the common assumption that pre-operative information can depict intra-operative morphology with sufficient accuracy. However, the heart is a soft-tissue organ prone to changes induced during access to the surgical targets. In addition to its clinical value for cardiac interventional guidance and assistance with the image- and model-to-patient registration, here we show how magnetically tracked TEE imaging, together with the registration techniques described in Chapter 4 can be used to estimate changes in the heart position and morphology of structures of interest at different stages in the procedure workflow of two types of interventions: model-enhanced US-guided guided procedures performed on swine models and robot-assisted CABG procedures performed in patients suffering of coronary artery disease.*

---

This chapter is adapted from Linte CA, Carias M, Cho SD, Moore J, Wedlake C, Bainbridge D, Kiaii B and Peters TM. Estimating heart shift and morphological changes during minimally invasive cardiac interventions. *Proc. SPIE Medical Imaging 2010: Visualization, Image-guided Procedures and Modeling*. Vol. 7625. Pp. 762509-1-11. 2010.

## 6.1 Introduction

As an alternative to conventional therapy approaches, performing interventions on the beating heart is considered to be the ultimate and least invasive cardiac therapy delivery technique. Nevertheless, the challenge lies within the ability to provide the interventionalist with a clear and intuitive display of the surgical field to enable target identification and surgical tool manipulation with sufficient accuracy and fidelity without compromising the therapy delivery outcomes.

For most of these procedures, in addition to the intra-operative visualization achieved using various medical imaging modalities, a pre-operative planning stage is often involved. In the case of CABG procedures, for example, a pre-operative computer tomography (CT) scan is used to assess patient candidacy for the robot-assisted procedure (i.e. the thorax anatomy of the patient allows the surgery to be performed using the surgical robot, ensuring the instruments can reach the heart without colliding with each other). Also based on the pre-operative dataset, the surgeon identifies the location of the target vessel - the left anterior descending (LAD) coronary artery, as well as the optimal location of the port incisions to ensure proper access to the LAD (**Fig. 6.1**).

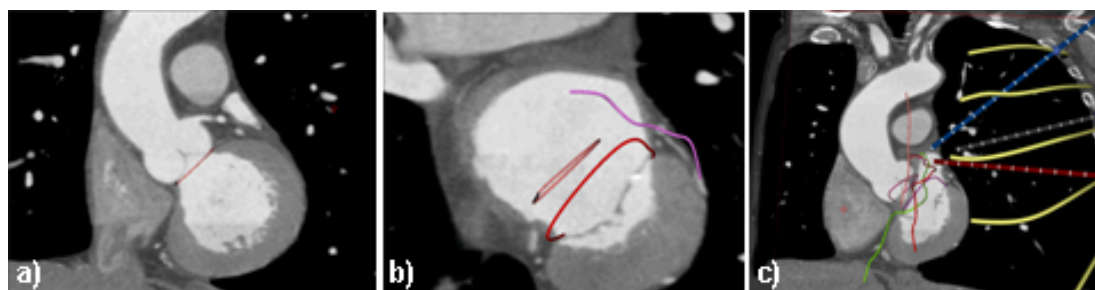


Fig. 6.1: Pre-operative planning stage showing patient's cardiac CT scan (a), the coronary vessel displayed relative to the valve annuli (b) and the port placement to ensure proper reach of the target vessel with the robotic instruments (c), where the yellow lines represent intercostal spaces.

Besides the CABG procedures, other novel minimally invasive interventions such

as the those guided using model-enhanced US-assisted guidance described in Chapter 5, involve an image-to-patient registration step [1], where real-time intra-operative US imaging is augmented with pre-operative anatomical models of the heart. A similar approach is presented by Ma *et al.* [2], where they use a feature-based approach to register pre-operative data to the intra-operative US images at a single stage before the procedure.

In both cases the pre-operative plan and the intra-operative visualization environment must adequately resemble the real surgical field to allow proper surgical navigation. Hence a clinically adequate alignment between the pre-operative models used in therapy planning and the intra-operative information used in therapy delivery is expected. In addition, it is worthwhile noting that the morphology of the features used for registration may differ between the pre- and intra-operative stages, simply due to a slightly different position of the subject, as well as changes induced during the peri-operative workflow of the procedure itself. Therefore, any information with regards to the changes in position, orientation and intrinsic morphology of these features is critical to either update a pre-operative plan or to provide a sufficiently accurate image- or model-to-patient registration.

This work is motivated by both our current developments in model-enhanced US intracardiac surgical navigation, as well as by a parallel project aimed at optimizing surgical planning and port placement for robot-assisted CABG procedures. Using the registration techniques described in Chapter 4, the changes the heart undergoes during the peri-operative workflow associated with these procedures, are estimated. The investigations were carried out in two porcine models undergoing beating heart interventions with intracardiac access achieved using the UCI, and four patients undergoing robot-assisted CABG intervention for coronary artery disease.

After observing the heart migration in patients undergoing robot-assisted CABG interventions, as a natural extension of this work toward improving procedure planning for the robot-assisted CABG interventions, a method to better predict of the

intra-operative location of the LAD, based on the pre-operative plan and the observed peri-operative migration, is proposed. This subsequent contribution is described in Appendix A.

All animal experiments described in this study were approved by the Animal Care and Use Committee of The University of Western Ontario and followed the guidelines of the Canadian Council on Animal Care. Also, all human data presented here were acquired following approval of the Research Ethics Board of the University of Western Ontario and patient consent.

## 6.2 Methodology

To estimate the changes in global position and morphology of the heart during the procedure workflow, we rely on features of the heart that are available in the pre-operative CT or MR images and that can also be readily obtained from real-time peri-operative US images of the subject's heart acquired at the various stages of the procedural workflow.

Here we use the mitral and aortic valves as the features of interest and assess their global movement and morphological changes during the intra-procedure workflow. As described earlier in Chapter 4 and Chapter 5, the valvular features (MVA and AVA) have been employed in the image- or model-to-subject registration of both patient and porcine image data, respectively. Moreover, they are also key features in another registration technique later presented in Appendix A that uses the left main coronary ostia (LMCO) and left ventricular apex (LVAp) in addition to the two valves, to map the pre-operative location of the LAD vessel to the corresponding peri-operative “instances” of the heart for improved planning and guidance of robot-assisted CABG procedures.

During the per-operative workflow, we are interested in the overall displacement of the heart — a measure of how much the heart itself shifts during the procedure, and



the morphological changes of the features of interest — a measure of the geometrical variation of the features of interest (i.e. MVA and AVA). The morphological changes of the valve annuli also provide a measure of the variability associated with their identification and segmentation, which, in turn, contribute to the uncertainty of any registration algorithm that relies on these features. In addition, their relative geometry provides a measure of the extent of local, non-rigid deformations that occur in the heart during the peri-operative workflow, which may or may not require the use of non-rigid registration to capture these changes between adjacent workflow stages.

## **6.2.1 Minimally Invasive Procedure Workflow**

### **6.2.1.1 Direct-access Off-pump Intracardiac Interventions via UCI**

Unlike a limited number of epicardial procedures that can be performed off-pump, most intracardiac procedures, including those performed under minimally invasive conditions, are carried out on the still drained heart. Minimal invasiveness is achieved by entering the thoracic cavity via smaller incisions with reduced tissue exposure, usually using a lateral minithoracotomy. In Chapter 5, we have demonstrated how model-enhanced US guidance can be used to implant a prosthetic mitral valve and repair a septal defect in live porcine subjects, with off-pump intracardiac access provided via the UCI.

After anesthesia and mechanical dual-lung ventilation, (Stage<sub>1</sub>), the heart is accessed via a minithoracotomy and the pericardial sac is opened for access to the chamber of interest (Stage<sub>2</sub>). The UCI is then attached to the left or right atrial appendage and the delivery instruments are inserted inside the chamber via the ports of the UCI (Stage<sub>3</sub>) (**Fig. 6.2**).

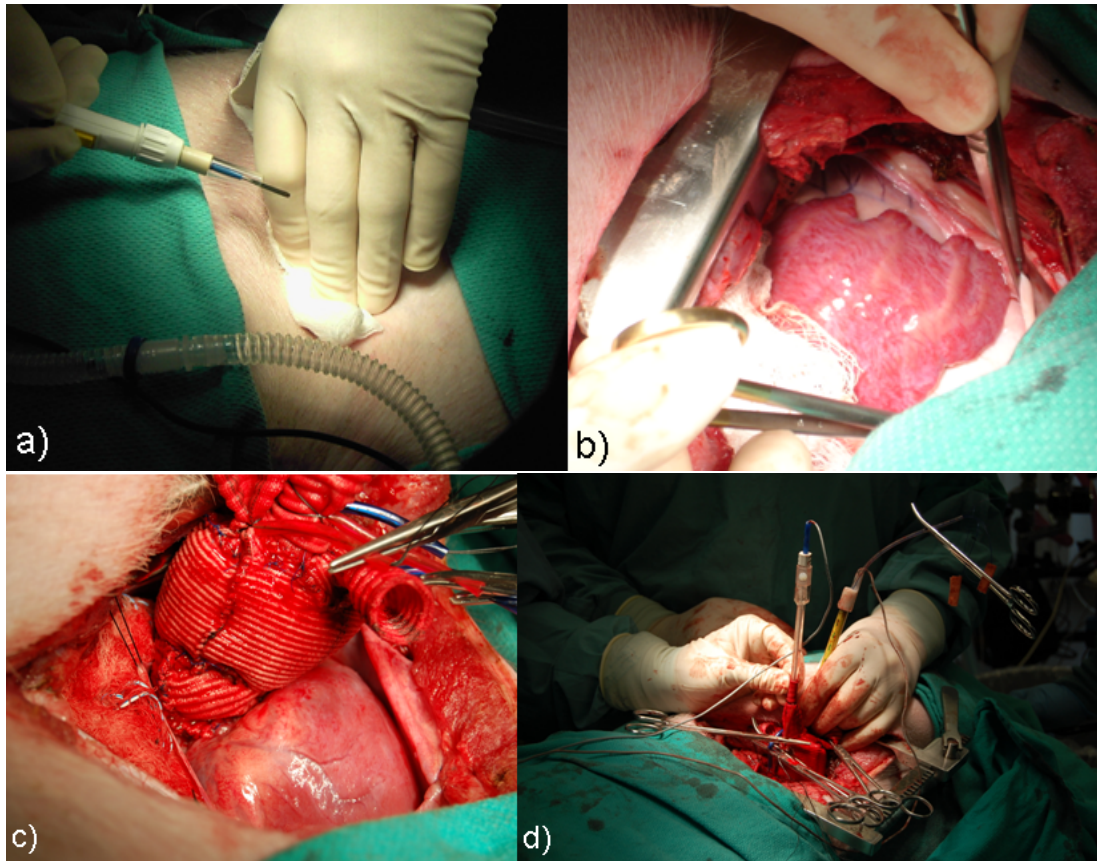


Fig. 6.2: Peri-operative workflow stages associated with the UCI-based intracardiac interventions: a) before opening chest; b) after minithoracotomy; c) after intracardiac access; d) during therapy delivery.

### 6.2.1.2 Robot-Assisted Coronary Artery Bypass Graft Interventions

Robot-assisted CABG procedures typically involve three peri-operative stages. Initially, the patient is anesthetized, with both lungs mechanically ventilated, and positioned in the right lateral decubitus position (Stage<sub>1</sub>). This stage closely resembles the pre-operative imaging setup when the patient's heart is imaged in the same position and under similar breathing conditions, but under no anesthesia. Hence the cardiac anatomy and morphology are thought to be very similar at these two stages. The left lung is then deflated to enable access to the heart (Stage<sub>2</sub>), while the patient undergoes single lung ventilation, followed by  $CO_2$  chest wall insufflation (Stage<sub>3</sub>) at

a target pressure of 10 cm  $H_2O$ .

## 6.2.2 Data Acquisition

### 6.2.2.1 Pre-operative Image Acquisition

**Porcine Image Acquisition:** A set of 20 high resolution ( $1.09 \times 1.09 \times 2.0 \text{ mm}^3$ ) ECG-gated MR volumes of the porcine subject’s heart was acquired throughout the cardiac cycle. A pre-operative surface model was constructed from the mid-diastole volume [3], consisting of the left ventricular myocardium (LV), left atrium (LA), right atrium and ventricle (RA/RV), and the mitral (MVA) and aortic valve annuli (AVA), similar to the techniques described in Chapter 5. For procedure guidance, a dynamic cardiac model can be obtained by animating the mid-diastolic model throughout the cardiac cycle using motion information extracted via non-rigid image registration [4] and synchronizing it with the ECG signal; however, for the purpose of this work, the mid-diastolic information is sufficient.

**Patient Image Acquisition:** For each patient undergoing robot-assisted CABG intervention, a high-resolution pre-operative CT scan (64 Slice LightSpeed VCT, General Electric, Milwaukee, WI, USA) was acquired as part of the clinical routine for candidacy assessment. Since X-ray contrast was used for the pre-operative scans, the images also provided accurate information about the location of the major blood vessels, including the LAD.

### 6.2.2.2 Peri-operative Image Acquisition

Magnetically tracked real-time TEE was employed to acquire “instances” of the heart at each stage in the peri-operative workflow and to track the cardiac features of interest. For both procedures the image acquisition was repeated at each stage of the peri-operative workflow.

For the patients undergoing robot-assisted CABG intervention, 2D US images were acquired using an Agilent Technologies TEE transducer (Agilent Technologies, Canada). The probe was modified by embedding a 6 DOF NDI Aurora magnetic sensor coil inside the encasing of the transducer and calibrated using the Z string technique [5, 6]. The magnetic field generator was located underneath the patient’s heart, under the operating table (**Fig. 6.3**).

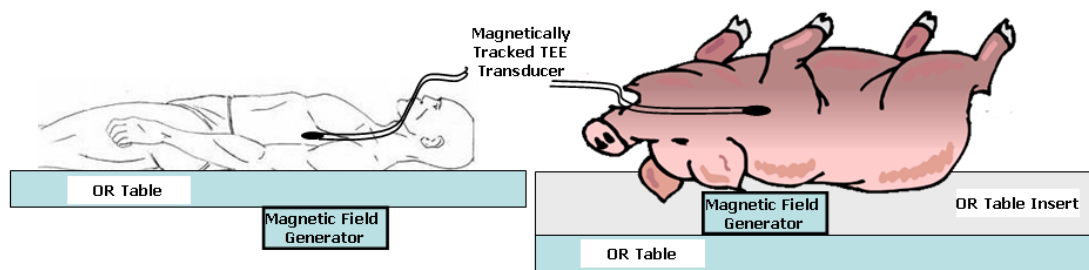


Fig. 6.3: Peri-operative setup of the a) patient during image acquisition prior to the robot-assisted CABG procedure, and b) porcine subject prior to the UCI-based off-pump intracardiac intervention.

In addition to spatial tracking, all images were acquired using ECG gating; the real-time US video feed was “frozen” at 75% of the R-R interval, corresponding to the mid-diastole time point. The mitral valve was imaged via a series of 6-10 mid-esophageal four-chamber acquisitions at 20° angular increments. The aortic valve was imaged using a 180° ± 10° long axis view and a 30° short axis view.

A similar acquisition protocol was used to acquire *in vivo* images of the porcine subjects during the UCI-based intracardiac intervention. However, instead of using the integrated magnetically tracked TEE probe, a similar transducer onto which the magnetic sensor coil was rigidly attached on the outside, was employed. Also, the field generator was located inside a mattress insert placed underneath the pig on the operating table (**Fig. 6.3**). The mitral and aortic valves were imaged at 10 – 20° angular increments, however difficulties were encountered during the aortic

valve image acquisition due to its obstruction by features belonging to the respiratory system.

### 6.2.2.3 Cardiac Feature Identification

The main advantage of the tracked image acquisition is the ability to interactively select features of interest in the image dataset at different times during the workflow, and display them relative to one other in the same coordinate system. As a result, all 2D image fans are inserted into the 3D volume according to their spatial stamp recorded by the tracking system.

Following image acquisition, all data processing was performed off-line, with the 2D images being reviewed by an experienced anesthetist. The features of interest were identified using a custom-developed tool that enabled the user to visualize each of the acquired 2D US images and interactively select points corresponding to the structure of interest. Each valve annulus was segmented by identifying the annular end points as seen in the 2D images acquired in angular increments (**Fig. 6.4**).

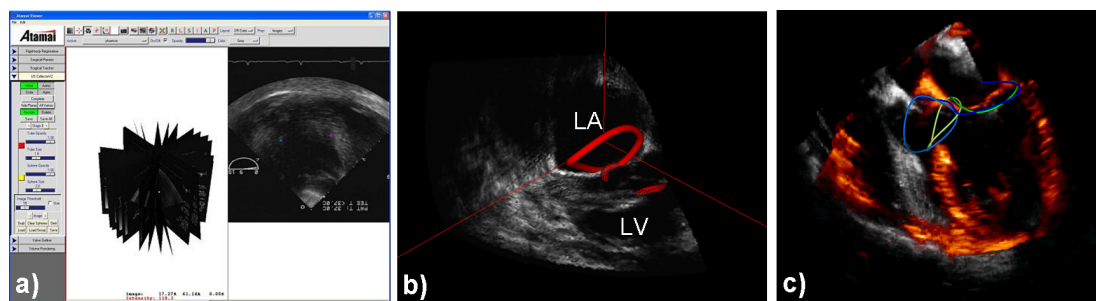


Fig. 6.4: a) Screen shot showing the US image collection and analysis tool used to extract the features of interest (b) from the peri-operatively acquired US images; c) Peri-operative US images at two different stages in the workflow showing the segmented mitral and aortic valve annuli.

The mitral and aortic annuli were reconstructed by connecting the corresponding points selected from the 2D images, resulting in a pair of continuous annuli at each peri-operative workflow stage. A similar tool was used to select the mitral and aortic

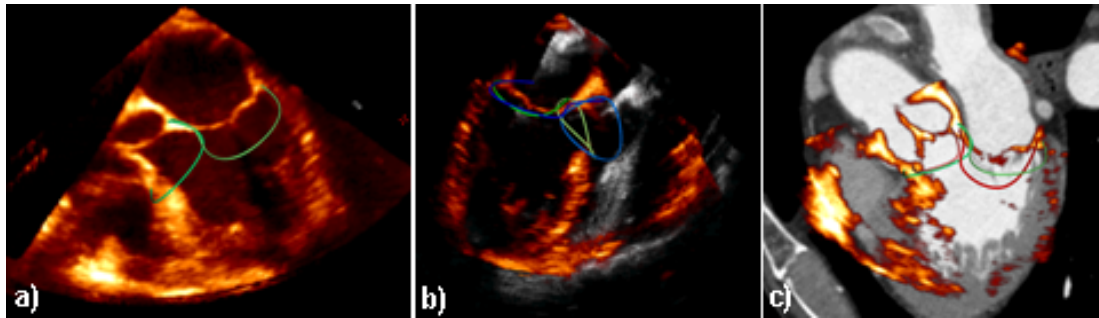


Fig. 6.5: a) Patient heart instance at Stage<sub>1</sub> acquired using tracked US and showing the valve annuli; b) Stage<sub>1</sub> (orange) and Stage<sub>2</sub> (gray) instances of the heart showing relative heart displacement and corresponding segmented valvular structures; c) Initial peri-operative US instance (Stage<sub>1</sub>) registered to the pre-operative dataset (Stage<sub>0</sub>) and displayed within the CT coordinate space.

annuli in the pre-operative CT and MR images. However, the process was facilitated by the superior image quality and 3D nature of the image datasets.

## 6.2.3 Data Analysis

### 6.2.3.1 Global Heart Movement

Since procedure planning is performed on the pre-operative dataset, the pre-operative image space was used as the fixed frame of reference. The peri-operatively acquired images were then transferred into the pre-operative coordinate system by aligning homologous features corresponding to the first peri-operative (Stage<sub>1</sub> US) and the pre-operative (Stage<sub>0</sub> CT) datasets (**Fig. 6.5**). These two stages are anatomically equivalent given the same subject position and dual-lung ventilation, and assuming that no major changes were induced by the anesthesia. As a result, the peri-operative displacements can be estimated with respect to the principal body axes.

The global motion of the heart was estimated according to the change in position of the mitral and aortic valve annuli between successive stages in the procedural workflow. The displacement was determined based on the locations of the centroid of the valve annuli expressed as a vector quantity. The movement between consecu-

tive stages was measured in the CT coordinate system with respect to the anterior-posterior (AP), superior-inferior (SI) and left-right (LR) axes of the body.

### 6.2.3.2 Morphological Feature Characterization

In addition to estimating the overall displacement of the features as a global measure of the position of the heart, we also characterized feature morphology in terms of annuli lengths and lengths of their principal axes, corresponding to the major and minor in-plane radii and polar radius, the latter being a measure of the out-of-plane properties. While the native valves are not exactly planar structures (in particular the mitral valve which is often referred to as saddle-shaped), the aortic valve annulus can nevertheless be usefully approximated as planar.

The morphological feature characterization was performed within a local coordinate system characterized by a basis consisting of three orthonormal vectors, which were identified using principal component analysis and eigenvalue decomposition of the covariance matrix of each valve annulus. The length of the in-plane and polar radii of each annular structure are directly proportional to the squared root of the eigenvalues in descending order, respectively. Furthermore, the directions of the principal axes of each feature were provided by the set of orthogonal eigenvectors, where the eigenvector corresponding to the lowest eigenvalue represented the normal of the orthogonal plane of best fit for each structure (**Fig. 6.6**). In other words, the lowest eigenvalue represents a measure of the “spread” of the feature in the out-of-plane direction, which for planar structures, such as the aortic annuli, are minimal.

Two other parameters were also estimated to provide a measure of local deformations within the heart: the inter-annular distance, represented by the distance between the centroids of the mitral and aortic annulus, and the relative annuli orientation, represented by the angle between the normals of the orthogonal plane of best fit of each annulus. Based on these parameters, one could assess whether significant local deformations occur between adjacent stages of the workflow, in which

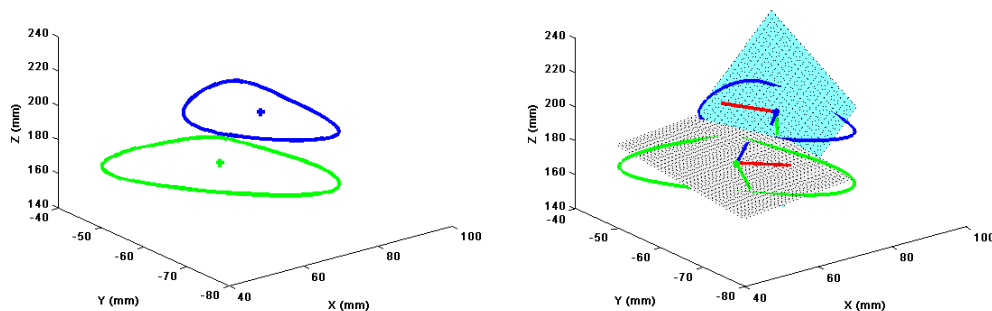


Fig. 6.6: a) Figure showing the mitral (green) and aortic (blue) shown before chest opening in the porcine subject; b) Orthogonal best-fit plane shown, together with principal in-plane directions (red and green) and normal unit vector (blue).

case a rigid registration algorithm may impose undesired limitations with respect to optimal procedure planning and guidance.

## 6.3 Results

### 6.3.1 Global Heart Displacement

#### 6.3.1.1 UCI-based Intracardiac Interventions

To evaluate the global motion of the heart during the peri-operative workflow, we first extracted the mitral and aortic annuli from each of the peri-operative US datasets. The peri-operative data were then registered into the same coordinate system as the pre-operative data using the homologous features at Stage<sub>1</sub> (before incision in the case of UCI-based intracardiac procedure or the dual-lung ventilation stage for the off-pump robot-assisted CABG procedure). **Table 6.1** includes a summary of the valvular and overall heart displacement across the three stages of the UCI-based procedure.

For an intuitive graphical display, we show below the mitral and aortic valve annuli at consecutive stages (**Fig. 6.7**), along with a generic model of the heart consisting of



Table 6.1: Valvular displacement in porcine subjects between consecutive stages of an off-pump UCI-based intracardiac intervention. Stage<sub>1</sub>: Before minithoracotomy; Stage<sub>2</sub>: After minithoracotomy; Stage<sub>3</sub>: After UCI attachment. Note: displacements are reported in mm according to the left/right (L/R), anterior/posterior (A/P) and superior/inferior (S/I) directions, where positive displacements are measured toward the right, anterior and superior directions, respectively.

Workflow Stage	Mitral Valve Shift (mm)			Aortic Valve Shift (mm)		
	L/R	A/P	S/I	L/R	A/P	S/I
Stage 1-2	13.7	-6.8	4.2	22.2	-17.6	4.3
Stage 2-3	-1.9	-2.8	1.5	-5.5	8.3	-3.3
Stage 1-3	11.7	-9.7	5.8	16.7	-9.4	1.0

the left atrium and ventricle and positioned according to the location and orientation of the mitral and aortic valve annuli (**Fig. 6.8**). Note that the three stages of the procedure are colour-coded using red, green and blue, which correspond to the Stage<sub>1</sub>: prior to minithoracotomy, Stage<sub>2</sub>: following minithoracotomy, and Stage<sub>3</sub>: post UCI attachment, respectively.

### 6.3.1.2 Robot-assisted CABG Interventions

The movement of the heart during the robot-assisted CABG procedure from Stage<sub>1</sub> (anesthetized, dual-lung ventilation) to Stage<sub>2</sub> (single-lung ventilation) averaged to  $\sim 24$  mm for the mitral valve and  $\sim 32.7$  mm for the aortic; from Stage<sub>1</sub> to Stage<sub>3</sub> (chest wall insufflation), the mitral valve experienced a movement of  $\sim 30$  mm and the aortic movement averaged to  $\sim 34$  mm. **Table 6.2** provides a summary of the valvular displacements with respect to the L/R, A/P and S/I axes across the patients observed.

**Fig. 6.9** shows the position of the mitral (solid ring) and aortic (wireframe ring) valve annuli colour-coded according to the three stages of the procedure.

For a better interpretation of the overall heart movement, **Fig. 6.10** shows the change in position of the epicardial surface of one patient’s heart segmented from the

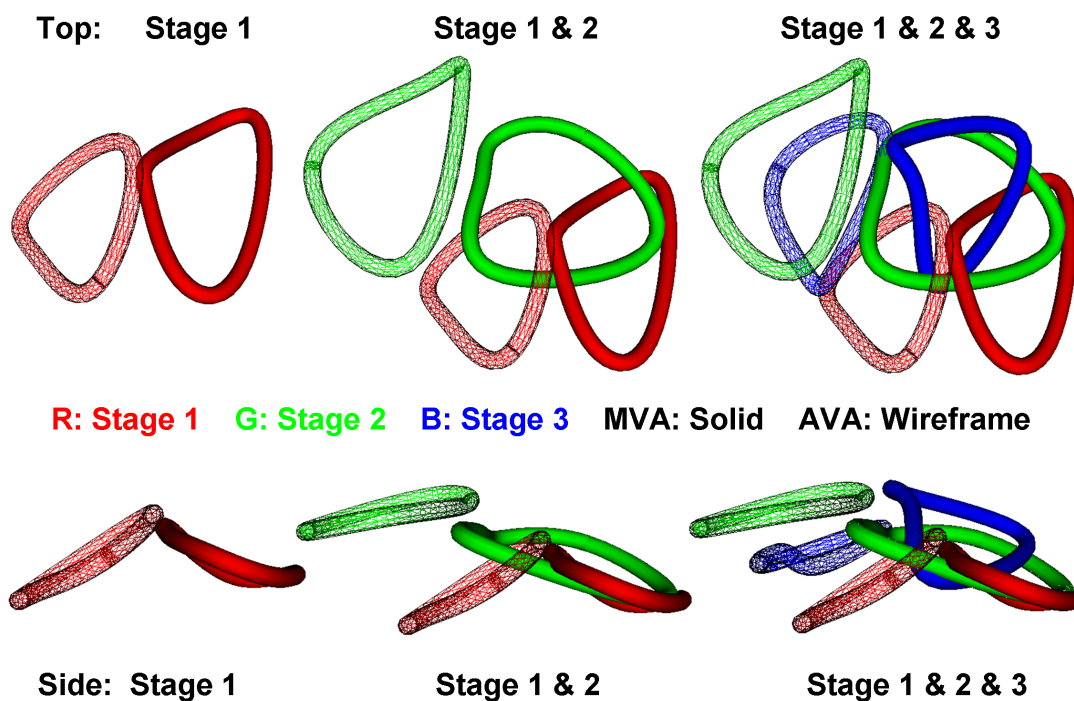


Fig. 6.7: Figure showing the mitral (solid ring) and aortic (wireframe ring) valve annuli at different stages of the UCI-based intracardiac procedure workflow in a porcine subject: Stage<sub>1</sub>: before minithoracotomy (red); Stage<sub>2</sub>: after minithoracotomy (green); Stage<sub>3</sub>: after UCI attachment (blue).

CT dataset and animated using the sequential peri-operative transforms at the three stages of the procedure: dual-lung ventilation shown in red, single-lung ventilation shown in green, and post chest insufflation, shown in blue.

### 6.3.2 Morphological Feature Characterization

Morphological changes of the annuli themselves were also assessed. Using principal component analysis and eigenvalue decomposition, we identified an orthonormal basis corresponding to each annulus; the eigenvectors corresponding to the largest and second largest eigenvalues were the principal in-plane orientations of the annulus, while the smallest eigenvector corresponded to the unit normal vector describing its

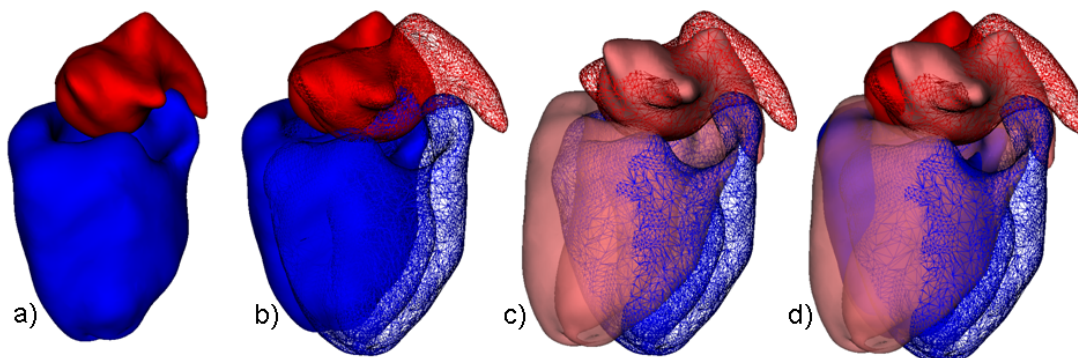


Fig. 6.8: Global porcine heart orientation (left ventricle and left atrium models shown) throughout the peri-operative workflow associated with the off-pump UCI-based intracardiac interventions on porcine subjects: a) Before opening chest; b) Before (surfaces) and after (wireframe) performing minithoracotomy; c) After minithoracotomy (wireframe) and after UCI attachment (light-coloured surface); d) All-in-one generic pre-operative shift.

orientation.

In addition, we estimated the effective perimeter of the mitral and aortic annuli, as well as the distance between the two valves and the angle between their planes of best fit at each stage in both the UCI-based porcine procedures and the robot-assisted CABG interventions. These parameters represent a measure of the morphology of the features of interest, and according to their variability across the procedural workflow, one can determine whether significant local deformations are induced and whether a rigid-body registration approach is sufficient. A summary of these results is included in **Table 6.3** for the UCI-based porcine interventions and in **Table 6.4** for the robot-assisted CABG procedures.

## 6.4 Discussion

The main focus of this work was to explore the displacement of the heart and features of interest within the heart during the peri-operative workflow of minimally invasive cardiac interventions. This work was motivated by our on-going develop-

Table 6.2: Mitral and aortic valve displacement in patients during off-pump robot-assisted CABG interventions. Stage<sub>1</sub>: Dual-lung ventilation; Stage<sub>2</sub>: Single-lung ventilation; Stage<sub>3</sub>: Chest insufflation. Note: displacements are reported in mm according to the left/right (L/R), anterior/posterior (A/P) and superior/inferior (S/I) directions, where positive displacements are measured toward the right, anterior and superior direction, respectively.

Workflow Stage	Mitral Valve Shift (mm)			Aortic Valve Shift (mm)		
	L/R	A/P	S/I	L/R	A/P	S/I
<b>Stage 1-2</b>	1.9	-1.6	6.8	2.6	-11.5	7.3
<b>Stage 2-3</b>	16.2	-2.6	-7.8	14.5	-2.8	-6.9
<b>Stage 1-3</b>	18.1	-4.2	-1.0	17.2	-13.9	0.4

Table 6.3: Characterization of the mitral (MVA) and aortic valve (AVA) annuli during the off-pump UCI-based procedure workflow in porcine subjects: Effective Perimeter (Length), Effective Major (MjA) and Minor axes (MiA), Inter-annular Distance (mm) and Inter-annular Angle (deg).

Workflow Stage	Mitral Annulus (MVA) (mm)			Aortic Annulus (AVA) (mm)			Annular	Annular
	Length	MjA	MiA	Length	MjA	MiA	Distance (mm)	Angle (deg)
<b>Pre-operative</b>	103.4	11.9	9.0	68.2	8.1	7.1	23.8	52
<b>Before Incision</b>	103.2	9.4	8.5	81.2	10.9	7.2	22.5	52
<b>After Incision</b>	109.4	14.4	8.9	107.8	11.1	8.9	26.4	39
<b>After UCI</b>	88.0	12.2	6.8	87.8	10.0	8.2	22.3	45

ments on the model-enhanced surgical guidance environment and its application in off-pump intracardiac intervention, where intracardiac access is achieved via the UCI. This novel therapy technique requires the registration of pre-operative images and models to the intra-operative US imaging environment, a process that involves features of interest that may undergo both location as well as morphological changes during the procedure workflow. We also extended this work toward a different application which was initiated by the need to update a pre-operative surgical plan according to changes induced during the peri-operative workflow. As such, we have used similar technique to estimate the location of the features of interest and the heart overall at different stages during the procedure and also evaluate the morphological variations of these features across the peri-operative workflow.

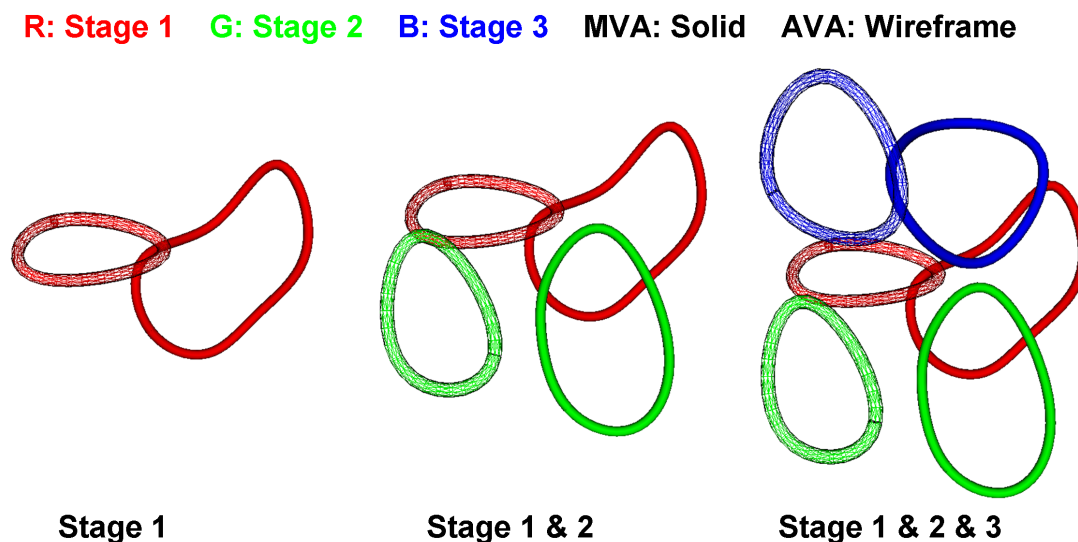


Fig. 6.9: Top view (upper panel) and side view (lower panel) of the mitral (solid ring) and aortic (wireframe ring) valve annuli at different stages of the robot-assisted CABG procedure workflow in a patient. Stage<sub>1</sub>: dual-lung ventilation (red); Stage<sub>2</sub>: single-lung ventilation (green); Stage<sub>3</sub>: chest insufflation (blue).

In the context of our original motivation — UCI-based off-pump intracardiac interventions — it appears that the porcine heart undergoes an overall movement of  $\sim 15$  mm in the lateral direction followed by a  $\sim 9$  mm movement in the anterior/posterior direction and a  $\sim 3$  mm movement in the superior/inferior direction between the initial peri-operative stage and the UCI attachment. These changes are sufficiently large to require the model-to-subject registration to be performed just before therapy

Table 6.4: Characterization of the mitral (MVA) and aortic valve (AVA) annuli during the robot-assisted CABG workflow in patients: Effective Perimeter (Length), Effective Major (MjA) and Minor axis (MiA), Inter-annular Distance (mm) and Inter-annular Angle (deg).

Workflow Stage	Mitral Annulus (MVA) (mm)			Aortic Annulus (AVA) (mm)			Annular	Annular
	Length	MjA	MiA	Length	MjA	MiA	Distance (mm)	Angle (deg)
Dual-lung Vent.	133.8	16.9	10.8	97.4	12.8	8.8	31.5	49
Single-lung Vent.	123.4	14.9	11.6	82.8	10.6	8.0	33.4	46
Chest Insufflation	123.2	14.6	10.9	106.0	12.5	7.2	31.5	55

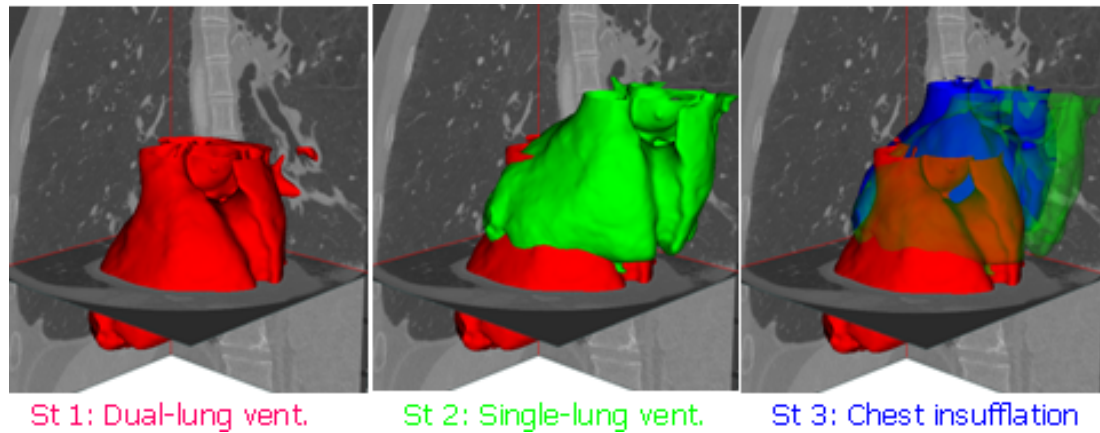


Fig. 6.10: Visual representation showing an automatically segmented epicardial model of a patient's heart animated using the sequential peri-operative transforms based on the valvular structures. Note: Stage<sub>1</sub> is shown in red, Stage<sub>2</sub> in green and Stage<sub>3</sub> in blue.

delivery, and therefore after UCI attachment and surgical tool insertion.

In the context of the robot-assisted CABG procedures, we have currently analyzed the data from four patients from a total of over 50 patients who have agreed to participate in the study. Similarly, we have noticed substantial movement of the heart and valvular structures caused by the lung deflation and chest insufflation. The overall heart displacement was  $\sim 17$  mm and  $\sim 9$  mm in the lateral and anterior/posterior direction, respectively, while the superior/inferior displacement was  $\sim 5$  mm. As a first attempt to make use of the peri-operative heart migration information toward improving pre-operative procedure planning, a proposed pre- to peri-operative registration technique is proposed in Appendix A as a means to update the pre-operative surgical plan with the migration information observed peri-operatively.

The morphological characterization of the mitral and aortic valve annuli has also revealed small variations in the effective perimeter and effective length of the major and minor axes of the valvular structures between the three stages for both types of procedure under investigation. Using the GraphPad Prism 4.0 statistical analysis package, a statistical comparison using two-way ANOVA was performed between the effective perimeter and effective long and short axes of the mitral and aortic annuli

across the patient sample. The results demonstrate that no significant differences ( $p > 0.1$ ) existed between these parameters at different procedure stage, except for those due to the patient variability, such as the size of the patients and their organs. Moreover, no significant differences were observed in the inter-annular distance ( $p > 0.1$ ). These two observations together suggest that no significant morphological changes have occurred during the procedure workflow and therefore a rigid body registration may be sufficient to either update the pre-operative surgical plan for robot-assisted CABG procedures, or to perform the model-to-subject registration for the UCI-based model-enhanced US guided procedures.

While this method is suitable to evaluate the changes in position of the heart and features of interest, we have nevertheless identified several challenges with respect to both data acquisition and post-processing. The peri-operative US images are acquired using a magnetically tracked transducer and the acquisition is gated to the ECG signal of the subject. For the porcine subjects the ECG gating was more consistent due to a better control of the heart rate compared to the patients. We have also observed some interference between the unshielded ECG leads and the tracking system, issue which can be addressed by using improved shielding of the ECG leads. However, the heart rate variability observed in the patients leads to the major concern in the image acquisition: the patients undergoing these procedures suffer from various medical conditions which lead to inconsistent heart rate and also prevent the administration of heart-rate controlling medication to the extent required for “clean” image acquisition. As such, the ECG trigger, although set for diastole, may actually trigger later in the cardiac cycle, leading to a systolic image acquisition, and hence a different position and orientation of the reconstructed annuli. These “artifacts” in fact explain the larger variations in the angle between the mitral and aortic valve annuli across the workflow stages in the patients undergoing robot-assisted CABG intervention.

Another challenge arises due to the large degree of manual intervention currently involved in the post-processing of the data. All peri-operative images are accessed

by the clinician off-line and the features of interest are segmented manually. In spite of manual segmentation being the clinical gold-standard procedure, we believe that there is an inherent degree of variability associated with the feature identification process, which, in turn, will affect the shape, position and orientation of the segmented features. To date we have not yet assessed the variability of the feature identification, but we plan to use the morphological characterization parameters to evaluate the repeatability and reproducibility of the segmentation as performed by different clinicians at different time points.

## 6.5 Conclusions

To conclude, this work was motivated by the well-known fact that pre-operative information can depict the intra-operative cardiac anatomy and morphology with limited fidelity and presents an analysis of the changes in location of the heart and the variations in morphology of features of interest arising during the workflow of minimally invasive procedures. The global heart displacement and morphological characteristics of the mitral and aortic valve annuli were estimated in two different minimally invasive procedures.

In terms of our UCI-based model-enhanced US guided interventions, this work allows us to estimate the effect of the procedure workflow on the model-to-patient registration, and suggests the need to update the registration prior to therapy delivery. In terms of the robot-assisted CABG procedures, this information is not only critical to assess anatomical differences induced during the procedure itself, but it also plays a crucial role in updating a pre-operative surgical plan. The work presented in Appendix A proposes a feature-based registration approach that predicts the intra-operative LAD location based on the pre-operative CT image and the peri-operative heart migration information.



# References

- [1] C. A. Linte, J. Moore, and C. *et al.* Wedlake. Inside the beating heart: An *in vivo* feasibility study on fusing pre- and intra-operative imaging for minimally invasive therapy. *Int J CARS*, 4:113–122, 2009.
- [2] Y. L. Ma, G. P. Penney, C. A. Rinaldi, M. Cooklin, R. Razavi, and K. S. Rhode. Echocardiography to magnetic resonance image registration for use in image-guided cardiac catheterization procedures. *Phys Med Biol.*, 54:5039–55, 2009.
- [3] W. E. Lorensen and H. E. Cline. Marching cubes: A high resolution 3d surface construction algorithm. *Computer Graphics*, 21, 1987.
- [4] M. Wierzbicki, M. Drangova, G. M. Guiraudon, and T. M. Peters. Validation of dynamic heart models obtained using non-linear registration for virtual reality training, planning, and guidance of minimally invasive cardiac surgeries. *Med Image Anal.*, 8:387–401, 2004.
- [5] D. G. Gobbi, R. M. Comeau, and T. M. Peters. Ultrasound probe tracking for real-time ultrasound/MRI overlay and visualization of brain shift. In *Lect Notes Comput Sci.*, volume 1679 of *Proc. MICCAI*, pages 920–27, 2008.
- [6] A. D. Wiles, C. A. Linte, J. Moore, C. Wedlake, and T. M. Peters. Object identification accuracy under ultrasound enhanced virtual reality for minimally invasive cardiac surgery. In *Proc. SPIE Medical Imaging 2008: Visualization, Image-Guided Procedures and Modeling*, volume 6918, pages 69180E1–12, 2008.

# Chapter 7

## Summary, Contributions and Future Directions

The work enclosed in this thesis describes the development of a multi-modality surgical guidance environment from initial concept, to *in vitro* evaluation, and all the way to pre-clinical implementation. The model-enhanced US-assisted surgical guidance environment represents one of the first attempts in cardiac IGS toward bridging pre-operative imaging and modeling, typically employed for procedure planning, with intra-operative guidance and therapy delivery. This environment is governed by the navigation-positioning paradigm, which was formulated in this thesis and is applicable to most image-guided interventions: every therapy delivery task consists of a navigation step — guiding the delivery instrument in the vicinity of the surgical target, followed by a positioning step — accurately place the tip of the delivery instrument on the surgical target.

In the context of the reality-virtuality continuum defined by Milgram *et al.* [1], the proposed platform is best classified as a mixed reality environment, leaning more

---

Portions of this work appear in Linte CA, Moore J and Peters TM. How accurate is accurate enough? An overview on accuracy considerations in image-guided cardiac interventions. *Proc. IEEE Eng Med Biol.* In Press. 2010. ©2010 IEEE. Reprinted, with permission, from IEEE.

toward the augmented virtuality end of the spectrum due to the extensive presence of virtual components (Fig. 7.1).

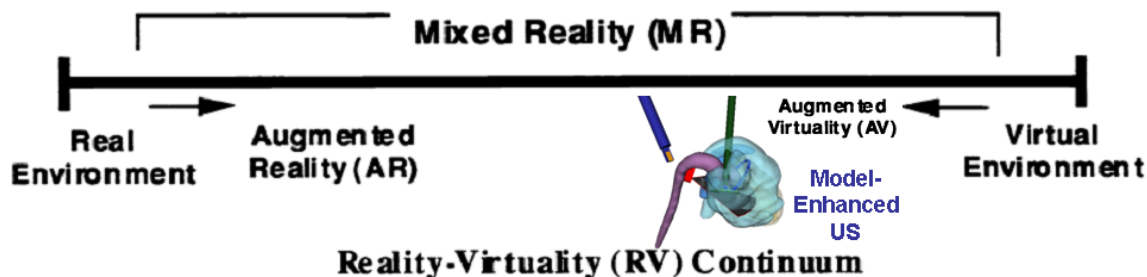


Fig. 7.1: Revisited schematic representation of the reality-virtuality continuum defined by Milgram *et al.* in 1994, showing the classification of the model-enhanced US-assisted guidance environment relative to the generic AR and AV environments. *Image adapted from Milgram et al. 1994.*

## 7.1 Summary of Contributions

The ability to accurately navigate the surgical tools to the target is essential for optimizing the surgical path that leads to achieving the desired therapeutic outcomes. TEE is an attractive modality for intra-procedure cardiac guidance and has become the clinical standard for interventional applications. However, despite real-time 2D ultrasound (US) images having relatively high spatial and temporal resolution, the context of the surgical site is generally incomplete, as 2D images cannot appropriately portray an entire 3D scene. While the recent release of 3D TEE technology may address some of the inherent challenges of interventional 2D TEE, its availability is still very limited. In addition, 3D TEE images possess a very restricted field of view and lower resolution than the 2D TEE images, making it difficult to visualizing both surgical targets and instruments in the same volume, leading to inadequate spatial context.

To ameliorate these situations, a key feature of the model-enhanced US platform is the combination of surgical tracking technologies and real-time US imaging. More-

over, the intra-operative images are augmented with pre-operative representations of the cardiac anatomy and virtual models of the delivery instruments tracked in real time using magnetic tracking technologies. As a result, the otherwise context-less 2D US images can now be interpreted within the anatomical context provided by the anatomical models. The virtual models assist the user with the tool-to-target navigation, while real-time TEE ensures accurate positioning of the tool on target, providing the surgeon with sufficient information to “see” and manipulate instruments in absence of direct vision.

The next research objective was to assess the accuracy with which a user can target specific features under guidance provided via the model-enhanced US-assisted environment. The experiments presented in Chapter 3 were designed around the hypothesis that the proposed platform would lead to improved targeting accuracy and shorter navigation times compared with 2D US image guidance alone; furthermore, the real-time US imaging would contribute to maintaining a consistent targeting accuracy under model-to-subject misregistrations.

Baseline accuracy measurements were obtained under endoscopic guidance, and were used as positive controls against which the other guidance modalities were tested. Our experimental results demonstrated that the proposed guidance environment led to an overall targeting error of under 3 mm, which represented a significant improvement from the accuracy recorded under 2D US image guidance alone (4-5 mm to as much as 15 mm targeting error). A comparison study between experts and novice users revealed that both groups achieved comparable targeting using model-enhanced US guidance, while the novice group showed a significant improvement over the expert group when employing the new environment, compared to the use of 2D US image guidance alone. Lastly, the studies also demonstrated that the real-time US imaging component provided sufficient information to correctly identify the intra-operative surgical target location following model-assisted navigation, and to compensate for any positioning errors due to misregistrations present between the heart/phantom

model and its physical counterpart, ensuring a consistent targeting accuracy within 1-1.5 mm.

The pre-operative anatomical models integrated within the proposed surgical environment are critical for ensuring appropriate tool-to-target navigation. As such, these models need to accurately depict the subject-specific anatomy and the location of the surgical target, and to provide the surgeon with the “big picture” of what he/she cannot see in absence of direct vision during beating heart interventions. The method proposed in Chapter 4 makes use of an average heart model previously developed in our laboratory [2] to generate dynamic subject-specific models from clinical 4D MR images. While similar techniques have previously been employed for diagnostic purposes [3], the models described here are intended for use in mitral valve interventional guidance. As reported earlier, the models can predict the location of the mitral valve annulus with a 3.1 mm accuracy throughout the cardiac cycle. Furthermore, using the feature-based registration method described in the same chapter, the models can be integrated within the intra-operative guidance environment with less than a 5 mm alignment error of the pre- and intra-operative anatomy in the region of interest.

Several pre-clinical acute evaluation studies have been conducted *in vivo* on swine models to assess the feasibility of the proposed environment in a clinical context. Following direct access inside the beating heart using the UCI, the proposed mixed reality environment was displayed to the surgeons via either standard operating room overhead monitors or head-mounted displays to provide the necessary visualization for therapy delivery. The integration of the proposed environment in the clinical workflow associated with mitral valve implantation and ASD repair procedures was described in Chapter 5. This work demonstrated the feasibility of the surgical platform for providing the required visualization and navigation information to position a prosthetic mitral valve on the the native annulus, or to place a repair patch on a created septal defect in a porcine model.

This work would be incomplete without exploring the effects of heart displacement

during the intra-operative procedure workflow as described in Chapter 6. The need for this investigation initially arose during the *in vivo* clinical evaluation of the model-enhanced US guidance platform presented in Chapter 5, as a consequence of the various stages involved in the workflow. Similar techniques were employed to assess the peri-operative migration of the heart due to the lung collapse and chest insufflation during robot-assisted CABG procedures in patient with coronary artery disease. Both procedures were shown to suffer from significant changes in the heart position, which need to be addressed during both the planning and guidance of these procedures.

The work in Appendix A is a natural extension of the findings described in Chapter 6 in the context of heart migration during robot-assisted CABG procedures. This research was performed in collaboration with a fellow student in the laboratory (Daniel S. Cho, Biomedical Engineering M.E.Sc. candidate) and it was aimed at investigating feasible techniques to improve planning of robot-assisted CABG procedures. In the effort to provide better planning of these interventions, this work proposes a modified version of the feature-based registration algorithm presented in Chapter 4 to predict the intra-operative location of the target vessel based on its pre-operative, CT-derived location and the peri-operative heart migration information explored using the techniques described in Chapter 6. A preliminary validation of the proposed technique was conducted *in vitro* using a beating heart phantom, and revealed a 3.5 mm RMS target registration error in predicting the LAD location.

## 7.2 Accuracy Considerations: Revisited

Recalling from Chapter 1, the success of an intervention is assessed from a clinical perspective according to the therapeutic outcome. From an engineering perspective on the other hand, navigation accuracy is constrained by the limitations of the IGS system [4]. To understand these limitations, it is necessary to estimate the errors at each stage of the IGT process and study their propagation through the entire

workflow, as suggested by Dr. Pierre Jannin from the Université de Rennes I (Rennes, France) [5]. However, these uncertainties are not unique, but rather application and system dependent. Thus, the aim of this section is to address these accuracy aspects from the point of view of the model-enhanced US-assisted surgical guidance environment and its applications in cardiac interventions, as described in this thesis.

### 7.2.1 Examples of Accuracy Expectations in the Clinic

While a formal definition is currently lacking, clinical accuracy may be defined as the maximum error that can be tolerated during an intervention without compromising the therapy or leading to increased risks to the patient. Such tolerances are difficult to define, as they are procedure and patient specific. A few examples are provided below.

In the case of an intracardiac ablation procedure, where the clinician aims to electrically isolate a region of tissue by forming a closed loop around the arrhythmia foci either via radio-frequency, cryo or thermal energy delivery, a 5 mm radius may provide a clinically adequate goal.

Another intervention in need of better guidance is the robot-assisted CABG procedure. As noted in Chapter 6, as many as 15-20% of the robot-assisted procedures are converted to traditional open-chest surgery [6] as the target vessel cannot be reached with the robotic instruments despite the port placement configuration having been determined based on the pre-operative plan. To avoid such situations, a better prediction of the intra-operative target vessel location is needed. The trocar can be repositioned in single rib space increments, hence a clinically-imposed accuracy on the order of one intercostal space (1-1.5 cm) is deemed sufficient, as described in Appendix A.

Lastly, based on our *in vivo* experience on swine models with mitral valve implantation or ASD repair procedures presented in Chapter 5, an overall  $\sim 5$  mm pre- and intra-operative anatomical alignment at the target region may be sufficient for

navigation, in the context of the navigation-positioning paradigm.

## 7.2.2 Identifying Engineering Accuracy Constraints

According to Jannin’s recommendations [5], the overall system accuracy is dependent on the limitations of its integrated components. Here we have broken down our mixed reality medical imaging platform into several parts including modeling, registration, surgical tracking, and overall tracking and reported on their individual accuracy constraints.

### 7.2.2.1 Modeling Accuracy

Within the framework of our model-enhanced US guidance environment, static and dynamic pre-operative models of the cardiac anatomy are generated using image segmentation from high-quality CT or MR images and used to provide visual cues for tool-to-target navigation. The accuracy of such anatomical models can be interpreted in terms of their fidelity in representing the subject’s organ. While the accuracy of the models generated via manual segmentation (**Fig. 7.2**) is difficult to assess, as manual segmentation itself is considered the gold-standard segmentation technique, one can nevertheless measure the uncertainties in the repeatability and reproducibility of the segmentations.

If the models are generated using an atlas-based approach [3, 7], their accuracy can be evaluated against that of the gold-standard models obtained by manual segmentation of the pre-operative images. Using similar techniques on human MRI data, subject-specific heart models (**Fig. 7.2**) for application in valvular interventions were generated by fitting an *a priori* heart model [2, 8] to a mid-diastolic subject MR image [9], as described in Chapter 4. These models enabled the prediction of the mitral valve annulus with an accuracy of 2.8 mm in diastole and 3.4 mm in systole.



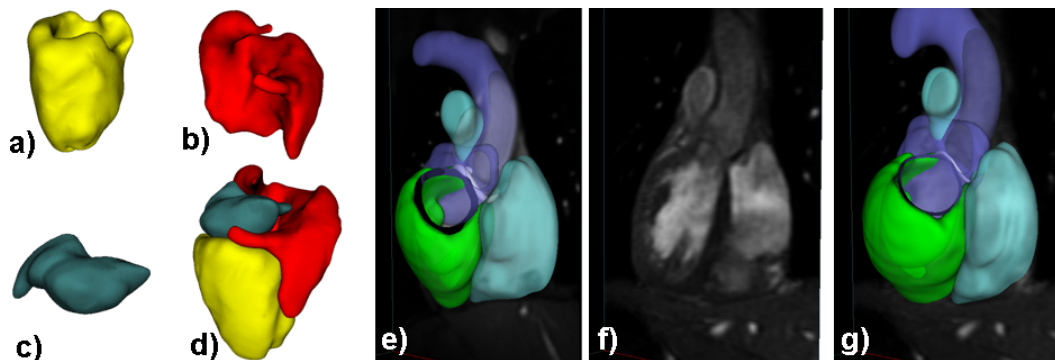


Fig. 7.2: Models of a porcine left ventricle (a), right atrium and ventricle (b), left atrium (c) and overall heart (d) obtained via manual segmentation of an MR dataset; e) *A priori* average heart model of a human heart; f) Clinical quality subject MR image; g) Subject-specific model obtained by fitting the atlas to a new subject's image dataset.

### 7.2.2.2 Registration Accuracy

As mentioned in section Chapter 1, computational complexity precludes some registration algorithms from use in time-critical interventions. Instead, fast, simple, and OR-friendly registration techniques are preferred [10, 11].

The feature-based registration technique proposed in Chapter 4 provided sufficiently accurate alignment (i.e. on the order of 4-5 mm) of the pre- and intra-operative anatomy in the region of interest [11, 12]. Similar results were achieved by Ma *et al.* [10] who proposed a feature-based registration technique that relied on the alignment of the left ventricular surface and the centerline of the descending aorta to fuse pre- and intra-operative data using a weighted iterative closest point (ICP) approach.

According to the navigation-positioning paradigm governing the model-enhanced US guidance environment, the achieved registration accuracy is suitable for tool-to-target navigation. Nevertheless, these results may not be suitable for model-guided therapy alone, without “refined guidance” provided via real-time US imaging.

Lastly, the method described in Chapter 4 was adapted to predict the change in location of the LAD coronary artery between the pre-operative plan and the intra-operative stage [13]. According to the phantom studies presented in Appendix A,

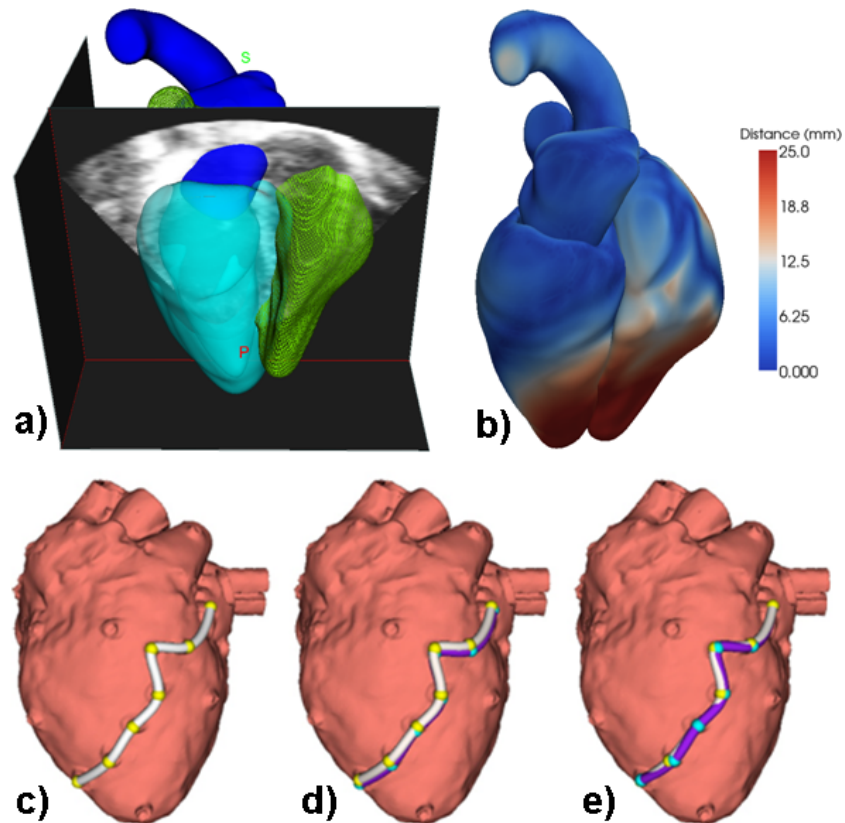


Fig. 7.3: a) US image augmented with pre-operative heart model; b) Error map showing registration error across the model; c) Phantom experiment showing gold-standard location of the target vessel along with its predicted location following lung deflation (d) and chest insufflation (e).

this technique yielded a RMS TRE of 3.5 mm along the LAD (**Fig. 7.3**) [13]. These accuracy figures are within the clinical requirements (10-15 mm) for the application, previously estimated as the width of one intercostal space (i.e. 10-15 mm).

### 7.2.2.3 Surgical Tracking Accuracy

Surgical tracking is essential for image-guidance and knowledge of tracking accuracy limitations is critical. For all intracardiac procedures, magnetic tracking technologies are employed exclusively [14, 15].

As described throughout this thesis, our augmented medical imaging platform

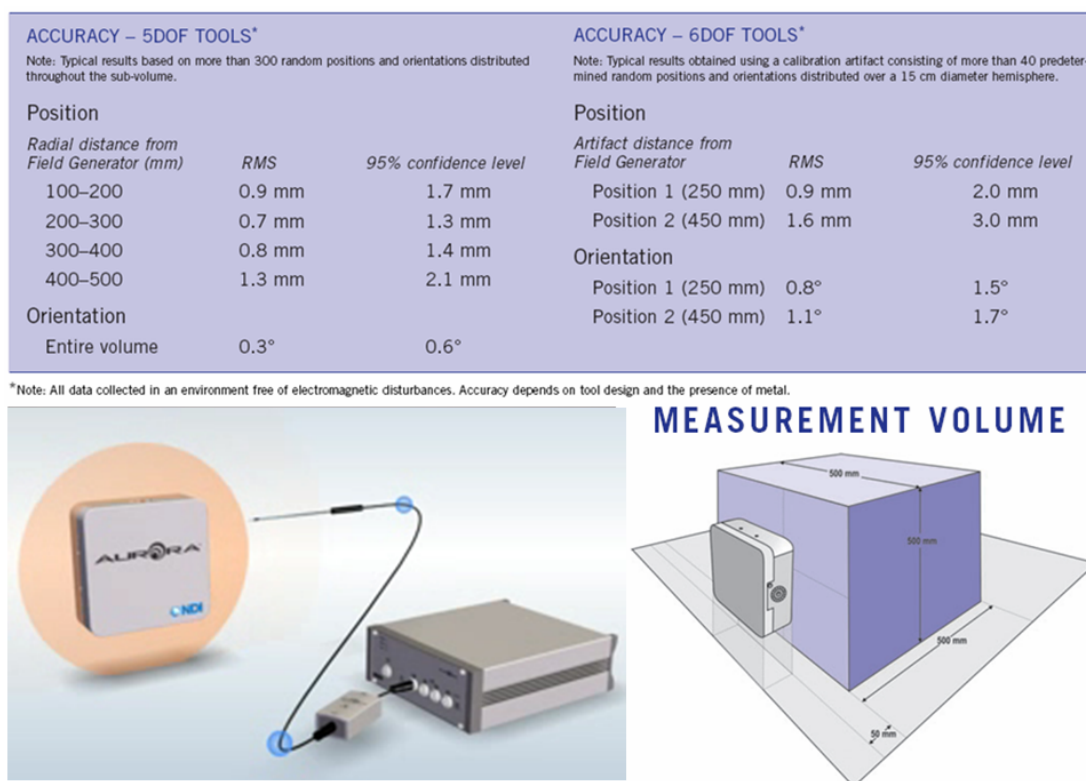


Fig. 7.4: The NDI Aurora<sup>TM</sup> magnetic tracking system, along with its specifications regarding optimal tracking volume and accuracy constraints. *Figure material adapted from the NDI Aurora<sup>TM</sup> technical brochure available at <http://www.ndigital.com>. Image courtesy of Northern Digital Inc., Waterloo, ON.*

employs the NDI Aurora<sup>TM</sup> MTS (**Fig. 7.4**). Both the surgical instruments (i.e. rigid tools or flexible catheters), as well as the US transducer are tracked using 6 DOF magnetic sensors. In addition, for the *in vitro* accuracy studies presented in Chapter 3, the surgical targets were also tracked using 5 DOF magnetic sensors. The system enables instrument tracking with an RMS accuracy of 0.7 mm and 0.9 mm in translation, and 0.3° and 0.8° in rotation, for the 5 and 6 DOF sensors, respectively [15].

### 7.2.2.4 Overall Targeting Accuracy

The targeting accuracy associated with an IGI system represents a measure of how well a user can guide a tracked instrument to a particular target under guidance provided by the system. According to the studies described in Chapter 3 that mimicked direct access and catheter-based procedures [16] (including analysis under model-to-phantom misregistrations similar to those encountered in the clinic), it was confirmed that real-time US guidance helped refine the model-assisted navigation accuracy, leading to targeting errors of  $\sim 1$  mm RMS (**Fig. 7.6**).

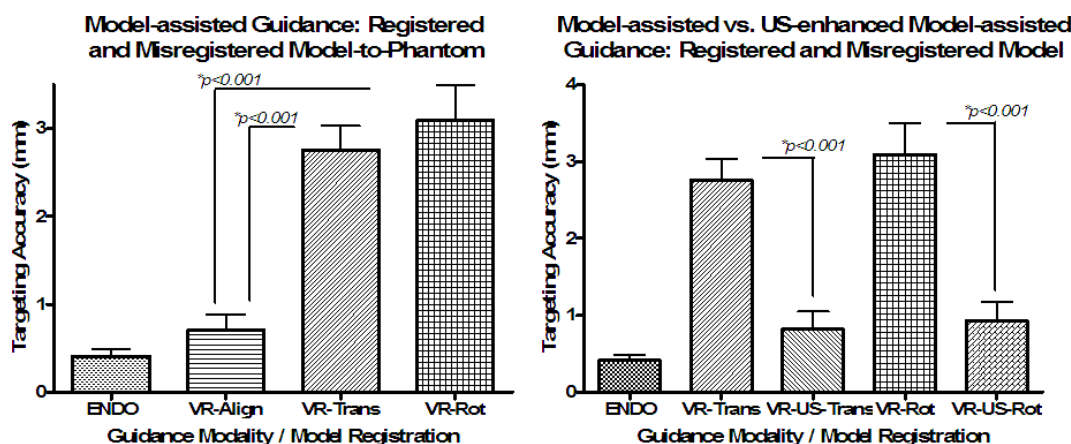


Fig. 7.5: *In vitro* evaluation of the targeting accuracy under optimal “world” registration (left panel), as well as in the presence of model-to-phantom misalignments (right panel). While model-assisted guidance alone provided accurate targeting under well-registered conditions (VR-Align), its accuracy decreased with the introduction of translational (VR-Trans) or rotational (VR-Rot) misalignments. However, superior targeting accuracy on the order of 1 mm RMS was achieved once real-time US imaging was used to complement the model-guided navigation, under both translational (VR-US-Trans) or rotational (VR-US-Rot) misalignments.

## 7.2.3 Monitoring, Improving and Providing Accuracy Feedback to the Surgeon

The registration and tracking accuracies of IGI platforms developed thus far have demonstrated errors on the order of several mm. These errors have the potential to

affect user decisions in a clinically significant manner. To further improve guidance accuracy, intra-operative real-time feedback can be presented along with uncertainty distributions, depending on the surgical task:

- To allow the surgeon to modify tool positioning to reduce the size of the uncertainty distribution if the estimated error is too large;
- To provide guidance on the appropriate size of the implant, if, for example, a larger patch may be required in cases with high uncertainty, when attempting to repair an atrial/ventricular septal defect;
- To provide a suggested search area in cases where multiple attempts may be required to hit the intended target - as in a catheter ablation procedures, for example;
- To provide the clinician with the opportunity to request additional secondary imaging if the uncertainty is high - for example in image-guided percutaneous valve delivery the surgeon may request additional angiographic images.

Based on the TRE models developed by Fitzpatrick *et al.* [17] and extended by Wiles *et al.* [18], the TRE information can be estimated and presented graphically to the surgeon using a 95% confidence ellipsoid, taking into account its anisotropic nature. Moreover, the error associated with the pre-operative anatomical models and the tracked surgical tools can also be incorporated and displayed to the operator.

On the other hand, presenting uncertainty distributions to the clinician may present some cognitive challenges. Such information would be a major paradigm change for a surgeon who is accustomed to directly visualizing a probe with respect to its intended target. Many cardiac procedures are performed very rapidly on a beating heart, and may involve multiple forms of image augmentation or multiple tracked tools. The addition of uncertainty information to the display may result

in cognitive overload; therefore, future studies are needed to explore an appropriate delivery approach of such information.

## **7.3 Summary of Lessons Learned during Clinical Translation**

Some of the challenges disseminated in the literature with respect to the clinical translation of new environments into the clinical setting have been mentioned in Chapter 1. Following the development, evaluation, and pre-clinical implementation of the model-enhanced US-assisted guidance platform described in this thesis, the lessons learned along the way are outlined below, together with the challenges that were addressed to ensure a smooth integration within the clinical environment of modern operating rooms.

### **7.3.1 Zoom in where Needed: Region of Interest Accuracy**

The feature-based registration technique presented in Chapter 4 was developed to provide optimal alignment of the pre- and intra-operative valvular structures for enhanced tool-to-target navigation during mitral valve implantation. While an accuracy of under 4 mm was achieved at the surgical target, remote regions of the heart experience larger registration errors. When extended to suit the application described in Appendix A, the features of interest bounding the upper and lower end of the target vessel — the left coronary ostium and left ventricular apex — were assigned a higher weighting factor compared to the other features employed, leading to an overall target registration error of  $\sim 2.5$  mm at the anastomosis site.

These are only two examples of situations where the registration techniques employed were adapted to suit the application and provide the desired anatomical alignment at the surgical site. However, this approach is common in IGS, as most tech-

niques designed for intra-operative use must be easily implemented and computationally efficient, while achieving the desired outcome.

### 7.3.2 Cutting-edge Hardware: Surgical Tool Design

Surgical tool manufacturing is a key component in IGS, especially when subject to multiple constraints imposed by the cardiac anatomy, interventional application, and surgical environment. Throughout the work described in this thesis, we have faced the challenge of designing and building our own instruments or adapting other available tools for the application at hand. For the pre-clinical *in vivo* evaluation studies, various iterations of prototypes of the valve- and ASD patch-guiding tools with embedded magnetic sensors were built and tested to ensure their compatibility with the surgical environment. Moreover, a laparoscopic stapler for abdominal interventions was adapted as a fastening device for securing the valve and ASD patch, in spite of its oversized dimensions for intracardiac applications.

Unfortunately, most off-the-shelf tools do not comply with the requirements imposed by the application; hence, a more efficient approach would be to involve a medical device manufacturer in the project to ensure that the developed tools were suitable for the application. For most interventional applications, sub-millimeter accuracy is meaningless unless appropriate surgical instruments are used for safe therapy delivery.

### 7.3.3 Minimizing “Footprint” in the Operating Room

A “busy” environment is not uncommon in an OR, raising the concern of using magnetic tracking technology as opposed to an optical system for surgical tool tracking, which, in turn implies the avoidance of any ferro-magnetic objects in close proximity to the magnetic field emitter [15]. Given that tracking accuracy decreases away from the magnetic field emitter, the field generator must be placed within a

range of 20-30 cm from the most probable tool location. Our initial implementation consisted of the magnetic field generator overhanging just above the surgical field.

To minimize the obstruction of the workflow, while maintaining tracking accuracy, the magnetic field generator was then embedded within the mattress of the operating table. It is worth noting that NDI has recently (June 2010) announced the release of a flat field generator that can be placed under the patient, directly on the operating table, even if it contains ferromagnetic components. This location has the additional benefit of placing tracked sensors closer to the field generator than large bodies of metal such as rib spreaders, making the MTS substantially more robust. A similar approach was undertaken during the peri-operative imaging of the patients undergoing robot-assisted CABG procedures, with all sensor cables placed under or along the OR table to be as unobtrusive as possible.

### **7.3.4 Making “the New” Look like “the Old”**

The mixed reality guidance environment is a novel surgical technique and, in spite of our efforts to make it a common part of the current operating rooms, we are well aware that it may not make its way into conventional surgery for a few years. Over the years, surgeons have become familiar with “standard views” of human anatomy. Although we are now able to provide an unlimited range of oblique views of tools and surgical targets, it is often best to use the views surgeons are most familiar with to maintain intuitive guidance. From our experience, the best approach is to make “the new” look much like “the old”, and instead of overwhelming the users with a lot of new technology at once, rather give them the time to get accustomed to the new environments.



### 7.3.5 Maximizing Returns: Optimal Information Display

Minimal invasiveness restricts both visual and surgical access. For off-pump intracardiac interventions, surgeons can't "see" what they do, and the guidance platform *is* their eyes. We have considered several approaches regarding the most appropriate display of the mixed reality environment to the surgeons, some of which were also mentioned in the introductory chapter. While some of these paradigms have been tested as part of parallel projects in our laboratory, others will be explored in our future work. Nevertheless, for the time being, our surgical team has been pleased with both overhead monitors and HMD units for visualization, in spite of their discomfort with the HMDs after prolonged use.

## 7.4 Future Directions

The mixed reality environment described in this thesis has been developed with the long-term objective to provide the surgeon with the necessary visualization and navigation information during beating heart procedures, in absence of direct vision. This environment can be adapted to suit the guidance of other interventions, and based on the infrastructure currently available in our laboratory, two future developments within an arm's length of the current work are identified here: integration of 3D TEE data within the mixed reality environment, and integration of electro-anatomical models with real-time image guidance for catheter-guided atrial fibrillation therapy.

### 7.4.1 Integration with 3D TEE

At the time this work was initiated, 3D TEE technology was still under development. From our experience, 3D trans-thoracic US provides limited flexibility for the surgeon to manipulate the US probe with one hand and the surgical instrument with the other. For enhanced navigation, magnetically tracked 2D TEE has been

integrated into the model-enhanced US environment.

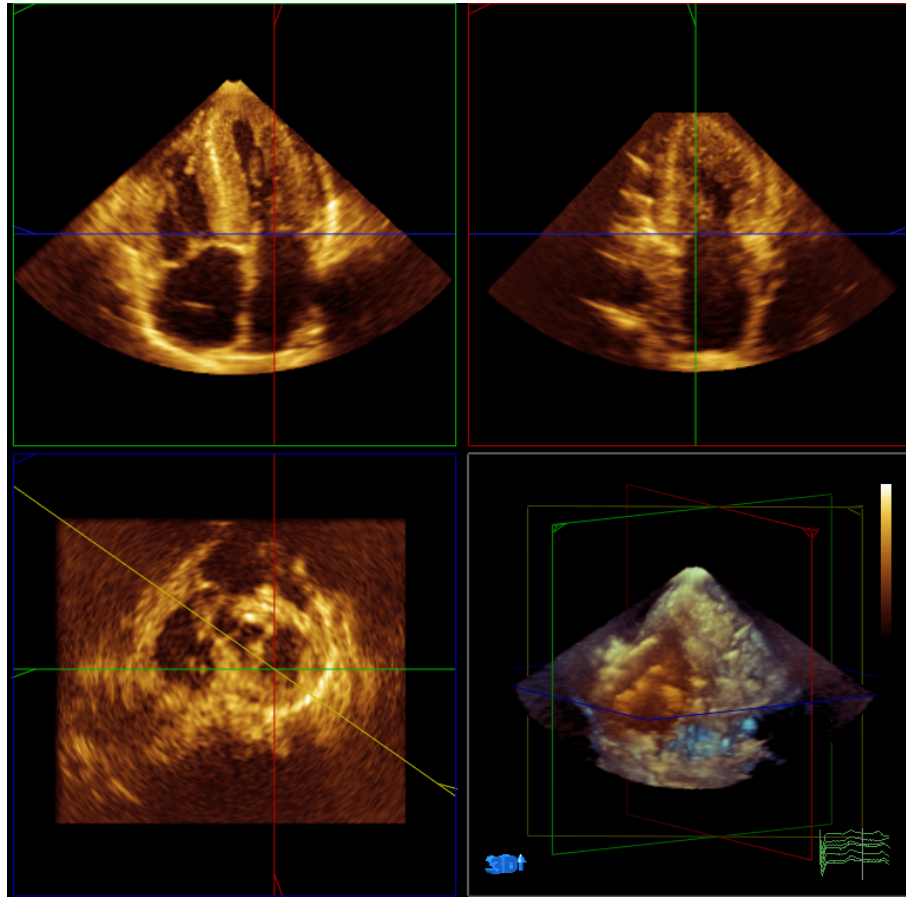


Fig. 7.6: Standard 2D views and volume rendered 3D display of the mitral valve apparatus acquired using the Philips real-time 3D TEE transducer and the IE33 scanner.

However, over the past three years, there have been significant developments in 3D TEE technology for both diagnostic and interventional imaging. As part of our future developments, we plan to investigate the integration of 3D US as the real-time imaging modality within the mixed reality platform. Several groups have demonstrated the added benefits of 3D TEE over the traditional 2D US images [19], for imaging both surgical targets as well as delivery instruments. This modality would enable a faster and more accurate identification and extraction of features of interest and surgical targets, which, in turn, may potentially provide the flexibility to update the pre- to intra-operative registration as often as needed during the procedure.

Provided similar calibration approaches can be developed to enable magnetic tracking of 3D TEE transducers, the proposed mixed reality environment described in this work could be “upgraded” to include real-time 3D TEE augmented with pre-operative anatomy and surgical instrument tracking.

### 7.4.2 Catheter-guided Atrial Ablation Therapy

Several other cardiac image-guidance techniques have been explored in our laboratory over the past five years that have the potential to provide enhanced intra-operative guidance. From a modeling perspective, Wilson *et al.* [20] demonstrated the extension of 3D static cardiac mapping environment into one that takes full advantage of 4D pre-operative modeling. Recorded EP data can be encoded according to their spatial and temporal time-stamps, as prescribed by the tracking system and ECG-gating, respectively. As such, 4D mapping enables the augmentation of the pre-operative models with functional data, leading to electro-anatomical models suitable for both surgical planning and intra-procedure guidance. A schematic illustration of the concept is included in **Fig. 7.7**, and a preliminary *in vivo* demonstration of this work has also been reported [20].

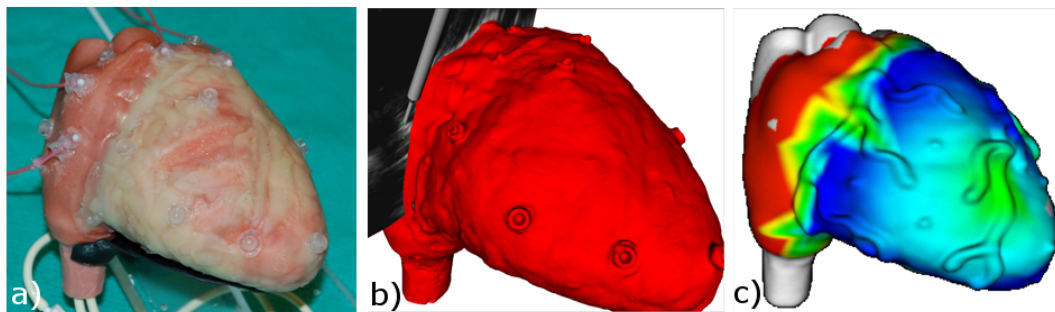


Fig. 7.7: a) Cardiac phantom used for *in vitro* experiments; b) Surface model of the phantom segmented from the CT image; c) Electro-anatomical model obtained by mapping EP data onto a pre-operative model to serve with surgical target identification. *Image courtesy of Kevin Wilson, MEdSc, Robarts Research Institute, London, ON*

From a navigation perspective, the work presented here has demonstrated the ca-

pabilities of the model-enhanced US environment to provide sufficient guidance under limited visualization. Moreover, a preliminary *in vivo* study on catheter navigation to clinically relevant sites in the right atrium of a porcine model has been performed, comparing navigation under model-enhanced US-assisted guidance vs. real-time US guidance. Our results have reported targeting errors of less than 5 mm and navigation times of  $\sim 20$  seconds under the hybrid guidance environment. These represents an improvement over US image guidance alone, which led to errors as high as 30 mm, achieved after durations twice as long as those recorded under model-enhanced US guidance(Fig. 7.8).

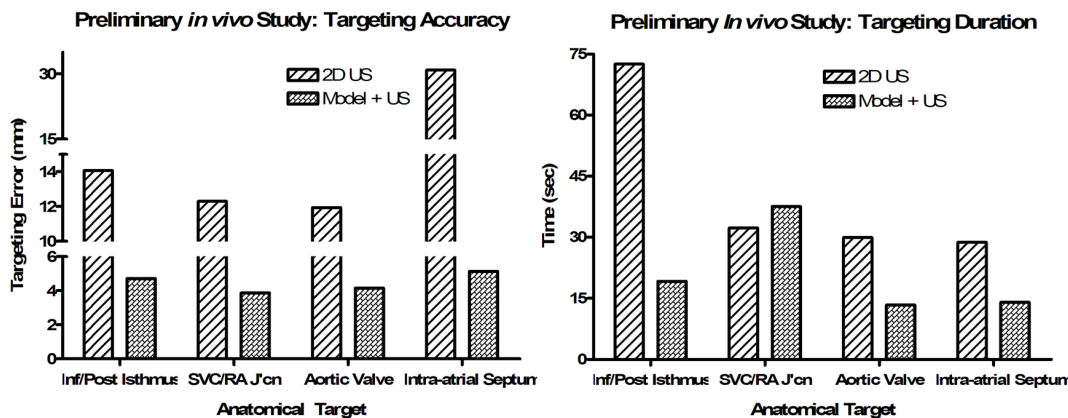


Fig. 7.8: Preliminary *in vivo* evaluation of model-enhanced US-assisted vs. 2D US image-guided catheter navigation in the right atrium of a porcine model. Navigation accuracy (mm) and duration (sec) were recorded while a magnetically tracked catheter was guided to clinically relevant sites (i.e. inferior/posterior isthmus, superior vena cava/right atrium junction, aortic valve, and intra-atrial septum) in the right atrium of a swine model.

By combining electro-anatomical modeling and model-enhanced US for intra-operative guidance of catheter-guided atrial fibrillation treatment, the hybrid environment would enable the mapping of dynamic EP data onto the pre-operative cardiac model and eliminate the risks associated with fluoroscopic imaging. Ultimately, clinicians can explore the intracardiac environment using registered pre-operative models as guides, and navigate surgical tools intrinsically relative to cardiac anatomy.

## 7.5 Concluding Remarks

In one of his articles at the turn of the millennium, Mack *et al.* [21] identified four themes in the context of minimally invasive cardiac interventions: increasing use of image guidance in lieu of direct vision during interventions; evolution of excision techniques for arrhythmia treatment into ablation therapy; use of reconstruction and self-anchoring devices as an alternative to traditional suturing; and therapy delivery via natural orifices or blood vessels as opposed to the traditional open heart approaches. Moreover, they also raised the need for a different workplace that can embrace these new techniques — the cardiac operating room of the future — featuring both multi-modality imaging and tele-surgery capabilities.

Looking back almost a decade later, we recognize that some of those advancements have indeed occurred: the devices have been built and the techniques have been developed and translated into clinical practice, enabling more efficient therapy delivery while reducing patient morbidity [22]. However, these developments would not have taken place without appropriate visualization and guidance provided via medical imaging.

Following further development and seamless integration into the clinical workflow, we hope that the model-enhanced US-assisted guidance environment described in this thesis may become a significant milestone toward enabling minimally invasive therapy on the beating heart.

# References

- [1] P. Milgram, H. Takemura, A. Utsumi, and F. Kishino. Augmented reality: A class of displays on the reality-virtuality continuum. In *Proc. SPIE 1994: Telemanipulator and Telepresence Technology*, volume 2351, pages 282–92, 1994.
- [2] M. Wierzbicki, J. Moore, M. Drangova, and T. M. Peters. Subject-specific models for image-guided cardiac surgery. *Phys Med Biol.*, 53:5295–312, 2008.
- [3] M. Lorenzo-Valdés, G. I. Sanchez-Ortiz, D. Mohiaddin, and D. Rueckert. Atlas-based segmentation and tracking of 3D cardiac MR images using non-rigid registration. In *Lecture Notes in Computer Science*, volume 2488 of *Proc. of Med Image Comput Comput Assist Interv.*, pages 642–50, 2002.
- [4] W. J. Viant. The development of an evaluation framework for the quantitative assessment of computer-assisted surgery and augmented reality accuracy performance. *Stud Health technol Inform.*, 81:534–40, 2001.
- [5] P. Jannin, J. M. Fitzpatrick, D. J. Hawkes, X. Pannec, R. Shahidi, and M. W. Vannier. Validation of medical image processing in image-guided therapy. *IEEE Trans Med Imaging*, 21:1445–49, 2002.
- [6] Jr Damiano, Ralph J. Robotics in cardiac surgery: The emperor’s new clothes. *J Thorac Cardiovasc Surg.*, 134:559–561, 2007.
- [7] M. Wierzbicki, M. Drangova, G. M. Guiraudon, and T. M. Peters. Validation of dynamic heart models obtained using non-linear registration for virtual reality training, planning, and guidance of minimally invasive cardiac surgeries. *Med Image Anal.*, 8:387–401, 2004.
- [8] J. Moore, M. Drangova, J. Barron, and T. M. Peters. A high-resolution dynamic heart model based on averaged MRI data. In *Proc. of Med Image Comput Comput Assist Interv.*, volume 2878 of *Lect Notes Comput Sci.*, pages 549–55, 2003.
- [9] C. A. Linte, M. Wierzbicki, J. Moore, G. M. Guiraudon, S. Little, and T. M. Peters. Towards subject-specific models of the dynamic heart for mitral valve

- surgery. In *Proc. of Med Image Comput Comput Assist Interv.*, volume 4792 of *Lect Notes Comput Sci.*, pages 94–101, 2007.
- [10] Y. L. Ma, G. P. Penney, C. A. Rinaldi, M. Cooklin, R. Razavi, and K. S. Rhode. Echocardiography to magnetic resonance image registration for use in image-guided cardiac catheterization procedures. *Phys Med Biol.*, 54:5039–55, 2009.
- [11] C. A. Linte, M. Wierzbicki, J. Moore, G. M. Guidardon, D. L. Jones, and T. M. Peters. On enhancing planning and navigation of beating-heart mitral valve surgery using pre-operative cardiac models. In *Proc. IEEE Eng Med Biol.*, pages 475–78, 2007.
- [12] C. A. Linte, J. Moore, C. Wedlake, D. Bainbridge, G. M. Guitaudon, D. L. Jones, and T. M. Peters. Inside the beating heart: An *in vivo* feasibility study on fusing pre- and intra-operative imaging for minimally invasive therapy. *Int J CARS*, 4:113–122, 2009.
- [13] S. D. Cho, C. A. Linte, E. Chen, J. Moore, J. Barron, B. Kiaii, R. Patel, and T. M. Peters. Predicting target vessel location for improved planning of robot-assisted CABG procedures. In *Proc. Med Image Comput Comput Assist Interv.*, volume *In Press* of *Lect Notes Comput Sci.*, 2010.
- [14] W. Birkfellner, F. Watzinger, F. Wanschitz, R. Ewers, and H. Bergmann. Calibration of tracking systems in a surgical environment. *IEEE Trans Med Imaging*, 17:737–42, 1998.
- [15] C. Nafis, V. Jensen, L. Beauregard, and P. Anderson. Method for estimating dynamic EM tracking accuracy of surgical navigation tools. In *Medical Imaging 2006: Visualization and Image-Guided Procedures*, volume 6141 of *Proc. of SPIE.*, pages 61410K–16, 2006.
- [16] C. A. Linte, J. Moore, C. Wedlake, and Peters. T. M. Evaluation of model-enhanced ultrasound-assisted interventional guidance in a cardiac phantom. *IEEE Trans Biomed Eng.*, *In Press*, 2010.
- [17] J. M. Fitzpatrick, J. B. West, and C. R. Jr. Maurer. Predicting error in rigid-body point-based registration. *IEEE Trans Med Imaging*, 17:694–702, 1998.
- [18] A. D. Wiles, A. Likholyot, D. D. Frantz, and T. M. Peters. A statistical model for point-based target registration error with anisotropic fiducial localizer error. *IEEE Trans Med Imaging*, 3:378–90, 2008.
- [19] P. M. Novotny, J. A. Stoll, N. V. Vasilyev, P. J. del Nido, P. E. Dupont, T. E. Zickler, and R. D. Howe. GPU based real-time instrument tracking with three-dimensional ultrasound. *Med Image Anal.*, 11:458–64, 2007.

- [20] K. Wilson, G. M. Guiraudon, D. L. Jones, and T. M. Peters. Mapping of cardiac electrophysiology onto a dynamic patient-specific heart model. *IEEE Trans Med Imaging*, 28:1870–80, 2009.
- [21] M. J. Mack. Minimally invasive and robotic surgery. *JAMA*, 285:568–72, 2001.
- [22] M. Eckert, D. Cuadrado, T. Steele, S. and Brown, M. Martin, and A. Beekley. The changing face of the general surgeon: National and local trends in resident operative experience. *Am J Surg.*, 199:652–6, 2010.



# Appendix A

## Predicting Target Vessel Location for Improved Planning of Robot-Assisted CABG Procedures

*This work is a continuation of the investigation on peri-operative heart migration during minimally invasive robot-assisted CABG procedures in Chapter 6. In common clinical practice, the pre-operative surgical plan is based on a CT scan of the patient acquired before the procedure, under the assumption that the heart does not undergo any significant changes between the pre- and intra-operative stages. However, as shown in Chapter 6, the peri-operative workflow itself leads to changes in heart position and, consequently, the intra-operative target vessel location. As such, the pre-operative plan must be adequately updated to adjust the target vessel location to better suit the intra-operative condition. Here we propose a technique to better predict the peri-operative target vessel location, which has the potential to improve procedure planning and help reduce the rate of conversion to traditional open-chest surgery.*

---

This chapter is adapted from Cho SD, Linte CA, Chen E, Wedlake C, Moore J and Peters TM. Predicting Target Vessel Location for Improved Planning of Robot-Assisted CABG Procedures. *Proc. Med Image Comput Comput Assist Interv. - Lect Notes Comput Sci. In Press: 2010.*

## A.1 Background and Motivation

Robot-assisted (RA) surgery represents a paradigm shift in the delivery of health care for both the patient and the surgeon [1] and it has been adopted as standard of care at many institutions worldwide [1]; one of the popular cardiac interventions performed under robot-assistance is the CABG procedures.

In current clinical practice, a pre-operative CT scan of the patient is used to assess his/her candidacy for undergoing a RA-CABG procedure. Based on the pre-operative scan, the surgeon identifies the location of the surgical target - the left anterior descending (LAD) coronary artery, examines whether there is sufficient workspace inside the chest wall for the robot arms, and ultimately estimates the optimal locations of the port incisions to ensure proper reach of the surgical targets with the robotic instruments (**Fig. A.1**). However, it is not unusual that after setting up the patient for the robot-assisted procedure, the surgeons encompass difficulties due to the inability in reaching the target, robot arm collisions or reduced dexterity [2]. In fact, 20-30% of the robot-assisted (RA)-CABG interventions require conversion to traditional open-chest surgery [3], mainly due to the migration of the heart during the peri-operative workflow, not accounted for in the pre-operative plan.

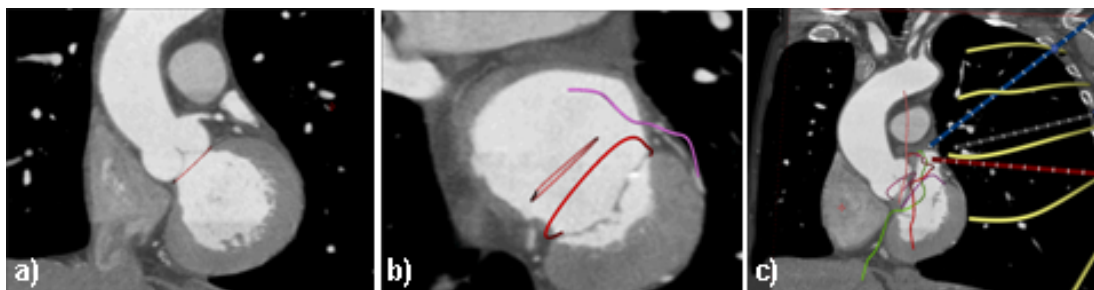


Fig. A.1: Pre-operative planning stage showing patient's cardiac CT scan (a), the coronary vessel displayed relative to the valve annuli (b) and the port placement to ensure proper reach of the target vessel with the robotic instruments (c), where the yellow lines represent intercostal spaces.

In a typical RA-CABG procedure, the patient is first imaged pre-operatively

(Stage<sub>0</sub>) in the same position as during the intervention. Peri-operatively, following intubation and anesthesia delivery (Stage<sub>1</sub>), the left lung is collapsed (Stage<sub>2</sub>), and the chest is insufflated (Stage<sub>3</sub>) to provide sufficient work space.

As described in Chapter 6, we have developed a feasible approach to “image” the patient’s heart at each peri-operative workflow stage using tracked US [4] and estimate its global displacement. To capture all of the necessary cardiac features, images were collected from three different views. For our work, mid-esophageal-4-chamber view images were captured at 20° increments from 0° to 180° for the mitral valve annulus (MVA) and the left ventricle apex (LVAp). Five long axis view images with 10° increments and one short axis view of the aorta at 30° were also acquired to visualize the AVA and the left main coronary ostium (LMCO).

The peri-operatively acquired instances were then transferred into the CT coordinate system by aligning homologous features corresponding to the first peri-operative (Stage<sub>1</sub> US) and the pre-operative (Stage<sub>0</sub> CT) datasets (**Fig. A.2**). These two stages are physiologically equivalent given the same patient position and dual-lung ventilation, and hence minimal anatomical variations are expected. As a result, the peri-operative displacements can be estimated with respect to the principal body axes.

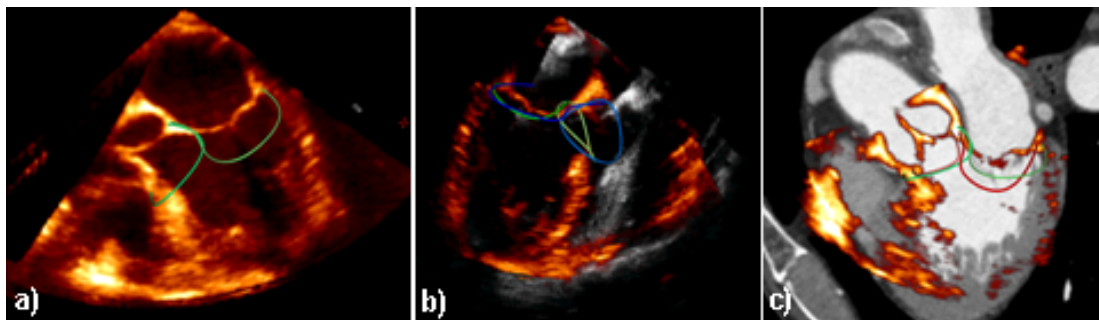


Fig. A.2: a) Patient heart instance at Stage<sub>1</sub> acquired using tracked US and showing the valve annuli; b) Stage<sub>1</sub> (orange) and Stage<sub>2</sub> (gray) instances of the heart showing relative heart displacement and corresponding segmented valvular structures; c) Initial peri-operative US instance (Stage<sub>1</sub>) registered to the pre-operative dataset and displayed within the CT coordinate space.

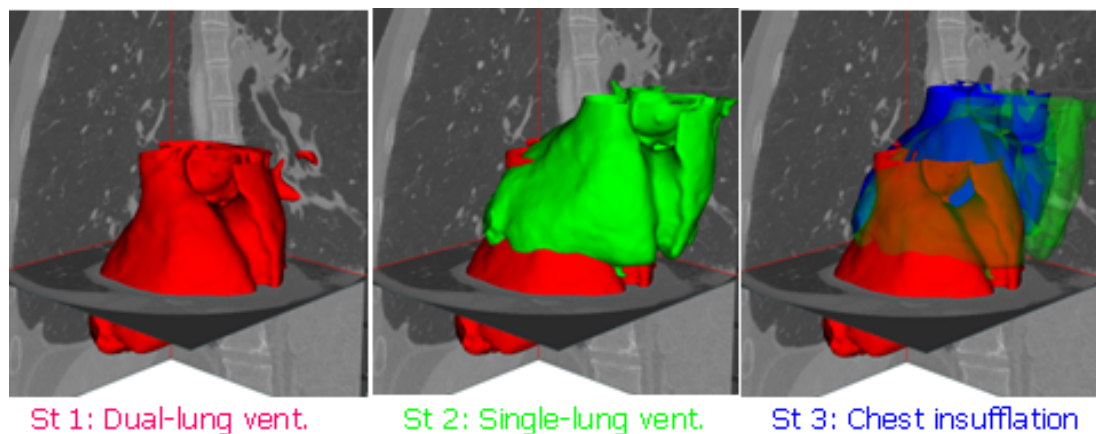


Fig. A.3: Visual representation showing an automatically segmented epicardial model of a patient’s heart animated using the sequential peri-operative transforms based on the valvular structures. Note: Stage<sub>1</sub> is shown in red, Stage<sub>2</sub> in green and Stage<sub>3</sub> in blue.

We have shown the migration patterns in four patients undergoing RA-CABG procedure [5]. Our clinical data have suggested that the heart undergoes considerable displacement during the workflow, which should not be ignored during the planning process. As an example, we show the change in position of the epicardial surface of one patient’s heart segmented from the CT dataset and animated using the sequential peri-operative transforms (**Fig. A.3**). Moreover, in spite of the observed displacements, the morphology of the identified features remains relatively consistent throughout the workflow [5], suggesting that no significant non-rigid deformations are occurring, as concluded in Chapter 6.

Based on these clinical observations, the pre-operative plan needs to be updated such that it better reflects the peri-operative migration of the LAD. To achieve this objective, here we propose a rigid-body feature-based registration that can be employed to predict the peri-operative location of the LAD vessel based on the pre-operative data. To validate our registration and overcome the clinical limitation arising due to the invisibility of the LAD in the US images, we simulated the heart migration *in vitro* and showed how accurately our technique predicts the LAD location.

While no known accuracy constraints have been reported for this specific applica-

tion, our collaborating cardiac surgeons have recommended that a maximum target prediction error on the order of one intercostal space ( $\sim 10$ - $15$  mm, depending on patient size) is desired. From a clinical feasibility perspective, this constraint is valid: as long as the intra-operative LAD location is correctly predicted to within one intercostal space from its actual location, it can be reached by positioning the trocar on either side of the adjacent rib.

## A.2 *In vitro* Experimental Validation

### A.2.1 Experimental Apparatus

Since the LAD cannot be identified peri-operatively using US imaging, we conducted an *in vitro* validation study to assess the accuracy with which our technique can predict the LAD location. The experimental apparatus was set up in a configuration similar to that typically found in the OR. The migration patterns of the heart observed during RA-CABG procedures were simulated *in vitro* by altering the position and orientation of a heart phantom (The Chamberlain Group, Great Barrington, USA).

Sixteen CT-visible fiducials were attached to the surface of the phantom: ten were used to assist with the CT-to-phantom registration and the remaining six were used to “define” the path of the LAD vessel. The position of the heart phantom was tracked throughout the study using a 6 DOF NDI Aurora<sup>TM</sup> magnetic sensor rigidly attached onto the phantom. Two different modalities (CT and US) were employed for image acquisition: a pre-operative CT scan was acquired and a virtual surface model was constructed using automatic segmentation tools; peri-operative images at each workflow stage were acquired using a magnetically-tracked TEE probe similar to the one used in the OR (**Fig. A.4**). The LAD vessel was initially identified from the CT image and its peri-operative location was predicted based on its pre-operative

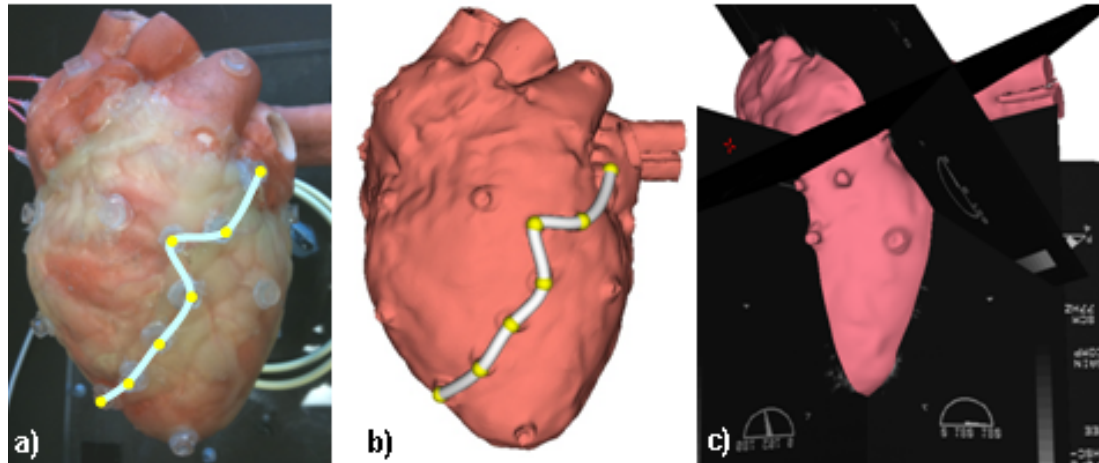


Fig. A.4: a) Image and (b) virtual surface model of the heart phantom showing the LAD path; c) Peri-operative US image acquisition protocol showing imaging of the apex and coronary ostia using incrementally tracked 2D US images.

location using the proposed registration.

## A.2.2 Intra-operative Image Acquisition

Since TEE is the standard of care for monitoring during cardiac procedures, in this study we collected the required tracked US images following the clinical workflow. The position of the heart was changed twice in order to mimic the actual intervention, the former location representing the displacement subsequent to collapsing the left lung, while the latter was the position subsequent to insufflating the thoracic cavity (**Fig. A.5**). In each position, the image acquisitions were repeated three times and the entire protocol was also conducted three times to minimize human errors. Four features were then extracted from the images using a custom-developed segmentation tool: MVA, AVA, left main coronary ostium (LMCO), and left ventricular apex (LVAp). All features were defined in the same 3D coordinate space; the mitral and aortic valves were represented as “rings”, while the ostium and apex were represented as points.

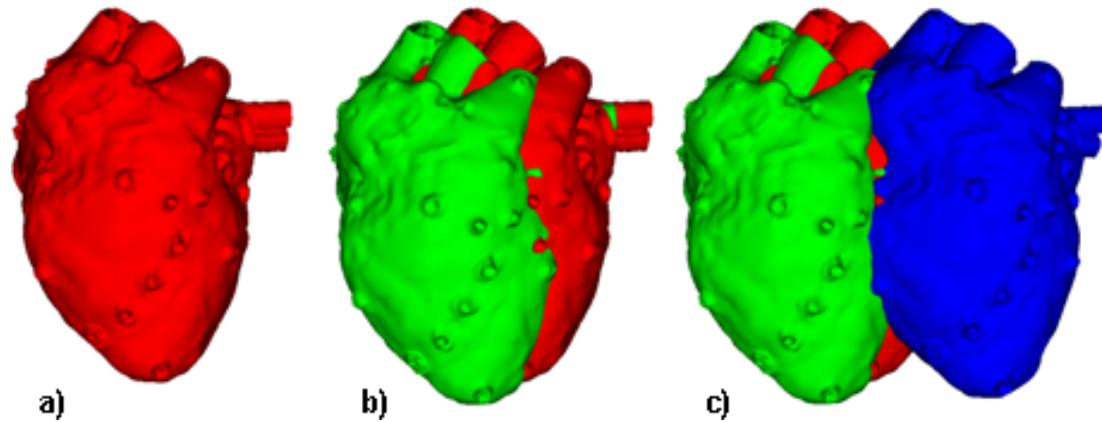


Fig. A.5: a) Virtual surface model of the heart phantom showing the subsequent stages in the peri-operative workflow simulating those observed in the clinical workflow. Note: Stage<sub>1</sub> is shown in red, Stage<sub>2</sub> in green and Stage<sub>3</sub> in blue.

### A.2.3 Feature-based Registration Technique

Since the LAD can only be clearly seen in the pre-operative CT image and not in the peri-operative US images, its peri-/intra-operative location has to be deduced based on the rest of the data available peri-operatively. Therefore, we chose to predict its location via a registration algorithm that involves the four features mentioned above. All of these features are easily identifiable in both modalities and sufficiently close to the target vessel to provide adequate alignment accuracy in the region of interest.

The registration algorithm employed here has been adapted from the feature-based technique presented in Chapter 4. According to cardiac anatomy, the LAD begins at the coronary ostia and runs toward the apex, close enough to the apical region of the left ventricle; moreover, the mitral and aortic valves are located on either side of the starting point of the LAD. A rigid-body registration driven by these four features was applied to map the pre-operative dataset to the peri-operative datasets, to predict the LAD location at each subsequent stage.

A rigid-body registration was first performed using the centroids of the four extracted features. Considering the proximity of the left main coronary ostium and left

Table A.1: Target registration error (TRE) measured along the left anterior descending coronary (LAD) vessel. (Mean  $\pm$  Sdt. Dev. and RMS (mm))

LAD Point	Stage <sub>0</sub> to Stage <sub>1</sub>		Stage <sub>0</sub> to Stage <sub>2</sub>	
	Mean $\pm$ SD (mm)	RMS (mm)	Mean $\pm$ SD (mm)	RMS (mm)
1	3.1 $\pm$ 0.9	3.2	2.9 $\pm$ 1.7	3.4
2	2.9 $\pm$ 1.3	3.2	3.4 $\pm$ 1.6	3.8
3	3.4 $\pm$ 1.4	3.7	3.3 $\pm$ 1.6	3.7
4	3.9 $\pm$ 1.9	4.3	3.8 $\pm$ 1.3	4.0
5	4.4 $\pm$ 2.3	5.0	3.9 $\pm$ 1.7	4.3
6	4.9 $\pm$ 2.6	5.5	4.5 $\pm$ 2.1	5.0
Overall	3.7 $\pm$ 1.9	4.2	3.6 $\pm$ 1.7	4.0

ventricular apex to the superior and inferior ends of the LAD, respectively, the initial alignment was then refined by minimizing the distance between the homologous features, while enforcing more stringent constraints on the distance between the two sets of features at each end of the LAD: the LMCO and LVAp.

### A.3 Assessing Intra-operative LAD Localization

The six fiducials positioned along the LAD path were used to assess the target registration error (TRE) computer between the predicted LAD fiducial locations and their gold-standard locations, at each stage in the workflow. The gold-standard LAD fiducial locations were determined by recording the LAD fiducial locations at each stage using a magnetically tracked pointer and confirmed using the point-based registration transform corresponding to each peri-operative stage. The predicted LAD location was identified by mapping the pre-operative LAD fiducials using the feature-based registration transform described in section **A.2.3**.

Three different RA-CABG-related workflows were simulated by altering the position and orientation of the heart phantom at three different stages. For each of the nine poses, we acquired three sets of tracked US images, defined the features of



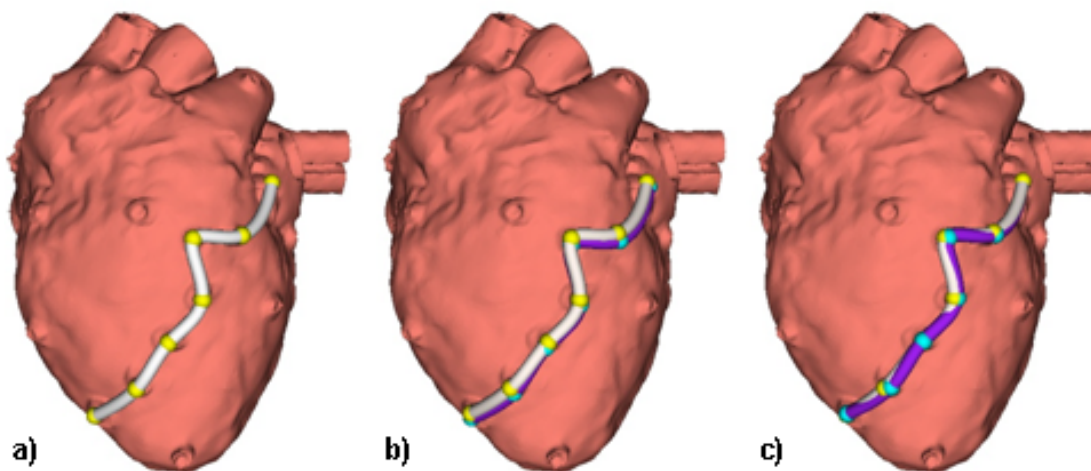


Fig. A.6: a) Pre-operative heart phantom model at Stage<sub>0</sub> showing the LAD vessel; Visual display of the LAD TRE at Stage<sub>1</sub> (b) and Stage<sub>2</sub> (c), showing the gold-standard LAD (seashell white) obtained using the point-based registration transform and the predicted LAD (purple) determined using the proposed feature-based registration transform.

interest, and used the proposed registration algorithm to predict the location of the LAD vessel. **Table A.1** summarizes the TRE between the actual locations of the LAD target fiducials (the gold-standard location) and their predicted locations from the registration.

For a visual interpretation of the LAD TRE, **Fig. A.6** shows the virtual model of the heart phantom along with the gold-standard and predicted LAD paths at both Stage<sub>1</sub> and Stage<sub>2</sub> in the peri-operative workflow, showing clinically-adequate alignment, well under the 10-15 mm intercostal space constraint.

Table A.2: Localization error of the features used in the registration. (RMS (mm))

Feature	Stage <sub>0</sub> (mm)	Stage <sub>1</sub> (mm)	Stage <sub>2</sub> (mm)
LVAp	2.3	4.7	4.0
AVA	1.4	1.3	1.2
MVA	0.6	1.9	1.5
LMCO	1.1	4.0	2.1

Moreover, considering that the target vessel location is predicted using a feature-based registration algorithm, we next assessed the error associated with the feature

localization. **Table A.2** includes a summary of the RMS localization error associated with the identification of each of the four features used to drive the registration: left main coronary ostium, left ventricular apex, and mitral and aortic valves. As expected, the localization of the left ventricular apex and coronary ostium was challenging, mainly due to the 2D nature of the US images used to identify a 3D structure.

## A.4 Discussion

This work constitutes the first steps towards optimizing pre-operative planning for RA-CABG procedures. Motivated by a recent clinical study that revealed substantial migration of the heart during the peri-operative procedure workflow, our ultimate goal was to predict the intra-operative location of the target vessel, to therefore provide the surgeon with an optimized surgical plan that better reflects the intra-operative stage.

As a bridge to the *in vivo* validation, considering the limitations arising due to poor visualization and identification of the LAD coronary vessel in clinical US images, the phantom study was performed to assess the accuracy with which a proposed feature-based registration technique can predict the location of a target vessel in a simulated workflow. Our results have shown an RMS TRE of  $\sim 3.5$  mm across the twenty-seven peri-operative poses simulated in our study. The feature localization errors explain the increased target registration error at the LAD fiducials closer to the apical region at both peri-operative stages. Moreover, considering that the actual anastomosis target site is located along the LAD path approximately two thirds of the way from the coronary ostia toward the apex, target registration error can be further improved near the inferior end of the LAD using a more robust apex localization approach from the US data. A possible solution would be to use the apical region as a registration constraint as opposed to a single point, and include a robust estimator to reduce the TRE, as suggested by Ma *et al.* [6]. Nevertheless, in spite of these slight inaccuracies,

our results are well within the 10-15 mm clinically-imposed constraint dictated by a typical intercostal space, allowing sufficient tolerance (over 10 mm) in the event that these errors amplify when using clinical data.

## A.5 Conclusions

Driven by the clinical motivation to improve the pre-operative planning of RA-CABG procedures, here we have proposed and evaluated a technique used to predict the intra-operative target vessel location. Our technique was validated in an *in vitro* study simulating the clinically-observed RA-CABG procedure workflow and yielded an overall RMS accuracy on the order to 3.5 mm in predicting the peri-operative LAD location. Provided an equally successful *in vivo* evaluation in our upcoming clinical studies employing dyna CT for intra-operative validation, we believe this technique has the potential to significantly improve the current pre-operative planning of RA-CABG procedures, and consequently lead to reduced rates of conversion to traditional open-chest surgery.

# References

- [1] P. Modi, E. Rodriguez, and W. R. Jr. Chitwood. Robot-assisted cardiac surgery. *Interact Cardiovasc Thorac Surg.*, 9:500–5, 2009.
- [2] A. L. Trejos, R. V. Patel, I. Ross, and B. Kiaii. Optimizing port placement for robot-assisted minimally invasive cardiac surgery. *Int J Med Robot.*, 3:355–64, 2007.
- [3] R. J. Damiano Jr. Robotics in cardiac surgery: The emperor’s new clothes. *J Thorac Cardiovasc Surg.*, 134:559–61, 2007.
- [4] J. T. Moore, A. D. Wiles, and C. *et al.* Wedlake. Integration of trans-esophageal echocardiography with magnetic tracking technology for cardiac interventions. In *Proc. of SPIE. - Medical Imaging 2010*, volume 7625, pages 76252Y–1–10, 2010.
- [5] C. A. Linte, M. Carias, and D. S. *et al.* Cho. Estimating heart shift and morphological changes during minimally invasive cardiac interventions. In *Proc. of SPIE. - Medical Imaging 2010*, volume 7625, pages 762509–1–11, 2010.
- [6] B. Ma, R. E. Ellis, and D. J. Fleet. Spotlights: A robust method for surface-based registration in orthopedic surgery. In *LNCS*, volume 1679 of *Proc. of MICCAI.*, pages 936–945, 1999.

## Appendix B

# Copyright Releases and Permissions



From: Christian A. Linte  
 Sent: July 16, 2010 2:58 AM  
 To: copyrights@ieee.org  
 Cc: Christian A. Linte  
 Subject: Copyright Permission for Use in Thesis/Dissertation  
 Importance: High

Dear Madam/Sir,

I am contacting you with regards to receiving permission to use the following published works in my doctoral dissertation in the Biomedical Engineering Graduate Program at the University of Western Ontario in London, Ontario, Canada.

The thesis is entitled Virtual and Augmented Reality Techniques for Minimally Invasive Cardiac Interventions: Concept, Design, Evaluation and Pre-clinical Implementation with the expected date of completion in August 2010.

Please find below the title and information related to the works that I am requesting permission to include in the thesis:

1. Linte CA, White J, Eagleson R, Guiraudon GM and Peters TM. Virtual and Augmented Medical Imaging Environments: Enabling Technology for Minimally Invasive Cardiac Interventional Guidance. IEEE Reviews in Biomedical Engineering. Submitted: July 2010. Submission No.: RBME-00013-2010.

2. Linte CA, Moore J, Wedlake C and Peters TM. Evaluation of Model-Enhanced Ultrasound-Assisted Interventional Guidance in a Cardiac Phantom. IEEE Transactions on Biomedical Engineering. In Press: 2010. DOI: 10.1109/TBME.2010.2050886.

3. Linte CA, Moore J and Peters TM. How Accurate is Accurate Enough? A Brief Overview on Accuracy Considerations in Image-Guided Cardiac Interventions. Proc. IEEE Engineering in Medicine and Biology Conference (EMBC 2010). In Press: 2010. Submission No.: 2151.

4. Linte CA, Wierzbicki M, Moore J, Guiraudon GM, Jones DL and Peters TM. On Enhancing Planning and Navigation of Beating-Heart Mitral Valve Surgery using Pre-operative Cardiac Models. Proc. IEEE Engineering in Medicine and Biology Conference (EMBC 2007). Pages: 475-478. DOI: 10.1109/IEMBS.2007.4352326.

Please note that I am planning to submit my thesis in the next week and it is the University of Western Ontario policy to have the permissions bounded in the thesis. If you can please assist me with getting the permissions within the next couple of day, I would really appreciate it! Also, if you require additional information, please do not hesitate to contact me anytime!

Thanks very much!

Regards,

CL  
 --  
 Cristian A. Linte, MEng  
 University of Western Ontario  
 Biomedical Engineering Grad. Program  
 Robarts Research Institute  
 Imaging Research Laboratories  
 100 Perth Dr. P.O.Box: 5015  
 London ON N6A 5K8 Canada



**informa**  
healthcare

**Title:** Virtual reality-enhanced ultrasound guidance: A novel technique for intracardiac interventions

**Author:** Cristian A. Linte, John Moore, Andrew D. Wiles et al.

**Publication:** Computer Aided Surgery

**Publisher:** Informa Healthcare

**Date:** Jan 3, 2008

Copyright © 2008 Informa Healthcare

Logged in as:

Cristian Linte

LOGOUT

#### Thesis/Dissertation Reuse Request

Taylor & Francis is pleased to offer reuses of its content for a thesis or dissertation free of charge contingent on resubmission of permission request if work is published.

BACK

CLOSE WINDOW

Copyright © 2010 [Copyright Clearance Center, Inc.](#) All Rights Reserved. [Privacy statement.](#)  
Comments? We would like to hear from you. E-mail us at [customercare@copyright.com](mailto:customercare@copyright.com)





**Title:** Towards Subject-Specific Models of the Dynamic Heart for Image-Guided Mitral Valve Surgery

Logged in as:  
Cristian Linte

**Author:** Cristian A. Linte

LOGOUT

**Publication:** Springer eBook

**Publisher:** Springer

**Date:** Oct 12, 2007

Copyright © 2007, Springer Berlin / Heidelberg

### Permission Request Submitted

**Your request is now under review.  
You will be notified of the decision via email.  
Please print this request for your records.**

[Get the printable order details.](#)

Order Number	500572025
License date	Jul 13, 2010
Licensed content publisher	Springer
Licensed content publication	Springer eBook
Licensed content title	Towards Subject-Specific Models of the Dynamic Heart for Image-Guided Mitral Valve Surgery
Licensed content author	Cristian A. Linte
Licensed content date	Oct 12, 2007
Type of Use	Thesis/Dissertation
Portion	Full text
Number of copies	1
Author of this Springer article	Yes and you are the sole author of the new work
Title of your thesis / dissertation	Virtual and Augmented Reality Techniques for Minimally Invasive Cardiac Interventions: Concept, Design, Evaluation and Pre-clinical Implementation
Expected completion date	Aug 2010
Estimated size(pages)	200
Total	Not Available

CLOSE WINDOW

Copyright © 2010 [Copyright Clearance Center, Inc.](#) All Rights Reserved. [Privacy statement.](#)  
Comments? We would like to hear from you. E-mail us at [customercare@copyright.com](mailto:customercare@copyright.com)



**Title:** Virtual Reality-Enhanced  
Ultrasound Guidance for Atrial  
Ablation: *In vitro* Epicardial  
Study

**Author:** Cristian A. Linte

**Publication:** Springer eBook

**Publisher:** Springer

**Date:** Oct 30, 2008

Copyright © 2008, Springer

Logged in as:  
Cristian Linte  
Account #:  
3000324124

LOGOUT

### Order Completed

Thank you very much for your order.

This is a License Agreement between Cristian A Linte ("You") and Springer ("Springer"). The license consists of your order details, the terms and conditions provided by Springer, and the [payment terms and conditions](#).

License number	Reference confirmation email for license number
License date	Jul 16, 2010
Licensed content publisher	Springer
Licensed content publication	Springer eBook
Licensed content title	Virtual Reality-Enhanced Ultrasound Guidance for Atrial Ablation: <i>In vitro</i> Epicardial Study
Licensed content author	Cristian A. Linte
Licensed content date	Oct 30, 2008
Type of Use	Thesis/Dissertation
Portion	Excerpts
Author of this Springer article	Yes and you are the sole author of the new work
Title of your thesis / dissertation	Virtual and Augmented Reality Techniques for Minimally Invasive Cardiac Interventions: Concept, Design, Evaluation and Pre-clinical Implementation
Expected completion date	Aug 2010
Estimated size(pages)	200
Total	0.00 USD

CLOSE WINDOW

Copyright © 2010 [Copyright Clearance Center, Inc.](#) All Rights Reserved. [Privacy statement](#).  
Comments? We would like to hear from you. E-mail us at [customercare@copyright.com](mailto:customercare@copyright.com)



**Title:** Targeting Accuracy under Model-to-Subject Misalignments in Model-Guided Cardiac Surgery  
**Author:** Cristian A. Linte  
**Publication:** Springer eBook  
**Publisher:** Springer  
**Date:** Oct 1, 2009  
 Copyright © 2009, Springer

Logged in as:  
 Cristian Linte  
 Account #:  
 3000324124

LOGOUT

### Order Completed

Thank you very much for your order.

This is a License Agreement between Cristian A Linte ("You") and Springer ("Springer"). The license consists of your order details, the terms and conditions provided by Springer, and the [payment terms and conditions](#).

License number	Reference confirmation email for license number
License date	Jul 16, 2010
Licensed content publisher	Springer
Licensed content publication	Springer eBook
Licensed content title	Targeting Accuracy under Model-to-Subject Misalignments in Model-Guided Cardiac Surgery
Licensed content author	Cristian A. Linte
Licensed content date	Oct 1, 2009
Type of Use	Thesis/Dissertation
Portion	Excerpts
Author of this Springer article	Yes and you are the sole author of the new work
Title of your thesis / dissertation	Virtual and Augmented Reality Techniques for Minimally Invasive Cardiac Interventions: Concept, Design, Evaluation and Pre-clinical Implementation
Expected completion date	Aug 2010
Estimated size(pages)	200
Total	0.00 USD

CLOSE WINDOW

Copyright © 2010 [Copyright Clearance Center, Inc.](#) All Rights Reserved. [Privacy statement](#).  
 Comments? We would like to hear from you. E-mail us at [customercare@copyright.com](mailto:customercare@copyright.com)



**Title:** Inside the beating heart: an in vivo feasibility study on fusing pre- and intra-operative imaging for minimally invasive therapy

**Author:** Cristian A. Linte

**Publication:** International Journal of Computer Assisted Radiology and Surgery

**Publisher:** Springer

**Date:** Jan 1, 2008

Copyright © 2008, CARS

Logged in as:

Cristian Linte

LOGOUT

### Order Completed

Thank you very much for your order.

This is a License Agreement between Cristian A Linte ("You") and Springer ("Springer"). The license consists of your order details, the terms and conditions provided by Springer, and the [payment terms and conditions](#).

[Get the printable license.](#)

License Number	2467300433701
License date	Jul 13, 2010
Licensed content publisher	Springer
Licensed content publication	International Journal of Computer Assisted Radiology and Surgery
Licensed content title	Inside the beating heart: an in vivo feasibility study on fusing pre- and intra-operative imaging for minimally invasive therapy
Licensed content author	Cristian A. Linte
Licensed content date	Jan 1, 2008
Volume number	4
Issue number	2
Type of Use	Thesis/Dissertation
Portion	Full text
Number of copies	1
Author of this Springer article	Yes and you are the sole author of the new work
Title of your thesis / dissertation	Virtual and Augmented Reality Techniques for Minimally Invasive Cardiac Interventions: Concept, Design, Evaluation and Pre-clinical Implementation
Expected completion date	Aug 2010
Estimated size(pages)	200
Total	0.00 CAD

CLOSE WINDOW

Copyright © 2010 [Copyright Clearance Center, Inc.](#) All Rights Reserved. [Privacy statement](#).  
Comments? We would like to hear from you. E-mail us at [customercare@copyright.com](mailto:customercare@copyright.com)

**SPIE** TRANSFER OF COPYRIGHT TO SOCIETY OF PHOTO-OPTICAL INSTRUMENTATION ENGINEERS (SPIE)

Title of Paper: Attuning heart shift and morphological changes during minimally invasive cardiac interventions

SPIE Paper Number: (xxxx-xx) 1625-8

Author(s): Linte; Carrau; Cho; Pace; Moore; Wedlake; Bainbridge; Ermi; Peters

*This signed statement must be returned to SPIE prior to the scheduled publication of the Proceedings or Journal in which the Paper will be published. The intent of this Agreement is to protect the interests of both SPIE and authors/employers and to specify reasonable rights for both parties related to publication and reuse of the material.*

The undersigned hereby assign(s) to Society of Photo-Optical Instrumentation Engineers (SPIE) copyright ownership in the above Paper, effective if and when the Paper is accepted for publication by SPIE and to the extent transferable under applicable national law. This assignment gives SPIE the right to register copyright to the Paper in its name as claimant and to publish the Paper in any print or electronic medium.

Authors, or their employers in the case of works made for hire, retain the following rights:

1. All proprietary rights other than copyright, including patent rights.
2. The right to make and distribute copies of the Paper for internal purposes.
3. The right to use the material for lecture or classroom purposes.
4. The right to prepare derivative publications based on the Paper, including books or book chapters, journal papers, and magazine articles, provided that publication of a derivative work occurs subsequent to the official date of publication by SPIE.
5. The right to post an author-prepared version or an official version (preferred version) of the published paper on an internal or external server controlled exclusively by the author/employer, provided that (a) such posting is noncommercial in nature and the paper is made available to users without charge; (b) a copyright notice and full citation appear with the paper, and (c) a link to SPIE's official online version of the abstract is provided using the DOI (Document Object Identifier) link.

**Citation format:**

Author(s), "Paper Title," Publication Title, Editors, Volume (Issue) Number, Article (or Page) Number, (Year).

**Copyright notice format:**

Copyright XXXX (year) Society of Photo-Optical Instrumentation Engineers. One print or electronic copy may be made for personal use only. Systematic reproduction and distribution, duplication of any material in this paper for a fee or for commercial purposes, or modification of the content of the paper are prohibited.

**DOI abstract link format:**

<http://dx.doi.org/DOI#> (Note: The DOI can be found on the title page or online abstract page of any SPIE article.)

If the work that forms the basis of this Paper was done under a contract with a governmental agency or other entity that retains certain rights, this Transfer of Copyright is subject to any rights that such governmental agency or other entity may have acquired.

By signing this Agreement, the authors warrant that (1) the Paper is original and has not previously been published elsewhere; (2) this work does not infringe on any copyright or other rights in any other work; (3) all necessary reproduction permissions, licenses, and clearances have been obtained; and (4) the authors own the copyright in the Paper, are authorized to transfer it, and have full power to enter into this Agreement with SPIE.

**WHO SHOULD SIGN.** This form must be signed by (1) at least one author who is not a U.S. Government employee and (2) the author's employer if the Paper was prepared within the scope of the author's employment or was commissioned by the employer. If not signed by all authors, the author(s) signing this Agreement represents that he/she is signing this Agreement as authorized agent for and on behalf of all authors.

	<u>CRISTIAN A. LINTÉ</u>	<u>02/11/2010</u>
Author's signature	Print name	Date (mm/dd/yyyy)

Author's signature	Print name	Date (mm/dd/yyyy)

Authorized Employer signature	Print name	Title	Date (mm/dd/yyyy)

**U.S. GOVERNMENT EMPLOYMENT CERTIFICATION**

A work prepared by a U.S. Government employee as part of his or her official duties is not eligible for U.S. Copyright. If all authors were U.S. Government employees when this Paper was prepared, and the authors prepared this Paper as part of their official duties, at least one author should sign below. If at least one author was not a U.S. Government employee, the work is eligible for copyright and that author should sign the Transfer of Copyright form above.

Author's signature	Print name	Date

# Appendix C

## Research Ethics Approvals



## Office of Research Ethics

The University of Western Ontario  
 Room 4180 Support Services Building, London, ON, Canada N6A 5C1  
 Telephone: (519) 661-3036 Fax: (519) 850-2466 Email: ethics@uwo.ca  
 Website: www.uwo.ca/research/ethics

### Use of Human Subjects - Ethics Approval Notice

**Principal Investigator:** Dr. T.M. Peters

**Review Number:** 13753E

**Revision Number:** 1

**Review Date:** December 01, 2008

**Review Level:** Expedited

**Protocol Title:** Towards Minimally-Invasive, Dynamic Characterization of the Mitral Valve Annulus using Subject-Specific Cardiac Models

**Department and Institution:** Medical Biophysics, Robarts Research Institute

**Sponsor:** CIHR-CANADIAN INSTITUTE OF HEALTH RESEARCH

**Ethics Approval Date:** December 01, 2008

**Expiry Date:** June 30, 2010

**Documents Reviewed and Approved:** Revised study end date.

#### Documents Received for Information:

This is to notify you that The University of Western Ontario Research Ethics Board for Health Sciences Research Involving Human Subjects (HSREB) which is organized and operates according to the Tri-Council Policy Statement: Ethical Conduct of Research Involving Humans and the Health Canada/ICH Good Clinical Practice Practices: Consolidated Guidelines; and the applicable laws and regulations of Ontario has reviewed and granted approval to the above referenced revision(s) or amendment(s) on the approval date noted above. The membership of this REB also complies with the membership requirements for REB's as defined in Division 5 of the Food and Drug Regulations.

The ethics approval for this study shall remain valid until the expiry date noted above assuming timely and acceptable responses to the HSREB's periodic requests for surveillance and monitoring information. If you require an updated approval notice prior to that time you must request it using the UWO Updated Approval Request Form.

During the course of the research, no deviations from, or changes to, the protocol or consent form may be initiated without prior written approval from the HSREB except when necessary to eliminate immediate hazards to the subject or when the change(s) involve only logistical or administrative aspects of the study (e.g. change of monitor, telephone number). Expedited review of minor change(s) in ongoing studies will be considered. Subjects must receive a copy of the signed information/consent documentation.

Investigators must promptly also report to the HSREB:

- changes increasing the risk to the participant(s) and/or affecting significantly the conduct of the study;
- all adverse and unexpected experiences or events that are both serious and unexpected;
- new information that may adversely affect the safety of the subjects or the conduct of the study.

If these changes/adverse events require a change to the information/consent documentation, and/or recruitment advertisement, the newly revised information/consent documentation, and/or advertisement, must be submitted to this office for approval.

Members of the HSREB who are named as investigators in research studies, or declare a conflict of interest, do not participate in discussion related to, nor vote on, such studies when they are presented to the HSREB.

Chair of HSREB: Dr. Joseph Gilbert

Ethics Officer to Contact for Further Information			
<input type="checkbox"/> Janice Sutherland	<input type="checkbox"/> Elizabeth Wambolt	<input checked="" type="checkbox"/> Grace Kelly	<input type="checkbox"/> Denise Grafton

*This is an official document. Please retain the original in your files.*

cc: ORE File  
LHR!



## Office of Research Ethics

The University of Western Ontario  
 Room 4180 Support Services Building, London, ON, Canada N6A 5C1  
 Telephone: (519) 661-3036 Fax: (519) 850-2466 Email: ethics@uwo.ca  
 Website: www.uwo.ca/research/ethics

### Use of Human Subjects - Ethics Approval Notice

**Principal Investigator:** Dr. B. Kiaii

**Review Number:** 15098

**Review Date:** July 14, 2009

**Revision Number:** 1

**Review Level:** Expedited

**Protocol Title:** Imaging Investigation to confirm ligation of the Left Atrial Appendage

**Department and Institution:** Surgery, London Health Sciences Centre

**Sponsor:**

**Ethics Approval Date:** July 14, 2009

**Expiry Date:** July 31, 2010

**Documents Reviewed and Approved:** Revised Study End Date

**Documents Received for Information:**

This is to notify you that The University of Western Ontario Research Ethics Board for Health Sciences Research Involving Human Subjects (HSREB) which is organized and operates according to the Tri-Council Policy Statement: Ethical Conduct of Research Involving Humans and the Health Canada/ICH Good Clinical Practice Practices: Consolidated Guidelines; and the applicable laws and regulations of Ontario has reviewed and granted approval to the above referenced revision(s) or amendment(s) on the approval date noted above. The membership of this REB also complies with the membership requirements for REB's as defined in Division 5 of the Food and Drug Regulations.

The ethics approval for this study shall remain valid until the expiry date noted above assuming timely and acceptable responses to the HSREB's periodic requests for surveillance and monitoring information. If you require an updated approval notice prior to that time you must request it using the UWO Updated Approval Request Form.

During the course of the research, no deviations from, or changes to, the protocol or consent form may be initiated without prior written approval from the HSREB except when necessary to eliminate immediate hazards to the subject or when the change(s) involve only logistical or administrative aspects of the study (e.g. change of monitor, telephone number). Expedited review of minor change(s) in ongoing studies will be considered. Subjects must receive a copy of the signed information/consent documentation.

Investigators must promptly also report to the HSREB:

- a) changes increasing the risk to the participant(s) and/or affecting significantly the conduct of the study;
- b) all adverse and unexpected experiences or events that are both serious and unexpected;
- c) new information that may adversely affect the safety of the subjects or the conduct of the study.

If these changes/adverse events require a change to the information/consent documentation, and/or recruitment advertisement, the newly revised information/consent documentation, and/or advertisement, must be submitted to this office for approval.

Members of the HSREB who are named as investigators in research studies, or declare a conflict of interest, do not participate in discussion related to, nor vote on, such studies when they are presented to the HSREB.

Chair of HSREB: Dr. Joseph Gilbert

Ethics Officer to Contact for Further Information			
<input checked="" type="checkbox"/> Janice Sutherland	<input type="checkbox"/> Elizabeth Wambolt	<input type="checkbox"/> Grace Kelly	<input type="checkbox"/> Denise Grafton

*This is an official document. Please retain the original in your files.*

cc: ORE File  
LHRI



<b>A. PROJECT/INVESTIGATOR INFORMATION</b>	
Investigator Name: Dr. Gerrard Guiraudon	Current Protocol #: 2007-021-10
Project Title: <i>This is a NEW title.</i> Yes <input type="checkbox"/> No <input type="checkbox"/> Closed Heart Surgical Techniques for Atrial Fibrillation	
<b>B. INVESTIGATOR DECLARATION</b>	
I. All animals used in this research project will be cared for in accordance with the recommendations of the Canadian Council on Animal Care and the requirements of the provincial legislation entitled, "The Animals for Research Act," of the Province of Ontario.	
II. I confirm that this <i>Animal Use Protocol</i> accurately represents the proposed animal use.	
III. I accept responsibility for procedures performed on animals in this project.	
IV. I will ensure that any individual who will perform any animal-related procedure(s) within this protocol will complete all related mandatory training AND will be made familiar with the contents of this document.	
1. I support the above declaration - YES <input checked="" type="checkbox"/> Today's Date mm/dd/yy: 11/05/09	
2. By checking 'YES' in this section, I authorize the submission of this form and its electronic delivery to auspc@uwo.ca YES <input checked="" type="checkbox"/> NO <input type="checkbox"/>	
3. I authorize Sheri Van Lingen (PI Designate) to submit this form and to receive a copy of authorization via email on my behalf. Today's Date (mm/dd/yy): 11/05/09	
AUS APPROVAL - AUS Office Use Only - Veterinary Authorization by Click Here Authorization Date (mm/dd/yy) / /	
Signature:	
<b>C. CHANGES AT RENEWAL CONFIRMATION – Pick One Only</b>	
<input checked="" type="checkbox"/> I confirm that NO CHANGES and/or NEW ELEMENTS to this AUP - other than staffing - have occurred since the last AUS Form submission.	

I confirm that all CHANGES and/or NEW ELEMENTS to this protocol not previously submitted WILL BE sent via a Protocol Modification form along with this Protocol Renewal Form.

**D. THREE R's PROGRESS REPORT**

Describe any progress made with respect to the Three R's of replacement, reduction and refinement of animal use during the PAST PROTOCOL YEAR. See the CCAC 3 R's Microsite: <http://www.ccac.ca/en/alternatives/>

- No additional animals were used during the past Protocol Year.  
 No additional animals were requested during the past Protocol Year.

**E. ANIMAL USE COMPLICATIONS PROGRESS REPORT**

Describe any complications beyond the expected experimental outcomes and end points encountered relative to animal use – e.g. unpredicted outcomes and any unexpected animal pain, distress, or mortality - AND indicate measures being undertaken to resolve these complications for the PAST PROTOCOL YEAR.

- No complications were encountered relative to animal use during the past Protocol Year.

**F. ANALGESIA ADMINISTRATION UPDATE**

Choose One of the Following Statements:

1. Analgesics were administered as outlined within the Animal Use Protocol  \*if checked, please list all analgesics currently used below:

Buprenorphine 0.01mg/kg

2. Analgesics are not indicated in this Animal Use Protocol

**G. PROTOCOL PERSONNEL UPDATE**

Complete for ALL Staff Working Under This Protocol for This Renewal Year

COMPLETE ALL COLUMNS BELOW PER PERSON				If 'YES' to HANDS-ON ANIMAL WORK, Complete This Section PER SPECIES	
FIRST	LAST	ROLE	EMAIL	HANDS	PROCEDURES PER SPECIES
				Expected	

NAME <i>Repeat For Each Species Used</i>	NAME <i>Repeat For Each Species Used</i>	(Role within this Protocol) <i>Researcher Staff Student</i>	Address <b>*Mandatory Field*</b> <i>UWO &amp; Affiliated Institution Emails Preferred</i>	ON Animal Work? YES or NO	One Species Per Row <i>Use an Additional Row for Each Species</i>	START DATE <i>mm/dd/yy</i>	1=Basic Handling 2=Health Monitoring 3=Blood Collection 4=Injections 5=Anaesthesia 6=Surgery-Recovery 7=Surgery-Non-Recovery 8=Euthanasia/Post Mortem 9=Other, <i>Provide Detail Below, e.g. suturing</i>													
							1	2	3	4	5	6	7	8	9					
Gerrard	Guiraudon	Researcher		Yes	Pig	10/10/07	<input type="checkbox"/>	<input type="checkbox"/>	<input type="checkbox"/>	<input type="checkbox"/>	<input checked="" type="checkbox"/>	<input type="checkbox"/>	<input type="checkbox"/>	<input type="checkbox"/>	<input type="checkbox"/>	<input type="checkbox"/>	<input type="checkbox"/>	<input type="checkbox"/>	<input type="checkbox"/>	
Doug	Jones	Researcher		Yes	Pig	10/10/07	<input type="checkbox"/>	<input type="checkbox"/>	<input type="checkbox"/>	<input type="checkbox"/>	<input type="checkbox"/>	<input checked="" type="checkbox"/>	<input type="checkbox"/>	<input type="checkbox"/>	<input type="checkbox"/>	<input type="checkbox"/>	<input type="checkbox"/>	<input type="checkbox"/>	<input type="checkbox"/>	
Dan	Bainbridge	Researcher		Yes	Pig	10/10/07	<input type="checkbox"/>	<input type="checkbox"/>	<input type="checkbox"/>	<input type="checkbox"/>	<input type="checkbox"/>	<input type="checkbox"/>	<input type="checkbox"/>	<input type="checkbox"/>	<input type="checkbox"/>	<input type="checkbox"/>	<input type="checkbox"/>	<input type="checkbox"/>	<input checked="" type="checkbox"/>	
Sheri	Van Lingen	Staff		Yes	Pig	10/10/07	<input checked="" type="checkbox"/>	<input checked="" type="checkbox"/>	<input checked="" type="checkbox"/>	<input checked="" type="checkbox"/>	<input checked="" type="checkbox"/>	<input checked="" type="checkbox"/>	<input checked="" type="checkbox"/>	<input checked="" type="checkbox"/>	<input checked="" type="checkbox"/>	<input checked="" type="checkbox"/>	<input checked="" type="checkbox"/>	<input checked="" type="checkbox"/>	<input type="checkbox"/>	
Amber	Parsons	Staff		Yes	Pig	08/10/09	<input checked="" type="checkbox"/>	<input checked="" type="checkbox"/>	<input checked="" type="checkbox"/>	<input checked="" type="checkbox"/>	<input checked="" type="checkbox"/>	<input checked="" type="checkbox"/>	<input checked="" type="checkbox"/>	<input checked="" type="checkbox"/>	<input checked="" type="checkbox"/>	<input checked="" type="checkbox"/>	<input checked="" type="checkbox"/>	<input checked="" type="checkbox"/>	<input type="checkbox"/>	
Karen	Siroen	Staff		Yes	Pig	10/10/07	<input checked="" type="checkbox"/>	<input checked="" type="checkbox"/>	<input checked="" type="checkbox"/>	<input checked="" type="checkbox"/>	<input checked="" type="checkbox"/>	<input checked="" type="checkbox"/>	<input checked="" type="checkbox"/>	<input checked="" type="checkbox"/>	<input checked="" type="checkbox"/>	<input checked="" type="checkbox"/>	<input checked="" type="checkbox"/>	<input checked="" type="checkbox"/>	<input type="checkbox"/>	
Terry	Peters	Researcher		No	Pig	11/03/08	<input type="checkbox"/>	<input type="checkbox"/>	<input type="checkbox"/>	<input type="checkbox"/>	<input type="checkbox"/>	<input type="checkbox"/>	<input type="checkbox"/>	<input type="checkbox"/>	<input type="checkbox"/>	<input type="checkbox"/>	<input type="checkbox"/>	<input type="checkbox"/>	<input checked="" type="checkbox"/>	
Chris	Wedlake	Staff		No	Pig	11/03/08	<input type="checkbox"/>	<input type="checkbox"/>	<input type="checkbox"/>	<input type="checkbox"/>	<input type="checkbox"/>	<input type="checkbox"/>	<input type="checkbox"/>	<input type="checkbox"/>	<input type="checkbox"/>	<input type="checkbox"/>	<input type="checkbox"/>	<input type="checkbox"/>	<input checked="" type="checkbox"/>	
John	Moore	Staff		No	Pig	11/03/08	<input type="checkbox"/>	<input type="checkbox"/>	<input type="checkbox"/>	<input type="checkbox"/>	<input type="checkbox"/>	<input type="checkbox"/>	<input type="checkbox"/>	<input type="checkbox"/>	<input type="checkbox"/>	<input type="checkbox"/>	<input type="checkbox"/>	<input type="checkbox"/>	<input checked="" type="checkbox"/>	
<b>PROCEDURE #9 DETAIL</b>																				
<b>EMERGENCY AFTER HOURS CONTACT NAMES &amp; NUMBERS - NO LAB PHONE NUMBERS -</b>																				
If applicable, provide POST-OP CARE personnel detail												PRIMARY EMERGENCY CONTACT NUMBER (HOME OR CELL):								
If applicable, provide MONITORING personnel detail												SECONDARY EMERGENCY CONTACT NUMBER (HOME OR CELL):								
												Emergency #:      Lab #:			mail:					
												Emergency #:      Lab #:			mail:					

## CURRICULUM VITAE

**Name:** Cristian A. Linte

### Education

- 2006 - Ph.D. - Biomedical Engineering,  
University of Western Ontario, London, ON, Canada
- 2004 - 2006 M.E.Sc. - Biomedical Engineering,  
University of Western Ontario, London, ON, Canada
- 2000 - 2004 B.A.Sc. - Mechanical & Materials Engineering,  
University of Windsor, Windsor, ON, Canada

### Scholarships, Fellowships and Other Funding Opportunities

- 2010 - 2012 Natural Sciences and Engineering Research Council (NSERC),  
Postdoctoral Research Fellowship (PDF) (\$40,000/yr)
- 2008 - 2011 Heart & Stroke Foundation of Canada (HSFC),  
Doctoral Research Award (\$21,000/yr)
- 2008 - 2010 International Society of Optical Engineers (SPIE),  
Scholarship in Optical Science and Engineering (\$2,500/yr)
- 2006 - 2008 Natural Sciences and Engineering Research Council (NSERC),  
Canada Graduate Scholarship - Doctorate (\$35,000/yr)
- 2004 - 2006 Natural Sciences and Engineering Research Council (NSERC),  
Postgraduate Masters Research Scholarship (\$17,300/yr)
- 2004 - 2006 Canadian Institute of Health Research,  
Strategic Training Program in Vascular Research (\$5,000/yr)
- 2004 - 2010 Western Graduate Research Scholarship,  
Biomedical Engineering, University of Western Ontario (\$7,000/yr)
- 2000 - 2004 Norah Cleary Scholarship - Dept. Mechanical & Materials Eng.  
University of Windsor (\$5,000/yr)
- 2003 NSERC Undergraduate Research Scholarship (\$4,500),  
Dept. Mechanical & Materials Eng. University of Windsor
- 2002 NSERC Undergraduate Research Scholarship (\$4,500),  
Dept. Biochemistry & Environmental Eng. University of Windsor

### Honours, Awards and Academic Accomplishments

- 2010 CARS 2010 Travel Grant (2,000 EURO),  
International Society for Computer Assisted Surgery
- 2010 Poster Award - Margaret Moffat Research Day,  
Schulich School of Medicine and Dentistry
- 2010 Young Investigator Forum Travel Grant (\$1,000),  
CIHR - Institute of Circulatory and Respiratory Health
- 2009 MICCAI 2009 Travel Grant (450 GBP),  
Imperial College London, London, United Kingdom
- 2009 Teaching Assistant Award, Dept. Mechanical & Materials Eng.,  
University of Western Ontario
- 2009 Young Investigators Forum Travel Grant (\$1,500),  
CIHR - Institute of Circulatory and Respiratory Health
- 2008 Canadian Cardiovascular Society (CCS) Have a Heart Bursary,  
Canadian Cardiovascular Congress, Toronto, Canada
- 2008 Margaret Moffat Research Day Poster Award - Biomedical Eng.,  
Schulich School of Medicine and Dentistry
- 2007 Michael B. Merickel Student Paper Award - Second Place,  
SPIE Medical Imaging Symposium, San Diego, CA, USA (\$500)
- 2007 Poster Award, Ontario Consortium for Image-Guided Therapy,  
Imaging Network Ontario Symposium, Toronto, Canada (\$100)

### Teaching Portfolio

- 2004 - 2010 Graduate Teaching Assistant, University of Western Ontario  
Faculty of Engineering - Dept. Mechanical & Materials Eng.  
*Courses: Rigid Body Dynamics; Mechanics of Materials*  
Schulich School of Medicine - Dept. Medical Biophysics  
*Courses: Medical Imaging; Biophysics for Engineers*
- 2001 - 2004 Undergraduate Teaching Assistant, University of Windsor  
Faculty of Science - Dept. Mathematics & Statistics  
*Courses: Vector Calculus; Differential Equations; Linear Algebra*  
Faculty of Science - Dept. Chemistry & Biochemistry  
*Courses: Chemistry for Engineers; Inorganic Chemistry I and II*

## Publications and Contributions

### *Peer-Reviewed Journal Articles*

1. **Linte CA**, White J, Eagleson R, Guiraudon GM and Peters TM. Virtual and augmented medical imaging environments: Enabling technology for minimally invasive cardiac interventional guidance. *IEEE Reviews Biomed Engin.* (Submitted: July 2010).
2. **Linte CA**, Moore J, Wedlake C and Peters TM. Evaluation of model-enhanced ultrasound-assisted surgical guidance in a cardiac phantom. *IEEE Trans Biomed Eng.* (In Press: 2010).
3. **Linte CA**, Moore, J, Wedlake C, Bainbridge D, Guiraudon GM, Jones DL and Peters TM. Inside the beating heart: An *in vivo* feasibility study on fusing pre- and intra-operative imaging for minimally invasive therapy. *Int J Comput Assist Radiol Surg.* 4(2): 113-23. 2009.
4. **Linte CA**, Moore J, Wiles, AD, Wedlake, C. and Peters TM. Virtual reality-enhanced ultrasound guidance: A novel technique for intracardiac interventions. *Comput Aided Surg.* 13(2):82-94. 2008.
5. **Linte CA**, Wierzbicki M, Peters TM and Samani A. Towards a biomechanics-based technique for assessing myocardial contractility: An inverse problem approach. *Comput Methods in Biomech Biomed Engin.* 11(3):243-55. 2008.

### *Full-length Refereed Conference Proceedings - MICCAI*

1. Cho DS, **Linte CA**, Moore J, Wedlake C, Chen E and Peters TM. Predicting target vessel location for improved planning of robot-assisted CABG procedures. *Proc. Med Image Comput Comput Assist Interv. (MICCAI). Lect Notes Comput Sci.* (In Press: 2010).
2. **Linte CA**, Moore J, Wiles AD, Wedlake C and Peters TM. Targeting accuracy under model-to-subject misalignments in model-guided cardiac surgery. *Proc. Med Image Comput Comput Assist Interv. (MICCAI). Lect Notes Comput Sci.* 5761:361-8. 2009.
3. **Linte CA**, Wiles AD, Moore JT, Wedlake C and Peters TM. Virtual reality-enhanced ultrasound guidance for atrial ablation: In vitro epicardial study. *Proc. Med Image Comput Comput Assist Interv. (MICCAI). Lect Notes Comput Sci.* 5242:644-51. 2008.
4. Wilson K, Guiraudon GM, Jones DL, **Linte CA**, Wedlake C, Moore J and Peters TM. Dynamic cardiac mapping on patient-specific cardiac models. *Proc. Med Image Comput Comput Assist Interv. Lect Notes Comput Sci.* 5241:967-974. 2008.

5. **Linte CA**, Wierzbicki M, Moore J, Guiraudon GM, Little SH and Peters TM. Towards subject-specific models of the dynamic heart for image-guided mitral valve surgery. *Proc. Med Image Comput Comput Assist Interv. MICCAI). Lect Notes Comput Sci.* 4792:94-101. 2007.

*Note:* The MICCAI manuscripts consist of full-length, 8-page papers that undergo double-blinded peer-review by 4-7 experts in the field, and only 25-30% of the submitted papers are accepted for publication in Lect Notes Comput Sci.

*Other Refereed Papers in Conference Proceedings*

1. **Linte CA**, Moore, J and Peters TM. How accurate is accurate enough? A brief overview on accuracy considerations in image-guided cardiac interventions. *IEEE Eng Med Biol. (In Press: 2010).*

2. **Linte CA**, Pace DF, Moore J, Cho S, Bainbridge D and Peters TM. Estimating heart shift and morphological changes during direct access off-pump intracardiac interventions. *Proc. SPIE - Medical Imaging. Visualization and Image-guided Procedures and Modeling.* 762509:1-11. 2010.

3. Moore J, **Linte CA**, Wedlake C and Peters TM. Overview of AR-assisted navigation: Applications in anesthesia and cardiac interventions. *Proc. AMI-ARCS.* 2-11. 2009.

4. Peters TM, **Linte CA**, Moore J, Wiles AD, Lo J, Pace D, Wedlake C, Bainbridge D, Jones DL and Guiraudon GM. Cardiac imaging and modeling for guidance of minimally invasive beating heart interventions. *Proc. FIMH. Lect Notes Comput Sci. Vol. 5528:466-75.* 2009.

5. **Linte CA**, Moore J, Wiles AD, Lo J, Wedlake C and Peters TM. In vitro cardiac catheter navigation via augmented reality surgical guidance. *Proc. SPIE - Medical Imaging. Visualization, Image-Guided Procedures and Modeling.* 721600:1-9. 2009.

6. **Linte CA**, Moore J, Wiles A, Lo J, Pace D, Wedlake C, Bainbridge D, Guiraudon GM, Jones D and Peters TM. Where cardiac surgery meets virtual reality: Pains and gains of clinical translation. *Proc. AMI-ARCS.* 18-27. 2008.

7. **Linte CA**, Wiles AD, Moore JT, Wedlake C and Peters TM. Surgical accuracy under virtual reality-enhanced ultrasound guidance: An *in vitro* epicardial dynamic study. *Proc. IEEE Eng Med Biol.* 62-5. 2008.

8. Peters TM, **Linte CA**, Moore J, Bainbridge D, Jones DL and Guiraudon GM. Towards a medical virtual reality environment for minimally invasive cardiac surgery. *Proc. MIAR. Lect Notes Comput Sci.* 5128: 1-11. 2008.

9. **Linte CA**, Wierzbicki M, Moore JT, Wiles AD, Wedlake C, Guiraudon GM, Jones DL, Bainbridge D and Peters TM. From pre-operative cardiac modeling to

intra-operative virtual environments for surgical guidance: An *in vivo* study. *Proc. SPIE - Medical Imaging. Visualization, Image-Guided Procedures and Modeling*. 69180D:1-12. 2008.

10. Wiles AD, Moore J, Wedlake C, **Linte CA**, Ahmad A and Peters TM. Object identification accuracy under ultrasound enhanced virtual reality for minimally invasive cardiac surgery. *Proc. SPIE - Medical Imaging. Visualization, Image-Guided Procedures and Modeling*. 69180E:1-12. 2008.

11. **Linte CA**, Wierzbicki M, Moore J, Guiraudon GM, Jones DL and Peters TM. On enhancing planning and navigation of beating-heart mitral valve surgery using pre-operative cardiac models. *Proc. IEEE Eng Med Biol*. 475-478. 2007.

12. **Linte CA**, Wiles AD, Moore JT, Wedlake C, Guiraudon GM, Jones DL, Bainbridge D and Peters TM. An augmented reality environment for image-guidance of off-pump mitral valve implantations. *Proc. SPIE - Medical Imaging. Visualization and Image-Guided Procedures*. 6509ON:1-12. 2007 (Second Place - Michael B. Merickel Student Paper Award).

13. Peters TM, **Linte CA**, Wiles AD, Hill N, Moore JT, Wedlake C, Jones DL, Bainbridge D and Guiraudon GM. Development of an augmented reality approach for closed intracardiac interventions. *Proc. IEEE ISBI*. 1004-07. 2007.

14. Wiles AD, Guiraudon GM, Moore JT, Wedlake C, **Linte CA**, Jones DL, Bainbridge D and Peters TM. Navigation accuracy for an intracardiac procedure using virtual reality-enhanced ultrasound. *Proc. SPIE - Medical Imaging. Visualization and Image-Guided Procedures*. 6509OW:1-10. 2007.

15. **Linte CA**, Wierzbicki M, Aladl U, Peters, TM and Samani A. Towards a biomechanical-based method for assessing myocardial tissue viability. *Proc. IEEE Eng Med Biol*. 2884-7. 2006.

16. **Linte CA**, Peters TM and Samani A. A method for myocardial contraction force reconstruction for tissue viability assessment. *Proc. SPIE - Medical Imaging. Physiology, Function and Structure from Medical Images*. 6143OW:1-10. 2006.

#### *Technical Articles*

1. Peters TM, Moore JT, Guiraudon GM, Jones DL, Bainbridge D, Wiles AD, **Linte CA** and Wedlake C. Inside the beating heart: Toward a less invasive approach to surgery. *International Society of Optical Engineers - SPIE Newsroom*. Biomedical Optics & Medical Imaging. Apr. 2007.

#### *Invited Presentations*



1. An example of a medical augmented reality: Our experience in cardiac interventions. *University of Oshawa Institute of Technology (UOIT) EMBS Student Club*. Oshawa, Canada. April 9th, 2010.
2. From cardiac imaging and modeling to augmented reality environments for minimally invasive interventional guidance. *CIHR Strategic Training Program in Vascular Research*. London, Canada. Mar. 15th, 2010.
3. Towards the integration of pre-operative models with intra-operative imaging for image-guided intracardiac therapy. *Image-guided Interventions Workshop - Innovation Centre for Computer-Assisted Surgery (ICCAS)*. Leipzig, Germany. Sept. 15-18th, 2009.
4. How to effectively deliver an oral presentation. *IEEE Engineering in Medicine and Biology Conference (EMBC 2010)*. Minneapolis/St. Paul, USA. Sept. 2-6th, 2009. (Co-presented with Jacquelyn Brinkman and Christopher James).
5. Augmented reality-enhanced surgical guidance inside the beating heart. *ORF Consortium on Imaging for Cardiovascular Therapeutics. Imaging Network Ontario Symposium*. Toronto, Canada, Sept. 28-30, 2008.
6. The beating heart from within: An augmented reality environment for intracardiac surgical navigation. *London Imaging Discovery*. London, Canada. June 5, 2008.
7. On the Development of Pre-operative Anatomical Models for Minimally Invasive Cardiac Therapy. *CIHR - ICRH Young Investigators Forum*. Montreal, Canada. May 2008.
8. Inside the beating heart: Towards the development, evaluation and clinical integration of novel image guidance techniques for minimally invasive therapy. *Canadian Surgical Technologies and Advanced Robotics (CSTAR) Research Forum*. London, Canada. April 17, 2008.
9. A virtual-reality enhanced computer-assisted navigation system for image-guided surgery and therapy. *Ontario Consortium for Image-Guided Therapy and Surgery (OCITS)*. Toronto, Canada, Mar. 28-29, 2007.
10. A method for myocardial contraction force reconstruction for assessment of cardiac tissue viability. *Ontario Consortium of Image-Guided Surgery and Therapy (OCITS)*. Toronto, Canada. April 3-4, 2006.
11. Applications of tissue biomechanics in medical imaging. *Workshop on Numerical Modeling and Simulation in Biomedical Engineering. Univ. of Western Ontario*. London, Canada. June 15, 2005.

*Other Podium Presentations*

12. Estimating heart migration and morphological changes during minimally invasive cardiac interventions. *SPIE - Medical Imaging Symposium. Visualization, Image-Guided Procedures and Modeling*. San Diego, USA. Feb. 13-18, 2010.
13. Exploring augmented reality-assisted navigation accuracy: Cardiac and spinal chord applications. *AMI-ARCS Workshop*. London, UK. Sept. 20-24, 2009 (Co-presented with John Moore.)
14. Where cardiac surgery meets augmented reality: Initiating clinical translation. *CIHR's ICRH Young Investigators Forum*. Ottawa, Canada. May 21-23, 2009.
15. Evaluating augmented reality-assisted catheter guidance in phantoms. *Canadian Student Conference on Biomedical Computing (CSCBC)*. Vancouver, Canada. March 12-14, 2009.
16. *In vitro* cardiac catheter navigation via augmented reality surgical guidance. *SPIE - Medical Imaging Symposium. Visualization, Image-Guided Procedures and Modeling*. Orlando, USA. Feb. 7-12, 2009.
17. Where cardiac surgery meets virtual reality: Gains and pains of clinical translation. *AMI-ARCS Workshop*. New York, USA. Sept. 5-10, 2008.
18. Surgical accuracy under virtual reality-enhanced ultrasound guidance: An *in vitro* epicardial dynamic study. *IEEE Engineering in Medicine and Biology Conference*. Vancouver, Canada. Aug. 20-23, 2008.
19. Inside the beating heart: An *in vivo* feasibility study on fusing pre- and intra-operative imaging for minimally invasive therapy. *Computer Assisted Radiology and Surgery*. Barcelona. Spain. June 25-28, 2008.
20. From pre-operative cardiac modeling to intra-operative virtual environments for surgical guidance: An *in vivo* study. *SPIE - Medical Imaging Symposium. Visualization, Image-Guided Procedures and Modeling*. San Diego, USA. Feb. 19-21, 2008.
21. On enhancing planning and navigation of beating-heart mitral valve surgery using pre-operative cardiac models. *IEEE Engineering in Medicine and Biology Conference*. Lyon, France. Aug. 23-26, 2007.
22. An augmented reality environment for image-guidance of off-pump mitral valve implantations. *SPIE - Medical Imaging Symposium. Visualization, Image-Guided Procedures and Modeling*. San Diego, USA. Feb. 17-22, 2007.
23. A virtual-reality enhanced computer-assisted navigation system for image-guided surgery and therapy: A study on mitral valve implantations. *Canadian Student Conference on Biomedical Computing (CSCBC)*. London, Canada, Mar. 16-18, 2007.
24. Towards a 3D biomechanics-based technique for assessing myocardial tissue

performance. *International Society of Magnetic Resonance in Medicine (ISMRM) - Workshop on Cardiovascular Flow and Motion*. New York, USA. July 14-16, 2006.

*Non Peer-Reviewed Contributions*

1. **Linte CA**. Student events around the world: The inauguration of the IEEE EMBS Izmir student chapter. *Student's Corner - IEEE Eng Med Biol*. Vol. 29(5). (*Ahead of Print: 2010.*)
2. **Linte CA**. Student events around the world: Launching an undergraduate research conference. *Student's Corner - IEEE Eng Med Biol*. Vol. 29(4). (*In Press: 2010.*)
3. **Linte CA**. Receiving the mentorship you need. *Student's Corner - IEEE Eng Med Biol*. 29(3). 2010.
4. **Linte CA**. Looking ahead! Tips on putting together a five year career plan. *Student's Corner - IEEE Eng Med Biol*. Vol. 29(2). 2010.
5. **Linte CA**. Looking back at EMBC'09: Student activities highlights. *Student's Corner - IEEE Eng Med Biol*. Vol. 29(1). 2010.
6. **Linte CA**. Student Activities around the World: IEEE EMBS UKRI Student Club Features PGBIOMED 2009. *Student's Corner - IEEE Eng Med Biol*. Vol. 28(6). 2009.
7. **Linte CA**. Medicine through the eyes of an engineer: Strengthening engineer-physician collaborations. *Student's Corner - IEEE Eng. Med Biol*. Vol. 28(5). 2009.
8. **Linte CA**. EMBC'09 at a glance. *Student's Corner - IEEE Eng. Med Biol*. Vol. 28(4). 2009.
9. **Linte CA**. Communicating your research in lay language. *Student's Corner - IEEE Eng. Med Biol*. Vol. 28(3). 2009.
10. **Linte CA**. The nuts and bolts of EMBS student chapters. *Student's Corner - IEEE Eng. Med Biol*. Vol. 28(2). 2009.
11. **Linte CA**. Retrospective: Student events at EMBC'08. *Student's Corner - IEEE Eng Med Biol*. Vol. 28(1). 2009.
12. **Linte CA**. Undergraduate student successfully invents artificial Golgi. *Student's Corner - IEEE Eng Med Biol*. Vol. 27(5). 2008.
13. **Linte CA**. The art of dissemination: What makes an effective scientific presentation? *Student's Corner. IEEE Eng Med Biol*. Vol. 27(4). 2008.
14. **Linte CA**. Writing for publication in biomedical engineering. *Student's Corner. IEEE Eng Med Biol*. Vol. 27(3). 2008.

## Research and Employment

- 2004 - Graduate Research Assistant,  
Robarts Research Institute, London, ON, Canada
- 2005 - 2006 Senior Instructor: Mathematics and Science,  
Seron Academy, London, ON, Canada
- 2003 - 2004 Undergraduate Research Assistant,  
University of Windsor, Dept. Mechanical & Materials Eng.
- 2002 - 2003 Junior Research Engineer,  
Ford Motor Company of Canada, Windsor, ON, Canada
- 2002 - 2003 Undergraduate Research Assistant,  
University of Windsor, Dept. Chemistry & Biochemistry

## Professional Associations & Scientific Societies

- 2008 - 2010 International Society of Computer Assisted Surgery (ISCAS)
- 2007 - 2010 Medical Image Computing & Computer Assisted Interventions
- 2006 - 2010 International Society of Optical Engineers (SPIE)
- 2005 - 2010 IEEE Engineering in Medicine and Biology Society (EMBS)
- 2000 - 2004 Society of Automotive Engineers (SAE)

## Conference Roles

- 2009 IEEE EMBC 2009, Minneapolis, USA  
*Session Co-chair: Computer Assisted Surgery*  
*Student Activities Theme: Co-chair*
- 2008 IEEE EMBC 2008, Vancouver, Canada  
*Session Co-chair: Computer Assisted Surgery;*  
*Catheter-Based Interventions and Endoscopy*  
*Student Activities Theme: Co-chair*
- 2007 IEEE EMBC 2007, Lyon, France  
*Session Co-chair: Computer Assisted Surgery*  
*Student Activities Theme: Volunteer*
- 2007 Canadian Student Conference on Biomedical Computing  
*Conference Chair*

### Scientific Review Boards

2009 - 2010	Journal of Physics in Medicine and Biology
2009 - 2010	Journal of Medical Physics
2008 - 2010	IEEE Transactions on Biomedical Engineering
2007 - 2010	IEEE Engineering in Medicine and Biology Conference
2007 - 2010	Journal of Engineering in Medicine
2007 - 2010	Medical Image Computing and Computer Assisted Interventions

### Committee Membership

2008 - 2010	IEEE Engineering in Medicine and Biology Advisory Board
2006 - 2009	CIHR - ICRH Young Investigators Forum Steering Committee
2006 - 2008	Biomedical Engineering Student Committee
2005 - 2007	Schulich School of Medicine - Graduate Research Committee
2005 - 2007	Schulich School of Medicine - Dean's Awards of Excellence Adjudication Committee
2005 - 2008	London District Science & Technology Fair

### Career Development

2010	IEEE EMBC 2010, Buenos Aires, Argentina Minisymposia Organizer: <i>Tips on Presentation Design and Delivery; Negotiating Your First Bioengineering Position; Lunch with Leaders</i>
2009	IEEE EMBC 2009, Minneapolis, USA Minisymposia Organizer: <i>Presentation Design and Delivery; Negotiating Your First Bioengineering Position; Lunch with Leaders</i>
2008	IEEE EMBC 2008, Vancouver, Canada Minisymposia Organizer: <i>Pathways to Success in Bioengineering; Negotiating Your First Bioengineering Position; Lunch with Leaders</i>
2007	IEEE EMBC 2007, Lyon, France Minisymposium Organizer: <i>Making and Impact in Bioengineering</i>